Single droplet drying to steer particle agglomeration during spray drying

Nienke M. Eijkelboom

Propositions

1. One can predict the morphology of a single dried droplet solely based on its temperature trajectory in time.
   (this thesis)

2. Chance co-determines the results of droplet collisions during spray drying.
   (this thesis)

3. Connecting different length scales in food science research is essential to improve food production.

4. Numerical models extend the interpretation of experimental observation.

5. To see science as just a puzzle to solve is misleading.

6. When research makes you smile, understanding sticks better.

7. For the inexperienced, shortcuts are actually detours.

8. Editing a manuscript is like maintaining a garden, removing the unnecessary and adding elements to obtain a clear structure.

Propositions belonging to the thesis, entitled

Single droplet drying to steer particle agglomeration during spray drying

Nienke M. Eijkelboom

Wageningen, 6 December 2024

Single droplet drying to steer particle agglomeration during spray drying

Nienke M. Eijkelboom

Thesis committee

Promotors

Prof. Dr Maarten A.I. Schutyser
Personal Chair at the Laboratory of Food Process Engineering
Wageningen University & Research

Prof. Dr Remko M. Boom
Professor of Food Process Engineering
Wageningen University & Research

Co-promotor

Dr Patrick F.C. Wilms
Assistant professor at the Laboratory of Food Process Engineering
Wageningen University & Research

Other members

Prof. Dr Jasper van der Gucht, Wageningen University & Research
Prof. Dr Andrew E. Bayly, University of Leeds, England
Dr Giulia Finotello, Eindhoven University of Technology
Dr Eline M. Verbaanderd-Both, FrieslandCampina, Wageningen

Single droplet drying to steer particle

agglomeration during spray drying

Nienke M. Eijkelboom

Thesis
submitted in fulfilment of the requirements for the degree of doctor
at Wageningen University
by the authority of the Rector Magnificus,
Prof. Dr C. Kroeze,
in the presence of the
Thesis Committee appointed by the Academic Board
to be defended in public
on Friday 6 December 2024
at 3.30 p.m. in the Omnia Auditorium.

Table of contents
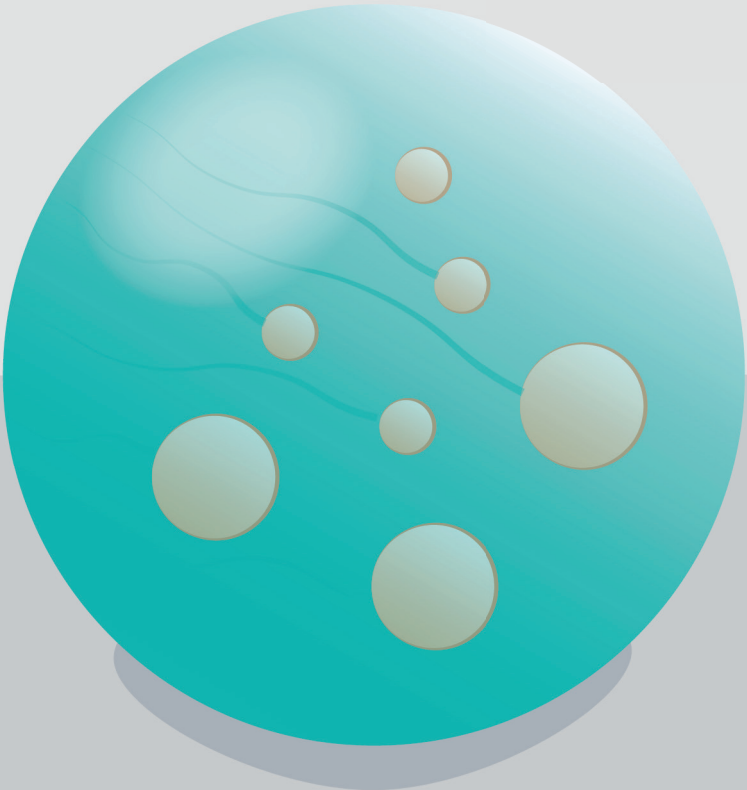
Chapter

Introduction and thesis outline

1

Throughout history, the introduction of food preservation techniques has greatly benefitted our food security. Foods can be preserved in many ways, for example by fermenting, by pickling and by drying. The development of large-scale food production has allowed us to mass-produce well-preservable food materials, such as dry powders. As an example, the commercial production of milk powders started in the early 1900s, and the global production of skim milk powder increased to almost 5 million tons in 2015 (CNIEL, 2016; Coulter, 1956). The drawback of food processing and in particular drying, however, is that it is energy intensive. The food sector is currently responsible for roughly 20% of the global greenhouse gas emissions, and for around 30% of the global primary energy use (FAO, 2011). Of this energy consumed by the food sector, around 40% is used for processing and distribution. Increasing the energy efficiency of food processing is therefore crucial to increase the sustainability of our food production.

Spray drying

Drying is a common processing step applied in the food industry. This process is not only about water removal to obtain a shelf-life stable product, but also about the formation of a micro-structured product. This micro-structure influences functional properties, especially in the case of a powder. One of the drying technologies commonly applied to produce a powder is spray drying (Sadek, Schuck, et al., 2015; Schutyser et al., 2018). Examples of food powders produced via spray drying are vitamins, enzymes, probiotics, flavorings, vegetables, whey protein, caseinates and milk (Anandharamakrishnan & Padma Ishwarya, 2015; Siccama et al., 2021). As an example to illustrate the scale of the spray drying industry, in the year 2000, Germany processed 4,000,000 tons of milk into 400,000 tons of skim milk powder. Approximately 99.5% of all this skim milk powder was produced by spray drying (Dairy Industries International, 2018; Ramírez et al., 2006). To achieve production of such amounts of powder, spray dryers can be scaled to a very large size. The dairy company Fonterra owns the largest spray dryer in the world which can produce 30 tons of milk powder per hour (Eagle, 2016).

Spray drying starts with the atomization of the liquid feed inside a drying chamber, creating a large number of very small droplets with a diameter in the range of 10-500 µm (Filková et al., 2006; Gianfrancesco, Turchiuli, & Dumoulin, 2008). In the drying chamber, the small droplets are contacted with hot air, which leads to very fast evaporation. The fast evaporation induces evaporative cooling, maintaining the droplet at the so-called wet-bulb temperature and thereby limiting the inactivation of heat-sensitive compounds (Cheuyglintase, 2009). While water evaporates, a solute concentration gradient develops within the droplet, with the highest solute concentration near the surface. During drying, eventually a viscoelastic skin forms at the surface of the droplet (Vehring et al., 2007). Due to the high solute concentration near the surface, internal moisture mass transfer will eventually become limiting which will reduce the evaporation rate of water. As a consequence, the drying will enter the falling rate period and the temperature of the particle will gradually increase to the dry bulb temperature (Schutyser et al., 2018). The

droplet residence time in a typical spray dryer ranges from only a few seconds to 30 s (Fox et al., 2014; Harvie et al., 2002). After drying, the powder is collected and cooled down to obtain an amorphous, glassy product (Cheuyglintase, 2009; Fox et al., 2014).

The quality of the obtained powder is generally assessed based on properties such as its mechanical stability, flowability, bulk density and reconstitution behavior. These functional properties are influenced by the micro-structure of the powder. Individual primary powder particles are known to have poor flowability, and their very small particle sizes cause dust issues. Spray drying allows for steering towards agglomerated powders. Agglomeration, resulting in an increase in particle size, benefits the techno-functional properties of a powder (Fröhlich et al., 2023).

Agglomeration

Agglomeration can be achieved with a fluidized bed after the spray dryer. This process has already been studied extensively, and models have been developed to understand the process (Du et al., 2022; Terrazas-Velarde Korina et al., 2011). However, agglomeration can also occur in the zone close to the spray nozzle inside a spray dryer. Within this nozzle zone, agglomeration is induced when a partially dried droplet collides with another partially dried droplet or with a fully dried particle. Recirculation of small, dried particles (fines) into the nozzle zone of the spray dryer can therefore enhance the agglomeration. However, a collision between a partially dried droplet and a fine particle does not always lead to agglomeration. Depending on the material properties, the degree of drying and the collision parameters, a collision can result in full coalescence, agglomeration or bouncing (van Boven et al., 2023) (Figure 1.1).
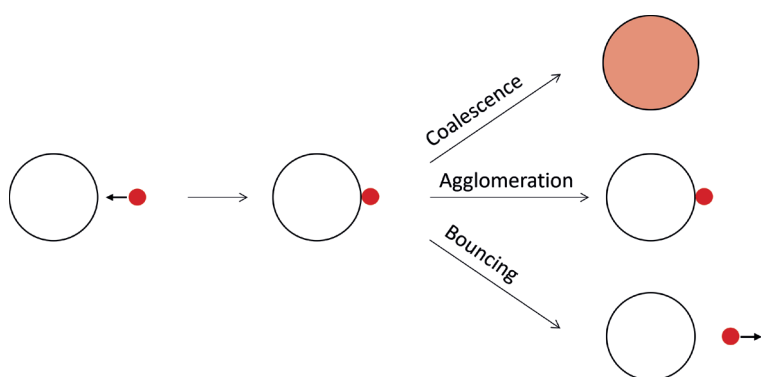

Figure 1.1. Schematic representation of the different collision outcomes between a drying droplet and a fine.

In industrial practice, optimization of the degree of nozzle zone agglomeration is generally achieved by adapting the drying conditions, the position and/or angle of the nozzles, and the choice of the position where the fines are recycled in the chamber. Unfortunately, mechanistic insight into the phenomenon of agglomeration inside spray dryers is lacking, which renders the optimization of agglomeration a difficult task, as this needs to be done empirically for each product formulation (Fröhlich et al., 2023). Failure of adequate particle agglomeration during large-scale production leads to product losses due to off-spec product formation, dust formation and fouling. The waste of material has a major impact on the economics of the process and on the sustainability of the entire powder production chain. To move away from empirical approaches for finding optimal agglomeration conditions, it is crucial to have a better mechanistic understanding of the agglomeration process. However, within a spray dryer, countless collisions occur simultaneously at different stages of the drying process, making it virtually impossible to obtain this mechanistic understanding within a spray dryer.

Single droplet drying

Single droplet drying is used to assess spray drying at the scale of a single droplet, thereby helping to create mechanistic understanding of the spray drying process. Different experimental single droplet drying techniques exist, using sessile, pendant, levitating or free falling droplets (Boel et al., 2020). The focus of single droplet drying studies performed up till now was mainly on drying kinetics and morphology development of the particle (wrinkled versus smooth particles) as a function of the droplet composition (e.g. type of solute and initial dry solids content) and processing parameters (e.g. drying temperature) (Both et al., 2019; Hülsmann et al., 2021; Siemons et al., 2020) (Figure 1.2).

Hitherto, a limitation of all single droplet drying setups is that the droplets are dried at a constant drying air temperature. This differs from what happens inside a spray dryer, where a droplet is subjected to a temperature-time trajectory due to the temperature of the inlet air of a spray dryer being much higher than the outlet air temperature. The temperature influences the drying kinetics of the droplet, and can influence the quality of the powder in various ways. It can for example affect the inactivation of heat-sensitive components present in the product (Perdana et al., 2013; Yamamoto & Sano, 1992), the morphology of the powder (Siemons et al., 2020), and phase separation in case of multicomponent systems (Both, Karlina, et al., 2018). This in turn has an impact on the droplet surface properties, and thus on the drying and agglomeration behavior. Therefore, performing studies on a single droplet drying platform that more closely mimics spray drying conditions is of great interest.
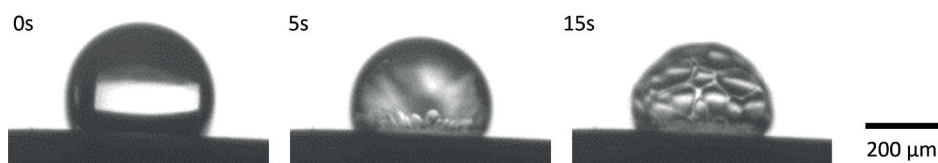
Figure 1.2. Morphological development of a drying 40% maltodextrin DE21 droplet dried with air of 90 °C having a velocity 0.3 m/s.

Droplet collisions

Drying kinetics and morphology development have strong implications for the flowability, bulk density and reconstitution behavior, but these properties are also largely influenced by the agglomeration of the powder (Fu et al., 2012; Sadek, Schuck, et al., 2015; Schutyser et al., 2018). Despite the importance of agglomeration for product quality, collision behavior at the droplet scale has obtained limited attention up till now. Most of the binary collision studies that have been performed focused either on collisions between a dry particle and a water droplet (Charalampous & Hardalupas, 2017; Pawar et al., 2016), or between two wet (solute-containing) droplets (Buck et al., 2018; Finotello, Kooiman, et al., 2018). While the latter type of collisions is of interest for inter-spray interactions in a spray dryer, nozzle-zone agglomeration is based on the collisions between a partially dried droplet and another partially dried droplet or a fully dried particle. Very recently, Sewalt (2024) created two different systems to study the collision outcomes of a drying droplet over time. In the first system, a dry particle is ejected onto a drying droplet. For the second system, a drying droplet falls onto a dry object. This work showed that the collision outcome changed from coalescence to sticking to bouncing depending on the drying time. However, it also showed that focusing on the time that the droplet needs to obtain a glassy surface was too simplistic to successfully predict collision outcomes. In this way, the work of Sewalt (2024) contributed to the mechanistic understanding of drying droplet collisions, but also shows that further investigations are needed to sufficiently understand the agglomeration process.

Modelling single droplet drying

Modelling the drying behavior of a single droplet provides insight into the transient droplet properties that cannot be measured experimentally. This includes, for instance, the development of the moisture content at the surface of the droplet and the resulting rheological properties. These transient droplet properties are expected to play a significant role in the agglomeration behavior, and a drying model could provide valuable information. Another benefit of using a numerical model, is that it makes it possible to rapidly investigate the impact of, for example, changing drying conditions on particle properties such as the retention of enzyme activity.

The predictions made by such a model rely heavily on the provided input parameters, e.g. the mutual solute-water diffusivity in the applied drying matrix. The diffusivity as a function of moisture content and temperature is not known for all drying matrices. Previously developed single droplet drying models focused on droplet volume, temperature, rheological properties and enzyme inactivation, and often considered maltodextrin as a model matrix (Perdana et al., 2013; Siemons et al., 2022). Maltodextrin is commonly added as a drying aid in the spray drying industry, and for maltodextrins the diffusivity under different conditions is well characterized. While maltodextrin can therefore serve as a well-characterized system to evaluate many aspects of morphology development and agglomeration, it is of limited value for many practically relevant spray drying processes. Most industrial applications use different matrices, such as mixed systems containing protein, oil and/or other carbohydrates. Unfortunately, diffusivities in these systems are not as well characterized as for maltodextrin.

Objective and approach

The aim of this thesis is to characterize the physical phenomena underlying the drying and agglomeration behavior of droplets during spray drying via single droplet drying experimentation. To do this, first a single droplet drying platform is developed that more realistically represents spray drying conditions by incorporating changing air conditions. As careful characterization of the drying droplets is required, the temperature of the drying droplets is tracked and their surface composition after drying is determined. To obtain information on the droplet properties that cannot be directly measured upon drying, a numerical model that predicts the drying dynamics of a droplet is employed. The drying platform is then adapted to study binary collisions. The drying model is used to relate the collision behavior to the transient properties of the drying droplets. Maltodextrin will be used as well-characterized model matrix material, but also other materials, such as whey and plant proteins, will be used.

Thesis outline

In the following paragraphs, the thesis outline is described per chapter, and a graphical representation is given in Figure 1.3.
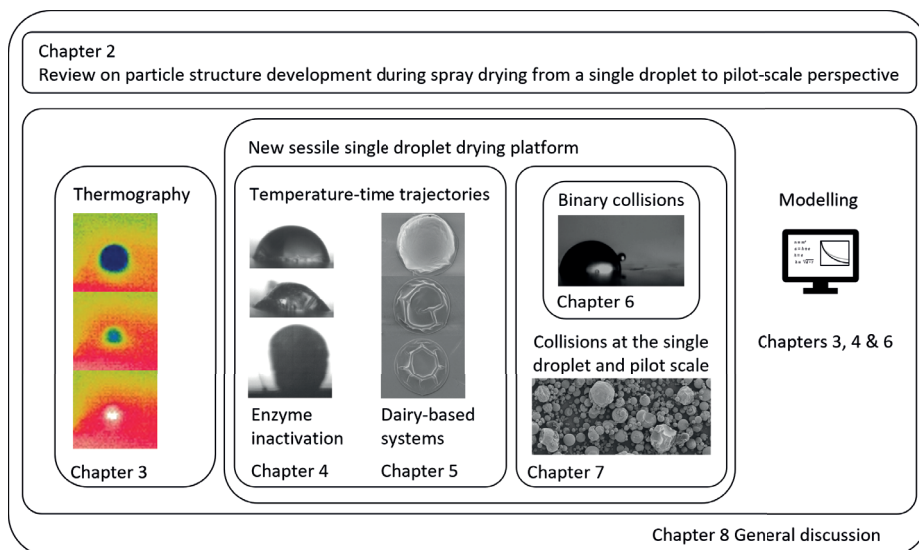

Figure 1.3. Graphical outline of the thesis content and chapter division.

In **Chapter 2** the current understanding of the potentials and limitations of single droplet drying approaches to unravel the evolution of primary particle morphology and the nozzle-zone agglomeration phenomenon during spray drying is reviewed.

To optimally design a spray drying process, it is important to know the drying kinetics of a droplet. While visual observations using a camera can provide information until the locking point, the drying kinetics after this point are also of interest. **Chapter 3** focuses on improved characterization of drying sessile single droplets. The drying behavior of droplets of different maltodextrin, whey protein isolate, and galacto-oligosaccharide solutions was investigated with high-resolution thermography and high-speed visual camera monitoring. A heat and mass transfer-based numerical model was used to predict the drying behavior of the droplets, including the droplet temperature during the constant rate period, the duration of this period, and the final droplet temperature.

To make a further step towards more realistic representations of industrial spray drying systems, a new sessile single droplet drying platform that can use changing drying air temperature-time trajectories has been developed. This new platform is described in **Chapter 4**, where single droplets of solutions containing β-galactosidase and maltodextrin are dried with different temperature-time trajectories. The inactivation of the enzymes was used as an indicator for the thermal load on the droplet. The β-galactosidase inactivation

was also predicted with a coupled drying and inactivation model.

In industry, spray drying is often applied to multicomponent systems, like milk. The drying of these multicomponent systems is more complex than that of a single solute system, as the distribution of components within the droplet generally becomes non-uniform upon drying. Therefore, in **Chapter 5** single droplet drying of dairy-based systems is studied, varying the composition and oil droplet size of the emulsion and the drying conditions applied. The influence on the locking point and the morphological development has been investigated, and confocal Raman microscopy was used to examine the surface composition of the dried droplet.

Collisions occur in the nozzle zone of a spray dryer due to recirculation of fines. To mimic these collisions between a drying droplet and a fine particle, the single droplet drying platform was extended to perform binary collision studies. This platform extension is introduced in **Chapter 6**, where it is used to investigate collisions between drying maltodextrin droplets and glass beads. The collisions resulted in three different outcomes, being merging, sticking and bouncing. To predict the regime when a collision can result in sticking, being the starting point of the formation of an agglomerate, a previously developed single droplet drying model was used.

To reduce the stickiness of sugar-rich products during spray drying, proteins can be added as a drying aid. In **Chapter 7** binary collisions are performed on systems containing maltodextrin and either whey protein isolate or pea protein isolate, characterizing the impact of the carrier composition (from dairy-based to plant-based proteins) on the drying and collision dynamics. To investigate the industrial relevance of the single droplet drying studies, the findings were extended with pilot-scale trials in which both agglomeration and yield were investigated.

Chapter 8 provides a general discussion of the results obtained in this thesis. Besides, it discusses additional work related to the impact of glass bead size on binary collisions, as fines within a spray dryer can have different sizes, further influencing collision behavior. The practical implications of the work performed are highlighted, and the chapter concludes with thoughts for future research.
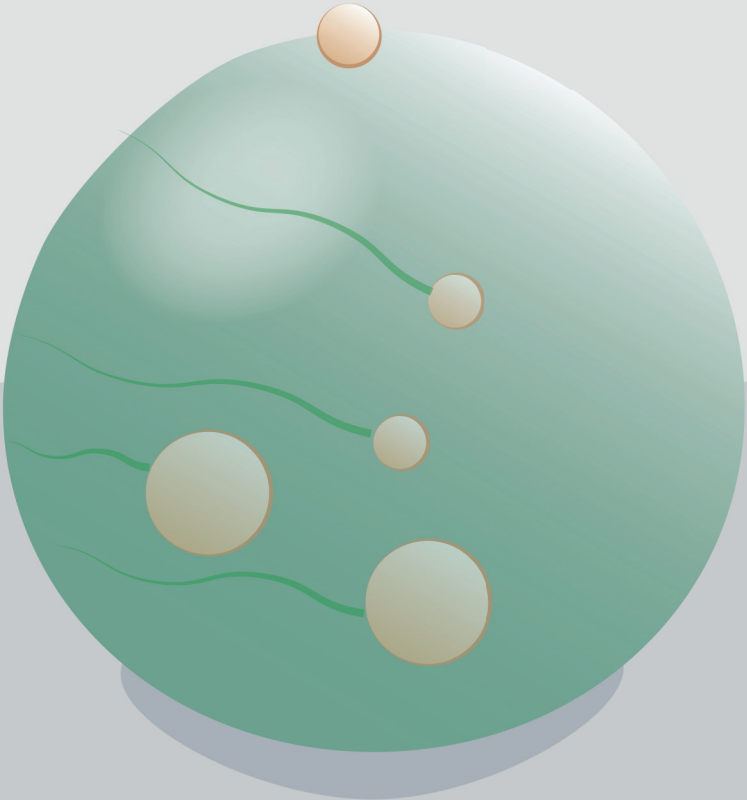
Chapter

Particle structure development during spray drying from a single droplet to pilot-scale perspective

N.M. Eijkelboom[1]
A.P. van Boven[1]
I. Siemons
P.F.C. Wilms
R.M. Boom
R. Kohlus
M.A.I. Schutyser

[1]: Shared first authorship, these authors contributed equally.

2

Abstract

Crucial for achieving premium agglomerated powder products through spray drying is that the primary particle morphology and the degree of agglomeration can be controlled. However, the costs of trial runs and the wide range of products properties complicate achieving this control of particle structure during spray drying. Single droplet drying approaches are employed to study the development of the primary particle morphology and the collision behavior of droplets under well-defined conditions. These studies shed light on the underlying mechanisms but have been related less often to realistic drying and especially agglomeration. This review focuses on the potential and limitations of single droplet drying approaches to unravel the evolution of primary particle morphology and nozzle-zone agglomeration phenomena during spray drying. We discuss advances in single droplet drying approaches and how to combine these with pilot-scale spray drying to obtain the desired particle structures.

Introduction

Spray drying is a widely used process in the food, chemical, pharmaceutical and cosmetic industry to transform liquids into powders. In the food industry, spray drying prolongs the shelf life and concentrates foods, making storage and transportation easier. A major advantage of spray drying compared to other drying techniques is that agglomerated powders can be produced with excellent functional properties such as flowability, reconstitution behavior, bulk density, and mechanical stability. Although the technique was invented 150 years ago (Percy, 1872), lack of understanding of the spray drying process frequently leads to low-quality products and poor process efficiency. Especially the spray drying of new products is challenging and can result in unnecessary waste generation and energy losses.

Both the composition of the liquid formulation and the spray drying conditions determine the properties of particles with specific size, surface composition, morphology and degree of agglomeration of the particles, which together determine the functionality. Smooth and spherical particles with limited surface distortions are for example preferred for a free-flowing powder, which is important for dosing, tableting, blending/mixing or coating (Both, Boom, & Schutyser, 2020; Capece et al., 2015; Walton, 2000). Powders comprising of particles with irregular shape, in other words wrinkles and folds, potentially interlock mechanically, leading to inferior flow properties. In addition, it is not uncommon to spray drying that a large number of small particles (< 100 μm) is formed, which negatively influences the flowability as well. To reduce the percentage of small particles, nozzle zone agglomeration is often used to cluster the primary particles into larger, porous agglomerates that have better flowability. Besides flowability, the particle structure influences the reconstitution behavior and the bulk density (Both, Boom, & Schutyser, 2020; Fu et al., 2020; Takeiti et al., 2008).

To better steer the particle properties of spray-dried powders, the particle morphology and agglomeration during spray drying were studied at different experimental scales. The experimental focus ranges from the single droplet to the laboratory and the pilot-scale (Boel et al., 2020). For example, larger scale spray drying studies were performed to investigate the critical formulation and process parameters to the particle morphology and subsequently analyzing particle morphologies produced using microscopy (Alamilla-Beltrán et al., 2005; Both, Boom, & Schutyser, 2020; Littringer et al., 2013; Paramita et al., 2010). For laboratory-scale spray dryers, such investigations are questionable since the short residence time requires the generation of droplets that are very small (1-10 μm) compared to droplets in industrial spray dryers. As a result, lab-scale produced powders often show poor flowability. For agglomeration studies it is required to perform experiments at the pilot-scale, and could involve the dosage of fines or controlled fines recycling in the nozzle zone (Fröhlich et al., 2020). Despite attempts using, for instance, a sampling device containing liquid nitrogen to capture and analyze drying droplets at different locations in a spray dryer (Pearce, 2007), the major disadvantage for all spray drying experiments is that the dynamics of drying of the individual droplets and their

collision behavior cannot be monitored directly. Therefore, single droplet drying (SDD) approaches have been developed.
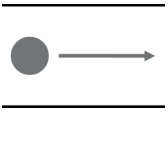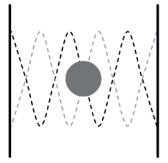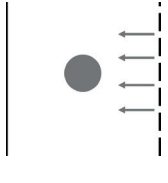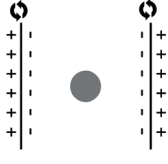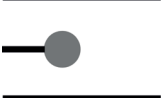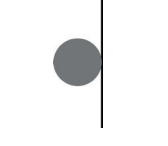
SDD has been successful in obtaining insight into the drying behavior of single droplets (Boel et al., 2020; Schutyser et al., 2019). Different SDD setups have been developed and used to characterize the drying kinetics and the impact of the drying conditions on the properties of the primary powder, such as the morphology and composition of the surface. A clear drawback of SDD is that the droplets are subjected to different conditions compared to droplets drying in a spray dryer. The droplets during SDD are larger and the drying air temperatures are constant, often made equal to the outlet air temperature of a spray dryer. This raises the question how SDD can be related to the complex dynamic drying behavior of droplets during spray drying, and how SDD can contribute to the development of rational guidelines to better control agglomeration processes at the larger scale. This includes the assessment of the extent to which SDD can be used to study binary collisions leading to coalescence, sticky or bouncing behavior. Whereas previous scientific reviews primarily provided an overview of single droplet drying research into the drying kinetics and morphology development of the primary droplets (Boel et al., 2020; Schutyser et al., 2019), this review focusses on the potential to bridge the gap between single droplet drying and pilot-scale spray drying, to better understand particle structure formation during spray drying.

The objective of this review is therefore to discuss the relevance of SDD for understanding the evolution of the morphology of the primary particles and the nozzle-zone agglomeration phenomena during spray drying. We first introduce different SDD techniques and discuss how these are used to monitor the drying kinetics in relation to process conditions. Subsequently, literature is discussed that specifically focused on morphology development. For this, amongst others, studies that compared results at the single droplet, lab, pilot, and/or industrial scale are reviewed (Both, Boom, & Schutyser, 2020; Nuzzo, Millqvist-Fureby, et al., 2015; Tran et al., 2017). The contributions that SDD may have to better understand nozzle zone agglomeration and how these may be combined with pilot-scale agglomeration studies will also be discussed. Finally, we conclude how this will contribute to our understanding for steering spray drying to obtain products with desired primary particle and agglomerate structure.

Single droplet drying techniques

SDD techniques mimic the spray drying process on the level of the individual droplet and thus can be used to thoroughly study the dynamics of the droplet drying process and its impact on, amongst others, morphology development. Different approaches have been developed throughout the years, including contactless methods such as free-falling columns (Fang et al., 2012; Hardy et al., 2021; Vehring et al., 2007), acoustic levitation (Boel et al., 2020; Groenewold et al., 2002; Schiffter & Lee, 2007), aerodynamic levitation (Adhikari et al., 2000; Archer et al., 2020; De Souza Lima et al., 2020) and electrodynamic levitation (Archer et al., 2020; Gregson et al., 2019), and contact-based methods such as

Table 2.1. Benefits and limitations of different SDD techniques.

	Free falling columns	Acoustic levitation	Aerodynamic levitation	Electrodynamic levitation	Pendant droplet	Sessile droplet
Schematic illustration						
Droplet size[1]	10-100 µm	> 300 µm	> 1 mm	10-100 µm	> 500 µm	> 200 µm
Measuring drying kinetics	Continuous monitoring is not possible, but it is possible to obtain samples at different positions in the drying tunnel	Entire drying process by monitoring mass	Entire drying process by monitoring mass	Entire drying process by monitoring mass	Entire drying process by monitoring mass	Only during constant rate period by visual observation
Measuring droplet temperature	No	Yes	Yes	No	Yes	Yes
Allows monitoring particle morphology evolution	Continuous monitoring is not possible, but it is possible to obtain samples and/or data at different positions in the drying tunnel	Yes	Yes, but it is difficult to keep the droplet in place, making constant monitoring more challenging	No	Yes	Yes
Suitable for particle analysis after drying	++	-	-	-	-	++
Remarks		Acoustic field influences the shape of the droplet and the rates of heat and mass transfer	The time frame at which particle crystallization occurs can also be identified		Contact area between filament and droplet affects heat and mass transfer and morphology development	Presence of surface affects heat and mass transfer and morphology development
References	(Fang et al., 2012; Hardy et al., 2021; Vehring et al., 2007)	(Boel et al., 2020; Groenewold et al., 2002; Schiffter & Lee, 2007)	(Adhikari et al., 2000; De Souza Lima et al., 2020; Winborne et al., 1976)	(Archer et al., 2020; Gregson et al., 2019)	(Charlesworth & Marshall, 1960; De Souza Lima et al., 2020; Nan Fu et al., 2011, 2012; Han et al., 2016; Lin & Chen, 2002)	(Perusko et al., 2021; Sadek, Schuck, et al., 2015; Siemons et al., 2020)

[1] The minimum droplet size is not only determined by the SDD method but also by the solutions studied, where it is far more challenging to dispense small droplets with increasing concentration and viscosity.

2

pendant droplet drying (Charlesworth & Marshall, 1960; De Souza Lima et al., 2020; Fu et al., 2011, 2012; Han et al., 2016; Lin & Chen, 2002) and sessile droplet drying (Both, Karlina, et al., 2018; Sadek, Schuck, et al., 2015; Siemons et al., 2020). Each approach has its benefits and limitations, which are summarized in Table 2.1.

In contactless free-falling columns, a single droplet or a stream of identical droplets, with a diameter in the micrometer range, is dried with a co- or countercurrent hot air flow. Hardy et al. (2021) used this technique to investigate the change in the droplet diameter and morphology by capturing samples at various heights. A drawback for this set-up is that continuous monitoring of a drying droplet is not possible (Fang et al., 2012; Vehring et al., 2007). Three different SDD approaches are based on levitation: acoustic levitation, aerodynamic levitation and electrodynamic levitation. In acoustic levitation, a droplet is suspended in hot air against gravity by using acoustic pressure from high intensity standing sound waves. The droplet is trapped in a node of the standing sound waves, such that it can be monitored while drying (Schiffter & Lee, 2007). A downside of the technique is that the acoustic field influences the shape of the droplet which will induce internal stresses as soon as the droplet developed a rigid skin, and intrinsically changes the rates of heat and mass transfer (Groenewold et al., 2002). In addition, the range of air flows that can be balanced by the acoustic field is limited. Aerodynamic levitation relies on an upward air flow that suspends the droplet. It is less frequently applied as it is challenging to control the droplet's exact position (Adhikari et al., 2000; De Souza Lima et al., 2020). Electrodynamic levitation has been more recently used for SDD and relies on levitation using an alternating-current electrical potential to focus a droplet and a direct-current electric potential gradient to balance the gravitational force (Archer et al., 2020; Gregson et al., 2019).

Contact-based SDD methods, including pendant and sessile droplet drying, are more straightforward to use but have the disadvantage that they are more intrusive. During pendant droplet drying, a relatively large (initial droplet size (d_0) = 1 mm) droplet hangs on a thin filament or glass capillary tube. Thanks to its simplicity, it has been widely employed and allows the monitoring of the overall mass, morphology and temperature in time (Charlesworth & Marshall, 1960; Fu et al., 2011; Lin & Chen, 2002). It was assessed that for droplets with an initial volume of 2 μL about 1% of the heat transferred is due to conductive transfer via the filament (De Souza Lima et al., 2020; Fu et al., 2012; Han et al., 2016). During sessile SDD, a droplet is deposited on a hydrophobic surface. The advantage is that the droplet can be accurately monitored by a camera and can be smaller than a pendant droplet (Both, Boom, & Schutyser, 2020; Sadek, Pauchard, et al., 2015; Siemons et al., 2020); its drawback is that the surface affects the heat and mass transfer to the droplet more strongly (Schutyser et al., 2012).

Drying kinetics of a drying droplet

The drying kinetics provide insight into the temporal evolution of the mass of a drying droplet. When a droplet is subjected to a convective air flow, an initial constant rate period

can be identified during which the drying rate is limited by the external rate of heat and mass transfer. This period is followed by a falling rate period, during which the moisture transfer is limited by internal diffusive mass transfer. Due to this limitation, an internal moisture gradient will develop, with the moisture content close to the surface lower than in the center of the droplet. For most food formulations, this moisture gradient coincides with a gradient in the viscoelastic properties of the material, and a skin may be formed that shows elastic, solid-like properties. These properties then affect the evolution of the particle morphology. During the constant rate period the droplet temperature settles at the wet bulb temperature. Subsequently, during the falling rate period, the droplet temperature increases due to limiting internal mass transfer and thus slower evaporation.

There are different possibilities to monitor the drying kinetics of a single droplet: camera monitoring, direct mass measurement and indirect moisture analysis of the drying air. Visual observation by camera is useful for monitoring the shrinkage behavior of droplets during the constant rate period, which can be translated into drying kinetics via image analysis. After skin formation the droplet resists further shrinkage, which makes it impossible to directly correlate the visual observation to the drying kinetics (Both, Karlina, et al., 2018). Data on the drying rate of the full drying period can be obtained by investigating the change in mass of the droplet during the drying process. Both pending and sessile SDD can be used to investigate the mass of a droplet, but for both techniques a relatively large droplet (mm range) is needed to have sufficient mass for accurate results (Boel et al., 2020; Lin & Chen, 2002; Sadek, Schuck, et al., 2015). For electrodynamic levitation, the required voltage to keep the droplet levitating is a direct measure of the mass of the droplet. Therefore, this technique can be used to obtain accurate results on the changing mass of small droplets (10-100 μm) (Colberg et al., 2004). Finally, measuring the moisture content of the outlet air stream can yield information on the drying rate of a drying single droplet. If the air flow and the moisture content of the in- and outgoing airstream are known, mass balances can be used to calculate the amount of moisture evaporated from the droplet (Groenewold et al., 2002). A disadvantage is that the differences when drying a single droplet can be minute and therefore require exceedingly accurate measurements.

The drying rate is influenced by several factors including: (i) the droplet size, (ii) the relative humidity of the air, (iii) the flow regime, and (iv) the temperature of the air. Another factor not considered here is obviously the type and concentration of the solute present but these will be chosen exactly the same during SDD and spray drying. (i) Droplets dried with SDD range in size from 10 μm to 9 mm (Archer et al., 2020; Boel et al., 2020; Hardy et al., 2021; Siemons et al., 2020), while the size of droplets inside a spray dryer is between 10 and 500 μm (Filková et al., 2006; Gianfrancesco et al., 2008). Theoretically, the drying time scales quadratically with the droplet diameter (Both, Karlina, et al., 2018). This is in close agreement with the experimental observations of Grosshans et al. (2016), who observed a 2.5 times faster drying rate for 10% (w/w) mannitol droplets of 370 μm compared to droplets of 600 μm dried with an acoustic levitator. Lin & Chen (2004) also showed that the drying time of pending single droplets of whole milk dried at 67.5 °C

scaled quadratically with the initial droplet diameter for droplets with an initial diameter between 1.15 and 1.83 mm. (ii) While the incoming air flow during spray drying has a low relative humidity, the relative humidity in close vicinity to the droplet increases due to evaporation. As a result, the drying rate decreases (Grosshans et al., 2016). This can be observed during SDD, in which the humidity can be better kept constant. Sadek et al. (2016) showed that the constant rate period for sessile casein micelle droplets dried in a 20 °C airstream was twice as long at a relative humidity of 40% as compared to a relative humidity of 2%. This longer constant rate period is related to a lower drying rate at higher relative humidty. Griesing et al. (2016) observed that for acoustically levitated 15% (w/w) mannitol droplets, an increase in relative humidity resulted in a delay in the onset of crust formation. Hence, a higher relative humidity leads not only to a lower drying rate but also to a delayed accumulation of components close to the surface. They also found a decrease in the porosity and diameter of the final particle with increasing relative humidity, which can be explained by the faster crust formation. (iii) The relative velocity of the air surrounding a falling, drying droplet within a spray dryer depends on both the set airflow rate and the falling speed of the droplet. The latter is influenced by the size and density of the droplet, as well as by interactions with other droplets. The air flow rate within a SDD is typically kept constant during the drying process, with a stagnant droplet resulting in a constant relative air velocity around the droplet. (iv) The hot inlet air that enters a spray dryer cools down during the drying process, leaving the spray dryer at a much lower temperature. SDD generally makes use of a constant air temperature in the range of the outgoing air temperature of a spray dryer. The consequence is that during SDD the initial drying rate will be lower than during spray drying, which may result in later skin formation leading to a longer constant drying rate period during SDD (Grosshans et al., 2016).

Evolution of the droplet temperature during drying

The differences in droplet size, relative humidity, flow regime and air temperature between SDD and spray drying not only influence the drying kinetics, but also the droplet temperature. Similar to the moisture content, the droplet temperature influences the rheological properties, and hence the morphology development, stickiness and agglomeration behavior, of a drying droplet (Figure 2.1). To investigate the temperature evolution of a drying single droplet, different techniques can be used.

The most straightforward method to monitor the temperature of a drying single droplet is direct measurement with a thermocouple (Han et al., 2016; Lin & Chen, 2002). The droplet must be sufficiently large relative to the thermocouple. Han et al. (2016) worked with 900 μm droplets of a mixture of n-Dodecane and n-Hexadecane and observed that the conductive heat transfer between the thermocouple and the droplet influenced the evaporation process. At air temperatures below 200 °C, the conduction mainly affected the initial evaporation stage, resulting in a more rapid increase in the droplet temperature and a faster decrease in the droplet size. Alternatively, the droplet temperature can be measured non-intrusively, for example by thermography using an infrared camera. This technique

has been applied to acoustically levitated, aerodynamically levitated and sessile droplets (Winborne et al., 1976). Even though thermography gives the surface temperature, while a thermocouple in principle gives the internal temperature, the temperature trajectories of drying suspension droplets as obtained by thermography are similar to those measured with a thermocouple.
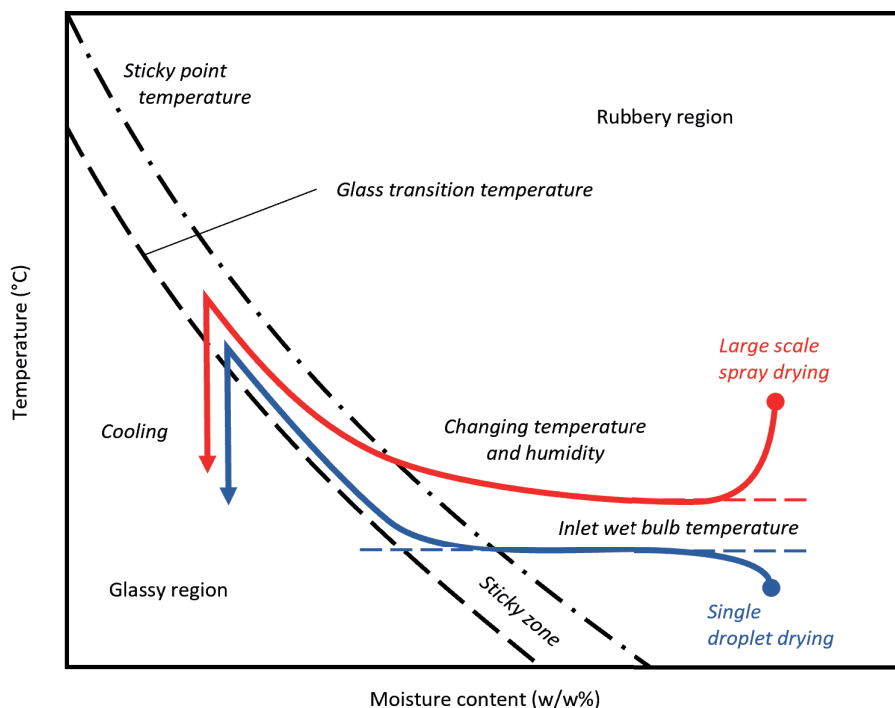
Figure 2.1. Schematic representation of the change in moisture content and temperature of the surface of a droplet during drying at either single droplet or large spray drying scale in the state diagram.

Although the overall, qualitative trend of the change in droplet temperature is the same for droplets drying at the single droplet and spray dryer scale, there are also differences. The temperature trajectories for both scales have been schematically depicted in Figure 2.1. In industrial practice, it is common that the feed material is preheated to temperatures up to 80 °C before spray drying (Pisecky, 2012). As a result of evaporative cooling, the droplet temperature initially decreases to the wet-bulb temperature. In SDD the feed generally has an initial temperature close to room temperature and will heat up to reach the wet-bulb temperature. Furthermore, during industrial spray drying processes, the temperature of the air surrounding a droplet changes over time. Typical air inlet temperatures are 100-150 °C for pharmaceutical products and up to 250 °C for food products (Pisecky, 2012). Due to fast evaporation of water from the drying droplets, the air quickly cools, creating a temperature gradient inside the dryer (Gianfrancesco et al., 2008). Not

considering the product type, the temperature of the outgoing airstream is typically in the range of 60-125 °C. Although the droplet temperature during spray drying cannot be monitored experimentally, it is know that the temperature of the final dried particle is generally 20 °C below the outlet air temperature (Selvamuthukumaran et al., 2020).

The temperature of a droplet, together with its moisture content and distribution, determine the proximity to the glass transition and properties of the surface of the droplet, such as its rheological properties. The droplet drying process can be presented in a state diagram, typically showing the gradual transition of the droplet surface from viscous to rubbery (viscoelastic), to sticky and finally to glassy, which will only be attained by cooling (Figure 2.1). The glass transition temperature, together with the droplet temperature, determines whether a droplet is sticky. In practice, the sticky point temperature is considered to be 20 to 30 °C above the glass transition temperature (Sewalt et al., 2020; Turchiuli et al., 2011) and is closely related to the very fast increase in viscosity close to the glass transition (also called Williams-Landel-Ferry behavior). A semi-dried particle is sticky when its temperature is within the range between the glass transition and sticky point temperature. The temperature of the droplet, which changes during the drying process, therefore influences the stickiness of a particle and other aspects of the rheology of the surface of the droplet, such as the development of elasticity. Since the temperature and concentration can be superimposed with regards to the rheological response of most carbohydrates, both a decrease in temperature and moisture content will generally increase the elastic as well as the viscous portion of the viscoelastic behavior. Therefore, both parameters have profound influence on the development of the morphology of the primary particle and on the agglomeration behavior (Siemons et al., 2020).

Primary morphology development

To improve the understanding and therefore the control of the morphology of the primary particle, researchers have investigated critical factors influencing the particle morphology, by systematically changing the spray drying process parameters and/or feed properties and subsequent microscopic analysis of particle morphologies (Alamilla-Beltrán et al., 2005; Littringer et al., 2013; Mezhericher et al., 2015; Paramita et al., 2010). However, the majority of the morphological research for spray drying has used SDD techniques, as these provide direct, dynamic observation of the evolution of the particle morphology during drying. In contrast to spray drying, SDD experiments can provide real-time information on the governing mechanisms of drying that give rise to specific morphology. This includes information on the shrinking dynamics of the droplets, the skin formation, and any mechanical instabilities that may occur, such as buckling or cracking (Sadek, Schuck, et al., 2015). Nonetheless, because of the differences in drying behavior at SDD and spray drying, the insights obtained at the single droplet scale can provide mechanistic understanding but usually no accurate predictions yet, as elaborated in the next section.

Sadek and colleagues (2013, 2015) and Yu et al. (2021) have for instance used sessile SDD to study the effect of protein composition on the mechanical instabilities triggered during

drying, such as wrinkling and vacuole formation. The effect of the solute composition on the skin formation and mechanical instabilities were also studied with sessile SDD by Siemons and colleagues (2020, 2021). The effect of the initial droplet size and the solids content at the onset of the formation of a solid skin, also called the locking point, was for example studied by Both et al. using SDD (Both et al., 2019). Other processing conditions affecting the morphology development, like the drying air temperature and the air humidity were investigated using various SDD techniques, including free-flight and acoustic levitation (Both, Karlina, et al., 2018; Bouman et al., 2016; Griesing et al., 2016; Rogers et al., 2012; Sadek et al., 2016). The effects of the drying conditions and process parameters on the overall morphology development have already been more extensively reviewed by Both et al. (2019) and Boel et al. (2020).

Despite the importance of SDD studies to study particle morphology development during drying, the question arises whether the results may be translated to large-scale spray dryers. Given the difference in drying conditions, it is not immediately evident whether the morphology development at a single droplet scale can be directly translated towards morphology development at an industrial scale.

Particle morphology development during single droplet drying and spray drying

A major cause of differences in drying kinetics are differences in droplet sizes. Droplets in an industrial spray dryer have much smaller initial droplet sizes (mean $d_0 \sim$ 30-250 μm depending on the atomization device (Selvamuthukumaran et al., 2020)) compared to SDD (Table 2.1), resulting in a reduced timescale of the drying process (since $t \sim d_0^2$) (Santos et al., 2018; Vehring et al., 2007). Powder particles are kinetically stabilized systems, with components migrating during the drying process, and therefore, it may be expected that the difference in droplet sizes and hence the difference in drying dynamics affects also the morphology development (Both, Boom, & Schutyser, 2020). Droplets with a large initial diameter have a smaller surface-area-to-volume ratio and thus require more time to dry at similar process conditions than smaller droplets, allowing more time for diffusional redistribution of the components depending on their characteristics and interactions (e.g. molecular weight, mutual diffusivities and surface activity) (Boel et al., 2020). Consequently, larger droplets may have a different surface composition when compared to smaller droplets, potentially influencing the rheological surface properties and therefore the mechanical instabilities occurring during drying. For this reason, comparisons between the particle morphologies generated at different drying scales (i.e. different droplet sizes), have received considerable attention (Both, Boom, & Schutyser, 2020; El-Sayed et al., 1990; Nuzzo et al., 2017; Ullum et al., 2010).

The study reported by El-Sayed et al. (1990) was one of the earliest studies comparing the particle morphologies of commercially spray-dried coffee and those obtained after free-falling SDD experiments for coffee extract. They observed that free-falling droplets with

sizes close to those encountered in commercial spray dryers reproduced the morphological properties of commercially spray-dried coffee, including the blowholes and surface irregularities. For the free-falling method, it may be expected that similar morphologies are produced as the flow regimes of industrial spray dryers are best reproduced; droplets can have roughly similar sizes to industrial spray drying operation and the drying air temperature profiles may be adjusted to mimic those of large scale dryers (Fu et al., 2012; Sadek, Schuck, et al., 2015).

Despite the droplet size differences, Ullum et al. (2010) found similar wrinkled particles for maltodextrin DE18 after acoustic levitation drying, even though the droplets were much larger ($d_0 \sim$ 500-700 μm) than those from spray drying. Nuzzo, Millqvist-Fureby, et al. (2015) further investigated the influence of the physical dimensions and droplet sizes on the development of the morphology, by comparing an acoustic levitator and a laboratory spray dryer for drying surface-active polymer-lactose systems. They demonstrated that the morphology of single particles produced by the acoustic levitator ($d_0 \sim$ 1 mm) can be well correlated to the morphology of laboratory spray-dried powders ($d_0 \sim$ 2-10 μm). Bovine serum albumin-lactose and hydroxypropyl methylcellulose-lactose mixtures at a mass ratio of 5:95 and 10% (w/w) total solids yielded creased/wrinkled particles with dents and ridges at the surface similar to what was found for laboratory spray-dried powders. Besides, poloxamer-lactose mixtures with similar mass ratio and total solids yielded smooth particles after both SDD and laboratory spray drying. Nuzzo, Millqvist-Fureby, et al. (2015) proposed that the main factor in the scaling effect was the surface activity of the polymers. A larger surface coverage by the polymers was found for the larger SDD particles as compared to spray-dried particles, which according to the authors, was caused by the longer drying time for larger droplets allowing for longer adsorption times. The morphology was mainly determined by the surface rheological properties of the feed solution, and to a lower degree by the surface composition.

In another study, the same authors researched the influence of the scale of drying and accordingly the droplet size on the surface morphology, surface composition and internal microstructure for drying of whole milk (Nuzzo et al., 2017). Whole milk particles as obtained after acoustic levitation ($d_0 =$ 800-1100 μm, 80 °C), laboratory spray drying ($d_0 =$ 2-10 μm, inlet air 210 °C), pilot plant spray drying ($d_0 =$ 4-20 μm, inlet air 155 °C) and industrial-scale drying ($d_0 =$ 4-30 μm, inlet air 210 °C) were compared using confocal Raman microscopy, low vacuum scanning electron microscopy (LV-SEM), and X-ray photoelectron spectroscopy (XPS). The different drying rates and, in particular, drying times affected the surface composition of the particles as revealed by XPS. The long drying times required during acoustic levitation allowed for a distinct rearrangement of the components close to the surface. The increased drying time resulted in an increase in the protein/lactose ratio at the particle surface when compared to the spray-dried particles. Despite the vast differences in drying times, the internal structures and the surface morphologies as investigated by LV-SEM (Figure 2.2) appeared similar. For the SDD scale, however, a more extended lactose enriched surface was found and for full-scale drying more folded surfaces were observed. According to the authors, the similarity of

the smooth surfaces obtained at the different drying scales may be attributed to the high viscosity of the matrices, overriding any potential differences of the surface elasticity at the different scales. The increased folding of the surface obtained after industrial-scale drying is ascribed to the different atomization technology, airflow, agglomeration and additional mechanical stress. The authors eventually suggested that single droplet dryers and pilot-scale spray dryers can be used for predicting the morphology at an industrial scale.
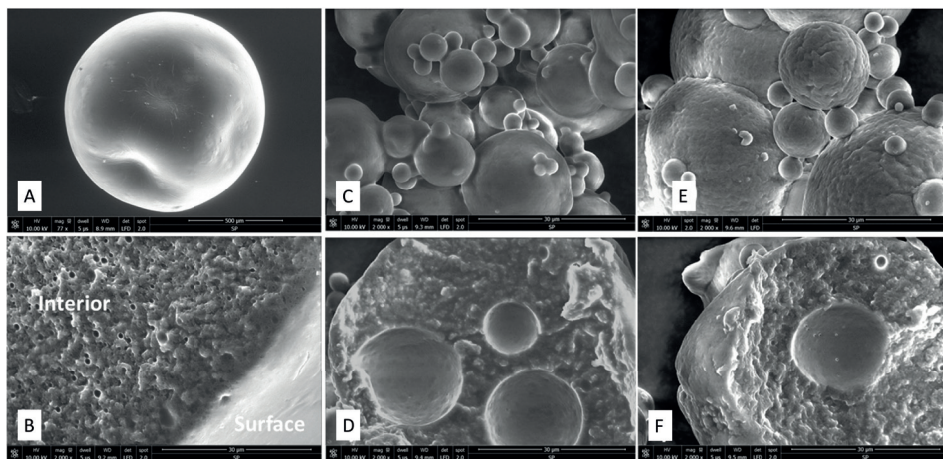
Figure 2.2. LV-SEM images of the morphology and interior of (A, B) SDD particle of whole milk (48% dry matter). Scale bar in (A) 500 μm, (B) 30 μm. (C, D) Pilot plant spray dried powder particle obtained from re-dissolved whole milk (48% dry matter), scale bars 30 μm. (E, F) Spray dried particle of condensed whole milk (50–52% dry matter) produced in an industrial sized dryer, scale bars 30 μm. Reproduced from Nuzzo et al. (2017) with permission of Elsevier.

Both et al. (2020) discussed pilot-scale spray drying of model formulations consisting of maltodextrin and whey protein (30% (w/w)), and compared the results to sessile SDD observations. The particle morphologies after pilot-scale spray drying were qualitatively evaluated with SEM and quantitatively with 2D image analysis for particle size and shape using a Malvern Morphologi 4 particle shape analyzer. Similar as obtained after SDD, they found on average more hollow particles for mixtures rich in whey proteins, while increasing the concentration of maltodextrins yielded more wrinkled particles. The authors also showed that the droplet size distribution greatly impacts the particle morphologies produced after pilot-scale drying. Larger particles (20-100 μm) were generally more wrinkled, while small particles (5-20 μm) were often classified as hollow (Figure 2.3). Interestingly, for single droplet drying this was the other way around. The relatively long drying time for SDD of ~ 1 mm droplets (~ 2-3 min) probably allows for surface enrichment with protein. A larger protein coverage of the surface results in an elastic skin that gives rise to cavitation and accordingly hollow particles (Both, Karlina, et al., 2018). Increasing the droplet size or decreasing the droplet drying air temperature during SDD experiments promotes this effect and consequently more hollow particles may be found (Figure 2.4). During pilot-scale drying, the initial sizes and, accordingly, the drying times are much shorter and
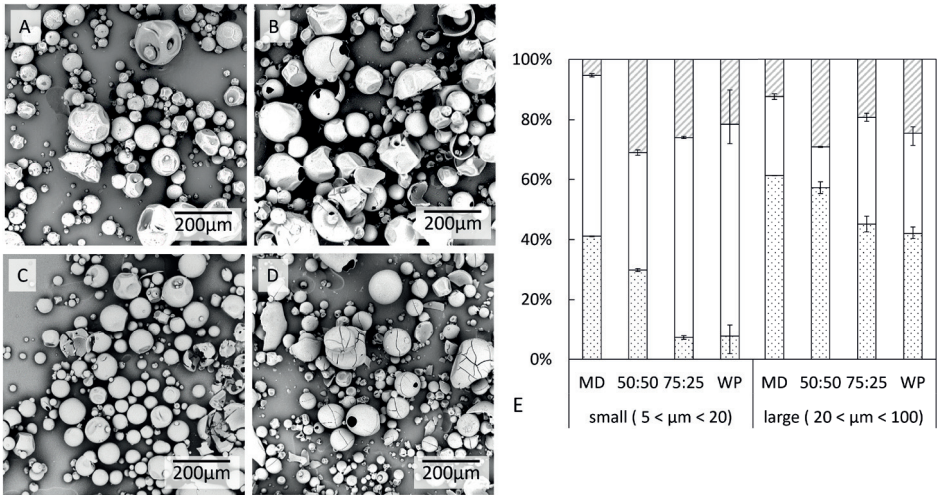
Figure 2.3. Particle morphologies of pilot spray dried powders (190 °C inlet, 8% outlet humidity): (A) SEM image of maltodextrin 30% (w/w), (B) SEM image of 50:50 whey protein-maltodextrin mixture 30% (w/w), (C) SEM image of 75:25 whey protein-maltodextrin mixture 30% (w/w), (D) SEM image of whey protein 30% (w/w). (E) Morphologi 4 analysis results with % wrinkled (dotted), % hollow (white), % other (diagonal lines), divided in particle size groups based on equivalent circular diameter. Adopted from Both et al. (2020).
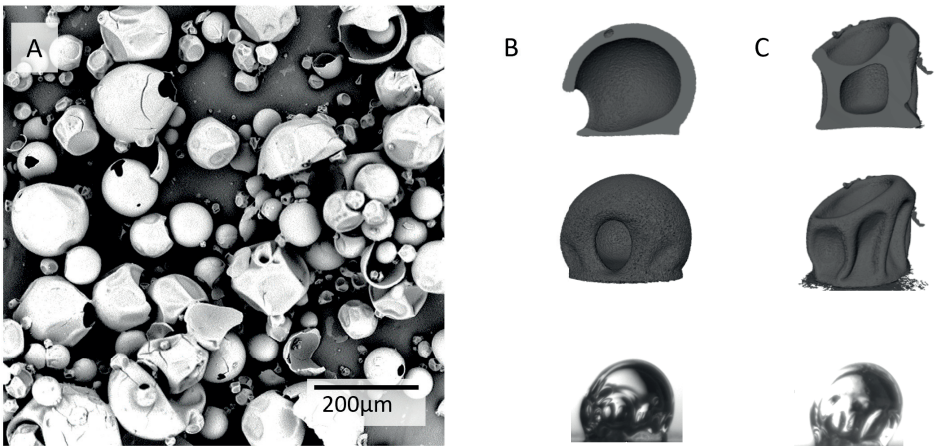

Figure 2.4. Particle morphologies of 50:50 whey protein-maltodextrin mixture 30% (w/w) dry matter: (A) after pilot-scale spray drying at 190 °C and 8% outlet humidity, (B) after SDD at 50 °C, and (C) after SDD at 70 °C with initial droplet size ~ 1 mm as reproduced from Both and colleagues (Both, Karlina, et al., 2018; Both, Boom, & Schutyser, 2020) with permission of Elsevier.

surface enrichment with a particular solute is therefore limited (Nuzzo et al., 2017). The finding that small particles are typically classified as hollow is likely related to faster heat and mass transfer for smaller droplets: smaller droplets deform much more quickly and therefore elasticity becomes prevalent earlier during the drying process and accordingly will prevent surface indentations, and give rise to cavitation. SDD experiments are thus less suitable to predict the development of the morphology at the very high drying rates that are present during spray drying of the small droplets.

Gouaou et al. (2019) compared the morphology of hydroxypropylated pea starch (HPS) particles using pendant SDD and pilot-scale spray drying at different temperatures and initial solids concentrations. The shrinking, deformation and breakage of the particles was attributed to stress distribution on the crust surface. Spray-dried HPS powder demonstrated a wide range of particle surface morphologies, with some particles completely smooth, and others rough with indentations. A higher degree of surface undulations and more dents were obtained for spray drying at lower drying air temperatures. Lower air temperatures result in a slower drying rate, requiring longer residence times, allowing for particle deformation and collapse. Increasing the solids concentration resulted in smoother surfaces, as attributed to the formation of a rigid shell that may sustain the surface structure. Similarly, SDD particles with lower initial solids content yielded wrinkled surfaces, while droplets made with higher initial solids content were generally smoother. X-ray microtomography of the SDD particles revealed collapsed particles for low initial solids concentrations dried at high drying air temperature, which was related to an inflation/deflation phenomenon occurring at air temperatures above 100 °C. Overall, the range of particle morphologies obtained after spray drying could be related to the morphologies produced after pendant SDD. The drying rate resulting from the processing conditions is considered the most important determining factor for the physical characteristics of the skin and accordingly the final particle morphology.

Despite the differences between SDD and large scale drying, i.e. droplet size and size distribution, the aforementioned studies demonstrated that the morphologies of the primary particle produced are often quite similar. This confirms that SDD techniques allow adequate analysis of the mechanisms governing morphology development during drying, which cannot easily be studied at larger scales. However, the development of the primary particles determines to a large degree how the agglomeration of the primary particles into larger agglomerates will take place, as these are the result of collisions between particles at varying states of drying. The agglomerates largely determine the properties of the ultimate powder obtained.

Nozzle zone agglomeration during spray drying

In addition to primary particles having different morphologies, they can also interact to form agglomerates. Agglomeration of primary particles is a key determinant of the functionality of the final powder, such as flowability and reconstitution behavior. Collisions between two (semi-dried) droplets can lead to the formation of small agglomerates.

Binary collisions have different possible outcomes: coalescence, sticking or bouncing (Finotello, De, et al., 2018). The type of collision behavior results in different appearance of the agglomerates. Coalescence of wet droplets does not result in structure formation: the droplets will fuse to form a new, albeit larger spherical droplet. Collisions between a wet droplet and a dry fine result in coating and creates onion-like agglomerates with different layers (Figure 2.5). These agglomerates are compact, difficult to dissolve and therefore usually undesired. Collisions between two sticky particles or between a sticky and a dry particle lead to either compact or 'loose grape' structures, which dissolve more easily due to their increased porosity (Pisecky, 2012). When a droplet and a dried particle collide, the penetration of the dried particle into the droplet can be characterized by the impact Weber number, which gives the relative importance of the inertia versus the capillary forces. A larger impact Weber number leads to deeper penetration (Mitra et al., 2014; van der Hoeven, 2008).
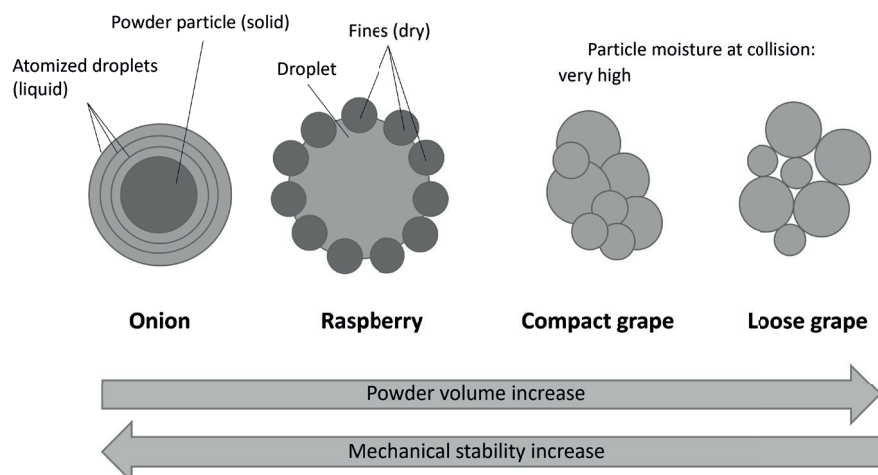

Figure 2.5. Different types of agglomerates, recreated from Pisecky (2012).

Although there are different agglomeration zones in a spray dryer, the nozzle zone has a dominant impact on agglomeration during spray drying (Schwartzbach & Masters, 2001). In the nozzle zone, the agglomeration is often enhanced by using multiple nozzles with overlapping sprays. Agglomeration can further be enhanced by dosing dry, fine particles into the spray drying chamber, leading to particle-drop collisions. From a study using marker powder in the fines recirculation, it was concluded that nozzle zone agglomeration is predominantly characterized by particle-drop interactions (Fröhlich et al., 2020). However, this research was conducted on a spray dryer with only one atomizer and the conclusions remain to be verified for spray drying systems with multiple atomizers. Note that a fluidized bed can be incorporated to induce agglomeration, either as a separate system after the spray dryer or integrated in multi-stage spray dryers. Experiments on pilot-scale spray dryers showed that the agglomeration efficiency (conversion efficiency

of the transformation from droplet's feed size distribution into the agglomerated size distribution) is more determined by the probability of successful agglomeration than by the rate of collision itself (Turchiuli et al., 2011; Williams et al., 2009). Thus, stickiness is a key aspect to control and steer agglomeration during spray drying.

Assessment of the stickiness and collision behavior at the droplet scale

Few studies used SDD to gain insights into stickiness and collision behavior. The fact that at least two droplets are involved during a collision complicates the use of SDD approaches. Some researchers applied a simplified approach to study binary collisions between non-drying droplets. Rabe, Malet, & Feuillebois (2010) investigated the impact parameters versus Weber number for binary collisions of water droplets and determined that coalescence of the droplets is only possible when their Weber number is smaller than 120, indicative of low cohesion relative to the impact velocity. Finotello, Kooiman, et al. (2018) investigated binary collisions of droplets consisting of reconstituted milk powder or glycerol varying in solid content, to simulate the increasing viscosity during drying. Droplets can bounce, coalesce or show reflexive separation upon an increase in Weber number. The authors found that the critical Weber number for droplet break-up is linearly related to the Ohnesorge (Oh) number, which relates the viscous forces to the inertial forces and the surface tension (Finotello, Kooiman, et al., 2018). At higher viscosities, a higher kinetic energy is required to achieve droplet break-up, favoring coalescence. However, solids content is not the only factor influencing viscosity and thus stickiness, but temperature also plays a role. Adhikari et al. (2004) studied the stickiness of single droplets and used it to predict when droplets would become non-sticky during drying. They experimented with droplets ($d_0 = 120$ μm) comprising of a mixture of maltodextrin DE6, low molecular weight sugars and organic acids. The stickiness was estimated using the droplets' surface glass transition temperature as an indicator. The addition of maltodextrin DE6 enabled quicker transition to the non-sticky drying regime which makes it an effective drying aid to prevent fouling, but this will be disadvantageous for agglomeration.

The different methods to assess the stickiness of powders can be divided into static and dynamic tests (Sewalt et al., 2020). Static tests provide information for long-term storage, while dynamic tests are more useful to evaluate powder processing. The evolution of the dynamic stickiness of single droplets was investigated by Petersen (2015). A moving piston was used to impact a drying droplet after a specific drying time. Visual inspection was used to observe the stickiness for skim milk and maltodextrin DE18 as a function of the drying time, temperature and relative humidity. The impact velocity of the piston affected the behavior, with a higher impact velocity being positively correlated to increased stickiness.

In short, while several groups have studied agglomeration on small scale by investigating stickiness in single droplets and by performing binary collision experiments, studies that

combine binary collision experiments with drying are lacking and provide opportunities for future research. This also includes the extension towards pilot- and industrial scale drying, which encompasses the multi-body interactions that are inherent to agglomeration, and which never have been studied on small scale.

Assessment of agglomeration at the pilot- and industrial scale

Researchers have tried to identify the sticky zones in a spray dryer to determine in which region droplet collisions are likely to form agglomerates (Figure 2.1). Sticky zones have been identified based on the surface properties of drying droplets in different regions of the spray dryer, which were correlated to the local temperature and humidities (Gianfrancesco et al., 2008). For example, Gianfrancesco et al. (2008) compared the sticky behavior of maltodextrin DE12 and DE21 during drying by combining data on drying rate, average particle water content, particle temperature, and glass transition temperature. They observed that a drying droplet of DE12 is sticky at higher moisture contents than DE21. Based on this observation, they hypothesized that particles of DE12 are sticky close to the atomizer, while particles of DE21 are sticky lower in the spray dryer. Similar conclusions were drawn in a following computational fluid dynamics (CFD) modeling study (Gianfrancesco et al., 2010). To further substantiate this hypothesis, an agglomeration study was carried out in which powder was reintroduced in different parts of the spray dryer during the drying of maltodextrin DE12 or DE21 (Turchiuli et al., 2011). The results underlined that the drying behavior largely influences the location of the sticky zones.

To reach the high throughputs necessary in industrial-scale spray drying, multiple atomizers are generally used. The overlapping spray cones increase the frequency of the droplet collisions. Unfortunately, pilot-scale spray dryers usually have limited evaporation capacity or too small diameters to allow for multiple atomizers. Zheng & Huang (2017) experimentally investigated droplet size distributions with three overlapping spray cones from pressure-swirl atomizers at ambient conditions. They found that coalescence into bigger droplets could be induced with a specific spatial arrangement of the atomizers. But since these droplets were not drying, it was not possible to study the agglomeration of sticky particles. Zbicinski, Ciesielski, & Ge (2022) reviewed single and multi-nozzle atomization in spray drying, and concluded that there is a strong effect of the nozzle locations related to the hot air inlet on the particle agglomeration mechanisms. Generally, a high air temperature in the atomization zone hinders agglomeration because this promotes earlier crust formation, lowering the stickiness. For a dual-lance setup, the authors concluded that the distance between the nozzles determines whether the collisions are wet-wet, sticky-sticky or sticky-dry, or dry-dry, resulting in different agglomerate structures (Figure 2.5). Given the experimental complexity of studying agglomeration, others have used computational modelling to obtain better understanding of the processes that determine the agglomeration process during spray drying with multiple atomizers

(Nhumaio et al., 2004, 2005; Verdurmen et al., 2006). This is still a developing field, where we expect that the ongoing increase in computational power will contribute to the design of models that are in semi-quantitative agreement with experimental observations, providing insights in the near future.

Concluding remarks

A range of single droplet drying (SDD) methods is available to mimic the spray drying process and monitor the drying kinetics and temperature evolution of individual droplets. SDD methods are especially suitable to characterize the particle morphology, although differences in drying rate due to droplet size and temperature profile differences do lead to differences between SDD and spray drying. For future research it may be considered to extend SDD approaches to facilitate more realistic simulation of spray drying conditions. This includes small droplet sizes and super-imposed temperature and relative humidity profiles providing higher drying rates that are similar to spray drying. Non-invasive measurements during SDD (e.g. thermography) are already used to collect information on drying droplet properties, but could perhaps be complemented with other analytical techniques (e.g. confocal Raman microscopy) to dynamically map the changing compositional surface properties if it is feasible to integrate these techniques in a SDD set-up (Both, Nuzzo, et al., 2018).

The development of the morphology of the primary droplets and the sticky behavior are very much governed by the rheological properties of the materials dried. Very recently, we proposed combining SDD models and rheology to predict mechanical skin properties (Siemons et al., 2020). This could be taken further to fully model morphology evolution.

SDD methods are intrinsically not suitable to characterize nozzle zone agglomeration but may be complemented with binary collision studies of droplets and/or particles. SDD set-ups could be extended to monitor binary collision behavior, e.g. by contacting a drying droplet with another wet, dry or drying particle. Better understanding of nozzle-zone agglomeration requires use of pilot-scale spray dryer set-ups that allow for controlled agglomeration, e.g. being able to dose fines and varying air flow conditions to steer agglomeration.

Ultimately, advanced CFD modelling approaches could prove useful to fully integrate the insights gained at the SDD and pilot-scale. However, such advanced CFD based models still have a long computation time. Therefore, a more direct translation of the insights generated by SDD into lumped models or at least into generic guidelines may aid industrial application and validation of findings on a large number of systems.
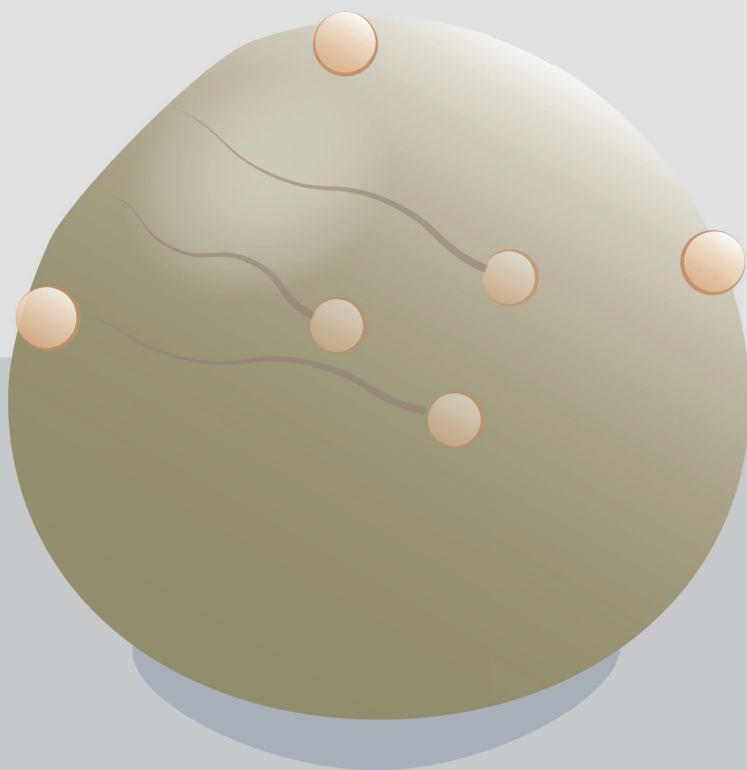
Chapter

3

High-resolution thermography and modelling allows for improved characterization of drying sessile single droplets

N.M. Eijkelboom
A.C.M. Swinkels
J. de Ruiter
R.M. Boom
P.F.C. Wilms
M.A.I. Schutyser

Abstract

Single droplet drying experiments help to understand droplet drying behavior during spray drying. In this study, high-resolution thermography and high-speed camera monitoring were used to characterize drying behavior of sessile single droplets containing solutes. Selected solutes were maltodextrin with a dextrose equivalent of 6, 21, and 38, whey protein isolate and galacto-oligosaccharide. A heat and mass transfer-based model was developed to describe the drying kinetics of the sessile droplets, assuming ideal shrinkage. This model accurately predicted the drying behavior of the droplets, including the droplet temperature during the constant rate period, the duration of this period, and the final droplet temperature. Remaining differences between measured and predicted droplet temperature are explained by skin formation and subsequent morphological development. Tracking temperature with thermography allows to more accurately follow and understand drying behavior, including morphology development of sessile droplets. It makes it possible to develop better models to translate the obtained insights to spray drying behavior.

Introduction

Spray drying is a common process to create a powder from a liquid feed, which is atomized into small droplets and exposed to hot drying air. Due to the large number of droplets, it is not possible to track and study the drying behavior of individual droplets during spray drying (Sadek, Schuck, et al., 2015). To increase the understanding of the drying behavior during spray drying, single droplet drying (SDD) approaches are often used to mimic spray drying at the scale of a single droplet (Boel et al., 2020; Eijkelboom, van Boven, et al., 2023; Fu et al., 2012). The initial droplet size and drying air conditions can be accurately controlled during SDD, which allows the investigation of their influence on drying. Previous SDD studies have, for example, investigated the impact of these parameters on heat-sensitive components, such as enzymes and living bacteria (Schutyser et al., 2012; Siemons et al., 2021), and particle morphology development (Both, Karlina, et al., 2018; Ge, 2005; Sadek, Schuck, et al., 2015; Siemons et al., 2020).

Several different single droplet drying techniques exist, each having their own benefits and limitations. Drying kinetics as assessed by contactless methods, such as free-falling columns, acoustic, aerodynamic or electrodynamic levitation, are not influenced by the presence of a contact area which could influence heat transfer. However, visual observations are more challenging for these contactless methods, as the position of the droplet is not fully static (Eijkelboom, van Boven, et al., 2023). Pendant droplet drying employs static droplets and allows monitoring mass changes as well as visual camera observations. For this technique a small contact area between filament and droplet is present, and relatively large (> 500 μm) droplets are required. Although sessile single droplet drying has the largest contact area, it is suitable for visual camera observations and uses smaller droplets (> 200 μm) (Eijkelboom, van Boven, et al., 2023). Unfortunately, monitoring drying kinetics during sessile droplet drying is more challenging, as the droplet mass is too small to measure directly with a mass balance. Visual observations can only provide insights into the drying kinetics until the locking point, i.e. the point at which shape deviation is visually observed (Siemons et al., 2020). Another approach to indirectly monitor the drying kinetics is by measuring the droplet temperature (Huelsmann et al., 2020). The droplet temperature stays constant during the constant rate period, increases during the falling rate period and becomes constant again when fully dried. Direct measurement of the droplet temperature also gives insights into the drying kinetics beyond the locking point.

Up till now, the measurement of the temperature of a droplet during drying has been challenging. Invasive methods disturb the droplet's drying behavior (Han et al., 2016), while non-invasive temperature measurements were not accurate enough for very small droplets (Chen et al., 2016; Duranty et al., 2020; Huelsmann et al., 2020). Infrared thermography has been used to investigate the temperature of drying droplets, but only for droplets of a larger size (1.5-2 mm) (Chen et al., 2016; Duranty et al., 2020; Huelsmann et al., 2020) compared to industrial-scale spray drying, where the droplet sizes are 10-500 μm (Patel & Chen, 2008).

Monitoring the droplet temperature of small drying droplets is important as it influences, together with moisture content, the viscoelastic properties of the material and especially that of the 'skin' with increased solute concentration which is formed at the surface of the drying particle (Siemons et al., 2022). Being able to follow the drying kinetics of a droplet in detail is key to steering particle properties, such as skin properties, which have a profound impact on stickiness and thus indirectly on the agglomeration and fouling during spray drying.

In addition to experimental methods, modelling work has been performed on the drying of droplets to increase the understanding of the drying kinetics. Different types of models have been developed for droplet drying such as multi-physics models (Shamaei et al., 2017; Siemons et al., 2022; Yang et al., 2014) as well as CFD models (Wegener et al., 2014; Woo et al., 2008). The models as developed by Siemons et al. (2022) and Yang et al. (2014) are specifically developed to describe the drying of sessile single droplets. However, these models have not yet been well validated because of the challenges to monitor mass and temperature of these drying droplets in-line (Perdana et al., 2013; Siemons et al., 2022). In sessile droplet drying models the conductive heat transfer was neglected as it was estimated that conductive heat transfer would be limited to 5% of the overall heat transfer or less (Perdana et al., 2013). However, since the impact of conductive heat transfer also depends on the experimental conditions (e.g., droplet size and material of the contact surface), it is important to quantify conductive heat transfer by direct droplet temperature measurement.

The focus of this chapter is therefore on the non-invasive analysis of the temperature of a drying sessile single droplet with microscopic infrared thermography and comparing this to modelling results. Drying experiments were performed for different drying matrices (maltodextrin DE6 (MD6), maltodextrin DE21 (MD21), maltodextrin DE38 (MD38), galacto-oligosaccharides and whey protein isolate) at solute concentrations of 20, 30 or 40% (w/w). The droplets had an initial radius of 200 ± 15 μm and were dried with a dry air flow of 0.3 m/s at 60, 75 or 90 °C. Results from this infrared thermography were compared to visual camera observations which were used to track the morphological change and initial drying rate via image analysis. A droplet drying model as developed by Siemons et al. (2022) was extended, by including, among others, conductive heat transfer to more accurately predict the experimentally obtained drying rates and temperature development.

Materials and methods

Materials
Polyethylene glycol with an average molecular mass of 400 g/mol (PEG400) was obtained from Sigma Aldrich (St. Louis, MO, USA) and was specifically used to investigate heating of a non-evaporating droplet. Maltodextrins with dextrose equivalence (DE) 6, 21 and 38 were obtained from Roquette Frères (Lestrem, France). Whey protein isolate (WPI) (Nutri Whey™ Isolate R, 90% protein) and galacto-oligosaccharides (GOS) (Vivinal GOS, 69% galacto-oligosaccharides, 23% lactose, 5% glucose and galactose, 3% water) were kindly

provided and characterized for their composition by FrieslandCampina (Amersfoort, the Netherlands). The powders were mixed with demineralized water to obtain solutions with a concentration of 20, 30 or 40% (w/w) of solute. Solutions containing WPI were stirred overnight, while the other solutions were stirred for 30 minutes.

Viscosity measurements

The viscosities of 20% (w/w) solutions of the different solutes were measured with a strain-controlled rheometer (MCR 301, Anton Paar, Austria). Shear rate sweeps were performed using a double gap geometry (DG26.7/T200/AL, Anton Paar). The shear rate was logarithmically increased from 0.1 to 100 s^{-1}, collecting 30 data points at logarithmically decreasing duration of 300 to 1 s. Subsequently, the procedure was reversed, using a logarithmically decreasing shear rate from 100 to 0.1 s^{-1} taking 30 data points at logarithmically increasing duration of 1 to 300 s. Samples of different solutes were measured in duplicate; once with and once without the reversed procedure.

Sessile single droplet drying

The drying of single droplets was performed with the sessile single droplet drying platform as described earlier by Siemons et al. (2020). The droplets were dispensed onto a hydrophobic membrane (Tetratex® ePTFE Polytetrafluoroethylene 3104 membrane, thickness 254 μm, Donaldson Nederland B.V., The Netherlands) using a PipeJet® NanoDispenser (BioFluidix, Germany) with ID500-S PipeJet® Pipes (BioFluidix, Germany). BioFluidix Control Software V2.9 (BioFluidix, Germany) was used to control the volume of the droplets (Biofluidix, Germany). The deposited droplets had an initial radius of 200 ± 15 μm, which is within the upper limit of the droplet size range in industrial spray dryers (Patel & Chen, 2008). Droplets were dried in a dry air stream (RH = 1.2%) of 60, 75 or 90 °C with a flow velocity of 0.3 m/s, which corresponds to a surface temperature of 53, 64 or 67 °C respectively. Independent experiments were performed to investigate either the morphological development or the temperature development of a drying droplet.

The morphological development, including particle size and shape, was investigated using a C-VIT high-speed camera (AOS Technologies AG, Switzerland) with a VZMTM 1000 Zoom Imaging Lens (Edmund Optics, Japan). AOS Imaging Studio v4 (AOS Technologies AG, Switzerland) was used to adjust the settings of the camera and to capture the movies. Movies were taken with a frame rate of 500 fps. The lens was set to a zoom of 2.5x and the image format of the camera was set to 360 x 200 pixels. As a light source, a PFBR 150SW MN (CCS Inc., Japan) with a 2" x 2" back-light module (Vision Light Tech, the Netherlands) was used. The exposure of the camera was set to 2000 μs. The movies were analyzed using a MATLAB (MATLAB R2018b, MathWorks, United States) image analysis script to determine the droplet size until the locking point, based on pixel count. The locking point was manually determined as the first visual observation of spherical shape deviation. The measurements were performed in triplicate. Volume data were extracted from a single representative movie for each experimental condition.

An infrared (IR) camera was used (PI 640 Microscope optics, Optris, Germany) to monitor the droplet temperature. The settings of the camera were controlled with Optris PIX Connect software (Optris, Germany). The camera operated in a temperature range of 0-250 °C and was set to an optical resolution of 640 x 120 pixels, which is paired with a framerate of 125 fps. As the Biot number is clearly lower than 0.4 (Patel & Chen, 2008), the droplet temperature can be assumed uniform. For the temperature measurement, 3 x 3 pixels were taken in the center of the droplet. The infrared measurements were carried out via an AMTIR-1 window (Edmund optics, United States) in the drying tunnel. A calibration curve was created to correct for the emissivity of the material and the transmissivity of the window (Appendix 3.A). For each different condition at least 5 droplets were investigated and representative movies were selected to construct the time-temperature trajectories.

The rate of temperature increase during the falling rate period was determined for the interval where the droplet temperature was in the range of 5 °C above the wet-bulb temperature and 5 °C below its final temperature. The rate of temperature increase is shown as the average value of the replicates investigated under the same conditions. Two-sample t-tests were run in Microsoft Excel (version 16.0, Microsoft Corporation, United States) to determine significant differences ($p < 0.05$) in the rate of temperature increase.

Single droplet drying modelling

The single droplet drying model used in this research was an effective diffusion drying model, and has been strongly based on the work of Siemons et al. (2022). It is a one-dimensional (1D) model where the droplet is considered to be a spherical cap. The droplet is divided into 20 numerical shells of the same volume and evaporation and heat flux is calculated per shell. An overview of the model parameters and a schematic overview of the model are depicted in Appendix 3.B. The model was implemented in Python (Python 3.6, Python Software Foundation, United States) and Spyder (Spyder 3.7, Spyder Project Contributors, United States) was used to run the model.

The effective diffusive drying model is based on mass and energy transfer theory and makes use of the following equations rewritten in a familiar form of Fick's and Fourier's law:

$$D_t c_w = \nabla \cdot D_m \nabla c_w \tag{3.1}$$

$$D_t \rho_{eff} c_{p,eff} T = \nabla \cdot \lambda_{eff} \nabla T \tag{3.2}$$

Where D_t is the time derivative in the Langrangian reference frame (s), c_w the mass concentration of water (kg/m³), D_m the mutual moisture diffusion (m²/s), ρ_{eff} the effective density (kg/m³), $c_{p,eff}$ the effective heat capacity (J/(kg·K)), T the droplet temperature (K), and λ_{eff} the effective heat conductivity (W/(m·K)). The energy and mass balances are solved in spherical coordinates with the cell-centered finite volume scheme, using central differencing, and simple Euler forward time integrations. The initial and boundary conditions applied are:

$$c_w(r, t = 0) = c_{w,0} \quad T(r, t = 0) = T_0$$

$$\partial_r c_w(r = 0) = 0 \quad \partial_r T(r = 0) = 0 \tag{3.3}$$

$$-D_m \partial_r c_w(r = R) = J_{evap}$$

$$-\lambda_{eff} \partial_r T(r = R) = h_{ext}(T - T_{air}) - \left[\Delta H_{evap,0} + (c_{p,v} - c_{p,w})(T - T_0)\right] J_{evap}$$

With r the radial coordinate (m), R the droplet radius (m), $c_{w,0}$ the initial water concentration (kg/m³), T_0 the reference temperature for the enthalpy of evaporation (273 K), T_{air} the temperature (K) of the bulk air, h_{ext} the external heat transfer coefficient (W/(m²·K)), $\Delta H_{evap,0}$ the heat of vaporization of water at 273 K (J/kg), and $c_{p,v}$ and $c_{p,w}$ the specific heat of, respectively, vapor and water (J/(kg·K)). The evaporative mass flux J_{evap} (kg/s) equals:

$$J_{evap} = f_{cap} 4\pi R^2 \beta_{ext} M_w \frac{p_0}{R_{gas} T_{avg}} \ln \left(\frac{p_0 - p_{air}}{p_0 - a_w p_{sat}(T)} \right) \tag{3.4}$$

With f_{cap} a geometric correction factor used to account for the fact that the droplet is sessile rather than spherical, β_{ext} (m/s) the external mass transfer coefficient, M_w (g/mol) the molecular weight of water, p_0 (Pa) the atmospheric pressure, p_{air} (Pa) the partial dry air pressure, a_w (-) the water activity, and $p_{sat}(T)$ the saturated water vapor pressure (Pa) at the droplet temperature T (K).

The model of Siemons et al. (2022) has been extended by incorporating conductive heat transfer q_c (W) between the droplet and the contact surface:

$$q_c = \frac{A_c(T_{surf} - T)}{\frac{L_m}{\lambda_m} + \frac{L_p}{\lambda_p} + \frac{1}{h_{tb}}} \tag{3.5}$$

Where A_c is the contact area (m²) between the droplet and the surface. T_{surf} and T are the temperature (K) of the contact surface and the droplet respectively. L_m and L_p are the thickness (m) of the membrane and the plate that the membrane is placed on, while λ_m and λ_p are the corresponding thermal conductivities (W/(m·K)). The heat transfer coefficient of the thermal boundary layer is represented by h_{tb} and is set to 1000 W/(m²·K), a typical value used for air which resulted in a good model fit.

The effective Flory-Huggins excess interaction parameter χ_{eff} (-) was corrected compared to the earlier model:

$$\chi_{eff} = \chi_0 + (\chi_{ws} - \chi_0)(1 - \varphi_w)^2 \tag{3.6}$$

With χ_0 and χ_{ws} the interaction parameters (-) of water and solute respectively, and φ_w the volume fraction of water (-).

The contact angle θ is one of the factors used to calculate the geometry of the droplet. Whereas the model of Siemons et al. (2022) considered a linear decrease of the contact angle during the constant rate period, this has been modified to align with our observation that the contact line between droplet and surface remains constant. These observations are in-line with our previous studies (Perdana et al., 2013; Siemons et al., 2020). Based on this contact line and the changing height of the droplet, the contact angle was recalculated for every iteration step:

$$\theta = cos^{-1}\left(1 - \frac{H_{drop}}{r_{cap}}\right) * \frac{180}{\pi}$$

(3.7)

With H_{drop} the height of the droplet (m) and r_{cap} the radius of the cap that is not part of the droplet (m), which is half of the contact line diameter.

Some other small adjustments were made compared to the model of Siemons et al. (2022) such as:

- The water content of the droplet is a fraction of the total droplet weight instead of the solute weight.
- The Stefan flux correction for the external evaporative mass flux was not taken into account because of the forced convection caused by the air flow.
- To calculate the diffusivity, the area of a spherical cap is used instead of that of a perfect sphere.

Results and discussion

Particle morphology development during single droplet drying

During drying of a single droplet, the droplet does not only shrink but also changes in shape. This can be seen in the time series of the morphology of the drying droplets shown in Figure 3.1. The change in shape is related to the development of a layer with a high solute concentration at the surface of the droplet, which is referred to as the 'skin'. The mechanical properties of this skin influence the drying behavior of the droplet and the morphology of the dried particle (Both, Tersteeg, et al., 2020; Sadek, Schuck, et al., 2015; Siemons et al., 2020).

From Figure 3.1 it can be seen that the DE value of maltodextrins influences both the morphology and the shrinkage. Generally, the morphology developed earlier, and shrinkage stopped earlier for lower DE values, indicating faster locking (locking point at 10.4 ± 1.8, 13.2 ± 1.2 and 14.2 ± 1.6 s for MD6, MD21 and MD38 respectively (Table 3.1). Consequently, the average moisture content of the droplet at the locking point was also higher for lower DE values (moisture content of 42.6 ± 1.1, 40.2 ± 0.4 and 35.6 ± 0.9% (w/w) for MD6, MD21 and MD38 respectively). During the constant rate period, droplets containing different solutes show a similar rate of evaporation (Figure 3.2), so an earlier locking point means that less water has evaporated before the locking point is reached.
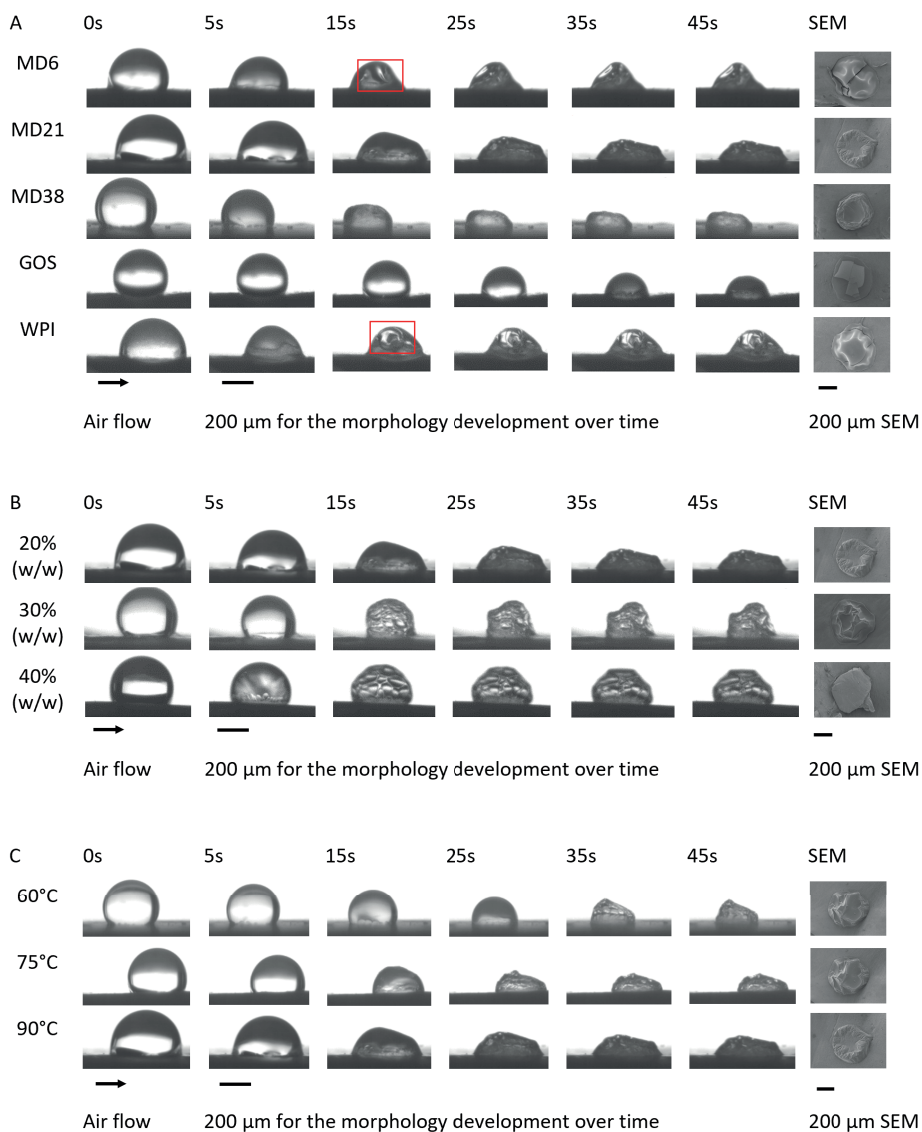
Figure 3.1. Morphology development in time for (A) 20% (w/w) solutions of different solutes dried at 90 °C, (B) MD21 solutions of different concentrations dried at 90 °C, and (C) 20% (w/w) MD21 solutions dried at different temperatures. The droplets had an initial radius of 200 ± 15 µm. The rectangles highlight the vacuoles. The droplets were dried with an air flow of 0.3 m/s coming from the left side. A SEM image of the dried particle is included.

Table 3.1. Locking point, moisture content at the locking point, and rate of temperature increase during the falling rate period (temperature between T_{wb}+5 and T_{end}-5 °C) for droplets containing an initial concentration of 20% (w/w) of different solutes, with different letters indicating a significant difference. Solutes are arranged based on their locking point. The viscosity of 20% (w/w) solutions of the solutes measured at 20 °C and a shear rate of 10–100 s^{-1} is also indicated.

Solute	Molecular weight (g/mol)	Viscosity (mPa·s)	Locking point (s)	Moisture content at locking point (% (w/w))	dT/t (°C/s)
WPI	22183[1]	7.91	8.2	47	1.09 ± 0.11[a]
MD6	3600[2]	11.37	9.8	46	1.05 ± 0.17[a]
MD21	857[2]	3.20	13.5	40	1.14 ± 0.13[a]
MD38	474[2]	3.15	15.8	35	1.42 ± 0.07[b]
GOS	504[3]	2.09	21.4	29	1.79 ± 0.22[c]

[1](Deeth & Bansal, 2019), [2](Dokic et al., 1998), [3](Warmerdam, 2013)

Also for WPI and GOS a difference in locking point and moisture content at the locking point were observed. The locking point of WPI was at 7.6 ± 0.7 s, while for GOS the locking point was observed at 19.2 ± 3.0 s. The moisture content at the locking point was 48.6 ± 2.5 and 29.2 ± 1.8% (w/w) for WPI and GOS respectively. These observations are in line with the observations of Sugiyama et al. (2006) and Siemons et al. (2020), where droplets containing solutes with a high molecular weight became non-spherical earlier in the drying process. At similar concentrations, solutes with a high molecular weight led to a higher viscosity of the solution (Table 3.1), leading to an earlier onset of skin formation and emergence of elasticity. When the elastic skin dries further, it will approach the glassy state, resulting in a very high viscosity, and the locking point will be reached (Siemons et al., 2020; Sugiyama et al., 2006). At any temperature, high molecular weight solutes have a glass transition at higher moisture content than low molecular weight solutes, so an earlier locking point is observed (Table 3.1).

The locking point of a droplet also depends on the initial solute concentration (Figure 3.1). The drying rate during the constant rate period is independent of the initial solute content (Figure 3.2), but droplets with a higher initial solid content show an earlier locking point (Both et al., 2019). Indeed, the locking points of droplets of 20, 30 and 40% (w/w) solutions of MD21 were observed at 13.2 ± 1.2, 7.8 ± 0.6 and 4.3 ± 0.7 s respectively. The respective average moisture contents at the locking points were 40.2 ± 0.4, 49.7 ± 2.1 and 59.0 ± 0.4% w/w. It is interesting to notice that an earlier locking point comes with a higher moisture content at the locking point, even when this is caused by an increase in the solute concentration. The slower diffusion of solutes within the droplet relative to the evaporation of water creates a solute gradient within the droplet. The water diffusivity in this skin is very strongly dependent on the solute concentration, and therefore this effect dominates the effect of the higher solute and thus the lower amount of water that needs to be evaporated.
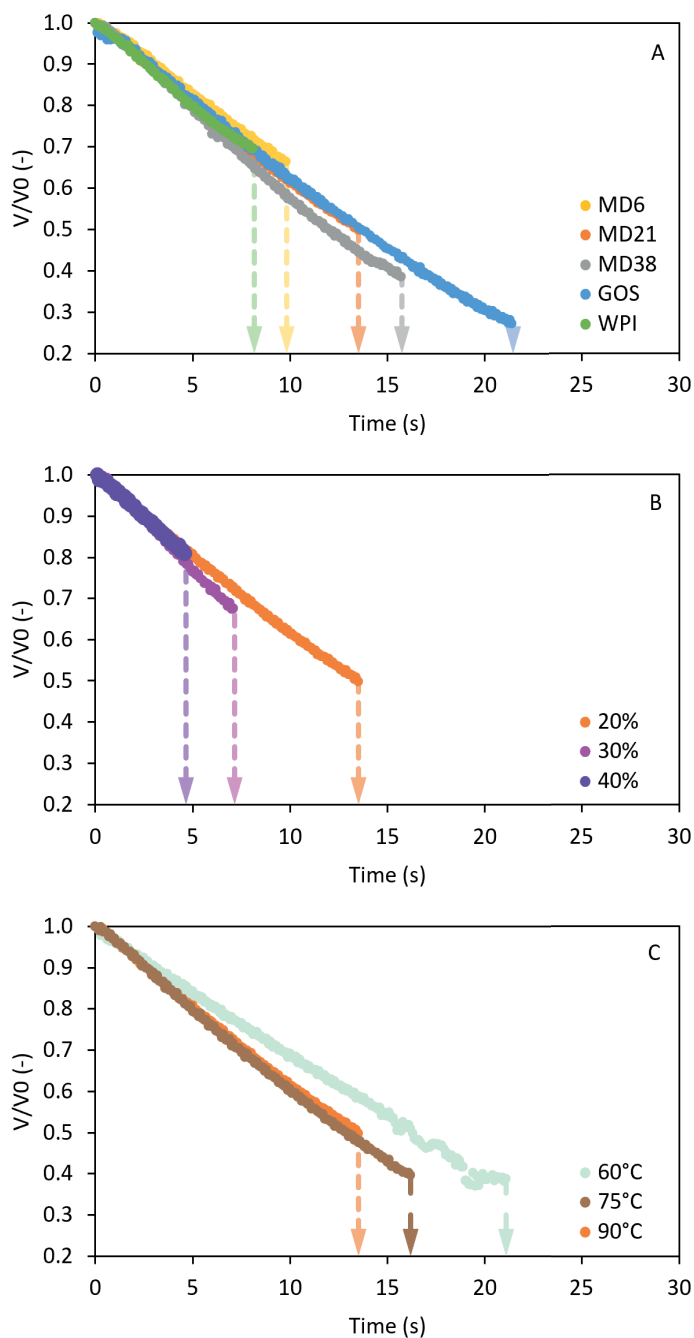
Figure 3.2. Volume decrease over time (dots) and locking point (dashed arrows) of drying droplets with an initial radius of 200 ± 15 μm as obtained via the high-speed camera observations for (A) 20% (w/w) solutions of different solutes dried at 90 °C, (B) MD21 solutions of different concentrations dried at 90 °C, and (C) 20% (w/w) MD21 solutions dried at different temperatures.

The influence of the air temperature on the drying behavior is shown for MD21 in Figure 3.1. Droplets dried at a higher air temperature dried faster and showed earlier skin formation, which is in agreement with the observations of Both, Karlina, et al. (2018) and Siemons et al. (2020). Especially the droplets dried at 90 °C showed a higher drying rate than the droplets dried at 60 or 75 °C (Figure 3.2). The locking points of droplets of a 20% (w/w) MD21 solution dried at 60, 75 and 90 °C were observed at 20.1 ± 1.1, 16.2 ± 1.4 and 13.2 ± 1.2 s respectively. The droplets dried at 60 and 75 °C show similar moisture contents at the locking point (36.9 ± 3.6 and 36.1 ± 2.4% (w/w)), while the moisture content of a droplet dried at 90 °C is a bit higher (40.2 ± 0.4% (w/w)). These observations are in the same order of magnitude as the observation of Lin & Chen (2004) and Siemons et al. (2020). They observed that the drying air temperature had only little effect on the normalized droplet radius at the locking point.

Droplet temperature

While visual camera observations provide insight into the drying rate until the locking point, the droplets become too irregularly shaped after the locking point, to enable the estimation of the droplet's volume. Droplet temperature measurements can however be used to assess the drying kinetics throughout the full drying period. High-resolution thermography was used to measure the temperature of the droplets during drying and an example of the images obtained during the measurements is shown in Figure 3.3. Figure 3.4 shows the temperature development of drying droplets containing different solutes.
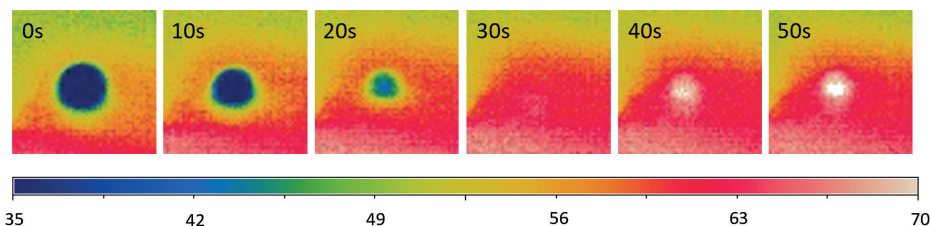

Figure 3.3. Infrared thermography images over time for a drying droplet of a 20% MD21 solution with an initial radius of 200 ± 15 μm, dried with air of 90 °C and a flow rate of 0.3 m/s. A color bar with reference temperatures for the droplet is also provided.

At the start of the drying process, during the initial heating period, the droplet temperature increases from room temperature to a constant temperature close to the wet-bulb temperature (Figure 3.4), although it may deviate somewhat due to the thermal contact between droplet and supporting plateau. The constant rate period sets in, during which the moisture content of the droplet is high and gas-phase transfer is limiting (Anandharamakrishnan & Padma Ishwarya, 2015; Boel et al., 2020). This is why this initial constant droplet temperature is independent of the nature and concentration of the solute (Figure 3.4).

While water evaporates from the surface of the droplet, the concentration of solutes at the surface increases. The increased solute concentration hinders water evaporation, which

is in line with the lower rate of volume decrease, and hence lower evaporation rate, that is observed for solute-containing droplets as compared to pure water (Figure 3.4) (Fu et al., 2013). The increase in solute concentration close to the surface eventually leads to the formation of a skin at the surface of the droplet. The diffusivity of water drops very sharply with decreasing moisture content, and the highly-concentrated skin therefore limits the transport of water to the surface. Hence, the evaporation rate drops, and temperature of the droplet increases and the falling rate period begins (Leniger & Beverloo, 1975).
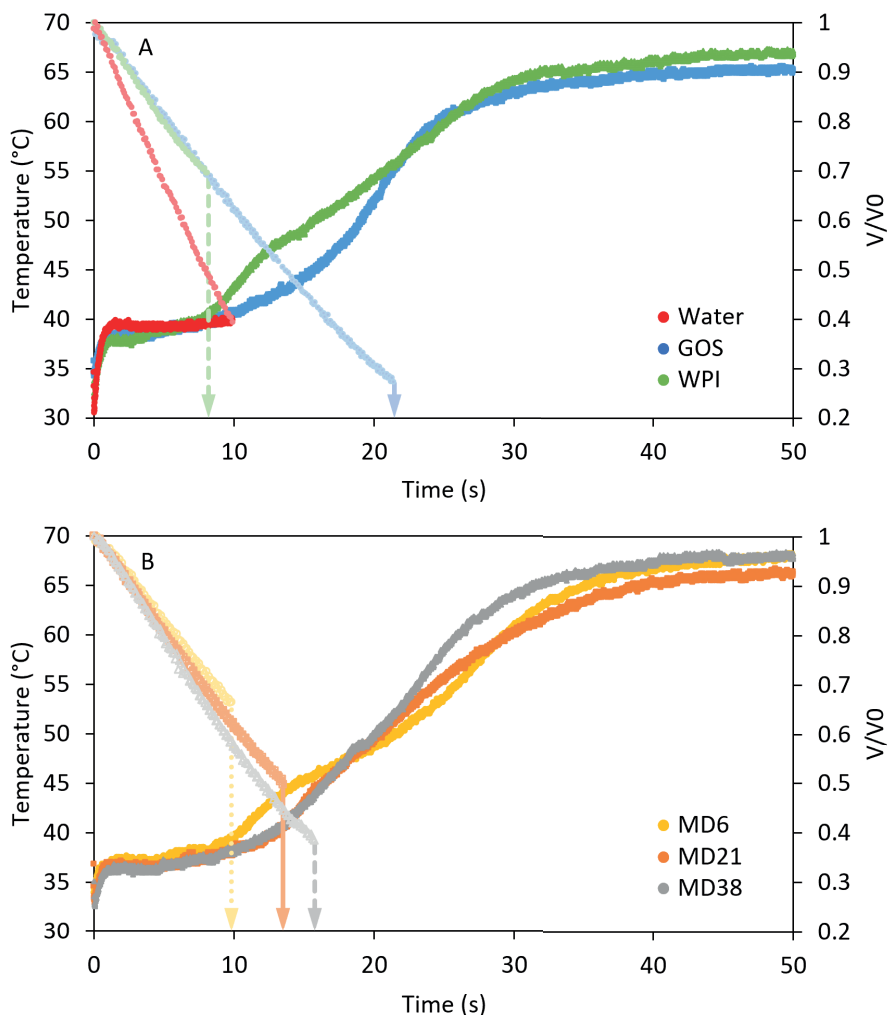

Figure 3.4. Time-temperature and time-volume curves of droplets dried at 90 °C with an air flow rate of 0.3 m/s. Temperature (bright dots), volume (pale dots) and the visually observed locking point (dashed arrows, Table 3.1) are indicated. Because droplet volume measurement is inaccurate after the locking point, measurements stop at this point.

For WPI, MD6 and MD21, the moment at which the droplet temperature starts to increase is almost identical to the visually observed locking point time (Figure 3.4). This is due to the formation of the skin at the surface of the droplet resulting in the start of morphological changes as well as the hindrance of evaporative cooling (Boel et al., 2020; Both et al., 2019). For GOS and MD38, there is no clear correlation between the end of the constant rate period and the visually observed locking point time (Figure 3.4). The GOS used in this study consist of a mixture of galacto-oligosaccharides with different degrees of polymerization (DP), with 95% of the oligosaccharides having a DP between 2 and 5. In addition, the powder contains 23% of lactose. For small compounds, such as MD38 and the lactose and low DP galacto-oligosaccharides present in GOS, the solute diffusivity is higher than for sugars with a higher DP value. This means that small compounds can better diffuse from the skin towards the bulk of the droplet, thereby not contributing as strongly to the formation of a dense skin at the surface. The onset of the morphological changes will therefore be delayed (Siemons et al., 2021).

The rate at which the temperature of the droplet increases, depends on the solute that is present and more specifically on its molecular weight (Table 3.1). The rate of temperature increase is lowest for WPI and low DE maltodextrins, higher for MD38 and the highest for GOS (Table 3.1). Because of the higher solute diffusivity, solute accumulation at the surface is slower, and hence the skin formation takes longer for low molecular weight compounds. This is in line with the later locking point of the MD38 and GOS droplets. As it takes more time before a skin is formed, more evaporation has taken place and the droplets will be smaller at the locking point. These smaller droplets have a larger surface area to volume ratio, which promotes faster heating (Mondragón et al., 2013). In addition, the droplets have a lower moisture content at their locking point, which results in a lower specific heat capacity. Consequently, the evaporation rate, and hence the level of evaporative cooling, is lower, causing a more rapid temperature increase.

The temperature increase after locking is more irregular for MD6 and WPI droplets than for MD21, MD38 and GOS droplets (Figure 3.4). While the temperature increase for MD21, MD38 and GOS is rather constant over time, MD6 and WPI show a plateau in their temperature increase. This is linked to differences in morphological development; the MD6 and WPI droplets form vacuoles while the MD21, MD38 and GOS droplets become wrinkled (Figure 3.1). Droplets that show vacuole formation have a more elastic skin, which can withstand deformation. When this elastic skin becomes rigid, further shrinkage of the droplet is prevented, but evaporation continues through the skin. This creates a local pressure minimum, and a vacuole forms inside the droplet. The vacuole results in an inward elastic stress, leading to rupture of the skin. This hole results in a sudden increase in the contact area with the environment, resulting in an increase in evaporation (Bouman et al., 2016). The enhanced evaporative cooling reduces the droplet's temperature increase, resulting in a small plateau in the droplet temperature development (Appendix 3.C). Therefore, the rate of temperature increase in this period after locking was considered to be a good indicator for the morphological development of a drying droplet.

The temperature of the drying particle increases until it reaches the temperature of its surroundings (Anandharamakrishnan & Padma Ishwarya, 2015; Boel et al., 2020). In the case of sessile SDD, this final temperature is equal to the temperature of the substrate that the dried particle is in contact with. This is in line with the experimental observations, where the particles reach a final temperature close to the substrate temperature of 67 °C when applying a hot air flow of 90 °C (Figure 3.4). The temperature of the substrate is lower than the air temperature due to heat loss via conduction.

Droplets of different initial concentrations of MD21 were dried to investigate the effects of the initial solute concentration on the temperature development of a drying droplet (Figure 3.5). For the three different MD21 concentrations investigated, the end of the constant rate period aligns well with the locking point (Figure 3.5). A locking point requires a minimum concentration of solute on the interface, to be in the region of dramatic reduction of the water diffusivity (Both, Karlina, et al., 2018; Siemons et al., 2020; Tran et al., 2016). At higher concentrations, this is reached earlier.
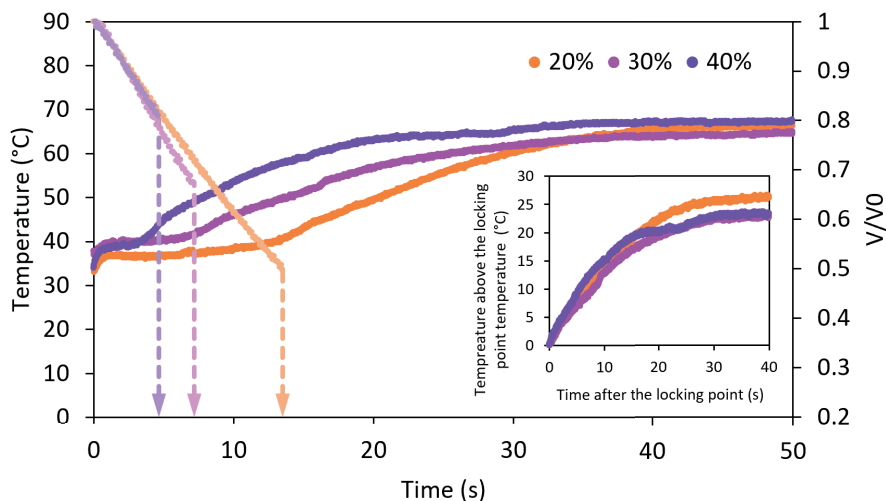

Figure 3.5. Droplets of MD21 solutions of different initial concentrations were dried at 90 °C with a flow rate of 0.3 m/s. Temperature (big bright dots), volume (small pale dots) and the locking point (dashed arrow), are indicated. Because droplet volume measurement is inaccurate after the locking point, measurements stop at this point. The insert shows the temperature increase after the locking point.

There is no significant difference in rate of temperature increase for the droplets with different initial MD21 concentrations (1.14 ± 0.13, 0.93 ± 0.13 and 1.06 ± 0.27 °C/s for the 20, 30 and 40% (w/w) solutions respectively). Gouaou et al. (2019) indicated that droplets with different initial solid contents in the decreasing flux period showed similar evaporative fluxes at a similar moisture content. Despite different initial concentrations, locking point formation starts when a specific, high concentration of MD21 is reached

at the surface of the droplet. This concentration is independent of the initial solute concentration, meaning that droplets of different initial MD21 concentrations are expected to have similar moisture contents at the surface of the droplet when skin formation starts. The mechanical properties of the skin will therefore be similar, which is also observed by the similar morphological development after the locking point (Figure 3.1). This indicates that, after the locking point, the rate of evaporative cooling is independent of the initial solute concentration, resulting in the same rate of temperature increase (Figure 3.5).

To investigate the influence of the drying air temperature on the drying kinetics of a sessile single droplet, droplets of a 20% (w/w) MD21 solution were dried at different temperatures (Figure 3.6). For the three different temperatures investigated (60, 75 and 90 °C), drying at a lower temperature results in a later locking point, which is in line with the observations of Both, Karlina, et al. (2018). At a lower air temperature, the driving force for evaporation is lower and hence the rate of evaporation is lower. As a result, the accumulation of solute in the skin is less extreme and the locking point comes later. The expected differences in the evaporation rate are, however, not large, especially at higher temperatures. Although the shrinkage of the droplet is the slowest at an air temperature of 60 °C, the shrinkage rates observed for the droplets dried at 75 °C and 90 °C are very similar. This is because the difference in heat transfer between 75 °C and 90 °C is not as large as between 60 °C and 75 °C, especially because of the limited difference of the temperature of the contact surface at these air temperatures (64 and 67 °C, respectively), which contributes to the heat supply to the droplet.
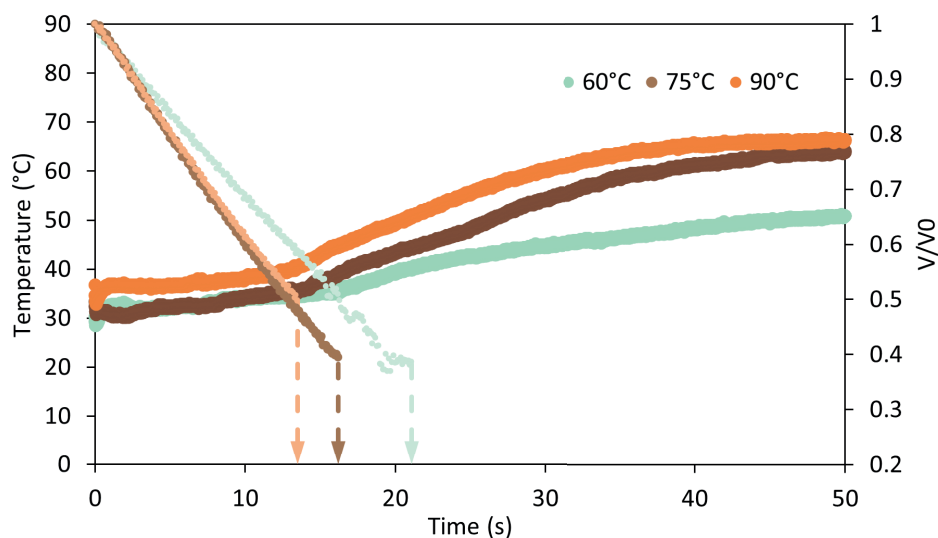

Figure 3.6. Droplets of MD21 solutions of 20% (w/w) were dried at different temperatures with a flow rate of 0.3 m/s. Temperature (big bright dots), volume (small pale dots) and the locking point (dashed arrow), are indicated. Because droplet volume measurement is inaccurate after the locking point, measurements stop at this point.

Model development

During preliminary experiments, it was found that sessile single droplets of, among others, maltodextrin solutions have a higher initial temperature than the wet-bulb temperature. This was assumed to be caused by conductive heat transfer from the surface on which the droplet was deposited. To estimate the rate of this heat transfer, the heating of a non-evaporating polyethylene glycol (PEG400) droplet and the evaporation of a water droplet without solute were studied. Next to adding a conductive heat transfer term in the model (Equation 3), the heat transfer via the air was modified to correct for the non-ideal spherical geometry of the droplet. This was done through the external mass transfer coefficient β_{ext} (m/s), which was originally based on a perfectly spherical geometry, to obtain a good description for heating of a PEG400 droplet and an evaporating water droplet (Figure 3.7). A good fit was obtained when the external mass transfer coefficient was corrected by $\beta_{ext,sessile} = 0.4 * \beta_{ext,sphere}$. The calculations then show that for the water droplet, 40% of the heat entering the droplet originates from conductive heat transfer. This relatively large contribution of the conductive heat transfer distinguishes a drying sessile single droplet from a droplet drying in a spray dryer. However, if the model that describes the drying behavior of a drying sessile droplet accurately predicts both conductive and convective heat transfer, the model results can be extrapolated to free flying droplets that rely on convective heat transfer.
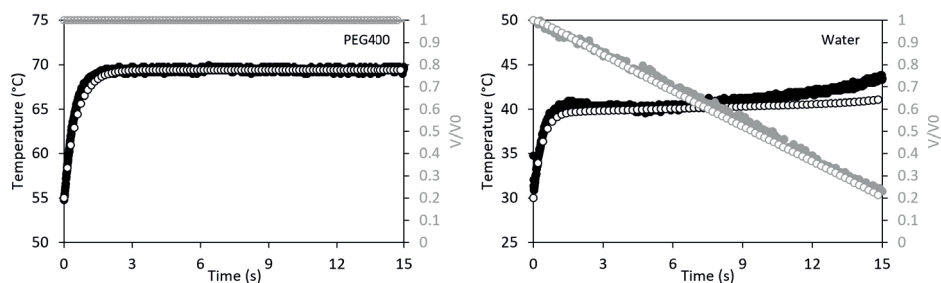

Figure 3.7. Temperature increase and volume decrease of a PEG400 and water droplet with an initial radius of 200 ± 15 μm dried at 90 °C, with the experimental droplet temperature (closed black dots), the droplet temperature as predicted by the model (open black dots), the experimental droplet volume (closed gray dots) and the model predictions regarding the droplet volume (open gray dots).

The improved sessile single droplet drying model (open symbols) was compared to the experimental measurements of the different solutions (closed symbols). The droplet temperature is shown for the full drying period, while the volume decrease of the droplet is only shown until the locking point (Figure 3.8). The reason for this is that from the locking point onwards the droplet becomes irregularly shaped (e.g., vacuole formation or wrinkling), which is not described by the one-dimensional drying model that is used. Until the locking point, the model predictions related to the volume decrease generally show a good match with the experimental results (Figure 3.8). This is especially true for the droplets of a 40% MD21 solution and a 20% GOS solution, which show smooth particles

with limited dents. Larger deviations in volume prediction, with lower predicted volume decrease compared to the experimental values, are observed for the droplets of a 20% DE6 and a 20% WPI solution (Figure 3.8), which are the droplets showing vacuole formation (Figure 3.8). It is unclear what causes these larger deviations, but it might be related to the earlier formation of a thin skin, hindering evaporation slightly but still allowing isotropic shrinkage.

The model adequately predicts the initial droplet temperature during the constant rate period, the duration of this period, as well as the final droplet temperature. During the time that the droplet temperature increases from the initial constant temperature to the final temperature, there are some deviations between the model predictions and the experimental results, with the model predicting a higher temperature than observed experimentally, which is related to the development of an irregular morphology. As was observed in Table 3.1, Figure 3.4 and Appendix 3.C, the rate of temperature increase depends on the morphological changes that occur during the drying process. The difference between the model and measurements can thus be considered as a fingerprint for morphology development: the difference between model and experiment is larger if the morphology is less spherical or contains a vacuole. The direct prediction of the irregularities would require a multidimensional model which was out of the scope of this study.

Conclusions

Single droplet drying studies are key to obtain insights into the impact of drying conditions on the drying kinetics of a droplet. While visual camera observations have been used to gain insights into the drying kinetics of drying sessile single droplets until the locking point, they failed until now to obtain relevant information further in the drying process (Siemons et al., 2020). High-resolution thermography is used within this research to obtain more relevant information during the entire drying process.

Droplets of 20% (w/w) solutions of MD6, MD21 and MD38, GOS and WPI were dried at 90 °C. For MD21 the influence of initial solute content was further investigated by drying droplets with an initial concentration of 30 and 40% (w/w). The impact of drying air temperature was examined by drying droplets of a 20% (w/w) MD21 solution at 60 and 75 °C. Both visual camera observations, as well as IR measurements, showed that the drying kinetics during the constant rate period depends on the drying air temperature, but not on the composition of the droplet. The duration of the constant rate period was found to be compound-specific and related to the morphological locking point of the droplet. The high concentration of solute at the surface leads to development of a skin, which is responsible for morphological changes as well as for the hindering evaporation, thereby inhibiting the droplet from staying at the wet-bulb temperature.

Although the IR measurements cannot be directly used to determine the particle morphology, the time-temperature results can serve as an indirect measure for
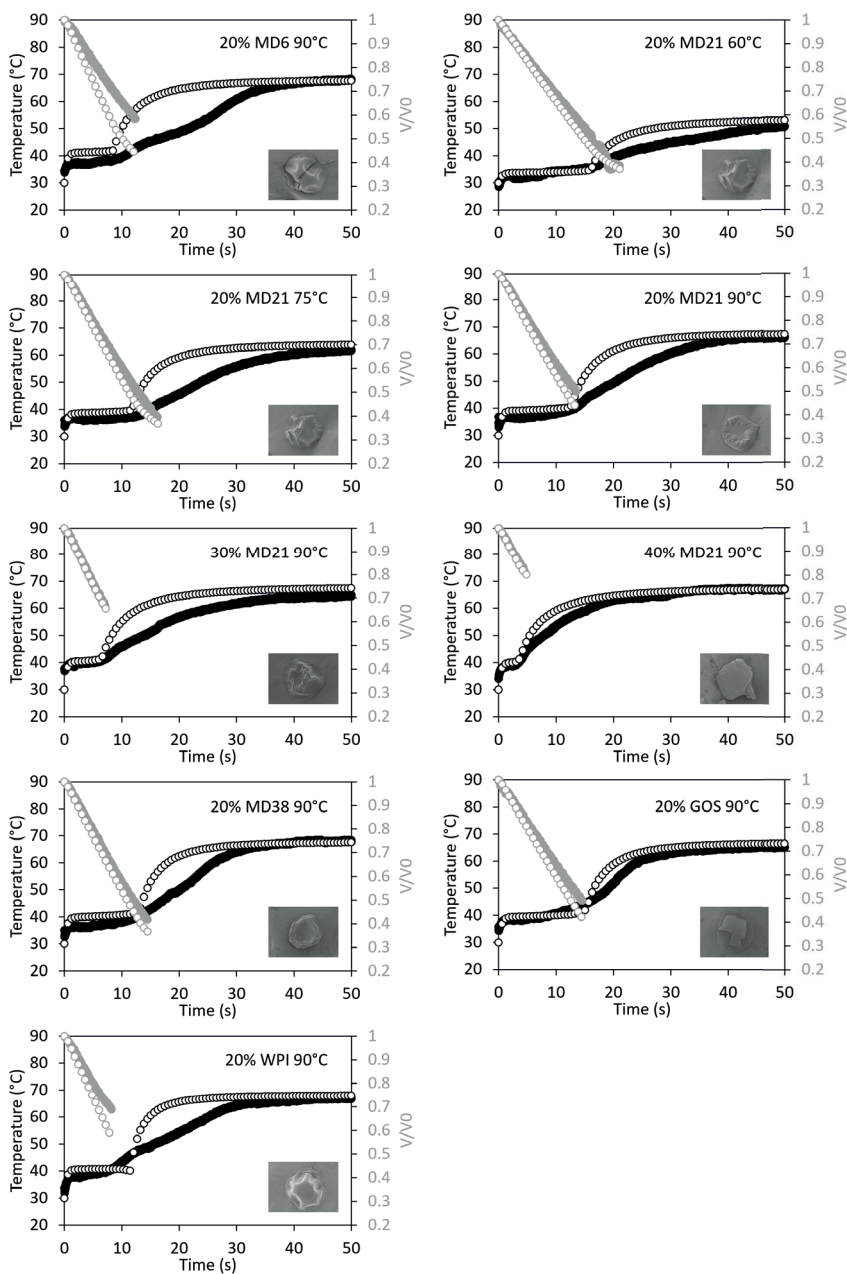
Figure 3.8. Temperature increase, volume decrease and final particle morphology of droplets of different solutions with an initial radius of 200 ± 15 μm dried at different air temperatures at a flow of 0.3 m/s. The graphs show the experimental droplet temperature as determined with the IR camera (closed black dots), the droplet temperature as predicted by the model (open black dots), the experimental droplet volume as determined with the visual camera observations (closed gray dots) and the model predictions regarding the droplet volume (open gray dots).

morphological development of the droplet. Droplets that form a vacuole during drying show a more irregular temperature increase, with a plateau of the droplet's temperature when the vacuole is formed. The formation of a vacuole can also be observed with the sessile single droplet drying model. Assuming morphological changes to be the main cause for the deviations between the predicted and experimentally observed droplet volume, these deviations can be considered a fingerprint for morphology development. A further understanding of these deviations could lead to insights into the drying behavior of a droplet. The combination of high-resolution thermography and an effective-diffusion-based model could thus provide valuable information to predict droplet surface properties during the entire drying process, not just until the locking point. This is an important step to steer spray drying processes to obtain powders with desired surface properties. Because of the profound impact of surface properties on stickiness and thus indirectly on agglomeration, this will help to control agglomeration and to prevent fouling in a spray dryer.
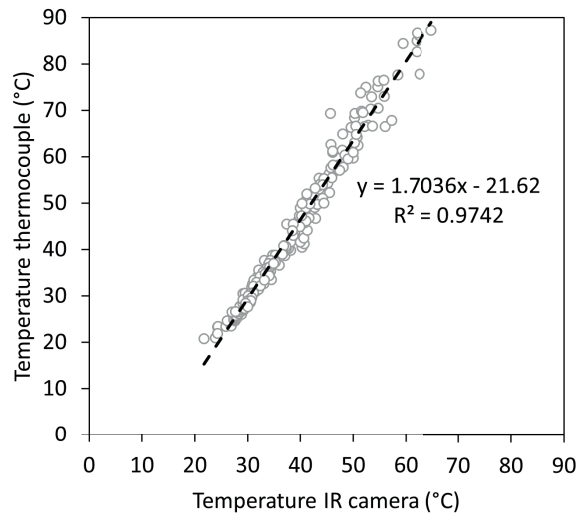
Appendix 3.A

Figure 3.A.1. Calibration curve as used for the infrared temperature measurements, with the dots showing the experimental measurement points and the dashed line the calibration curve. Measurements were performed with a larger volume of water or 40% MD21 solution.

Appendix 3.B

Table 3.B.1. Nomenclature as used in this chapter.

Abbreviations

DE	Dextrose equivalence
GOS	Galacto-oligosaccharides
IR	Infrared
MDX	Maltodextrin with dextrose equivalence X
SDD	Single droplet drying
WPI	Whey protein isolate

Symbols

|	
A_c	Contact area between droplet and surface (m²)
a_w	Water activity (-)
$c_{p,eff}$	Effective heat capacity (J/(kg·K))
$c_{p,v}$	Specific heat of vapor (J/(kg·K))
$c_{p,w}$	Specific heat of water (J/(kg·K))
C_w	Mass concentration of water (kg/m³)
$C_{w,0}$	Initial water concentration (kg/m³)
D_m	Mutual moisture diffusion (m²/s)
D_t	Time derivative in the Langrangian reference frame (s)
f_{cap}	Geometric correction factor (-)
H_{drop}	Height of the droplet (m)
h_{ext}	External heat transfer coefficient (W/(m²·K))
h_{tb}	Heat transfer coefficient thermal boundary layer (W/(m²·K))
J_{evap}	Evaporative mass flux (kg/s)
L_m	Thickness of the membrane (m)
L_p	Thickness of the plate (m)
M_w	Molecular weight of water (g/mol)
p_0	Atmospheric pressure (Pa)
p_{air}	Partial dry air pressure (Pa)
$p_{sat}(T)$	Saturated water vapor pressure at the droplet temperature T (Pa)
q_c	Conductive heat transfer (W)
R	Droplet radius (m)
r	Radial coordinate (m)
r_{cap}	Radius of the cap that is not part of the droplet (m)
T	Droplet temperature (K)
T_0	Reference temperature for the enthalpy of evaporation (273 K)
T_{air}	Temperature of the bulk air (K)
T_{surf}	Temperature of the contact surface (K)
β_{ext}	External mass transfer coefficient (m/s)
$\Delta H_{evap,0}$	Heat of vaporization of water at 273 K (J/kg)
θ	Contact angle (°)
λ_{eff}	Effective heat conductivity (W/(m·K))
λ_m	Thermal conductivity of the membrane (W/(m·K))
λ_p	Thermal conductivity of the plate (W/(m·K))
ρ_{eff}	Effective density (kg/m³)
φ_w	Volume fraction of water (-)
χ_0	Interaction parameter of water (-)
χ_{eff}	Effective Flory-Huggins excess interaction parameter (-)
χ_{ws}	Interaction parameter of solute (-)
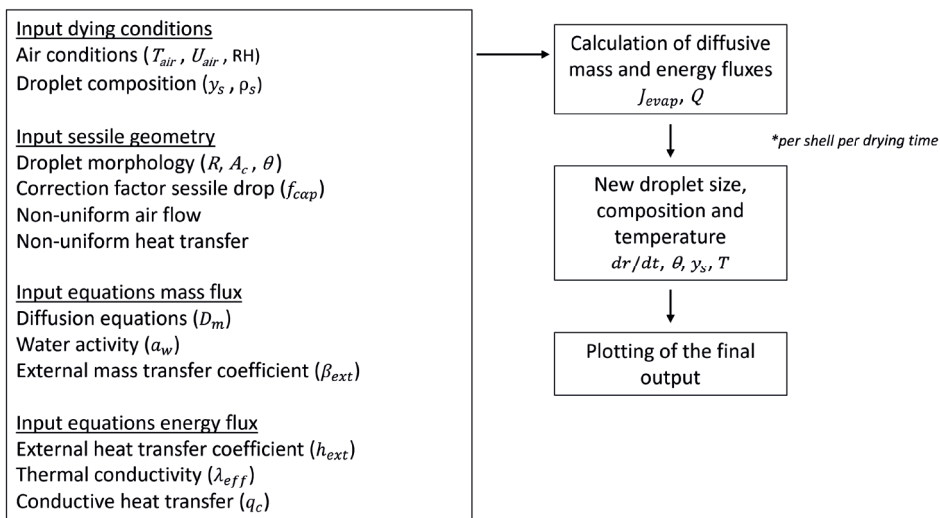
Figure 3.B.1. Schematic diagram of the sessile single droplet drying model, adapted from Siemons et al. (2021).

Appendix 3.C

Scan the QR code to see the video on morphology, volume and temperature development over time of droplets dried at 90 °C with an air flow rate of 0.3 m/s for different 20% (w/w) solutions.
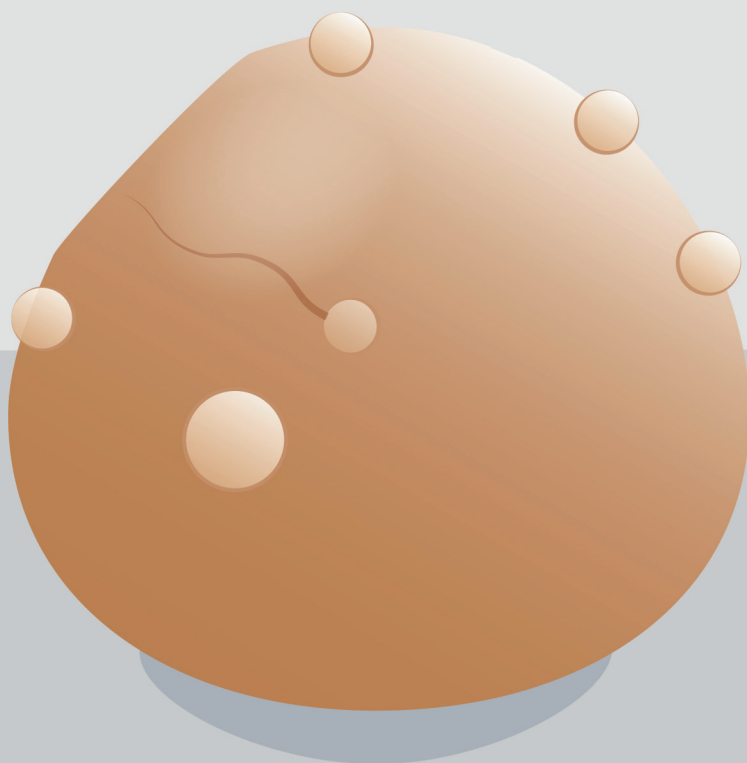
Chapter **4**

Single droplet drying with stepwise changing temperature-time trajectories: influence on heat sensitive constituents

N.M. Eijkelboom
K. Gawronska
J.M. Vollenbroek
G.J.C. Kraaijveld
R.M. Boom
P.F.C. Wilms
M.A.I. Schutyser

Abstract

Optimization procedures for industrial spray drying processes mainly rely on empirical understanding. Mechanistic understanding of the process is limited, but can be enhanced by studying the drying of single droplets. We here report on a new sessile single droplet drying platform, using two air streams to represent the inlet and outlet air of a spray dryer to simulate changing conditions in a spray dryer. Accurate temperature measurements confirmed the temperature profiles and their imposition onto a drying droplet. Single droplets of solutions containing β-galactosidase and maltodextrin were dried with different temperature-time trajectories, with the inactivation of the enzyme as indicator for the thermal load on the droplet. The locking point is found to be an important parameter: the air temperature before this point does not influence the enzyme inactivation much, but a high air temperature after the locking point results in significant inactivation. The β-galactosidase inactivation was also successfully predicted with a coupled drying and inactivation model.

Introduction

Spray drying is commonly applied in industry, for example for the downstream processing of bioactive ingredients, and for preservation and structuring of food ingredients (Huang et al., 2017; Peighambardoust et al., 2011). Due to the fine atomization of the liquid feed and the resulting fast evaporation of water, the conditions during spray drying are relatively mild. However, thermal degradation of bioactive ingredients cannot be completely avoided. In industrial practice, empirical procedures are used to obtain the optimal drying conditions for good quality powders with a desired retention of bioactivity. These empirical procedures require considerable amounts of materials and energy, especially when executed on large scale. It would thus be preferred to use an experimental assessment that accurately mimics the spray drying process at a smaller scale to more systematically perform the optimization. During drying of a single droplet, the external properties which are related to the drying of the droplet, such as the drying air conditions, can be controlled. This allows us to accurately and reliably investigate the influence of these properties on the drying behavior of a droplet and the characteristics of the powder particle obtained, like the activity of bioactive ingredients (Perdana et al., 2013; Schutyser et al., 2012, 2018).

Different approaches to single droplet drying exist, each having their own benefits and limitations (Eijkelboom, van Boven, et al., 2023). A limitation of all current approaches is that they use a constant drying air temperature. During industrial spray drying, the air entering the spray dryer is much warmer (e.g. 220 °C) than the air leaving the spray dryer (e.g. 80 °C). The droplet is therefore subject to a time-temperature trajectory, being in contact with the inlet air for just a few seconds before the air temperature rapidly decreases (Anandharamakrishnan & Ishwarya, 2015). The drying kinetics influence the droplet's morphology, with lower drying temperature resulting in smooth, but hollow particles, whereas particles dried at higher temperatures tend to acquire a wrinkled surface (Both, Karlina, et al., 2018). Porosity is also influenced by the drying kinetics, with faster drying resulting in more porosity (Janocha & Tsotsas, 2022). Second, in a system with multiple solutes, phase separation of the solutes may result, and droplets dried at a lower temperature may show more phase separation (Both, Karlina, et al., 2018). Third, the drying kinetics influence the inactivation of heat sensitive components: for example, enzyme activity after drying decreases with increasing drying air temperature (Perdana et al., 2013; Yamamoto & Sano, 1992). All these effects can be seen with spray drying, although the effect of the outlet temperature on the inactivation of heat sensitive components is known to be more pronounced than the effect of the inlet temperature (Ruprecht et al., 2023). It is not known what the role is of the intermediate temperature trajectory between entrance and exit of the droplet, and therefore it is relevant to investigate this further.

To better understand the impact of a stepwise changing drying air temperature on droplet drying, we here introduce a new sessile single droplet dryer which allows the use of a controlled temperature–time (T, t) trajectory. With this dryer, we investigate the impact of the temperature-time trajectories on the drying behavior of single droplets. This includes

the change in droplet volume, the development of the temperature of the droplet, and the degree of inactivation of the bioactive compound β-galactosidase. The data are interpreted with a sessile single droplet drying model which was presented in earlier work, which here is optimized to accurately predict the drying behavior of droplets dried with the new platform, and is extended to predict the β-galactosidase inactivation.

Materials and methods

Sample preparation

Buffer solution was prepared by mixing 0.2 M Na_2HPO_4 (Sigma-Aldrich, Germany) and 0.1 M citric acid (Sigma-Aldrich, Germany) solutions in a 3:2 ratio. The pH of the buffer was adjusted to 6.00 ± 0.01. Enzyme solutions with a concentration of 10% (w/w) were prepared by dissolving β-galactosidase from Aspergillus oryzae (Sigma-Aldrich, Germany) in the buffer solution. Maltodextrin solutions with a concentration of 25 or 50% (w/w) were prepared by dispersing maltodextrin with a dextrose equivalence (DE) of 21 (Roquette Frères, Lestrem, France) in the buffer solution. The β-galactosidase and maltodextrin solutions were mixed at a 1:4 ratio to obtain solutions with a β-galactosidase concentration of 2% (w/w) and a maltodextrin concentration of 20 or 40% (w/w).

Sessile single droplet drying with temperature trajectories

The sessile single droplet drying (SDD) platform is shown in Figure 4.1 (Technical Development Studio, Wageningen, the Netherlands). Before a droplet was dried, the drying tunnel was preheated for 60 s using air of the same temperature that the drying air will have (200, 220 or 250 °C). Next, the air flow was stopped to allow the drying table to cool to 80 °C. At this moment, a single droplet (initial radius of 200 ± 15 μm) was dispensed using a PipeJet® NanoDispenser (BioFluidix, Germany) using 500-S, coated PipeJet® Pipes (BioFluidix, Germany). A stroboscope (BioFluidix, Germany) which was connected to BioFluidix Controle Software V2.9 (BioFluidix, Germany) was used to control the droplet volume. The droplet was dispensed on a piece of PTFE coated glass fabric (PTFE glass fabric 0.18 AD, self-adhesive, High-tech-flon, Germany). The contact angle of water on this fabric is lower compared to pure Teflon or the Tetratex® ePTFE Polytetrafluoroethylene 3104 membrane which was used in previous single droplet drying research (Eijkelboom, Swinkels, et al., 2023). However, the ability of the material to handle high temperatures and the self-adhesiveness of the material is critical for the high temperature SDD drying experiments in this study and allows handling of the dried particles afterwards. Once the droplet was dispensed, an automated shutter covered the small opening at the top of the drying tunnel, preventing the loss of hot air during drying.

The droplet was dried with dry air (absolute moisture content of 3.5 g/kg) of which the temperature and flow rate were controlled by a mass flow controller (EL-FLOW® Select F-201 CV, Bronkhorst, the Netherlands). The air stream representing the inlet air was set to 200, 220 or 250 °C at a flow rate of 20 L/min (0.8 m/s), while the stream representing the outlet air had a temperature of 70, 80 or 90 °C and a flow rate of 10 L/min (0.4 m/s). During

drying, the position of the heating blocks can change within 1 s, thereby changing the air stream that is supplied to the droplet. This change results in a temperature trajectory. The temperatures of the drying table and of the air in the drying tunnel (6 mm above the drying table) were measured with thermocouples (IEC fine gauge exposed welded tip thermocouple type K with 0.076 mm Teflon® PFA insulated conductors) throughout the drying process. Heat conduction interferences of the thermocouples are assumed to be negligible, as the length to diameter ratio of the thermocouple is significantly larger than 200 (Heitor & Moreira, 1993). The different temperature trajectories used to dry the droplets are indicated in Figure 4.2. As the dried droplets had an initial size near the upper limit of the droplet size range in industrial spray dryers (Patel & Chen, 2008), the applied drying time was kept to 30 s to ensure complete drying. This drying time is at the higher end of the range of particle residence times in spray driers (Ruprecht et al., 2021; Schmitz-Schug et al., 2013). During drying, the droplet was filmed with either a high-speed camera (C-VIT, AOS Technologies AG, Switzerland) to observe morphological changes or with an infrared camera (PI 640 Microscope optics, Optris, Germany) to measure the droplet temperature. The video recording procedures were described in more detail in our previous work (Eijkelboom, Swinkels, et al., 2023). The experiments were performed in triplicate and representative results are shown.
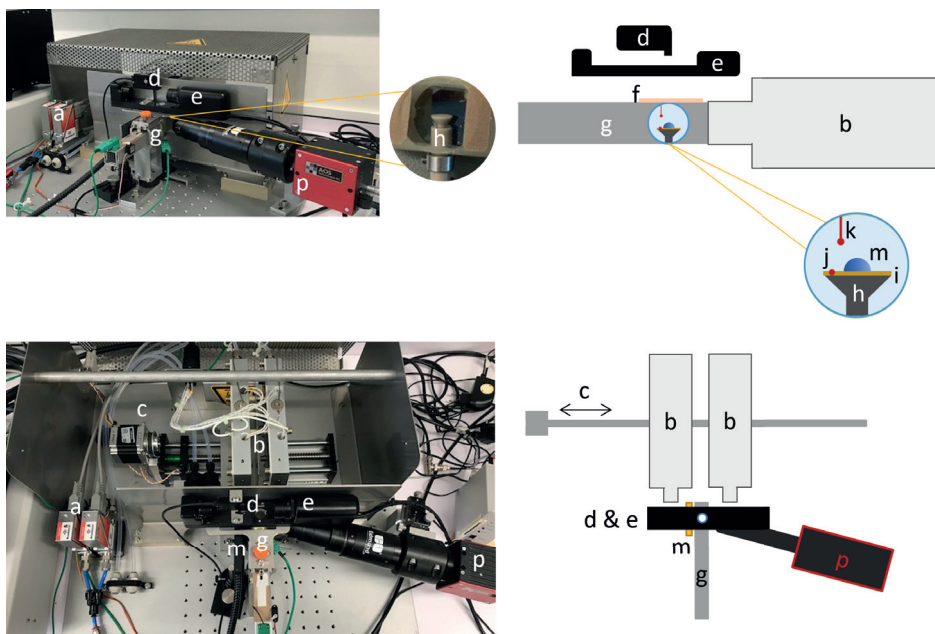

Figure 4.1. New sessile single droplet drying platform with mass-flow controllers (a), heating blocks (b), moving rail (c), droplet dispenser (d), stroboscope (e), automated shutter (f), drying tunnel (g), drying table (h), hydrophobic tape (i), thermocouple to measure contact surface temperature (j), thermocouple to measure air temperature near the droplet (k), droplet (m), backlight (n) and camera (p).
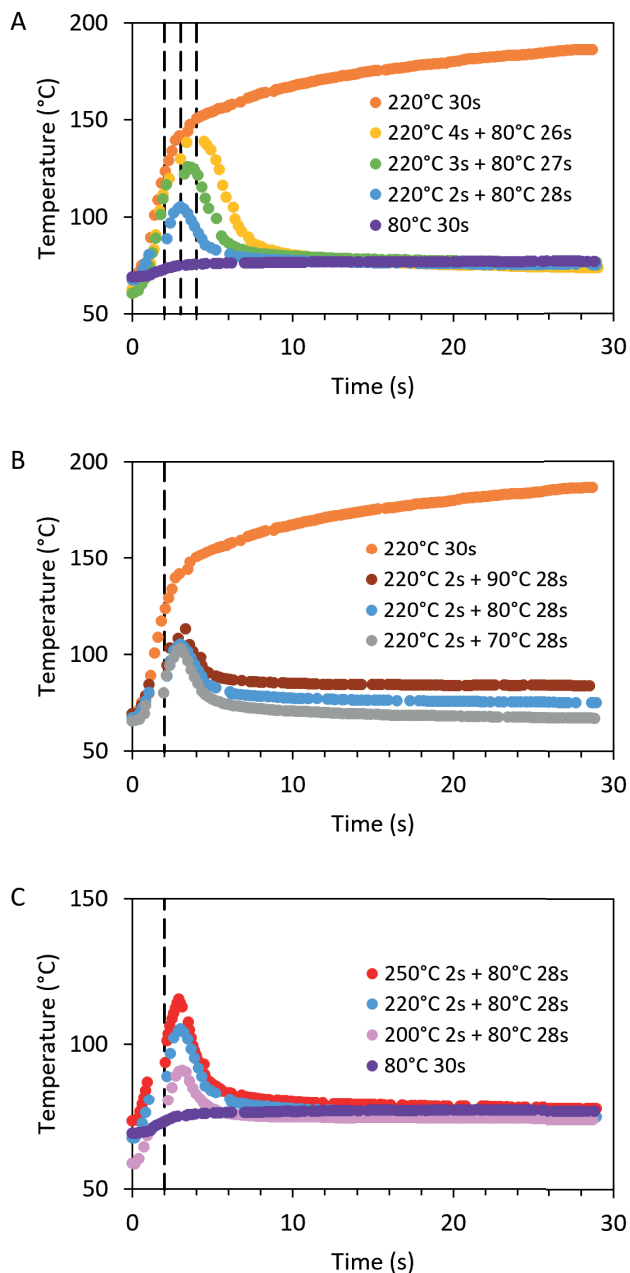
Figure 4.2. Experimental temperature of the drying air near the droplet (k in Figure 4.1) for different drying trajectories. Drying trajectories with a different drying time at in- and outlet temperature (A), different outlet temperatures (B), and different inlet temperatures (C) were measured. The annotations in the legend indicate the combination of air temperature and drying time at this temperature. The vertical dashed lines indicate the timepoints of a change in airflow. Note that the scale on the y-axis differs per plot.

β-galactosidase activity

After drying, the PFTE tape with the dried droplet was carefully removed from the drying table and put into a 2 mL Eppendorf tube for further analysis. The activity of β-galactosidase in the dried droplets was determined with an O-nitro-phenyl-β-D-galactopyranoside (ONPG) assay (Sigma–Aldrich, United States) as described by Perdana et al. (2012). After incubation and enzyme inactivation, the absorbance of the sample was measured at 420 nm using a spectrophotometer (DR6000, HACH, United States). For each drying trajectory, the β-galactosidase activity was measured for at least five individual single droplets. For the β-galactosidase inactivation, the activity in the dried droplet was compared to the activity in a non-dried droplet.

Single droplet drying model

A numerical SDD model was used in this study to interpret the results. The model is based on the SDD model that is described in more detail in our earlier work (Eijkelboom, Swinkels, et al., 2023; Siemons et al., 2022). Some changes have been made, however. The number of numerical shells was increased from 20 to 40, increasing the accuracy, especially at higher drying rates. The other change is related to the external mass transfer coefficient. For validation purposes and for determining heat transfer parameters, a non-evaporating polyethylene glycol (PEG400) droplet and a pure water droplet without solute were employed. As these droplets of single components will not develop an internal concentration gradient upon drying, internal diffusion was not taken into account in this case. Although it is known that the evaporation along the surface of a sessile droplet is non-uniform (Janocha & Tsotsas, 2021), for simplicity reasons the model considered the droplet to be a homogeneous, uniformly drying droplet. The validation showed us that the external mass transfer coefficient for a sessile droplet was lower than that of a free falling sphere: $\beta_{ext,sessile} = 0.03 * \beta_{ext,sphere}$ (Figure 4.3).
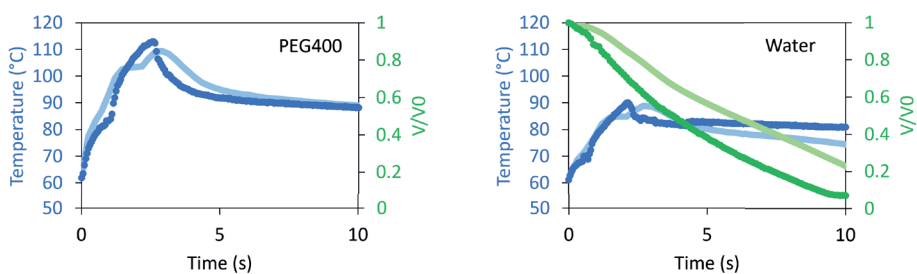

Figure 4.3. Temperature (blue) and volume (green) development of a PEG400 and water droplet dried with a temperature–time trajectory as generated by drying with a 20 L/min, 220 °C airstream for 2 s, followed by a 10 L/min, 80 °C airstream. The experimental values are represented by the dark colors, and the model predictions by the light colors.

Instead of using a fixed temperature profile and air speed, the experimentally measured contact surface temperatures, drying air temperatures, and air speed were used as input into the model. The model was then extended to predict the inactivation of β-galactosidase as function of temperature and moisture content. We made use here of the β-galactosidase inactivation kinetics reported by Zhang et al. (2017). To take the impact of the non-uniform solute distribution into account, the droplet was divided into 40 numerical shells of equal volume. The thickness of the shells changed over time, as the droplet shrinks during the course of drying due to the evaporation of water. For every timestep in the model, the inactivation constant k and, based on that, the inactivation of β-galactosidase was calculated per shell. The accumulated β-galactosidase activity of all shells was used to calculate the inactivation of the whole droplet. The model was implemented in Python (Python 3.11, Python Software Foundation, United States) and included the numpy, matplotlib and openpyxl packages. Spyder (Spyder 5.4.2, Spyder Project Contributors, United States) was used to run the model.

Results and discussion

Drying behavior of single droplets
Drying droplets with 40% maltodextrin of DE 21 (MD21) using different temperature-time trajectories yielded a locking point after 1.3 s of drying. During this initial part of drying, the temperature of the air close to the droplet was similar for all experiments, resulting in similar evaporation rates (Figure 4.2, Appendix 4 Figure 4.A.1). Due to the rather high initial solute content, not much evaporation was needed until skin formation started, therefore showing this early locking point for all drying conditions.

The droplets dried with different temperature trajectories showed similar morphological development, except for the droplets continuously dried at 220 °C (Figure 4.3). After an initial decrease in the droplet volume due to drying, these droplets then inflated. This can be explained by initial drying and subsequent skin formation hindering water evaporation, after which vapor accumulates inside the droplet. The pressure increase inside the droplet eventually leads inflation of the particle (Figure 4.4) (Bouman et al., 2016). The other droplets showed ideal shrinkage till the locking point. Since the locking point is at the same time for all droplets, the observed initial volume reduction is similar as well. After the locking point, the droplet shrinkage was limited due to the skin formed around the droplet. The droplet volume remains rather constant after the locking point, as long as the skin can withstand lower internal pressure due to the diffusion and evaporation of the moisture (leading to a cavity) or a higher internal pressure due to the temperature getting above the boiling point (Eijkelboom, Swinkels, et al., 2023; Siemons et al., 2020). However, a similar volume change after the locking point does not necessarily mean that the evaporation rates of the droplets are similar. Evaporation is still expected to be faster at high temperatures, so a higher drying temperature after the locking point is still likely to result in a faster decrease in droplet mass (Tran et al., 2016). A lower outlet air temperature resulted in a larger final particle volume (Appendix 4 Figure 4.A.1B). Such a

lower air temperature is expected to result in slower evaporation, resulting in less volume reduction within the observed 30 s.
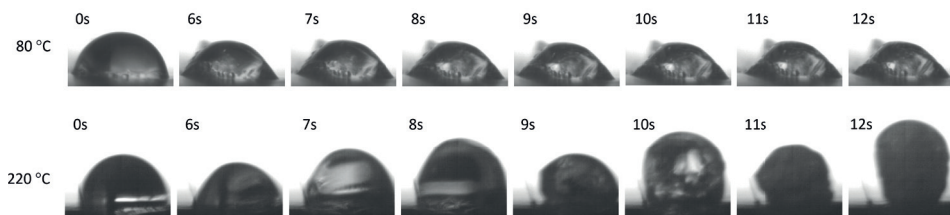

Figure 4.4. Morphological development of a single droplet of a 40 % MD21 + 2 % β-galactosidase solution drying at 80 °C or 220 °C.

As to be expected, variation of the two drying periods (representative of the higher inlet and lower outlet temperatures in a spray dryer) results in differences in the droplet temperature (Figure 4.5). Droplets that are subjected to hot inlet air for a longer time show a higher maximum in the droplet temperature. The temperature of droplets that are subjected to air of 220 °C for 30 s even rises to values considerably above the boiling point. When this happened, the droplet inflates most probably due to steam formation (Appendix 4 Figure 4.A.1). For droplets that are subjected to two different consecutive air temperatures, the droplet temperature increases roughly until the moment that the air stream is switched to the lower temperature (representative of the outlet air temperature of a spray dryer). Switching to this colder air stream is not instantaneous and takes roughly 1 s, which results in some delay before the reduction in air and droplet temperatures is observed. Besides, the heated air in the drying tunnel needs some time to fully converge to the set lower temperature (Figure 4.2), giving more delay in the reduction of droplet temperature. The droplet then converges to a temperature close to that of the air stream. This is in line with previous research, in which final droplet temperatures were also close to the temperature of the applied air stream (Eijkelboom, Swinkels, et al., 2023; Hülsmann et al., 2021). It represents the falling rate regime, in which not heat transfer, but the diffusion of the moisture through the skin is limiting. However, this convergence is relatively slow, and differences in final droplet temperature could still be observed. With the final droplet temperature only slowly converging to the air temperature, a higher outlet air temperature resulted in a higher final droplet temperature (Figure 4.5B).

Differences in the inlet air temperature had no substantial impact on the final droplet temperature (Figure 4.5C). The droplet temperature is initially limited by the wet bulb temperature (Boel et al., 2020), which for the inlet air streams of 200, 220 and 250 °C is respectively 46.3, 48.3 and 51.1 °C. These values are comparable and therefore result in similar droplet temperatures. We note, however, that the observed droplet temperatures are higher than the wet bulb temperatures, which is caused by heat transfer from the contact surface to the droplet. Nonetheless, initial droplet temperature differences were limited.
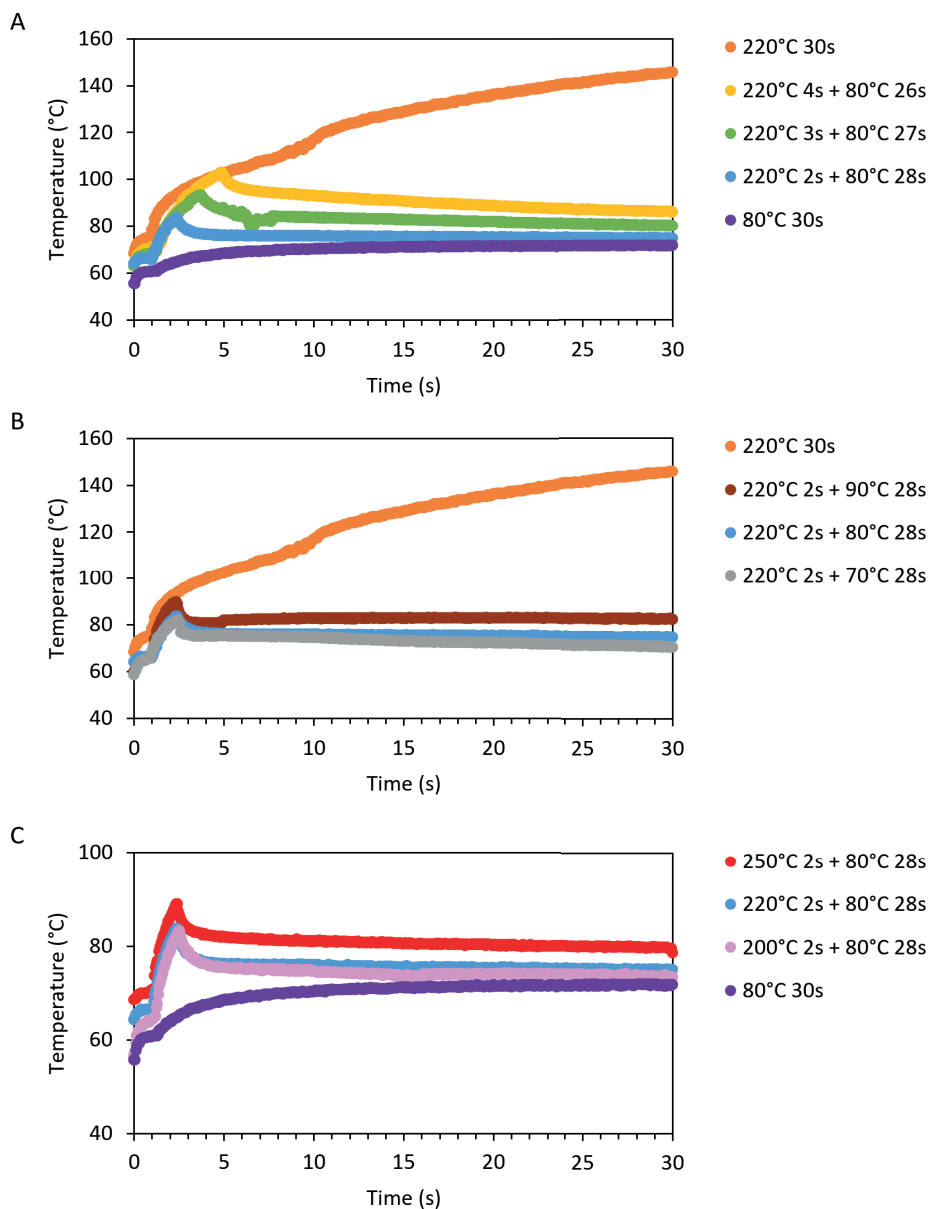
Figure 4.5. Experimental temperature development of drying droplets of 40% MD21 and 2% β-galactosidase dried under different trajectories. Drying trajectories with a different drying time at in- and outlet temperature (A), different outlet temperatures (B), and different inlet temperatures (C) were applied. The annotations in the legend indicate the combination of air temperature and drying time at this temperature. Note that the scale on the y-axis differs per plot.

β-galactosidase inactivation

The different temperature trajectories during the drying of the droplets also impacts the thermal load on the constituents, which we assess by following the level of inactivation of the enzyme β-galactosidase. Both dehydration and heating co-determine the inactivation during drying. During drying, the moisture content of the droplet decreases, which reduces the inactivation rate. Simultaneously, the droplet temperature increases, which increases the inactivation rate (Perdana et al., 2012). The impact of the specific drying trajectories on the inactivation of β-galactosidase in dried droplets found experimentally with our SDD system is shown in Figure 4.6 (fully filled bars). The modeling results shown in Figure 4.6 will be addressed in the next section.

Drying at the higher inlet air temperatures for extended times resulted in a higher enzyme inactivation of the dried particle (Figure 4.6A). Before the droplets reach their locking point, their temperature is around the wet bulb temperature, which is low enough to prevent strong inactivation of β galactosidase. After passing the locking point, the evaporative cooling declines quickly due to diffusion limitation through the skin, and the droplet heats up, leading to inactivation. Our hypothesis is that less enzymatic inactivation is obtained if the drying air is switched to the outlet temperature before the locking point is reached. Unfortunately, the fast locking in the current experiments prevented us from evaluating this here. However, one can observe that with shorter times at the high temperature, the inactivation is less. In addition, the enzyme inactivation of the droplets is less when dried with lower air temperatures after the locking point. A lower air temperature during this falling rate period, results in a lower droplet temperature during this stage and in less enzyme inactivation (Figure 4.6B). This is in line with previous spray drying research, where lower outlet temperatures resulted in less inactivation of bioactive compounds (Kim & Bhowmik, 1990; Ruprecht et al., 2023; Schaefer & Lee, 2015).

Differences in enzymatic inactivation for the temperature-time trajectories with different inlet temperatures were limited (Figure 4.6C). These droplets hardly showed any differences in droplet volume reduction and droplet temperature increase during drying (Figure 4.5C, Appendix 4 Figure 4.A.1C). This can be understood from the fact that the wet bulb temperatures are much lower than the high dry bulb temperatures in the initial stage. As inactivation of β-galactosidase depends on moisture content and temperature, no big differences in inactivation were expected. These results are in line with other research which stated that the impact of the inlet temperature on the inactivation of bioactive compounds was much less pronounced than the effect of outlet air temperature (Huang et al., 2017; Poozesh & Bilgili, 2019; Ruprecht et al., 2023).
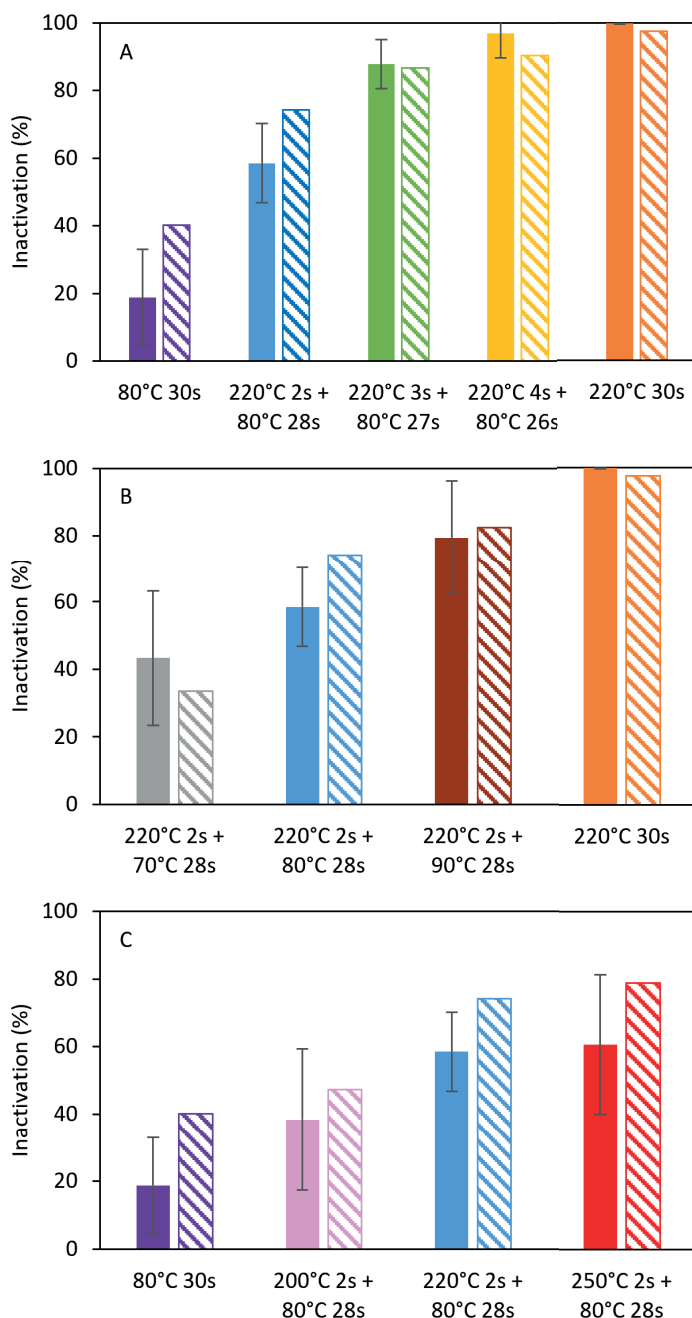
4

Figure 4.6. Experimental results (full fill) and model predictions (dashed fill) of β-galactosidase inactivation in 40 % (w/w) MD21 + 2% β-galactosidase droplets subjected to different drying trajectories. Drying trajectories with a different drying time at in- and outlet temperature (A), different outlet temperatures (B), and different inlet temperatures (C) were applied.

Modelling drying and β-galactosidase inactivation

The previously described numerical heat and mass transfer model was used to calculate drying of 40% MD21 and 2% β-galactosidase containing droplets dried under different conditions (Figure 4.7). The experimental observations and modelled predictions on volume decrease align well up to the locking point, but after this point, deviations become visible. Both the experimental as well as the modelled droplet volume are in essence no longer fully accurate after the locking point, since the morphology after the locking point will deviate from that of a dense sphere cap. A vacuole may be formed inside the droplet, and the surface may accommodate volume reductions by wrinkling up, thus retaining a larger surface area. These morphological changes are not taken into account with the current volume analysis based on two-dimensional images, while our one-dimensional drying model cannot take these morphological changes into account either.

The model adequately predicts the general trend in temperature changes. There is a general agreement on the point in time at which the droplet reaches its maximum temperature. In addition to deviations caused by morphological differences, deviations between model and experiments could also originate from differences in the temperatures of the contact surface (platform) and the drying air. While we did use the actual experimental temperatures as input for the model, these values were measured with thermocouples on the contact surface and in the drying air close to the droplet. Temperatures at the exact position of the droplet may well deviate from these values. For example, the thermocouple measuring the contact surface temperature may be too far away to experience the initial cooling effect of the tiny droplet on the platform, resulting in deviations in the prediction of the initial droplet temperature. The final droplet temperature is more accurately predicted by the model, as at that stage, the effects of the evaporative cooling on the temperature of the contact surface have become negligible. Note that for drying temperatures above the boiling point, predictions become difficult, since the internal boiling of moisture eventually results in inflation of the particle (Figure 4.4). This creates larger discrepancies between the experimental results and the model outcome.

The model was then used to predict the inactivation of β-galactosidase during drying, based on the predictions of the droplet moisture content and droplet temperature (Figure 4.8). As the droplet initially had a temperature close to the wet bulb temperature, inactivation of the enzyme was limited. As soon as the droplet temperature increased, more inactivation becomes visible. The level of inactivation within the droplet is not uniform: as the outside of the droplet dries faster and contains less moisture, less enzyme inactivation was observed here than in the wet core of the droplet. This is in line with other research on inactivation of proteins at different moisture contents, observing more inactivation at higher moisture contents (Ruprecht et al., 2023; Samborska et al., 2005; Siguemoto et al., 2023). This is explained as water is required for protein mobility during the unfolding process of denaturation (Mallamace et al., 2011).
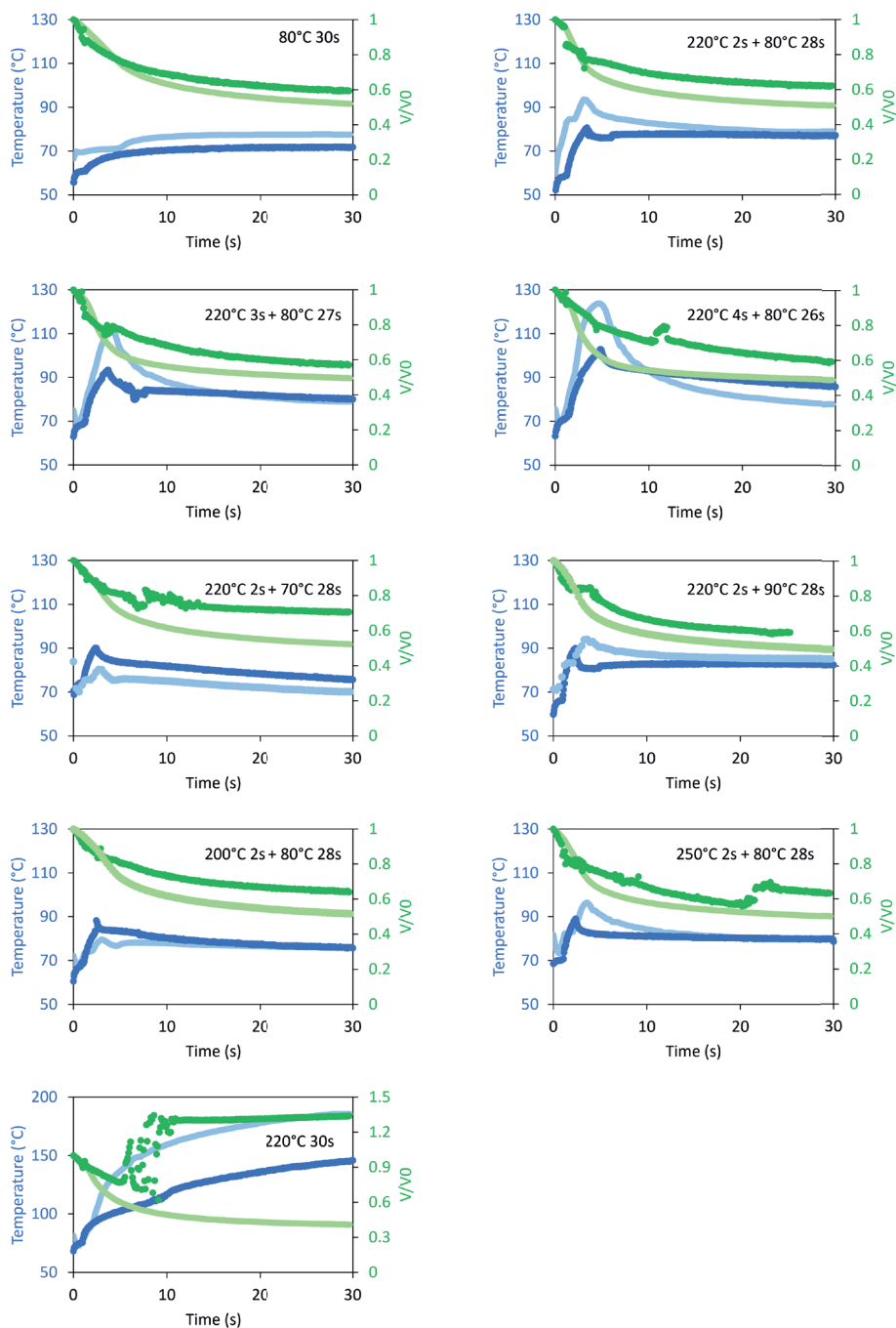
4

Figure 4.7. Temperature (blue) and volume (green) development of 40% MD21 droplets dried at different temperature–time trajectories. The experimental values are represented by the dark colors, and the model predictions by the light colors.
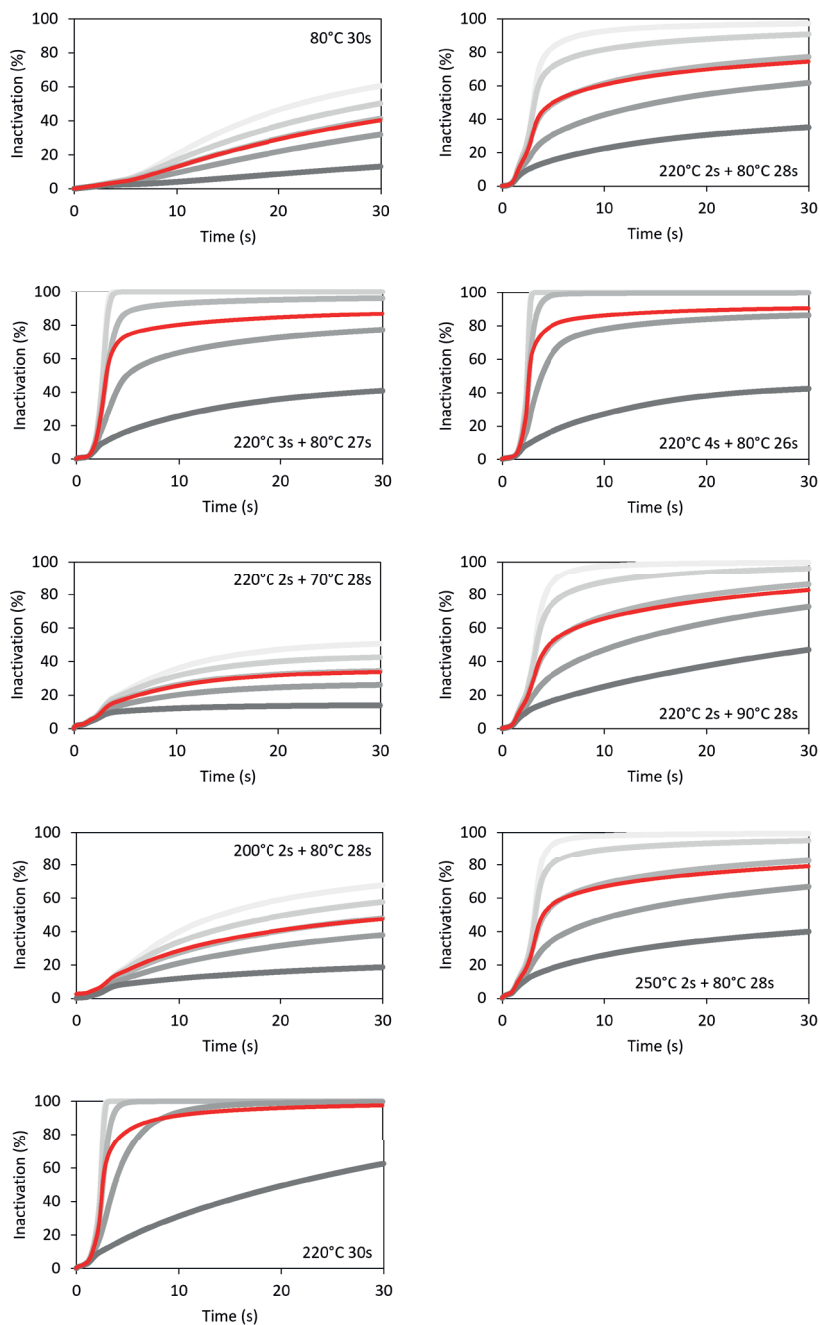
Figure 4.8. Predictions on β-galactosidase inactivation in the drying droplets, for different shells of the droplet (shell 1 (core of the droplet), 10, 20, 30 and 40 (outside of the droplet), presented by gray lines with increasing darkness for increasing shell number) as well as for the overall droplet (red) over time.

During the course of drying, there are some differences between the model and the experiments when it comes to droplet volume and droplet temperature (Figure 4.7). Consequently, these differences lead to differences related to the final level of β galactosidase inactivation. In addition, minor variations in droplet size contribute to relatively large experimental standard deviations (Figure 4.6), as this strongly influences the amount of enzyme present. Nonetheless, the model predictions are still in range of the experimental observations and show the same trends when it comes to changes in temperature-time trajectories (Figure 4.6, Figure 4.9).
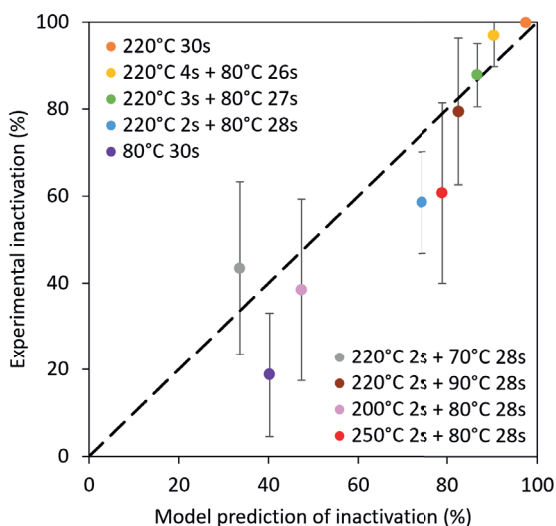

Figure 4.9. Parity plot of the inactivation of β-galactosidase as predicted by the model and determined experimentally.

The model can be employed to find the optimal drying conditions, for example by looking at the time it takes till the droplet has obtained a specified moisture content and the β-galactosidase inactivation at this time. Ideally, a product dries quickly and has a low β-galactosidase inactivation. However, the faster the droplet dries, the higher the inactivation of β-galactosidase becomes (Figure 4.10). Therefore, one should find the optimum balance between these two criteria. Depending on the importance of each criterium, optimal drying conditions can then be selected.

Drying droplets with a reduced solute content
To further investigate the impact of the inlet air temperature on the droplet drying rate and temperature development, droplets with an initial MD21 concentration of 20% (w/w) were dried. Previous research on maltodextrin droplets dried at constant air temperature showed that droplets with a lower initial solute concentration have a later locking point (Eijkelboom, Swinkels, et al., 2023). A later locking point enhances the temporal resolution of differences in drying behavior. Drying with temperature-time trajectories
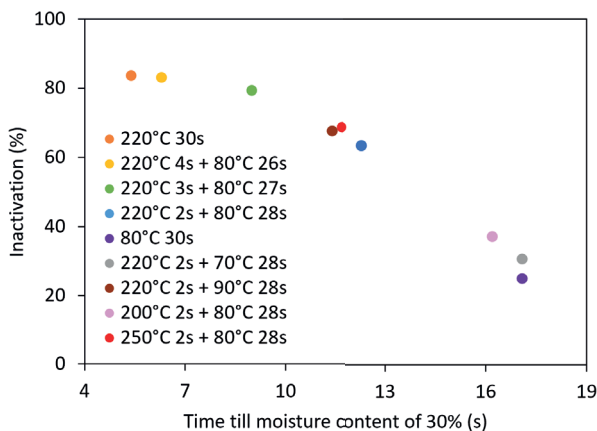
Figure 4.10. The predicted β-galactosidase inactivation at the predicted time that the moisture content of the sample has decreased to 30% for the droplets initially containing 40% MD21 dried at different temperature-time trajectories.

did also result in a later locking point for these droplets with a lower solute concentration. The 20% MD21 droplets continuously dried at 80 °C, showed locking at 5.1 ± 0.2 s. For the 200, 220 and 250 °C inlet air temperatures, locking occurred at 4.5 ± 0.2, 4.3 ± 0.4 and 3.7 ± 0.1 s respectively. Higher air temperatures result in faster evaporation and therefore lock earlier.

The lowered solute content resulted in different droplet volume development during drying (Figure 4.11, Appendix 4 Figure 4.A.1). The 20% MD21 droplets showed a rapid decrease in volume for a longer period of time and the lower solid content implies a smaller final volume than with 40% MD21 droplets. While the volume development for the 40% MD21 droplets was independent of the initial air temperature, the volume development of 20% MD21 droplets did depend on the initial air temperature. Higher air temperatures resulted in faster droplet shrinkage and a smaller final droplet volume (Figure 4.11). These differences in droplet volume at the end of the experiments might indicate that the droplets are not fully dried yet. As the drying rate is lower at the lower drying air temperatures, these droplets might still contain more water, resulting in a larger volume. Another possible explanation for the differences in the final droplet volume is a difference in the density of the dried droplets. No differences in morphological development, like vacuole formations, were visible, but the decreased detected droplet volume of the droplets dried at higher temperatures could be a result of a lower porosity. Due to the high air temperatures, the drying solution are less viscous, which might result in more deformability and the creation of a more compact dried particle.

The droplets with a lower initial solute content remained more dilute for a longer time, and this shows in the droplet temperature (Figure 4.5, Figure 4.12). As the locking point was delayed till after the point in time where the drying air was changed from hot to

cooler (inlet to outlet) conditions, the droplet was not yet fully in the falling rate regime. The droplets therefore remained cooler for a longer time than the 40% MD21 droplets (Figure 4.5, Figure 4.12). However, the heat transfer from the contact surface caused the droplet temperature to already rise above the wet bulb temperature. After the locking point, all droplet temperatures converged to a temperature close to that of the air (Figure 4.5, Figure 4.12).
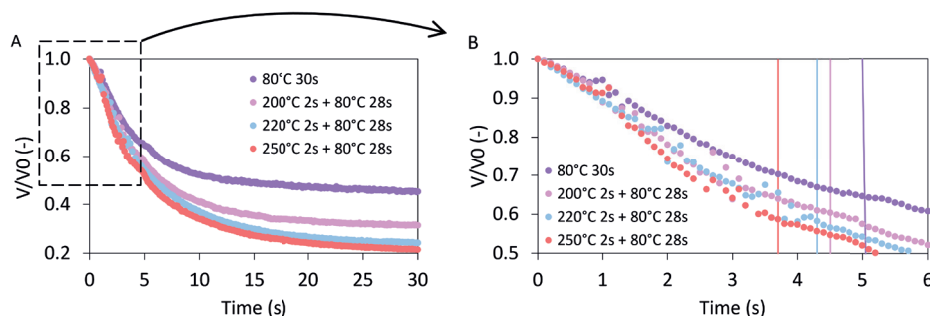

Figure 4.11. Experimental volume change over time for single droplets of a 20% MD21 + 2% β-galactosidase solution dried with different drying trajectories, for the full drying period (A), and zoomed in to the first 6 s (B). The annotations in the legend indicate the combination of air temperature and drying time at this temperature. The vertical lines in B indicate the locking points.
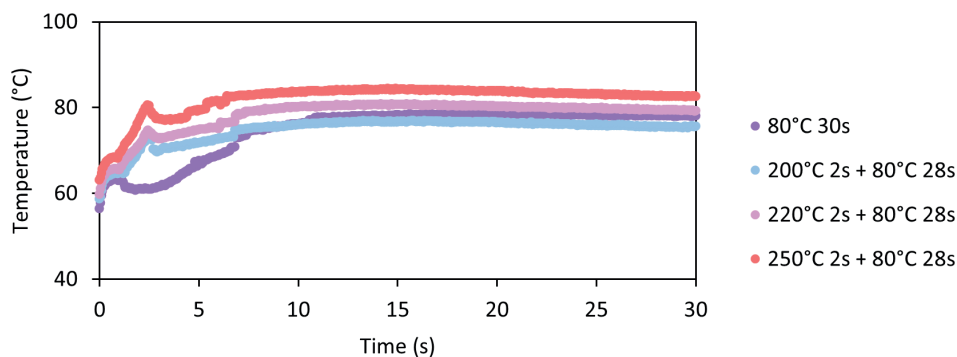

Figure 4.12. Experimental temperature development of single droplets of a 20% MD21 + 2% β-galactosidase solution dried with different drying trajectories. The annotations in the legend indicate the combination of air temperature and drying time at this temperature.

Based on the different volumes and temperature trajectories of the droplets with a lower initial solute content, we expected that the inactivation of β-galactosidase would also differ from that with 40% maltodextrin. The higher moisture content of a droplet with a lower solute content enhances the inactivation, while the initially lower droplet temperature reduces the inactivation (Perdana et al., 2013). To investigate the overall impact of the decreased solute content on β-galactosidase inactivation, the SDD model which was

shown to be able to predict β-galactosidase inactivation was applied (Figure 4.13). For drying at a constant temperature of 80 °C, the model predicted less β-galactosidase inactivation when starting with a 20% MD21 solution than with a 40% MD21 solution. For the drying trajectories with an initial high inlet temperature, the model predicted more β-galactosidase inactivation when starting with a 20% MD21 solution than with a 40% MD21 solution.
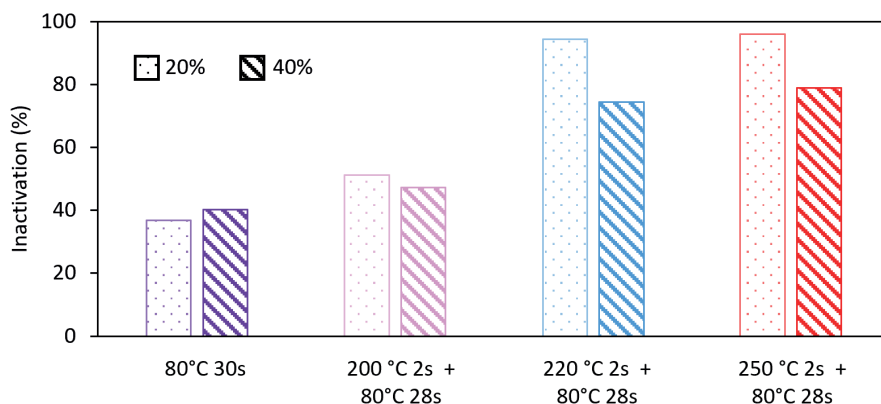

Figure 4.13. Model predictions of β-galactosidase inactivation in 20 % and 40 % (w/w) MD21 + 2 % β-galactosidase droplets subjected to different drying trajectories.

When using constant air temperatures, the SDD model predicts that minimal enzyme inactivation after drying is obtained with a low initial solute content. However, using temperature-time trajectories, a high initial solute content is predicted to be favourable to achieve minimal enzyme inactivation. These differences stress the importance to include temperature-time trajectories during SDD. The new sessile single droplet drying platform can be used to understand the impact of composition and more realistic drying conditions on droplet drying kinetics. Combined with the SDD model including β-galactosidase inactivation kinetics it can thus help to optimize spray drying conditions of β-galactosidase in maltodextrin. Now the SDD approach with stepwise temperature change has been validated, new SDD experiments with different formulations may be done for understanding their drying behavior as well. The SDD numerical model can then be of help to extrapolate the results of the SDD experiments to full scale spray drying if desired.

Conclusions

Assessing spray drying using single droplets can be done with a SDD platform that allows using a temperature-time trajectory. In this work, a sessile SDD platform is presented that contains two separate heating blocks that allow for a switch in air temperature during a

single measurement. The resulting temperature-time trajectory can be set to represent both the initial drying period at inlet air temperature and the part at the lower outlet air temperature. We used β-galactosidase as an indicator for the thermal load on the dried solids.

The temperature of the first stage (representing the inlet air) hardly influenced the drying behavior and inactivation of droplets containing an initial MD21 content of 40%. This is because the droplet temperature was limited to the wet bulb temperature. The later stage (outlet) air temperature however significantly influences the drying behavior of the droplets. A higher later stage air temperature results in higher droplet temperatures and a higher thermal load, and more inactivation of the β-galactosidase.

For droplets with a lower initial solute content of 20% MD21, later locking points were observed, resulting in a higher temporal resolution of the drying behavior. For these droplets, different initial air temperatures did result in different drying behavior and inactivation. With an increase in inlet air temperature, faster initial drying rates and earlier locking points were observed. Based on this, the model predicts more β-galactosidase inactivation with higher first stage (inlet) air temperatures.

The drying behavior and β-galactosidase inactivation was predicted using a numerical SDD model, making predictions that are in line with the experimental observations. The predicted β-galactosidase inactivation was lower at the dry outside of the droplet than in the wet core. Besides, the model predicts the needed drying time and β-galactosidase inactivation under different drying conditions. This is a first step to allow for the prediction of optimal drying conditions during spray drying, which should balance the energy efficiency of the process and the powder quality, including enzyme activity.
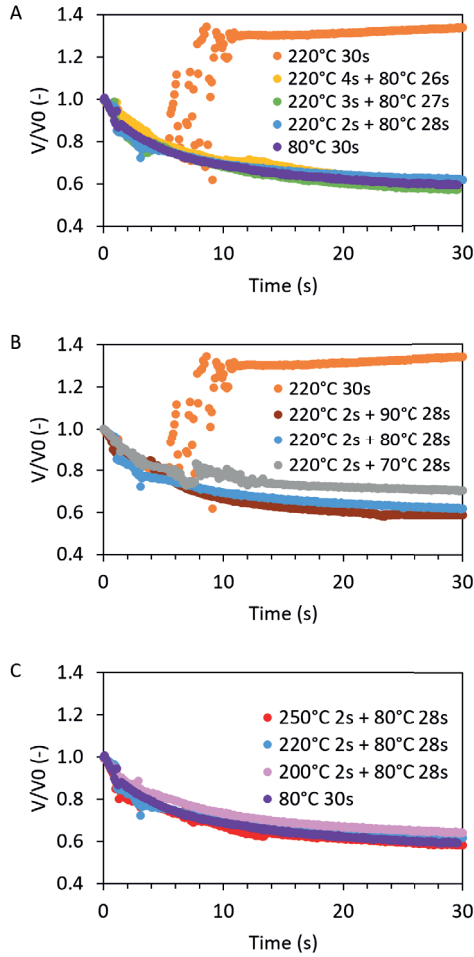
Appendix 4

Figure 4.A.1. Experimental volume change over time for single droplets of a 40% MD21 + 2% β-galactosidase solution dried with different drying trajectories. Drying trajectories with a different drying time at in- and outlet temperature (A), different outlet temperatures (B), and different inlet temperatures (C) were applied. The annotations in the legend indicate the combination of air temperature and drying time at this temperature.

Chapter

5
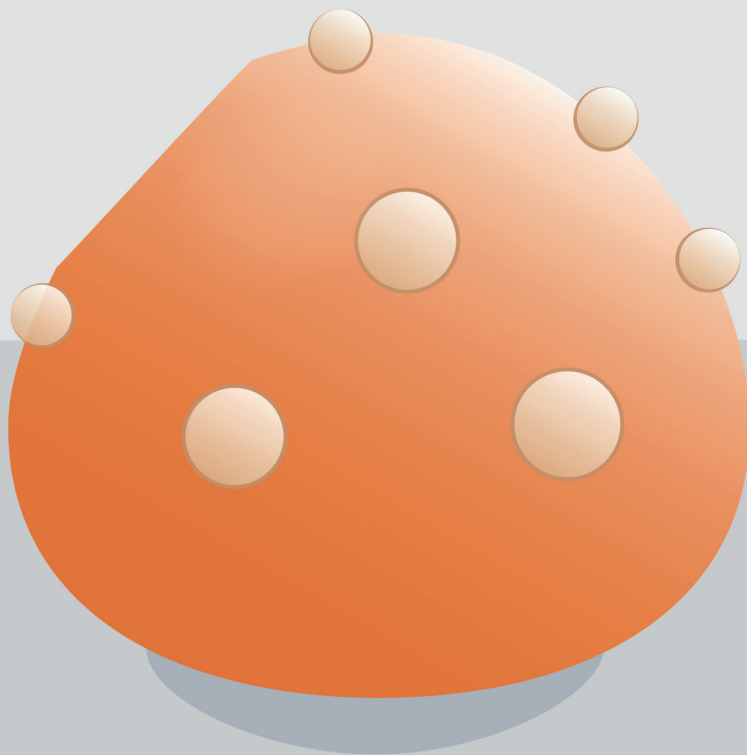
Single droplet drying of dairy-based systems at spray drying like temperature-time trajectories

N.M. Eijkelboom

E. Hooiveld

J. Kingma

R.M. Boom

P.F.C. Wilms

M.A.I. Schutyser

Abstract

Upon spray drying of dairy powders, the distribution of components within the droplets can become non-uniform. In this study, the influence of the composition on the drying behavior, morphological development and surface composition were studied using single droplet drying. The addition of fat was found to result in an earlier locking point (1.1 instead of 1.8 s). The fat content did not influence the morphological development, but the protein and lactose ratios did influence whether the dried particle was smooth or wrinkled. Confocal Raman microscopy revealed that the initial fat, lactose and protein contents influenced the dry surface composition. For example, fat was found on the surface of emulsions that were either rich in fat or in whey protein.

Introduction

The dairy industry processes a wide variety of emulsified products. Milk itself is an oil-in-water emulsion stabilized by proteins (Langevin, 2020). These complex, multi-component systems are often processed into powders by spray drying, as powdered dairy products have an increased shelf life and are easier to handle, store and transport compared to fresh dairy products. Moreover, spray drying can provide excellent encapsulation efficiency of the oil present in an emulsion (Höhne & Gaukel, 2024; Tabatabaei et al., 2022). However, the production of these spray dried dairy powders is very energy intensive, and reducing the energy consumption of the process, while still ensuring excellent quality powder, is important. To do this, we need better understanding of the underlying mechanisms involved in spray drying.

Single droplet drying is a promising technique to gain mechanistic understanding of spray drying processes (Schutyser et al., 2019). While typical single droplet dryers subject a droplet to a constant temperature, this is not the case in an industrial spray dryer. However, the impact of the more complex temperature-time trajectories in industrial dryers on the drying of individual droplets is unknown. We have recently introduced a custom-made single droplet dryer that allows two-step simulation of spray drying temperature-time trajectories (Eijkelboom, Gawronska, et al., 2024). However, in the latter work, we focused on single component model systems, while industrially dried systems, like dairy systems, typically contain multiple components. Interactions between the components could influence the drying behavior, and is therefore of interest to investigate.

A common effect observed for multi-component systems upon drying is component segregation, which can occur due to phase separation or differences in diffusivities, and creates differences in composition between the core and the surface of the dried product. The surface composition of a powder is strongly correlated to product properties such as flowability, sticking behavior and reconstitution behavior (Porowska et al., 2016). The distribution of the different components in the final dry particle will highly affect the powder quality and product performance. As an example, lipid oxidation reduces if the amount of surface fat is lower (Granelli et al., 1996). Besides, surface fat contributes to caking of powders during storage (Foster et al., 2005).

To investigate segregation of components in powders, confocal Raman microscopy can be applied. This technique does not require any pre-treatment of the sample but does require spectral resolution of the investigated components (Hooiveld et al., 2023). Components that are of interest within the food industry, like lipids and proteins, however, do show a big overlap in their Raman spectra. Therefore, for these components, the interpretation of the data depends on specific peaks rather than on the full spectrum (Dahl et al., 2023). Previous research used confocal Raman microscopy to study component segregation in single droplets of multicomponent mixtures that were dried at constant air temperatures (Both, Nuzzo, et al., 2018; Nuzzo, Millqvist-Fureby, et al., 2015). For systems containing lactose and surface-active components, component segregation was observed, and the

surface of the dried particle was enriched in the surface-active components (Nuzzo, Sloth, et al., 2015). Systems containing protein, lactose and fat showed a very thin layer of protein at the surface (Both, Nuzzo, et al., 2018). However, for both studies the interpretation of the results was based on auto-generated images from on the full Raman spectrum, rather than using component-specific peaks. Besides, component segregation is a temperature-dependent process, and drying a droplet with a temperature-time trajectory rather than with a constant temperature may influence the segregation process.

The objective of this study is, therefore, to investigate the drying behavior of multicomponent dairy systems dried with temperature-time trajectories mimicking co-current spray drying conditions. The locking point and morphology of the dried droplets are determined, as well as the dried surface composition based on confocal Raman microscopy. The interpretation of the confocal Raman data is based on component-specific peaks that are determined using pure components. The obtained results help to understand component segregation in multicomponent systems upon spray drying and thus create powdered products of excellent quality.

Materials and methods

Materials
Lactose (Lactopure®, 99.7% lactose), whey protein isolate (WPI) (Nutri Whey™ Isolate R, 90% protein content) and micellar casein isolate (MCI) (Refit™ micellar casein isolate, 88% protein, of which 90% is casein) were kindly provided and characterized for their composition by FrieslandCampina (the Netherlands). Sunflower oil was obtained from Coppelia (Cargill, USA). Demineralized water was used.

Preparation of the drying solution
Dairy emulsions with a water content of 80% (w/w) were prepared. Different ratios of lactose, whey protein isolate, casein isolate and sunflower oil were used (Table 5.1). After mixing the ingredients for 2 h, the solution was pre-emulsified by using a rotor-stator homogenizer (T18 digital Ultra-turrax®, IKA, Germany). For all different compositions, mixing for 2 min at 10,000 rpm combined with three cycles through a high-pressure homogenizer (M-110Y Microfluidizer, Microfluidics, USA) with an F12Y and APM H30Z chamber with an inlet pressure of 80 PSI (552 kPa) was used. For the Standard composition, two more preparation techniques were used. The first one was identical to the previously described method, except for a change in inlet pressure of the high-pressure homogenizer to 40 PSI (276 kPa). For the second preparation technique, only the rotor-stator homogenizer was used. The solution was mixed for 10 min at 15,000 rpm.

Oil droplet size determination
The size distributions of the oil droplets in the prepared emulsions were determined in triplicate using laser diffraction with a Mastersizer 3000 (Malvern Panalytical, UK). A Hydro MV dispersion unit was used, operating at a stirring speed of 1400 rpm. The

Table 5.1. Composition of the different samples investigated in this research on wet base.

Sample name	Fat (w/w %)	Lactose (w/w %)	WPI (w/w %)	MCI (w/w%)
Standard	2.0	9.0	4.5	4.5
No fat	0.0	10.0	5.0	5.0
High fat	6.7	6.7	3.3	3.3
High lactose	2.0	14.0	2.0	2.0
High protein	2.0	4.0	7.0	7.0
High WPI	2.0	9.0	1.8	7.2
High MCI	2.0	9.0	7.2	1.8
Lactose + WPI	0.0	10.0	10.0	0.0
Lactose + MCI	0.0	10.0	0.0	10.0

refractive index was set to 1.456 for the dispersed phase and to 1.330 for the dispersant. An absorption index of 0.01 was applied. The Mie theory is used for oil droplet size determination.

The oil droplet size distribution of the Standard emulsion prepared in different ways is depicted in Figure 5.1. All other emulsions prepared by using the rotor-stator homogenizer for 2 min at 10,000 rpm plus three 80 PSI cycles with the high-pressure homogenizer had similar oil droplet size distributions as the Standard emulsion, which should, therefore, not influence the drying behavior. The obtained most common oil droplet sizes for the different preparation techniques of 0.08, 0.2 and 0.4 μm are all at the smaller end of the size range of oil droplet sizes in homogenized bovine milk, human milk and infant milk formula (Gallier et al., 2015; Michalski et al., 2005; Mulet-Cabero et al., 2019). Since high stresses during atomization can lead to further oil-droplet breakup, it is expected that these smaller oil droplet sizes well represent the oil droplet size in a dairy slurry to be spray dried (Taboada et al., 2021).
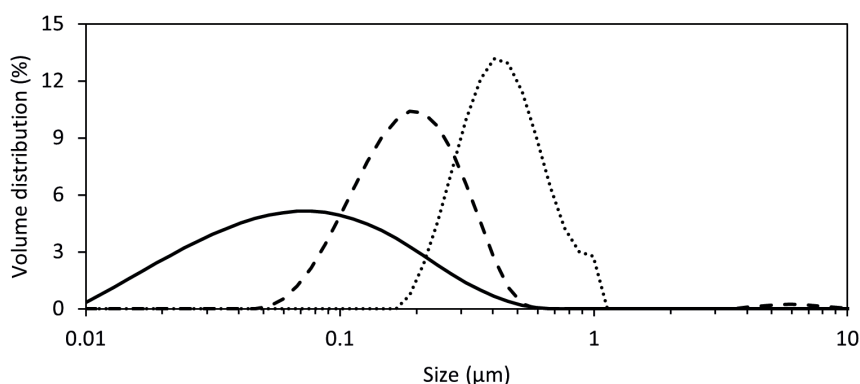

Figure 5.1. Oil droplet size distribution for the Standard emulsions prepared by using the rotor-stator homogenizer for 2 min at 10,000 rpm plus three 80 PSI cycles with the high-pressure homogenizer (full line), using the rotor-stator homogenizer for 2 min at 10,000 rpm plus three 40 PSI cycles with the high-pressure homogenizer (dashed line), and using the rotor-stator homogenizer for 10 min at 15,000 rpm (dotted line).

Single droplet drying

Drying of single droplets was performed with the sessile single droplet drying platform that was earlier described in more detail (Eijkelboom, Gawronska, et al., 2024). The droplets had an initial radius of 200 ± 20 μm. For all different compositions investigated, droplets were dried with a temperature-time trajectory that starts with an inlet air of 220 °C flowing at 20 L/min for 2 s, followed by air of 80 °C flowing at 10 L/min for 28 s. For the Standard composition, drying trajectories that start with an inlet air of 150 °C or 80 °C at 20 L/min for 2 s, followed by air of 80 °C flowing at 10 L/min for 28 s were also applied. For all solutions, three individual droplets were dried. The temperature of the air near the droplet was monitored throughout the drying process (Figure 5.2). The drying process was filmed at 100 fps with a high-speed camera (C-VIT, AOS Technologies AG, Switzerland) equipped with a VZMTM 1000 Zoom Imaging Lens (Edmund Optics, Japan). The movies are used to visually observe the morphological development and the locking point, i.e. the first point at which shape deviation from a spherical cap is visually observed (Siemons et al., 2020).
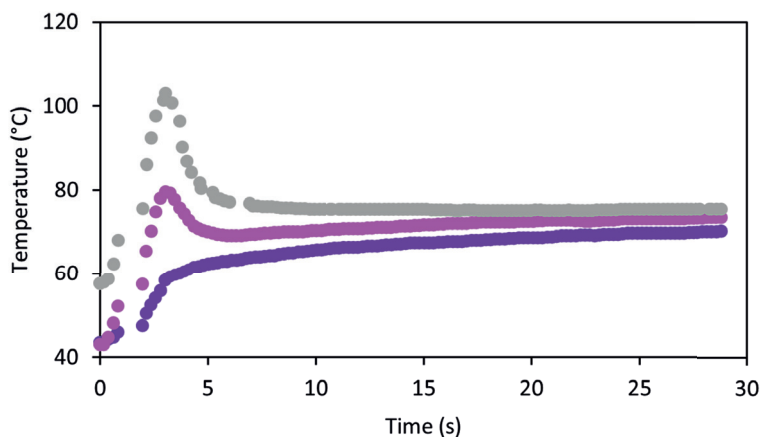

Figure 5.2. Temperature of the air near the droplet during the drying process for different temperature-time trajectories; 80 °C 20 L/min for 2 s + 80 °C 10 L/min for 28 s (purple), 150 °C 20 L/min for 2 s + 80 °C 10 L/min for 28 s (pink), 220 °C 20 L/min for 2 s + 80 °C 10 L/min for 28 s (gray).

Scanning electron microscopy

Of each sample type, one dried droplet was visually inspected using a JCM-7000 SEM (JEOL, Japan). The dried droplets were coated with gold using a JEOL Smart-Coater (JEOL, Japan). The images were taken at an acceleration voltage of 5.0 kV.

Confocal Raman microscopy

To investigate the distribution of components within the dried droplets, confocal Raman microscopy (Alpha300 R, WITec, Germany) was applied. A 100x air-objective with a numerical aperture of 0.9 and a laser with an excitation wavelength of 532 nm were used.

For the three different components present, i.e. lactose, protein and fat, single spectra of the pure components were obtained using 100 accumulated measurements with an integration time of 0.5 s (Figure 5.3). Based on these raw spectra, component characteristic peaks could be identified. For lactose, these peaks are at 355 and 468 cm^{-1}, in line with values reported in literature (Khan et al., 2023; Pax & Sheehan, 2020). Protein-specific peaks were observed at 755, 1560 and 3060 cm^{-1}, also in line with values reported in literature (Chen et al., 2014; Dahl et al., 2023; McColl et al., 2003). For fat only one specific peak could be identified, at 1750 cm^{-1}, which again is in line with values reported in literature (Khan et al., 2023; Pax & Sheehan, 2020). For further analysis we zoomed in to only one characteristic peak per component, being the 355 cm^{-1} for lactose and the 1560 cm^{-1} for the protein, as these peaks showed the clearest change in intensity upon changing the composition.
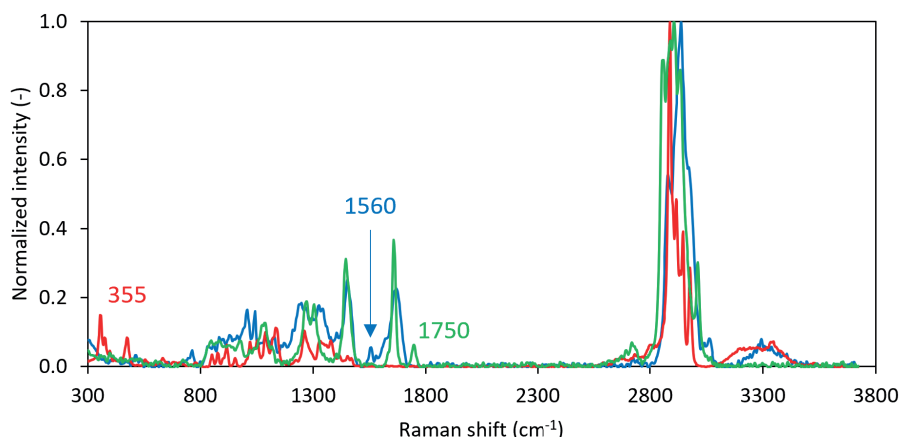

Figure 5.3. Raman spectra of pure fat (green), protein (blue) and lactose (red) and their component specific peaks.

For the dried particles, depth scans were taken to investigate the inward gradient of the Raman signal. The scans were taken with an image size of 40 (width) by 100 (depth) points, applying a point size of 0.5 μm. An integration time of 0.5 s was applied. The signals were cleaned by cosmic ray removal with a filter size of 2 and a dynamic factor of 8, average smoothing with a spectral filter size of 3 and a spatial filter size of 0, and background subtraction with a shape size of 300.

A MATLAB script (MATLAB R2018b, MathWorks, United States) was developed to analyze the confocal Raman spectra. The spectra were binned per depth layer, generating an average spectrum per depth. This was done for the top 10 μm of the droplet, as the Raman signal decreases with the depth (Everall, 2010) and preliminary experiments (results not shown) indicated that there was no detectable signal for deeper measurements. The Raman spectra at different depths within a droplet were compared (Figure 5.4A). Due to loss of scattering and absorption of the excitation and emission light, it is not immediately clear whether the changes can be attributed to overall signal decreases or to compositional

changes (Macdonald & Vaughan, 2007). Therefore, to compare the compositions of the droplet at different depths, the Raman signals were normalized, based on the total integral of the Raman spectrum. This clarified that there was no clear difference in composition over the investigated 10 μm (Figure 5.4B). This is only shown for one of the samples, but this observation holds for the other samples as well (results not shown).

As our samples showed no difference in normalized Raman spectra for the different depths, only the average spectrum of the depth showing the strongest absolute signal was used for further data interpretation. This strongest signal was assumed to be present at the interface between the droplet and the surrounding air. To compare the spectra of different samples, the absolute intensities were normalized over the intensity of the peak near 2950 cm^{-1}, which is caused by C-H bonds (Zhang et al., 2011). As the characteristic Raman shift of the C-H peak might slightly change depending on the measurement, the maximum intensity in the range of Raman shifts of 2915 to 2985 cm^{-1} was used. As C-H bonds are present in all the components used in the emulsions investigated in this research, this should not distort the results. Measurements have been performed in duplicate, but the result of only one of the measurements is shown. The noise level and the exact value of the normalized intensity vary between samples of the same initial composition (Appendix 5 Figure 5.A.1), but the presence or absence of component-specific peaks is consistent. We can therefore draw qualitative conclusions but have to refrain from quantitative interpretation.
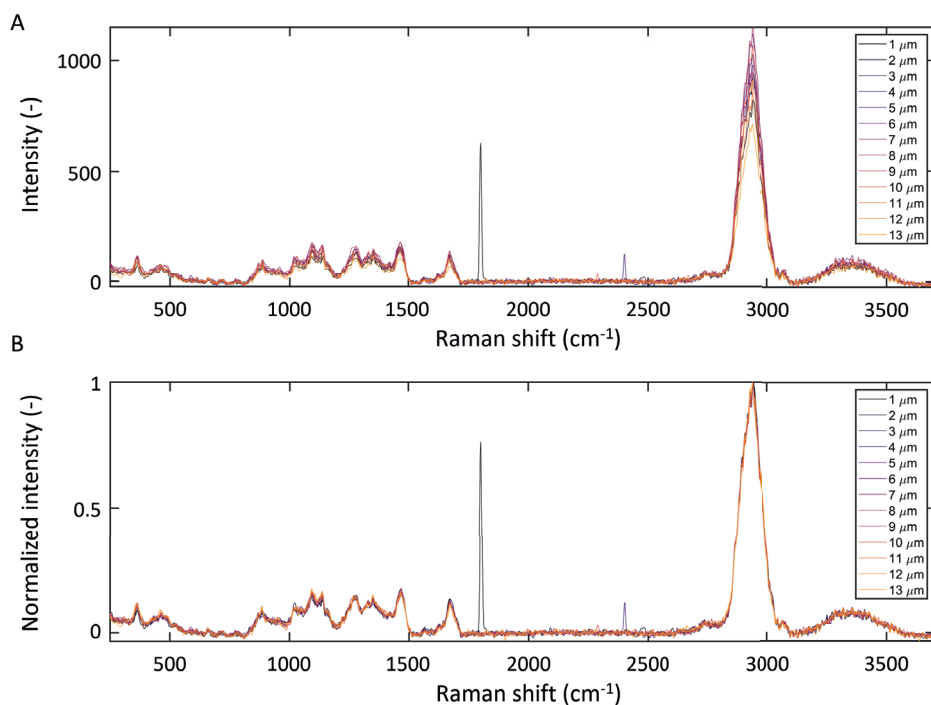

Figure 5.4. General (A) and normalized (B) confocal Raman spectra at different depths of a dried droplet with Standard composition dried with air of 220 °C 20 L/min for 2 s + 80 °C 10 L/min for 28 s.

Experimental design and statistics

For all different feed solutions, the oil droplet size was determined in triplicate, and the results of one representative sample are shown. Per solution three individual droplets were dried and filmed with a high-speed camera. The locking points are based on the average values of the three droplets, and standard deviations are indicated. Initial indications of the morphology of the dried particles can be obtained from the high-speed camera movies for all droplets, and per sample type one representative droplet is used to obtain a scanning electron microscopy image. Confocal Raman microscopy is performed on two droplets per sample type, and the results of one of these droplets is shown.

Results and discussion

Fat content

Upon drying droplets with different initial fat contents, the addition of fat resulted in an earlier locking point. For the No fat, Standard and High fat samples, the locking points were determined at 1.8 (± 0.1), 1.1 (± 0.1), and 1.1 (± 0.2) s, respectively. This is in line with the observations of Shamaei et al. (2016), who concluded that an increase in oil concentration results in an earlier locking point. The increase in the diffusion path of the moisture in the droplet hinders evaporation earlier on, which may be the cause of this earlier locking point.

The morphological development of the droplets did not differ upon changing fat content (Figure 5.5). This is in line with the research of Both, Nuzzo, et al. (2018), who also observed no impact of fat on the particle morphology and who hypothesized that fat present in the form of emulsified droplets does not impact the structural strength of the skin.
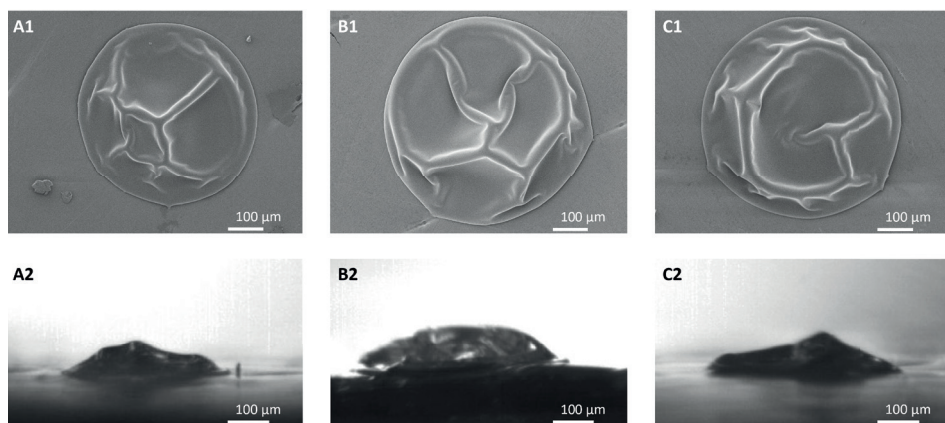

Figure 5.5. Top-view (1) and front-view (2) morphology of dried particles of the No fat (A), Standard (B) and High fat system (C).

Confocal Raman microscopy was used to investigate the presence of lactose, fat and protein at the surface of the dried droplets. For the No fat and Standard compositions, both lactose and protein were present at the surface of the dried droplet (Figure 5.6 lactose and protein, indicated by the presence of a peak), while fat was absent (Figure 5.6 fat, indicated by the absence of a peak). The dried droplet from the High fat matrix showed no presence of lactose and protein at the surface (Figure 5.6 lactose and protein, absence of a peak), but fat was definitely present (Figure 5.6 fat, presence of a peak).
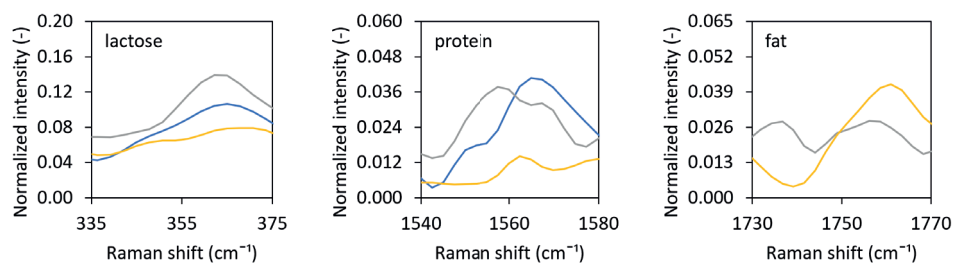

Figure 5.6. Normalized Raman intensity at the lactose, protein and fat specific Raman shifts for dried droplets of the No fat (blue), Standard (gray) and High fat system (yellow).

Earlier work by Nuzzo et al. (2017) investigated the surface of a whole milk particle dried with ultrasonic levitation based single droplet drying. The droplet had an initial dry matter content of 48%, an initial size in the range of 800-1000 µm, and was dried with air with a relative humidity of 7% and a temperature of 80 °C. They observed that the surface of the dried droplet consisted of an outer layer dominated by proteins, and an inner layer dominated by lactose. Fat globules were present in the core of the dried droplet. However, they also observed that droplets of similar composition dried in a pilot plant or full-scale spray drier, showed a different surface composition compared to that for single droplet drying. The droplets dried at a larger scale had a smaller initial size and were dried at high inlet air temperature, resulting in faster drying, and allowing less time for depletion or enrichment of specific components at the surface. Although the droplets dried in our study have a higher initial moisture content, they are smaller and are dried at higher initial air temperatures than those applied by Nuzzo et al. (2017). For the No fat and Standard droplet compositions, drying was fast enough to avoid the separation of lactose and protein at the surface.

Fat at the surface of the dried droplet was only detected for the High fat sample. This may be explained by the higher fat to protein ratio. At a 1:1 fat-to-protein weight ratio, the protein content might be insufficient to stabilize all oil droplets. The presence of oil at the surface is also observed for industrially dried milk powder. High pressure atomization of the milk can lead to rupture of oil droplets, resulting in the emergence of surface fat during drying (Foerster et al., 2016; Nuzzo et al., 2017).

Oil droplet size
The stability of the oil droplets in an emulsion is influenced by their size, with smaller oil

droplet sizes having a higher stability against rupture by shear (Santos et al., 2022). Since the emulsion stability might influence the results, we investigated standard compositions emulsified with different intensity to obtain different oil droplet sizes.

Only small differences in locking point were observed. The locking point of the emulsions with oil droplet sizes of around 0.08, 0.2 and 0.4 μm were at 1.3 (± 0.1), 1.2 (± 0.1), and 1.1 (± 0.1) s, respectively. Concerning morphological differences, an increase in oil droplet size led to more spreading and hence more flattened dried droplets (Figure 5.7). As the contact surface below the droplet was made of a hydrophobic material, this might be a first indication that the droplet surface is richer in hydrophobic components, i.e. fat.
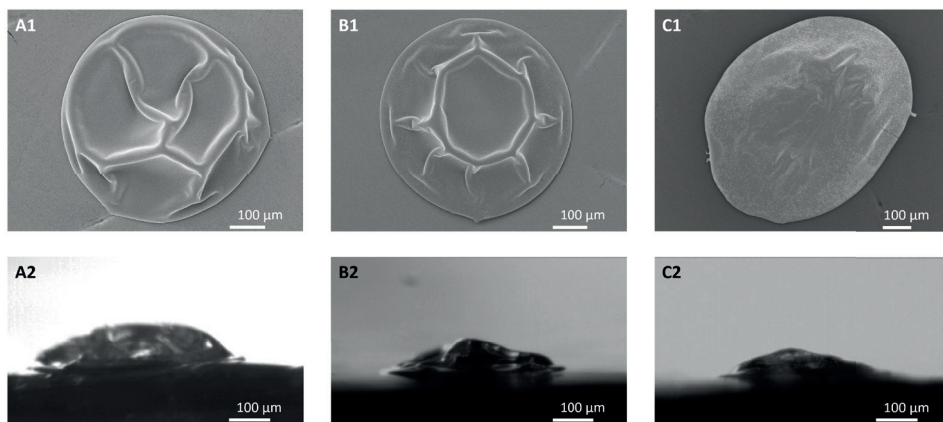

Figure 5.7. Top-view (1) and front-view (2) morphology of dried particles of the Standard composition with different oil droplet sizes; 0.08 μm (A), 0.2 μm (B), or 0.4 μm (C).

Nonetheless, this difference in presence of fat on the surface was not observed with the confocal Raman microscopy (Figure 5.8). Within the oil droplet size range investigated, the presence of components on the surface of the dried droplet did not differ. All dried droplets showed the presence of lactose and protein on the surface, while fat was not detected. This was not expected based on the work of Linke et al. (2020), where an increase in oil droplet size resulted in a decrease in oil encapsulation efficiency during pilot scale spray drying. However, they used much lower protein to oil ratios of 0.02 to 0.22% (w/w), which results in less stable emulsions. This indicates that all investigated emulsions in our research are stable, with no indication of any rupture of oil droplets or presence of surface fat.

Lactose-to-protein ratio
Because of their emulsifying properties, proteins influence the stability of oil droplets in an emulsion (Euston & Hirst, 2000). Changing the protein content by altering the lactose-to-protein ratio may therefore influence the emulsion stability, and hence component segregation. Upon changing the lactose-to-protein ratio of the drying droplet, the locking point remained unchanged. For the High lactose (7:2 lactose to protein ratio), Standard
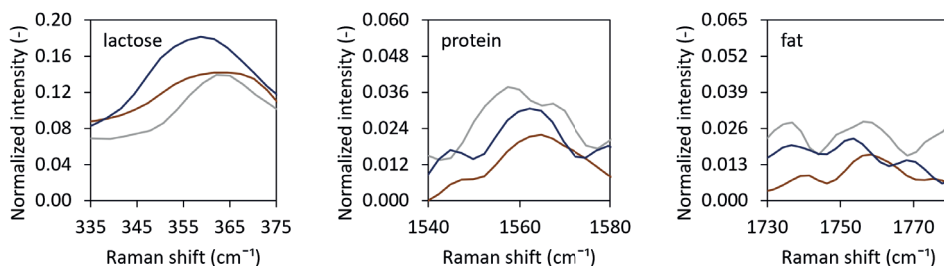
Figure 5.8. Normalized Raman intensity at the lactose, protein and fat specific Raman shifts for dried droplets of the Standard composition with different oil droplet sizes; 0.08 μm (gray), 0.2 μm (dark blue), or 0.4 μm (brown).

(1:1 lactose to protein ratio) and High protein (2:7 lactose to protein ratio) slurries, the locking point was, respectively, at 0.9 (± 0.1), 1.1 (± 0.1) and 0.8 (± 0.2) s. In previous research on solutions dried at lower temperatures, high molecular weight compounds such as proteins gave an earlier locking point than low molecular weight compounds (Eijkelboom, Swinkels, et al., 2023; Siemons et al., 2020; Sugiyama et al., 2006). At higher drying temperatures, drying goes much faster, and the locking point is obtained earlier, making differences in locking point too small to detect.

Differences were observed regarding the morphology of dried droplets containing different lactose-to-protein ratios (Figure 5.9). The High lactose system dried into a smoother particle, while the addition of protein resulted in a more wrinkled morphology. A droplet of the High protein system showed vacuole formation, resulting in a larger, partially puffed particle. Vacuole formation for protein and smooth particle formation for small sugar matrices was also observed in previous studies. Small sugars contribute to viscous behavior and thus more gradual skin formation, resulting in continuous shrinkage and the formation of a dense, spherical particle. Proteins may jam at high concentrations and form an elastic skin, which becomes rigid and then can no longer shrink. The internal pressure will drop due to proceeding water evaporation, creating a vacuole (Eijkelboom, Swinkels, et al., 2023; Siemons et al., 2021).

Confocal Raman microscopy showed that varying the lactose-to-protein ratio did influence the composition on the surface of the dried droplet. While the Standard composition showed the presence of both lactose and protein at the dried surface, the dried surface of the lactose enriched sample only contained lactose without much evidence of protein, and that of the protein enriched sample only contained protein, without indication of lactose (Figure 5.10). This indicates that lactose and protein can outcompete each other at the surface of the dried particle, based on their relative presence in the drying matrix.

Whey-to-casein ratio
Different proteins have different emulsifying properties. Whey protein is a good emulsifier, while micellar casein is a poor emulsifier (Euston & Hirst, 2000). A change in the whey-to-casein ratio might influence the emulsion stability. The locking point of the drying
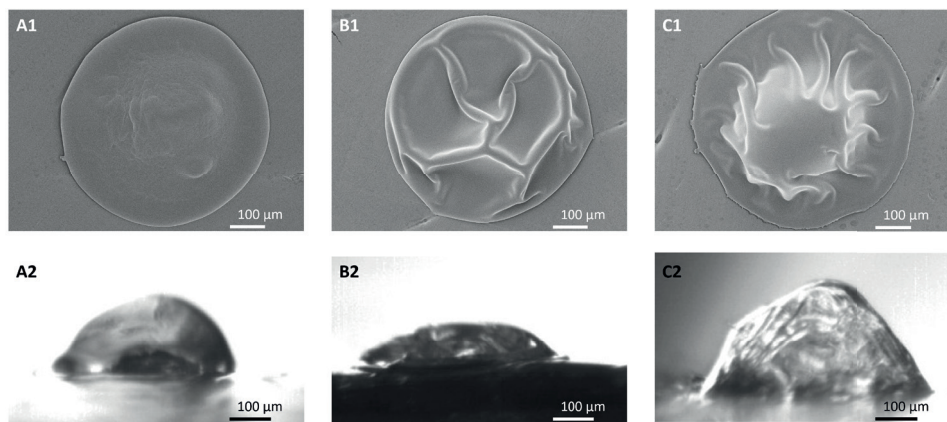
Figure 5.9. Top-view (1) and front-view (2) morphology of dried particles of the High lactose (A), Standard (B) and High protein system (C).
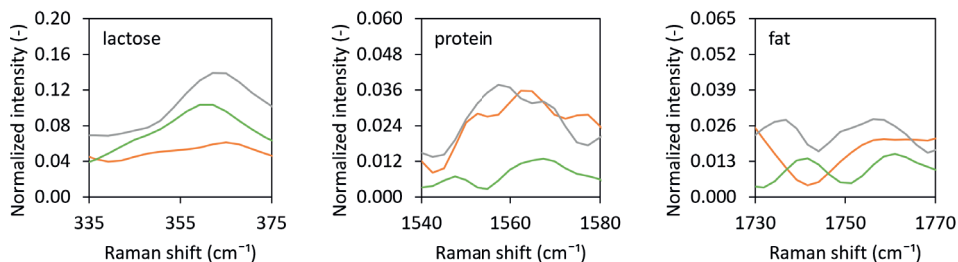

Figure 5.10. Normalized Raman intensity at the lactose, protein and fat specific Raman shifts for dried droplets of the High protein (orange), Standard (gray) and High lactose system (green).

droplet did not change upon changing the whey-to-casein ratio. For the High MCI (4:1 MCI to WPI ratio), Standard (1:1 MCI to WPI ratio) and High WPI (1:4 MCI to WPI ratio) solutions, the locking points were observed at 1.1 (± 0.1), 1.1 (± 0.1), and 1.0 (± 0.1) s, respectively. Nonetheless, morphological differences were clearly there (Figure 5.11), being in line with the work of Sadek et al. (2014), Bouman et al. (2016) and Both, Nuzzo, et al. (2018). While the system rich in MCI becomes more wrinkled, the system rich in WPI is smooth, with probably a vacuole. Upon drying, jamming of whey protein, which are "rigid sphere" proteins, results in the formation of relatively rigid shells. Casein micelles, which are "soft sphere" proteins, can deform after jamming, making the shell more flexible and resulting in a wrinkled morphology.

The surface composition of the dried droplets did differ based on the WPI-to-MCI ratio. While the surface of the Standard and High MCI sample contained lactose and protein, the surface of the dried High WPI solution only contained fat (Figure 5.12). Independent of the type of protein used, the high protein-to-fat ratio and small oil droplet size in all emulsions make it unlikely that any of them will be unstable. The fatty surface of the High WPI sample was, therefore, not expected. This result was even more surprising since
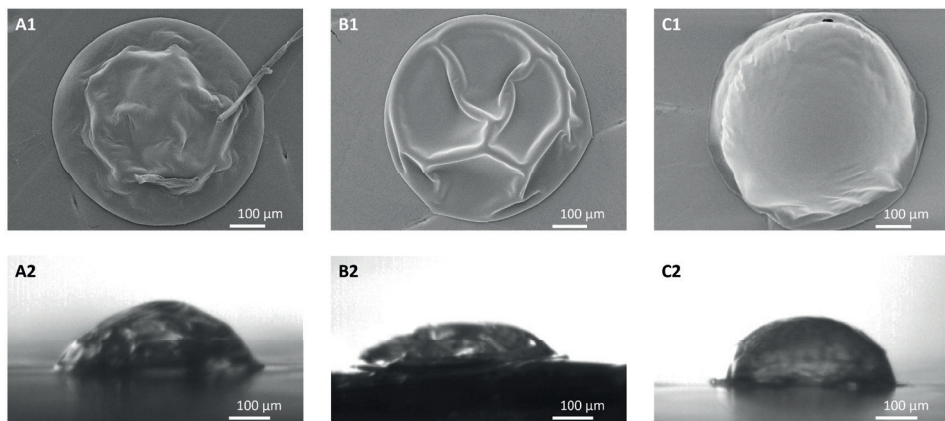
Figure 5.11. Top-view (1) and front-view (2) morphology of dried particles of the High MCI (A), Standard (B) and High WPI system (C).
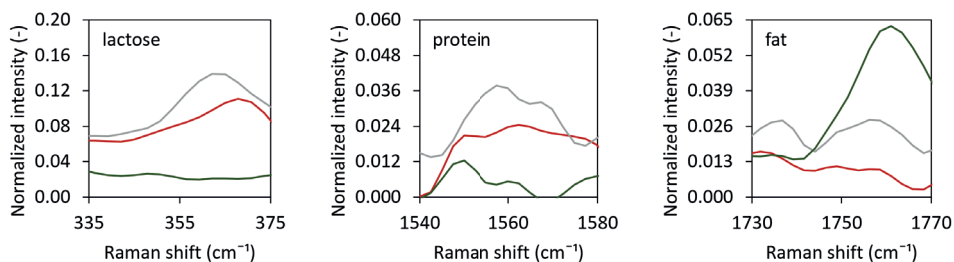

Figure 5.12. Normalized Raman intensity at the lactose, protein and fat specific Raman shifts for dried droplets of the High MCI (red), Standard (gray) and High WPI system (dark green).

the emulsifying properties of WPI are better than those of MCI (Euston & Hirst, 2000). Differences in the surface composition related to the morphological differences observed. The High WPI system turned into a smooth and hollow particle, instead of a wrinkled system. Although not clearly visible in the images provided, previous research indicated that skin rupture was observed for drying droplets with a vacuole (Bouman et al., 2016; Eijkelboom, Swinkels, et al., 2023). Through such a rupture, oil could have leaked out, covering the surface.

Fat free products

To complement our findings on the impact of the whey-to-casein ratio, fat free slurries with different whey-to-casein ratios were also investigated. The locking point of these fat free systems did not differ, as was the case for their fat containing counterparts. For the Lactose + MCI, Lactose + MCI + WPI and Lactose + WPI sample the locking points were respectively at 1.8 (± 0.1), 1.8 (± 0.1) and 1.6 (± 0.2) s. The fat free products do have a later locking point than their fat containing counterparts (High MCI, Standard and High WPI), which is in line with the results obtained for the samples differing in fat content. The same morphological differences, with the MCI system resulting in more wrinkled
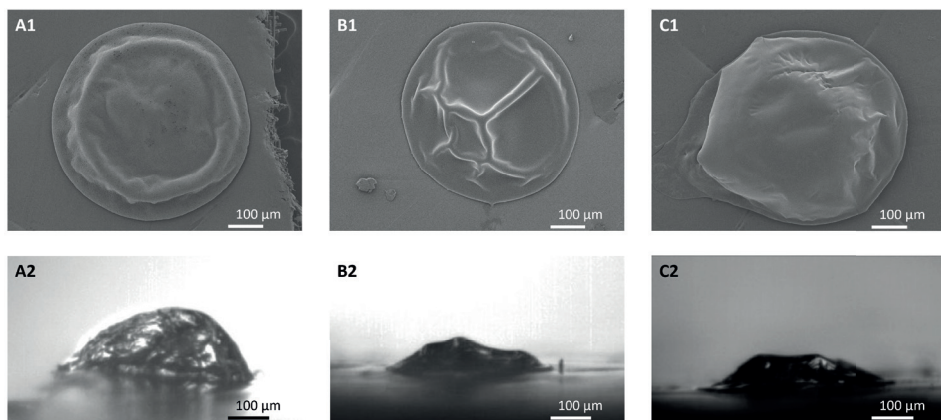
Figure 5.13. Top-view (1) and front-view (2) morphology of dried particles of the Lactose + MCI (A), Lactose + MCI + WPI (B) and Lactose + WPI system (C).

particles and the WPI in a smoother particle, were also observed (Figure 5.13).

Regarding the surface composition of the dried droplets that did not contain any fat and varied in WPI to MCI ratio it was observed that the surface of the dried droplet that was composed of lactose and MCI only consisted of lactose. The surface of the other dried droplets, where only WPI or a mixture of WPI and MCI was present as the protein source, was composed of both lactose and protein (Figure 5.14). This indicates that the smaller molecules, i.e. the lactose and whey protein, are present at the surface of the dried droplets, while the large micellar casein is not. This is in contradiction to previous confocal Raman measurements on dried single droplets which indicated that the outermost layer was dominated by the larger components (Both, Nuzzo, et al., 2018; Nuzzo et al., 2017). However, the stratification of small molecules at the top of a drying object was seen before in drying films (Fortini et al., 2016; Fortini & Sear, 2017; Schulz & Keddie, 2018). These authors concluded that stratification of small particles on top may occur when the solvent evaporation rate is sufficiently high. In that case, the moving interface creates a pressure gradient, pushing large particles away from the interface faster than it pushes small particles. In the work of Both, Nuzzo, et al. (2018) and Nuzzo et al. (2017) larger droplets (800-1200 µm) were dried with air of a constant temperature (70-90 °C), resulting in slower drying. These lower evaporation rates might have been insufficient to cause this small-on-top stratification.

Inlet temperature

To investigate whether slower drying does indeed result in component segregation, the Standard emulsion composition was dried with different temperature-time trajectories. A higher drying air temperature results in faster drying and hence an earlier locking point (Eijkelboom, Gawronska, et al., 2024; Shamaei et al., 2017). For the temperature-time trajectories with an initial drying air temperature of 80, 150 and 220 °C the locking points
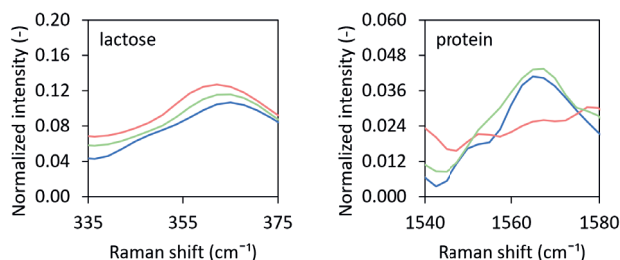
97

Figure 5.14. Normalized Raman intensity at the lactose and protein specific Raman shifts for dried droplets of the Lactose + MCI (pink), Lactose + MCI + WPI (blue) and Lactose + WPI system (green).

were at 1.7 (± 0.1), 1.5 (± 0.1), and 1.1 (± 0.1) s, respectively.

Based on top-view images, the morphologies of the droplets of the Standard emulsion dried at different temperature-time trajectories are different, with the droplet initially dried with air of 150 °C being smoother (Figure 5.15). Based on the side-view, the morphology of the droplets of the Standard emulsion dried at different temperature-time trajectories are however quite similar (Figure 5.15). In the work of Siemons et al. (2021) this was also observed for 20% (w/w) maltodextrin DE5 solutions dried at 90 °C, resulting in both smooth and dented particles. In general, an increase in drying temperature and the resulting faster skin formation led to more irregularly shaped, hollow or collapsed
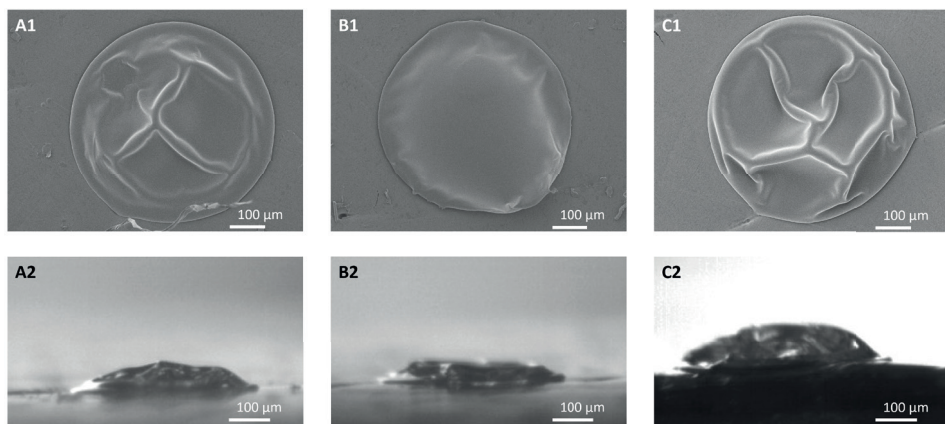
Figure 5.15. Top-view (1) and front-view (2) morphology of dried particles of the Standard composition dried with different air profiles; 2 s 80 °C 20 L/min + 28 s 80 °C 10 L/min (A), 2 s 150 °C 20 L/min + 28 s 80 °C 10 L/min (B) and 2 s 220 °C 20 L/min + 28 s 80 °C 10 L/min (C).

particles (Boel et al., 2020). This may be less apparent in in the current work due to the small differences in locking points, and hence in the speed of skin formation.

Independent of the temperature-time trajectory applied, both lactose and protein were

present at the surface of the dried droplet (Figure 5.16). However, no distinction between WPI and MCI can be made based on confocal Raman data, and it is therefore unknown
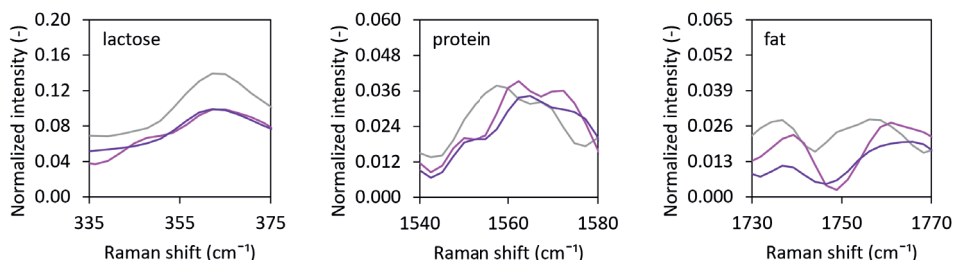

Figure 5.16. Normalized Raman intensity at the lactose (a), protein (b) and fat (c) specific Raman shifts for dried droplets of the Standard composition dried with different air profiles; 2 s 80 °C 20 L/min + 28 s 80 °C 10 L/min (purple), 2 s 150 °C 20 L/min + 28 s 80 °C 10 L/min (pink) and 2 s 220 °C 20 L/min + 28 s 80 °C 10 L/min (gray).

whether the stratification with smaller molecules accumulated at the surface occurred under all drying conditions.

Conclusion

Feed formulations dried within a spray dryer are commonly multicomponent systems, like dairy systems. The composition of such a system may influence the locking point and the morphology of the obtained powder particles. Moreover, an inhomogeneous component distribution could develop during drying, which influences the final powder quality and product performance. We investigated the locking point, morphology, and dried surface composition of dairy-based systems with different ratios of lactose, proteins and fat. Formulations dried under different conditions and with different oil droplet sizes were studied as well.

The presence of fat within the drying matrix reduces the moisture diffusivity, thereby resulting in an earlier locking point. With the applied drying conditions, other compositional changes, i.e. the ratio of lactose and protein, the presence of different types of dairy proteins and the oil droplet size, did not influence the locking point. Changing the drying conditions, and hence the drying rate, resulted in small differences in the locking point, with earlier locking at higher air temperatures. However, the applied drying conditions did not lead to discernible morphological differences. For that, more extreme temperature conditions might need to be applied. The presence of fat within the matrix did not influence the morphology either. The ratios between lactose and protein, and between different types of protein, did influence the morphology of the dried particle, and could therefore be relevant to obtain desired powder quality. Systems high in lactose formed smoother particles, while high protein contents resulted in hollow particles. A high MCI content resulted in wrinkling, while a high WPI content resulted in smoother particles

with a vacuole. Upon increasing the oil droplet size, the sessile droplet spreads out more on the hydrophobic surface, which can be attributed to the presence of surface fat.

Different components at the dried droplet's surface were detected with confocal Raman microscopy. Because of the large overlap in the Raman spectra of the pure components, peaks that are specific for individual components were used to identify the presence of the components. The obtained results were used to draw qualitative conclusions, but no quantitative data could be obtained with this technique For most of the dried droplets investigated, the surface was composed of a mixture of lactose and proteins. This is desired since the presence of fat on the surface increases the level of lipid oxidation and promotes caking of the powder. Nonetheless, surface fat was detected for the samples High in fat and High in WPI. As the surface fat of the sample High in WPI could be related to the formation of a vacuole which may result in hole or crack formation, morphology development should be one of the focus points when developing a fat-containing spray dried product.

Fat-free samples showed evidence of stratification of small components on the surface of the dried droplets. It is interesting to note that this observation, as well as some of our other results, were not always in line with earlier work (Both, Nuzzo, et al., 2018; Nuzzo et al., 2017). These authors focused on the surface composition of larger droplets dried at constant air temperatures. The differences that we obtained therefore indicate that the temperature-time trajectory is important for the surface composition, just as it is for the general drying behavior and inactivation of heat-sensitive components (Eijkelboom, Gawronska, et al., 2024). As the temperature-time trajectories applied in our work are more in line with realistic spray drying conditions, it is expected that these give a better indication of the surface composition of industrially spray dried powders. Future research on the component segregation of multicomponent dairy systems at the pilot scale should be performed to verify this.

Appendix 5
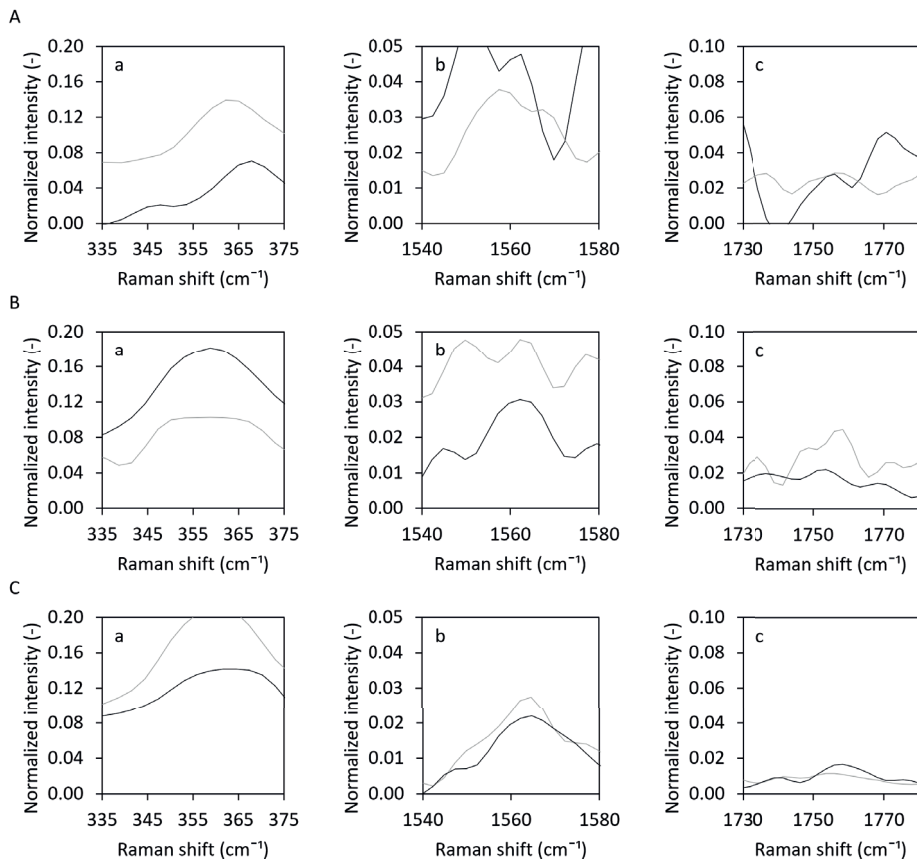
Figure 5.A.1. Duplicate of the normalized Raman intensity at the lactose (a), protein (b) and fat (c) specific Raman shifts for dried droplets of the Standard composition dried with the standard drying conditions (2 s 220 °C 20 L/min + 28 s 80 °C 10 L/min) with an oil droplet size of 0.08 µm (A), 0.2 µm (B), or 0.4 µm (C), different lines indicate the different samples.

Chapter

6
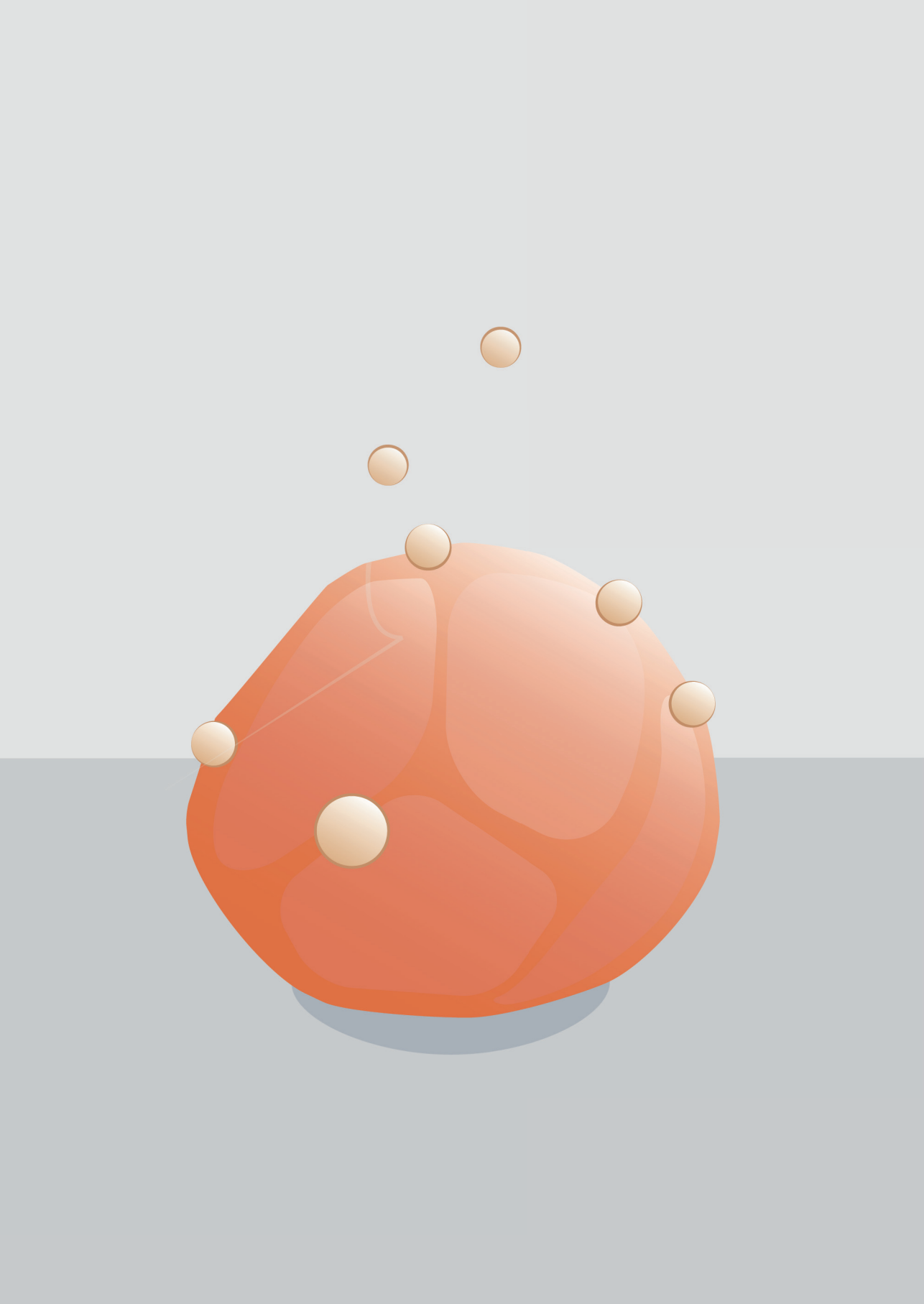
Binary collisions of drying maltodextrin droplets and glass beads

N.M. Eijkelboom
V.J. Rang
S. Breevaart
R.M. Boom
P.F.C. Wilms
M.A.I. Schutyser

Abstract

Spray drying is often used in combination with agglomeration to produce powders with good functional properties, yet the mechanistic understanding of this agglomeration is limited. This research is a fundamental study into the binary collision dynamics underlying agglomeration, identifying specific collision outcome regimes. A sessile single drying droplet was subjected to collisions with glass beads. For maltodextrins with a dextrose equivalent of 6, 21 and 38, collisions were performed at different time points in the drying process. A shift in the collision outcome was observed during drying. The transition from merging as sole collision outcome to a regime where also sticking and bouncing were observed was linked to the locking point of the drying droplet. The sticking regime was observed from 0.75 to 1.5 $t_{collision}/t_{lock}$. This indicates that precise timing of the collisions between drying droplets and dry fines is needed to optimize the agglomeration within a spray dryer.

Introduction

During spray drying a liquid feed is atomized into droplets which are then transformed into a dried and agglomerated powder. Spray dried powder particles can be characterized by their size and degree of agglomeration, which co-determines their techno-functional properties (Buchholz et al., 2022). Agglomeration can be enhanced after spray drying by using a spray fluidized bed. This process has already been extensively studied, and models have been developed to simulate the process (Du et al., 2022; Terrazas-Velarde Korina et al., 2011). However, agglomeration can also occur within a spray dryer. After atomization, droplets in a spray can collide. With an increasing frequency of droplet collisions the degree of agglomeration increases, thereby improving the rehydration properties of the final powder (van Boven et al., 2023). The presence of dried particles that have hardly agglomerated is less desired in spray dried powders, as these small particles negatively affect the flowability, dispersibility and handling properties (Fröhlich et al., 2021).

During spray drying, small particles, also called fines, are usually recovered during subsequent fluidized bed drying, and are recirculated into the spray dryer, where they can enhance the agglomeration by colliding with drying droplets (Williams et al., 2009). The collision between a fine particle and a drying droplet can lead to merging, sticking or bouncing off each other (van Boven et al., 2023). When the drying droplet is still very liquid, the fine particle will generally merge with the droplet, leading to one single dried circular particle. At later stages in the drying process, the droplet is more rigid, and the fine particle may bounce off, which does not lead to any agglomeration. Successful collisions are those that result in an intermediate between merging and bouncing: the fine particle sticks onto the surface of a droplet but does not (fully) merge with it. Several of these sticking collisions lead to the formation of agglomerated powder particles which is therefore desired. During spray drying, recirculation of fines is done to enhance the formation of agglomerates during so-called nozzle zone agglomeration, but this is hitherto empirical and needs to be adjusted for every ingredient (Fröhlich et al., 2023; van Boven et al., 2023). Better mechanistic understanding of the collision process between particles and drying droplets is important for finding rational guidelines for nozzle zone agglomeration.

It is virtually impossible to obtain this mechanistic understanding on droplet-droplet and droplet-particle collisions within a spray dryer, as countless collisions occur simultaneously at different stages of the drying process. Earlier research focused primarily on binary collisions of wet droplets (Finotello, De, et al., 2018; García Llamas et al., 2024), however, for agglomeration especially collisions between drying droplets and fine particles are relevant. Fewer studies focused on droplet-particle collisions. For example, collisions were studied between water droplets and glass beads (Pawar et al., 2016). Unfortunately this does not allow the evaluation of the drying stage on the outcome of the collisions, as sticking and bouncing is not observed with water droplets. The observation of different collision regimes, i.e. merging, sticking and bouncing, requires collisions between drying solute-containing droplets and solid particles, which has not been studied yet. Therefore, in this study, we examine binary collisions between drying sessile droplets of maltodextrin

solutions and small glass beads, representing the fines that are conveyed in a hot air stream in a spray drying process.

We use a modified single droplet drying (SDD) setup to study these binary collisions. Single droplet drying (SDD) studies are common to investigate the impact of the drying conditions on heat sensitive components or particle morphology development, and thereby improve our understanding of the spray drying process (Eijkelboom, van Boven, et al., 2023). Previous SDD research has shown that the choice of the solute and the drying conditions both influence skin formation and the subsequent development of the morphology of the drying droplets (Eijkelboom, Swinkels, et al., 2023; Siemons et al., 2020). For example, maltodextrins with a high dextrose equivalent (DE) show later locking points and give different droplet morphology than maltodextrins with a low DE. In addition, the skin of dried droplets made with high DE maltodextrin was predominantly viscous, while those with low DE maltodextrins formed an elastic skin (Siemons et al., 2020). These differences in locking point and rheological properties of the skin are expected to also influence the sticking behavior after a collision between a drying droplet and a particle.

The objective of this study is to identify the regimes for merging, sticking and bouncing with colliding drying droplets and particles. For this we characterize the drying droplet-particle collision behavior for maltodextrins of varying dextrose equivalent, i.e. DE6, 21 and 38, and glass beads. To create the unique possibility to investigate collision between a drying droplet and a dry particle, a single droplet drying system is adapted, by adding a dispensing system for glass beads, upstream in the air flow. The collisions are observed using high-speed imaging, and the collision outcomes are coupled to the collision parameters, drying conditions and evolving viscoelastic properties of the drying droplets. To relate the collision outcomes to the transient viscoelastic properties of the surface of the drying droplets, we employ a previously developed model for single droplet drying (Eijkelboom, Gawronska, et al., 2024). This drying model builds on work earlier developed by Siemons et al. (2022) and predicts the transient rheological properties of maltodextrin solutions during drying as function of the drying time and location inside the droplet.

Materials and methods

Sample preparation
Maltodextrin with a DE of 6, 21 or 38 (MD6, MD21 and MD38, respectively) (Roquette Frères, France) was added to demi-water and stirred for 30 min to obtain transparent 20% (w/w) solutions. The molecular weight distribution of the maltodextrins can be found in Appendix 6.A.

Single droplet drying with collisions

The single droplet drying platform used in this study is an extended version of the platform used in previous work (Eijkelboom, Gawronska, et al., 2024) and is schematically illustrated in Figure 6.1 (Technical Development Studio, Wageningen, the Netherlands). Before a droplet was dispensed, the drying tunnel was preheated for 30 s using air of 80 °C with a flow rate of 10 L/min (0.4 m/s) with the camera backlight (PFBR 150SW MN (CCS Inc., Japan) with ½" x 12", flexible fiber optic light guide (Edmund Optics, United States) and 28 mm fiber-lite focusing assembly for hybrid/semi-rigid (Edmund Optics, United States)) turned off. Next, the air flow was stopped to allow the drying table (i in Figure 6.1) to cool to 50 °C. When the drying table was at 50 °C, the camera backlight was turned on. To prevent extensive heating of the drying tunnel by the light source, the glass in between the light source and the drying tunnel was covered with a heat repellent foil that blocks infrared radiation but allows most of the visible light to pass through (GSW® Ice Cool super plus 78 Extern, Raamfoliewebshop, the Netherlands).
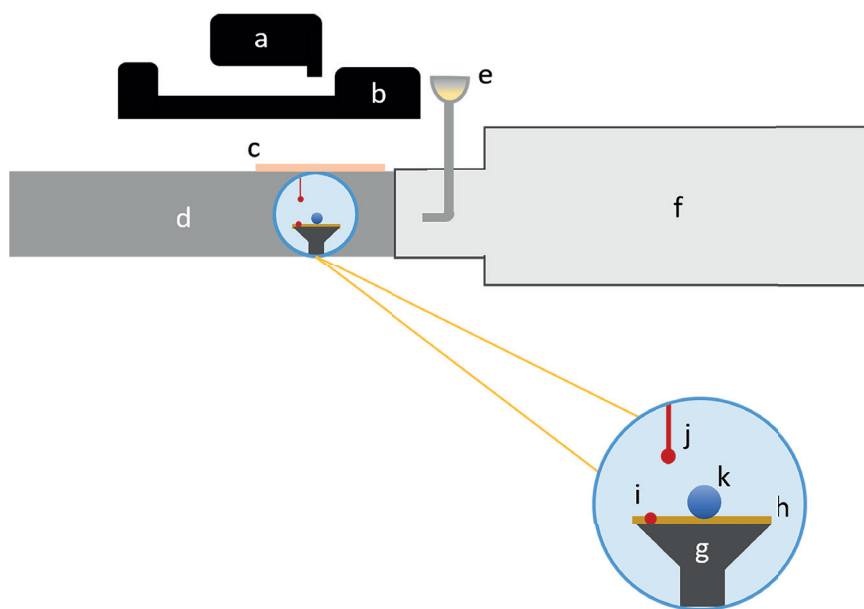
Figure 6.1. Schematic overview of the sessile single droplet drying platform with dispenser (a), stroboscope (b), automated shutter (c), drying tunnel (d), powder reservoir (e), electric heating block (f), drying table (g), hydrophobic tape (h), thermocouple to measure contact surface temperature (i), thermocouple to measure air temperature near the droplet (j) and droplet (k).

A single droplet (initial radius of 200 ± 15 μm) was dispensed using a PipeJet® NanoDispenser (BioFluidix, Germany) equipped with 500-S, coated PipeJet® Pipes (BioFluidix, Germany). A stroboscope (BioFluidix, Germany) connected to BioFluidix Controle Software V2.9 (BioFluidix, Germany) was used to control the droplet volume.

The droplet was dispensed onto a piece of PTFE coated glass fabric (PTFE glass fabric 0.18 AD, self-adhesive, High-tech-flon, Germany) to attain an almost spherical droplet. Once the droplet was dispensed, an automated shutter covered the small opening at the top of the drying tunnel, preventing the loss of hot air during drying. To dry the droplet, dry air (absolute moisture content of 3.5 g/kg) with a temperature of 80 °C and a flow rate of 10 L/min (0.4 m/s) was supplied to the droplet for 30 s. These conditions represent the outlet air of a spray dryer, and result in a drying rate allowing the accurate investigation of different collision regimes. The temperature and of the air in the drying tunnel (6 mm above the drying table) during these 30 s are indicated in Figure 6.2.
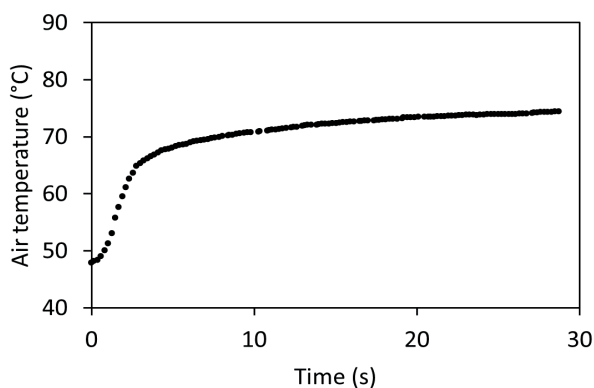

Figure 6.2. Temperature of the drying air near the droplet (j in Figure 6.1) as applied during the drying experiments in this research.

To introduce fine particles in the airstream and induce collisions, a funnel was employed to dose the particles close to the outlet of the heating blocks. For every experiment, around 25 mg of glass beads (70-110 µm, density of 3.22 kg/m³, EPCE Bouwstoffen B.V., the Netherlands, see Appendix 6.B for the exact size distribution) were added into the funnel. The particles were released using an automated control system. At a pre-selected time (1 to 10 s, with 1 s intervals), the beads flowed down the funnel and entered the heated air stream. The beads were entrained by the air stream and travelled towards the drying droplet. A few of these collided by chance with the drying droplet. The total number of collisions observed for droplets with MD6 was 106, for droplets with MD21, 226, and for droplets with MD38, 99.

The drying process and collisions were recorded with a high-speed camera (C-VIT, AOS Technologies AG, Switzerland) with a VZMTM 1000 Zoom Imaging Lens (Edmund Optics, Japan). Recording occurred in three blocks with different frame rates: before the collisions, during the collisions, and after the collisions. Before and after the collisions the camera operates at a frame rate of 100 fps, while a frame rate of 10,000 fps is used during the collisions. The movies are used to visually observe the locking point, i.e. the first point at which shape deviation from a sphere is visually observed (Siemons et al., 2020). A MATLAB (MATLAB R2018b, MathWorks, United States) image analysis script

was used to determine the droplet size until the locking point. The collision outcomes (merging, sticking or bouncing) were observed with the high-speed clips. The clips were analyzed with a MATLAB (MATLAB R2018b, MathWorks, United States) image analysis script to determine the collision speed, the collision angle and the impact parameter. The collision angle was determined relative to the surface contact line of the sessile droplet (Figure 6.3A). The measurement was performed with the camera footage and was determined based on the exact droplet shape at the time of collision. Only collisions with a collision angle between 0° and 90° were taken into account. To calculate the impact parameter (B), a slightly adapted version of the definition as generally used for the impact parameter between two free-flying droplets is used (Finotello, De, et al., 2018). Assuming that the path of the glass beads is parallel to the drying table, the impact parameter (B) was defined as the distance between the center of the droplet and the bead (b), normalized by the height of the drying droplet (h_d) and the diameter of the bead (d_b):

$$B = \frac{2b}{h_d + d_b}$$
(6.1)

As a result, the impact parameter can have values between -1 and 1 (Figure 6.3B); a value of zero implies a collision where the centers of both particles are on the trajectory of the particle, a value of 1 indicates a collision at the top of the droplet, and a value of -1 indicates a collision at the bottom of the droplet.
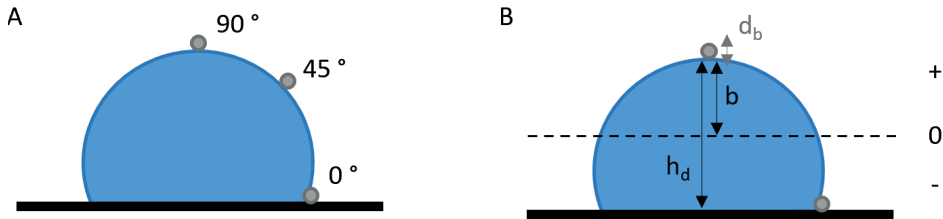
Figure 6.3. Schematic representation of the determination of the collision angle (A), and the impact parameter (B).

Single droplet drying model

To predict the drying behavior and rheological properties of the drying droplet, we used a model that was developed earlier by Siemons et al. (2022), and that was adapted as described in earlier work (Eijkelboom, Gawronska, et al., 2024; Eijkelboom, Swinkels, et al., 2023). The model is a one-dimensional (1D) effective diffusion drying model, considering the droplet to be a spherical cap. This cap is divided into numerical shells of the same volume, and evaporation and heat flux is calculated per shell. For a full description of the model and equations we refer to our earlier work (Eijkelboom, Gawronska, et al., 2024; Eijkelboom, Swinkels, et al., 2023; Siemons et al., 2022). The external mass transfer coefficient of the model was calibrated using the data of a water droplet without solute (no internal diffusion limitation) drying under the exact same conditions as all other

experiments performed in this research. This indicated that the external mass transfer coefficient had to be adapted to $\beta_{ext,sessile} = 0.15 * \beta_{ext,sphere}$ (Appendix 6.C).

Data analysis for the collision outcomes

For the collision outcomes, data analysis was performed using Python (Python Software Foundation, United States) (van Rossum & Drake, 1995) using external libraries for data handling (McKinney, 2010), statistical analysis (Seabold & Perktold, 2010; Virtanen et al., 2020) and data visualization (Hunter, 2007). Reproducible computational workflows were established using Jupyter Notebooks (Project Jupyter, United States) (Kluyver et al., 2016), which can be made available upon request.

Kernel density estimation is used to generate probability plots. To compare the average collision speed, the collision angle and the impact parameter between the droplets with different maltodextrins and between the different collision outcomes, a two-way ANOVA followed by a Tukey HSD post-hoc test was performed. Assumptions of ANOVA were validated through Shapiro-Wilk Test for normality, visual inspection of Q-Q plots and Levene's test for homogeneity of variances.

Results and discussion

Skin formation of the drying maltodextrin droplets

The visually observed locking point is often linked to the skin formation point, the point in time when a solute-rich skin has formed at the outside of the droplet. As the formation of such a skin is expected to influence the collision outcomes, the locking point is expected to be an important parameter to characterize collisions. For the specific settings applied in this research, the locking points of drying droplets containing MD6, MD21 and MD38 were observed at 3.1 (± 0.3), 4.8 (± 0.6) and 6.6 (± 0.3) s, respectively. Previous research into the drying behavior of maltodextrins already revealed an earlier locking point for droplets containing a maltodextrin with lower DE values. A lower DE value also results in a higher moisture content at the locking point and a slower temperature increase after the locking point. There are also differences in skin development and morphology: a solute with a low DE value develops a skin that quickly acquires elasticity, resulting in smooth, hollow particles. A solute with high DE values results in the formation of a more flexible and more viscous skin which generally leads to denser and more wrinkled particles (Eijkelboom, Swinkels, et al., 2023; Siemons et al., 2020).

Collisions between sessile drying droplets and glass beads

When a glass bead collides with a sessile drying droplet, three different types of results can be observed. The first possibility is that the droplet and the particle merge, when the glass bead collides with the droplet and sinks into it (Figure 6.4, Appendix 6.D). The second possibility is sticking. In this case, the glass bead collides with the droplet and remains located at the surface of the droplet (Figure 6.4, Appendix 6.D). The third possible result is bouncing: the glass bead collides with the droplet, but is taken up by the airflow again (Figure 6.4, Appendix 6.D).
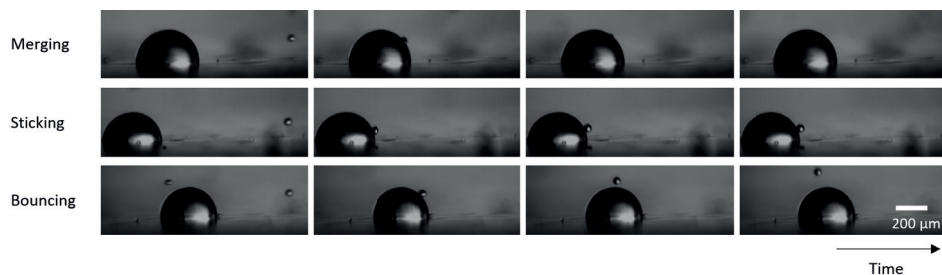
Figure 6.4. Different possible collision outcomes when a glass bead hits a sessile drying droplet.

Differences in rheological properties of maltodextrins with different DE values are expected to influence the collision outcomes for a drying droplet and a dry particle. To investigate this, the collision outcomes are studied for three different drying maltodextrins (Figure 6.5A) as a function of collision time. We observed that the start of the sticking regime was delayed when using a maltodextrin with a high DE value. As a high DE value results in a later locking point, it takes longer until the droplet is dry enough that not all collisions will result in merging. Also, the onset of the bouncing regime is later, as the skin is more viscous compared to the more elastic skins formed for low DE maltodextrins. Due to the slower changes in the rheological properties, the merging and sticking regimes are also spread over a longer time.
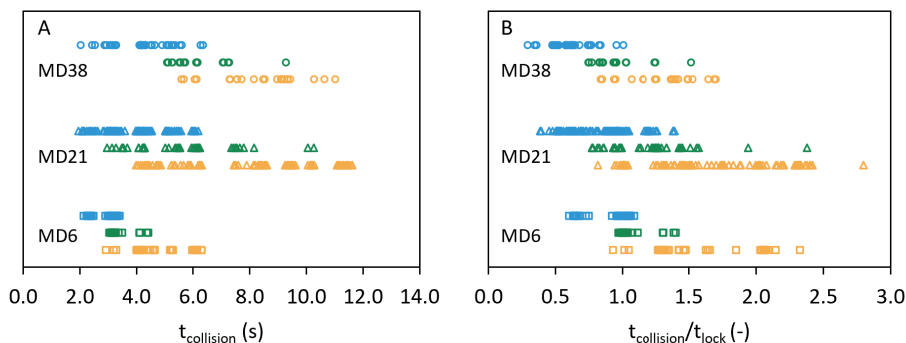
Figure 6.5. Collision outcomes over time (A) and over normalized time (B) for maltodextrin DE6 (squares), DE21 (triangles) and DE38 (circles), with merging indicated in blue, sticking in green, and bouncing in yellow.

As the formation of a skin will influence collision outcomes, the collision time was normalized with respect to the average locking point time (Figure 6.5B). After normalization, the distribution of collision outcomes for different maltodextrins shows more similarity, indicating the relevance of the locking point in the collision process. Merging is already observed from the start of the drying process but continues until after the locking point. For all three DE values, the first observation of sticking is at $t_{collision} \approx 0.75\ t_{lock}$, with this onset point of the sticking regime being somewhat earlier if

the DE value is higher. Based on the experiments, the endpoint of the sticking regime is at $t_{collision} \approx 1.5\ t_{lock}$ for all DE values, except for a few outliers. By the time that sticking is observed, some collisions also result in bouncing. Bouncing then continues to be observed from the locking point onwards and becomes the only type of collision outcome after the sticking regime has ended.

There are several factors influencing the collision outcome, and since not all of those can be controlled in our experiments, the collision outcomes are partially stochastic. Local differences in skin properties due to inhomogeneous drying of the droplet, small variations in locking points, as well as differences in droplet and glass bead size will add a level of randomness to the outcomes. Probability plots can be generated based on kernel density estimation to visualize the chance of observing a specific collision outcome (Figure 6.6). The probability plots indicate that the maximum probability of observing sticking differs per maltodextrin type, with the highest probability observed for MD38. These differences might be caused by the rheological properties of the skin that is formed. The viscous skin that is formed for maltodextrins with a high DE value promote sticking more than the elastic skins for maltodextrins with a low DE value (Siemons et al., 2020). Note that, because of the relatively limited sample size for each point in time, the kernel density algorithm also estimates the (small) chance of observing a specific collision outcome at a point in time when it was not observed experimentally. The probability plots for example show a slight probability of observing bouncing already before a probable collision outcome of sticking is observed.
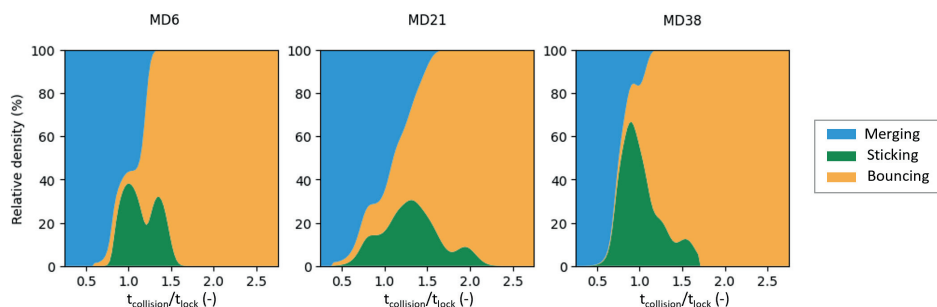
Figure 6.6. Stacked area charts for different maltodextrins based on kernel density estimation values relative for each collision outcome across $t_{collision}/t_{lock}$ (-).

Influence of the collision speed on collision outcomes

At the times when a collision could result in several outcomes, it is expected that other factors than drying time might determine the collision outcome. For colliding liquid droplets, it is known that the Weber number, the ratio of the inertial forces to the cohesion forces such as surface tension, co-determines the collision outcome. Since the collision velocity is a factor in the inertial forces, it impacts the Weber number and hence the collision outcome of wet collisions (Finotello, Kooiman, et al., 2018; Li et al., 2016; Qian &

Law, 1997). It is expected that collision velocity will also influence the outcome of a collision between a drying droplet and dry particle.

Although the speed of the air entraining the colliding particles was kept constant at 0.4 m/s, differences in collision speed were observed. The observed speeds ranged from 0.3 to 3.0 m/s, which is similar to the relative collision speeds observed within a spray dryer, i.e. 0.5-3.5 m/s, as mentioned in other research (Hussain et al., 2022; Li et al., 2016). However, within the range of collision speeds that we observed, the speed had no clear impact on the collision outcome. This is also evidenced by the distributions of the frequency of the types of outcomes as function of the collision speed, for all different collision outcomes and maltodextrin types (Figure 6.7). Only between MD6 and MD21 a significant difference in speed for bouncing outcomes was observed (mean difference 0.25 m/s, p = 0.036).
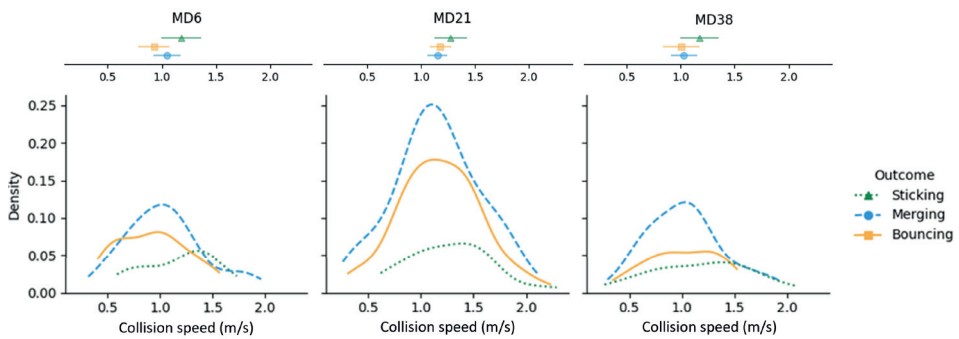
Figure 6.7. Confidence interval and density plots for collision speed, comparing outcomes and experiments.

Pawar et al. (2016) did observe an influence of the Weber number on collision outcome for collisions between solute-free water droplets (initial diameter of 2939 ± 125 μm) and glass beads (diameter of 2500 or 4000 μm). The relative velocity in their experiments ranged from 0.065 to 1.15 m/s, partially overlapping with our collision speeds. Within the work of Pawar et al. (2016), it was observed that the collision outcomes changed from resulting in agglomeration to showing stretching separation upon increasing the Weber number. The difference in the (relative) sizes of the droplet and particle compared to our experiments could have contributed to the different observations of the impact of the Weber number. The smaller droplets (initial diameter of 400 μm) and glass beads (diameter of 30-110 μm) in our experiments result in a lower Weber number, possibly being below the limit to observe an influence on collision outcome. For these smaller particles, the relative velocity differences may therefore not be important. In spray dryers, a similar size difference between drying primary particles and colliding fines is expected, but it remains to be verified if one can extend these observations.

Influence of the collision angle on collision outcomes

Previous research on binary collisions focused on free flowing, non-drying droplets, being uniform in shape and composition. The presence of a hot surface on which the sessile droplet is deposited, hinders the droplet from drying completely uniform. Therefore, the location of the collision, which can be indicated by the collision angle (Figure 6.3A), could potentially influence the collision outcome in this situation. For MD21 a significant difference in collision angle distribution between bouncing and merging (mean difference of 8.9°, $p = 0.041$), and between bouncing and sticking (mean difference of 14.4°, $p = 0.012$) was observed, showing that a small collision angle more often resulted in bouncing. This could be when the lower part of the droplet, closer to the contact surface area, dries faster, leading to an earlier change from sticking to bouncing. Although no significant difference was observed for MD6, the trend of more frequent bouncing at a lower collision angle seems to be present (Figure 6.8), but might be non-significant due to the lower sample size. The trend was not observed for MD38 (Figure 6.8). The differences between the different maltodextrins could be a result of their different rheological properties. An elastic skin that quickly becomes glassy as for MD6 and MD21 will result in more bouncing, while the more viscous skin of MD38 still shows more sticking.
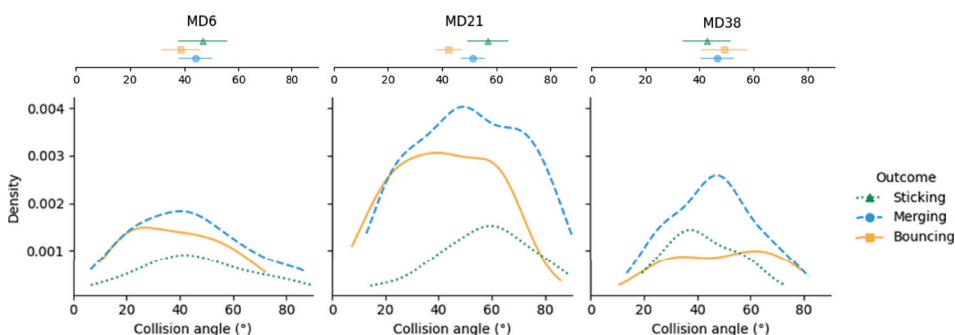
Figure 6.8. Confidence interval and density plots for collision angle, comparing outcomes and experiments.

Influence of the impact parameter on collision outcomes

The impact parameter, as calculated from Eq. (6.1), was expected to influence the collision outcome. The impact parameter is related to the collision angle (Figure 6.3), because they both take the position of the collision into account. Next to this, the impact parameter is based on the size of the droplet and bead, which in principle is kept constant in our experiments, but does show some natural variation.

Previous work on droplet-droplet interactions revealed that a change in impact parameter did influence the collision outcome, with a general trend of collision outcomes changing from reflexive separation, to coalescence, to stretching separation, to bouncing upon an increasing impact parameter (Finotello, Kooiman, et al., 2018; Qian & Law, 1997). The impact parameter was also found to impact the outcome of collisions between water

droplets (initial diameter of 2939 ± 125 μm) and glass beads (diameter of 2500 or 4000 μm), with an increase in impact parameter resulting in the collision outcome changing from agglomeration to stretching separation (Pawar et al., 2016).

For the experiments performed in this study, there was, however, no influence of the impact parameter on the collision outcome (Figure 6.9). For all different maltodextrins and outcomes, no significant differences in impact parameter distribution were observed. An important difference between the previous research and our current work is that previous research made use of two moving objects, while we use a stationary droplet. In previous research, the distance between the droplet centers was determined in the plane perpendicular to the relative velocity vector. Because of the stationary droplet in our work, and the assumption of the glass bead flying parallel to the surface that the droplet is sitting on, the relative velocity vector is constant in our case. The differences in experimental procedure and in the approach of obtaining the impact parameter might contribute to the difference in observed influence. In addition, the two-dimensional, instead of three-dimensional, observation of the collision outcome could result in small mismatches between the real and observed impact parameter, if the glass bead does not move in the center plane. As the collision angle and impact factor are highly correlated factors, the difference in the correlations found with collision outcomes is surprising. This most likely has to do with the mathematical concept behind the kernel density estimation. The estimation values are relative to the total area under the density curve, and differs between the contact angle and impact parameter due to different scales on the x-axis.
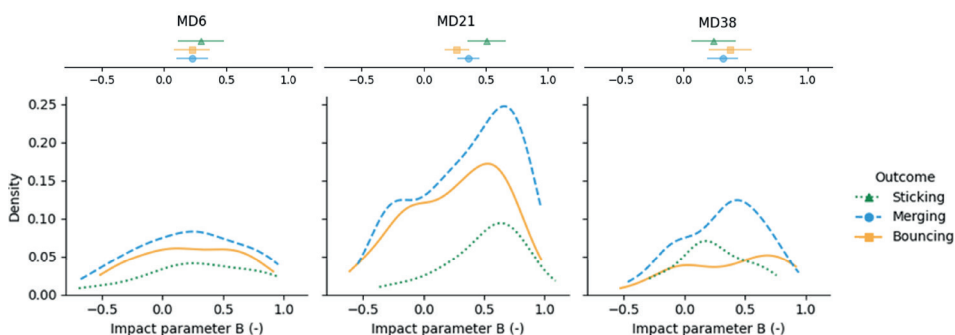
Figure 6.9. Confidence interval and density plots for impact parameter, comparing outcomes and experiments.

Modelling

Based on the experimental results, the time of collision with respect to the locking point of the drying droplet is the main parameter to indicate the collision outcome. Experimental data showed that sticking generally occurs when $t_{collision}/t_{lock}$ is between 0.75 and 1.5, and the kernel density algorithm estimates this timeframe to be even a bit wider. To get a rough estimation if sticking can occur at a specified time, it would therefore be desired to predict the locking point of the drying droplet with a model. Previous work has already focused on

the development of a sessile single droplet drying model to predict the change in droplet volume, (uniform) droplet temperature and rheological properties (Eijkelboom, Swinkels, et al., 2023; Siemons et al., 2022). This showed that, for maltodextrins with different DE values, at the skin formation point the change in concentration of maltodextrin in the outer shell can be linked to specific rheological properties. The skin formation point was indicated by the steepest increase in the logarithmic value of the storage modulus (log G') in combination with a characteristic change in the loss factor (tan δ) (Siemons et al., 2022). Also the onset of the increase in droplet temperature has been linked to the locking point (Eijkelboom, Swinkels, et al., 2023). Therefore, having a single droplet drying model that properly predicts the drying behavior and change in rheological properties of the droplet as examined in our experiments, will help to make predictions on locking point and collision outcomes.

Calibration of the existing single droplet drying model with a pure water droplet showed us that the external mass transfer coefficient had to be adapted to $\beta_{ext,sessile} = 0.15 * \beta_{ext,sphere}$ (Appendix 6.C). This adapted model was applied for the different drying maltodextrin systems used in this research (Figure 6.10).

Figure 6.10. Model predictions related to droplet temperature and volume development (including experimental data in green), and rheological development the outer volumetric shell of drying particles of 20% maltodextrin DE 6, 21 and 38 solutions, with the mutual solute-water diffusion coefficient based on the Darken relation.

The rapid temperature increase, steepest increase in log(G') and characteristic change in tan δ happen, respectively, at 8.7, 8.8 and 9.0 s for MD6, MD21 and MD38. The trend of having a later locking point for higher DE values does align with the experimental results. Nonetheless, the predictions deviate quite substantially from the experimentally

observed locking points (respectively 3.1 (± 0.3), 4.8 (± 0.6) and 6.6 (± 0.3) s). To find the cause of this deviation, sensitivity analyses were carried out for the external mass transfer coefficient and number of volumetric shells (results not shown). In case of the mass transfer coefficient, a larger mass transfer coefficient results in an earlier locking point, but it also results in a faster decrease in droplet volume, which no longer matches the experimental observations. Considering the good match between predicted droplet volume decrease and experimental results (Figure 6.10), the external mass transfer coefficient was therefore assumed to be correct. In the case of the number of volumetric shells, an increase in number of shells would make the simulation of a thin skin layer more accurate, and could thereby result in a different timing of characteristic changes in rheological properties. However, no such effect was observed. By using 40 volumetric shells, for MD6 the outer shell has a thickness of 0.80 μm and a moisture content of 0.54 g/g at the locking point. After increasing the number of volumetric shells to 400, the outer shell still had a moisture content of 0.52 g/g at the locking point, which is not a sufficient reduction to make a substantial difference. Another possible explanation for the differences between experiment and model could be a discrepancy between the calculated and actual mutual solute-water diffusivity. A difference in the mutual solute-water diffusivity in the droplet would result in the same, correct, predictions for the total volume decrease, but would influence the timing of the changes of the properties of the outer shell of the droplet. The current model uses the mutual diffusion coefficient that is based on the Darken relation to calculate the internal water diffusion. Alternatively, one can use the formula obtained by Räderer et al. (2002) which is based on experiments with maltodextrin DE33 (Figure 6.11). This formula has also been applied in a previous single droplet drying model by Perdana et al. (2013). The diffusion coefficients as a function of the water content based on the Darken relation for MD21 and based on the relation suggested by Räderer et al. (2002) can be found in Appendix 6.E.

With this adapted version of the model, the predicted rapid temperature increase, steepest increase in log(G') and characteristic change in tan δ all happen at 6.8 s, independent of the DE value of the maltodextrin. For MD38, this aligns well with the experimentally observed locking point. For MD6 and MD21, the predicted locking points are closer to the experimental locking point than for the model with the mutual solute-water diffusion coefficient based on the Darken relation, but do still deviate. It is known that the diffusion is dependent on the type of solute present, with a general decrease of the diffusivity of water as the molecular weight of the solute increases (Adhikari et al., 2002). However, maltodextrins consist of a mixture of molecules with different molecular weights and the specified DE value thus represents an average. Unfortunately no information is presented regarding the true molecular weight distribution of the MD used by Räderer et al. (2002). Nonetheless, it is expected that the molecular weight distribution of their maltodextrin DE33 is closest to our MD38. In the case of MD21 and MD6, the average molecular weight will be higher and will thus show a lower diffusivity than what is currently predicted. This will result in an earlier locking point, which is in line with the experimental observations. By using the diffusion equation as suggested by Räderer et al. (2002), the drying model

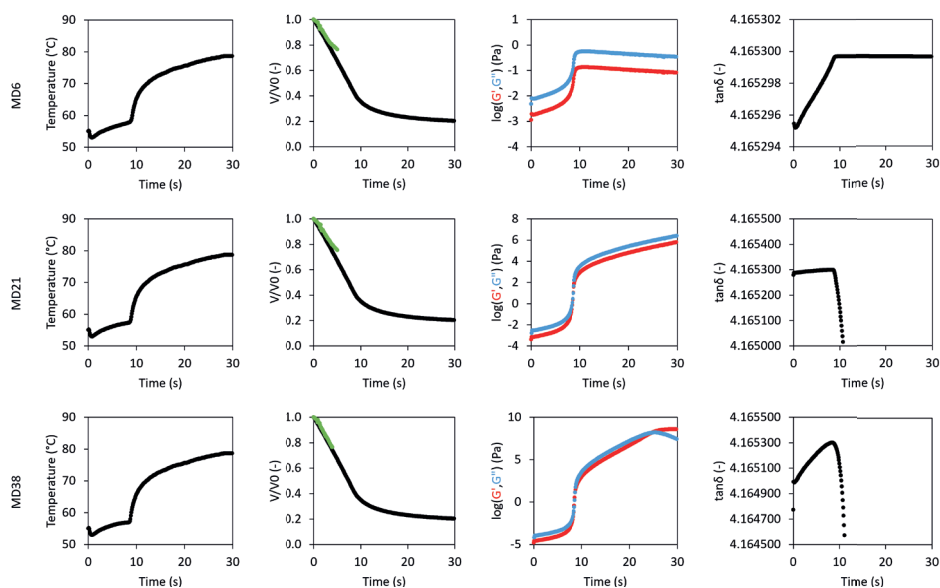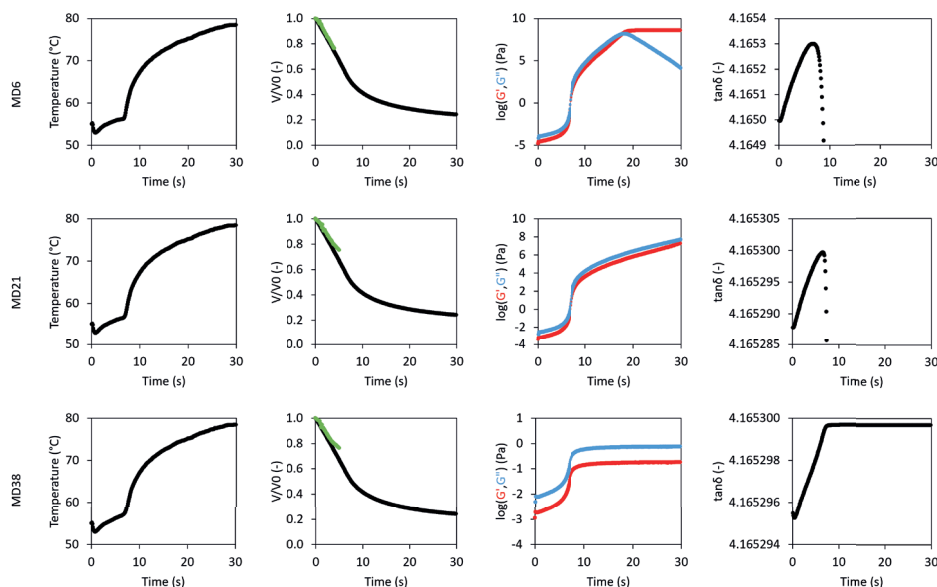**Figure 6.11.** Model predictions related to temperature, volume (including experimental data in green), and rheological development of drying particles of 20% maltodextrin DE 6, 21 and 38 solutions, with the mutual solute-water diffusion coefficient based on Räderer et al. (2002).

already gives a decent first indication of the locking point for maltodextrins with a high DE value. The model can already be used to a get a first indication of the sticking regime that ranges from 0.75 to 1.5 $t_{collision}/t_{lock}$. In the future, more accurate determination of the mutual solute-water diffusivity in different solute systems could help optimize locking point predictions.

Conclusion

To obtain better insight in the collision behavior between drying droplets and fine particles during spray drying, a sessile single droplet drying platform was extended to assess binary collision outcomes between a drying droplet and glass beads. We used drying droplets containing different maltodextrins (DE 6, 21 and 38) and performed collisions at several timepoints throughout the drying process.

Outcomes of the binary collisions depended on the timing of the collision. Collisions at the start of the drying process only resulted in merging, while later in time also bouncing and sticking were observed. The transition from merging to other collision outcomes occurred at different absolute times, depending on the dextrose equivalent of the maltodextrin. For maltodextrins with increasing DE value, the transition to sticking and bouncing occurs later, because of the later locking points of these droplets. If the collision time was corrected for the locking point, the different maltodextrins showed a similar sticking regime, ranging from 0.75 to 1.5 $t_{collision}/t_{lock}$. Due to the formation of a viscous, rather than

an elastic, skin, the maximum probability to obtain sticking was higher for MD38 than for the lower DE maltodextrins.

For all investigated systems, the observed collision outcome over time is stochastic. For the viscous skin forming MD38 no significant impact of collision speed, collision angle or impact parameter on the collision outcome was observed. For low-DE maltodextrins that form an elastic, glassy skin, the collision angle had a minor impact on the collision outcome. Bouncing was more likely to result at low collision angles, i.e. where the droplet is in contact with the support surface and dries faster.

The impact of particle properties, like density, is still to be examined. For now, it is expected that the lower density of the fines in industrial spray dryers compared to the glass beads used in this work will result in more sticking. Work of Hussain et al. (2022) indicated that in order to obtain sticking, the collision velocity needs to be below a specific critical velocity. A decrease in particle density results in an increase in this critical velocity, probably resulting in a larger range where sticking can be observed.

The collision time relative to the locking point is the key parameter to determine the collision outcome. It would therefore be of interest to predict the locking point time, and thereby have a prediction for the collision outcome, with a drying model. A numerical model that combines the drying of a single droplet with the rheological properties of the matrix was used to predict the locking point. The results were in reasonable agreement with the experimentally determined locking points. Especially the mutual solute-water diffusivity is found to play a major role, and accurate determination of the diffusion coefficient could further improve the locking point estimation.

The extended sessile single droplet drying platform allowed us to identify the different collision outcomes for drying droplets and particles. The found consistency of the sticking regime relative to the locking point provides a new step towards better control of agglomeration processes.

6

Appendix 6.A

Molecular weight distributions of the different maltodextrins were determined by High Performance Liquid Chromatography (HPLC) using a Shodex KS-802 (7 μm) 8.0 × 300 (mm) + Guard column. The column is operated at 50 °C and connected to a refractive index (RI) detector (Shodex RI-501). Milli-Q water was used as eluent with a flow rate of 1 mL/min.
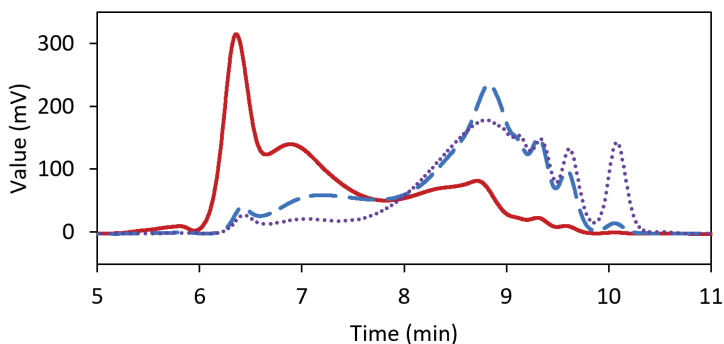
Figure 6.A.1. Molecular weight distribution for maltodextrin DE6 (red full line), DE21 (blue dashed line) and DE38 (purple dotted line). Molecules with higher molecular weight elute first, followed by low molecular weight components.

Appendix 6.B

The size distribution of the glass beads (70-110 μm, EPCE Bouwstoffen B.V., the Netherlands) has been measured with the Mastersizer 3000 with the Aero S dry powder disperser (Malvern Inc, United Kingdom). The gap between the feed tray and hopper was set to 3 mm. An air pressure of 1 bar, a feed rate of 35% and particle analysis based on the Fraunhofer theory was used. Measurements were performed 5 times, and the results of one representative measurement are shown (Figure B.1). The observed D10, DE50 and D90 values were, respectively, 54, 77 and 109 μm.
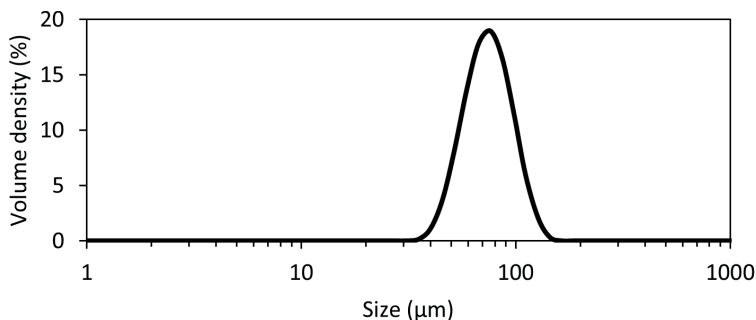
Figure 6.B.1. Size distribution of the glass beads.

Appendix 6.C
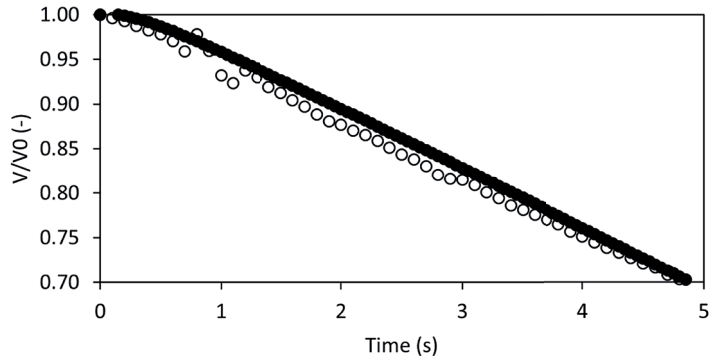
Figure 6.C.1. Volume reduction over time for a drying water droplet subject to dry air (absolute moisture content of 3.5 g/kg) with a temperature of 80 °C and a flow rate of 10 L/min (0.4 m/s) as measured experimentally (open circles) and predicted by the model (closed circles).

Appendix 6.D

Scan the QR code to see the video of different binary collision outcomes.

Appendix 6.E

The predicted moisture diffusion within the droplet depends on the formula applied, the moisture content within the droplet and the temperature of the droplet (Figure E.1).
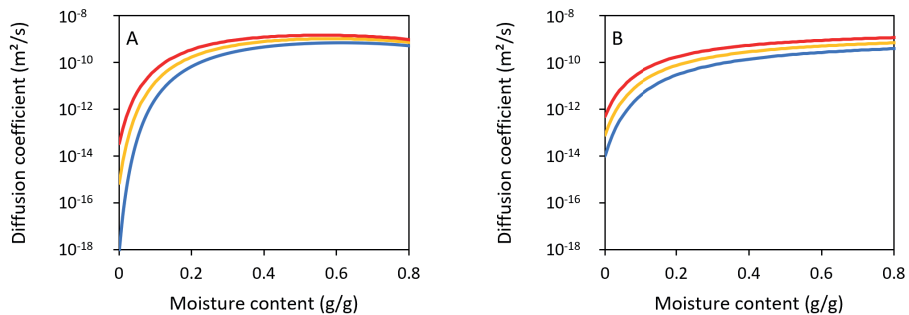
Figure 6.E.1. Diffusion coefficient of water as a function of moisture content as calculated by the Darken relation for maltodextrin DE21 (A) and by the relation suggested by Räderer et al. (2002) (B) at 60 °C (blue), 80 °C (yellow) and 100 °C (red).
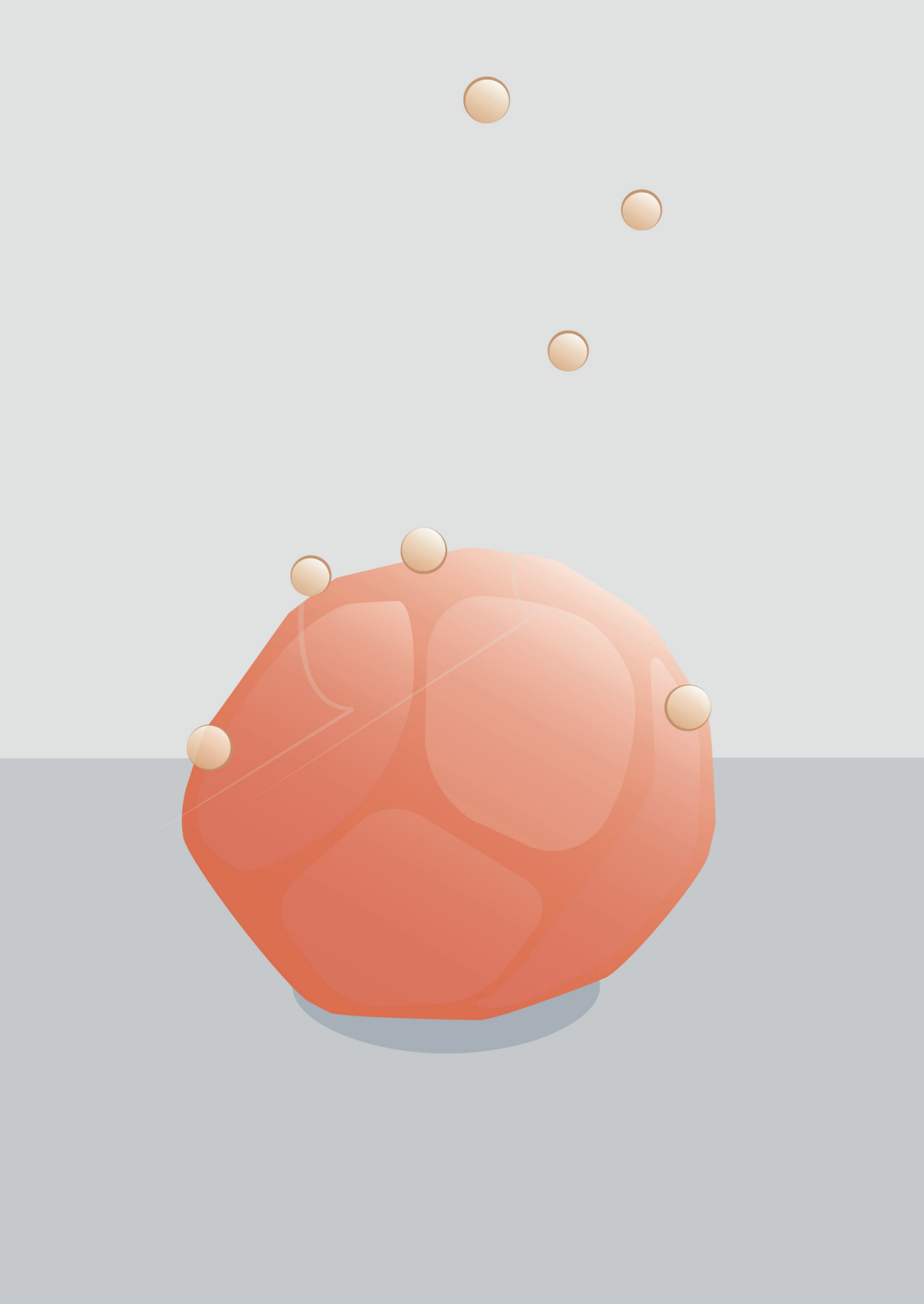
Chapter

7

A multiscale investigation on protein addition toward steering agglomeration and yield in spray drying

A.P. van Boven[1]
N.M. Eijkelboom[1]
K.J. Fentsahm
M.J. Gruson
R.M. Boom
P.F. C. Wilms
R. Kohlus
M.A.I. Schutyser

[1]: Shared first authorship, these authors contributed equally.

Abstract

The positive effect of protein drying aids that reduce the stickiness of sugar-rich products on the spray drying yield is known. However, as agglomeration also depends on stickiness, one can expect an effect of these drying aids on interparticle collisions. Therefore, the effect of protein addition to maltodextrin systems on agglomeration and yield in spray drying was investigated using single droplet drying and pilot-scale spray drying experiments. Single droplet drying was used to compare the sticking regimes of whey and pea proteins at different concentrations. Adding protein increased the chance of creating agglomerates upon forced collisions between a drying droplet and a glass bead. This was reflected in an increased fraction of agglomerated particles in pilot-scale experiments with injection of fines. Pea protein decreased the fraction of non-agglomerated primary particles from 38% to 22% when the protein concentration in the liquid feed was 5% dry basis. In pilot-scale spray drying, protein addition improved the yield. Industrially, these results can be used to steer formulations regarding agglomeration and yield.

Introduction

Many liquid products are dried into powders in the food industry as well as in other industries such as chemicals and pharmaceuticals. Powders have a longer shelf life due to their low water activity, are more convenient for transportation and storage due to their reduced bulk volume. A commonly used process to transform liquids into powders is spray drying. A benefit of spray drying over other drying methods is that it allows for more precise control of the particle size by steering the degree of agglomeration, resulting in superior techno-functional properties such as flowability and reconstitution behavior (van Boven et al., 2023).

Agglomeration is the process during which particles collide and cluster together to form larger structures called agglomerates. In industrial spray drying, agglomeration is enhanced by the recirculation of small particles (fines). These fines are separated from the rest of the product in an internal or external fluid bed, and are reintroduced into the nozzle zone of the dryer. In the nozzle zone, the fines can collide with atomized droplets. To form an agglomerate, it is important that particles not only collide but also stick together. Whether or not they stick depends on the extent of drying. When the droplets are still wet, no structure formation occurs as they merge/coalesce completely. As drying progresses, particles enter the sticky regime, which typically occurs at a temperature of 10 to 30 °C above the glass transition temperature (T_g) (Eijkelboom, van Boven, et al., 2023; Palzer, 2005). While the droplets are sticky, a collision can result in the formation of an agglomerate. As drying progresses further and the surface of the particles becomes completely dry, a collision will result in bouncing, and no agglomerates are formed (Eijkelboom, van Boven, et al., 2023; Gianfrancesco et al., 2009).

Stickiness does not only help to form agglomerates, it is also responsible for undesired fouling in spray dryers. During drying, particles collide with the walls of the spray drying chamber. If the particles are still wet or sticky during such a collision, they adhere to the wall. Ozmen & Langrish (2003) summarized why this is undesired. First, product that deposits on the wall reduces the yield of the drying process and cannot be sold. Second, there is a chance that larger powder lumps fall from the wall and mix with the rest of the product. After being exposed to high temperatures for longer periods of time, this product can be overdried which compromises the quality of the product. Third, continued build-up of material on the walls requires cleaning of the dryer. Finally, powder deposits in the chamber pose a safety risk: especially, powder deposits close to the hot air inlet can become very hot and may start to smolder, eventually leading to a fire or a dust explosion.

Excessive fouling is mainly observed for materials with a low T_g, for example products that are rich in sugar. To reduce fouling, the material-based approach has been developed and is widely used. In this approach, drying aids, also called drying agents, carriers, carrier agents, or wall material, are added to the feed to increase the T_g (Mirlohi et al., 2022). Drying aids are usually high molecular weight compounds, the most commonly used examples being maltodextrins (MD) and gum arabic. A drawback of using these drying

aids is that a high mass ratio may be required, depending on the material. Samborska et al. (2023) reviewed literature about maltodextrin addition for spray drying of honey and fruit juices and found that the drying aid content in the final product for honey may exceed 50% dry basis (db) and varies between 35 and 75% db for different fruit powders. An alternative to using polysaccharides as drying aids is using proteins, which requires less mass addition in the final product. Proteins are efficient drying aids due to their surface activity and film-forming properties (Samborska et al., 2023). During spray drying, proteins accumulate near the surface of the drying droplets, due to their relatively slow diffusion relative to low-molecular weight sugars, and due to their surface activity. Over time, this protein rich layer solidifies into a skin. Because the T_g of this skin is higher than that of the rest of the feed, stickiness is reduced. Mirlohi et al. (2022) reviewed literature on binary sugar-protein model systems and concluded that all types of proteins improve the spray drying yield. The observed relation is dose-dependent until saturation is achieved at only 1-2.5% protein ratio on db. This point varies per protein type. Dairy proteins are usually more effective in improving the yield than plant-based alternatives. However, the altered stickiness might also affect the agglomeration behavior, which affects the powder properties. To date, the impact of protein addition on agglomeration has not been addressed in literature.

While pilot-scale spray drying research can be used to investigate the level of agglomeration of the final product, it does not provide mechanistic insights into the collision behavior. For this, the individual collisions between droplets and particles need to be investigated. Binary collision behavior has been studied for wet droplets, and collision regime maps have been created for these situations (Finotello, De, et al., 2018; Focke et al., 2013). However, for agglomeration in spray dryers, collisions between drying droplets and dry particles are more relevant. Recently a single droplet drying approach was proposed to identify the different collision regimes, i.e. merging, sticking and bouncing (Eijkelboom, Rang, et al., 2024). This approach has been used to identify collision regimes for glass beads and droplets containing maltodextrins of different dextrose equivalents, but the impact of protein addition on collision behavior is still unknown. In addition, the mechanistic insights of obtained collision regimes have not yet been translated to larger scale spray-drying operations.

Therefore, with this research we aim to quantify the effect of protein addition on multiple scales, namely on the collision behavior on single-droplet scale and agglomeration and yield on pilot-scale. Ultimately, these results can be used to develop guidelines to optimize product formulation to facilitate agglomeration and reduce fouling in spray drying. Maltodextrin with a dextrose equivalent (DE) of 38 was used as model system for sugar-rich products. Different concentrations of protein were added to assess changes in collision behavior. A dairy protein (whey protein isolate (WPI)) was compared to a plant-based alternative (pea protein isolate (PPI)). Collisions between drying single droplets and glass beads were performed to investigate collision outcomes over time and to create probability plots for the collision outcomes. Next, the findings were extended with pilot-scale trials in which both agglomeration by morphology assessment and yield were investigated.

Materials and methods

Materials

Maltodextrin DE38 (MD38) (Glucidex 38, Roquette Frères, France, molecular weight of 474 g/mol) was used as model material. The proteins used were whey protein isolate (WPI) (FrieslandCampina, the Netherlands) and pea protein isolate (PPI) (Nutralys S85F, Roquette Frères, France). In the pilot-scale experiments, antifoam was added to the feed solution (Antifoam A concentrate A5633 (Sigma Aldrich, USA) dissolved in 1,2-propanediol (Merck, Germany)). Maltodextrin DE21 (MD21) (Glucidex 21, Roquette Frères, France) was used to produce the fine particles used in the pilot-scale experiments. For the binary collision studies, glass beads with a size of 70-110 μm were used (EPCE Bouwstoffen B.V., the Netherlands). The protein size was analyzed using SDS-PAGE supplied by Bio-Rad (Bio-Rad Laboratories B.V., the Netherlands).

Protein characterization

Protein size

The protein composition of both protein isolates was analyzed using SDS-PAGE. Solutions of 2 mg/mL and 5 mg/mL from both protein isolates were made in Milli-Q water. The samples were heated for 30 min at 60 °C and subsequently centrifuged. For non-reducing conditions, 50 μL of the supernatant was diluted 1:1 with 2x Laemmli sample buffer. For reducing conditions, 50 μL of the supernatant was diluted 1:1 with reducing agent (10 mM dithiothreitol (DTT) in 2x Laemmli sample buffer). All samples and a protein marker (10-250 kDa) were heated in a 100 °C water bath for 10 min to obtain fully denatured protein, after which the samples (not the protein marker) were centrifuged for 1 min at 14,000 rpm (17,530 xg) at room temperature. Before the samples were loaded on the SDS-PAGE gels, running buffer was added to the gasket to rinse the walls of the gels. Then the SDS-PAGE gels were loaded; the non-reducing and reducing conditions were loaded on separate 12% TGX gels. For the marker, 10 μL was added to the gels and for the protein samples 20 μL was added. The samples were loaded in duplicate. Running buffer was added to the outside chamber. Electrophoresis was performed at 200 V. The gels were washed three times for 10 min with Milli-Q water using a shaker, after which the gels were stained using Coomassie Biosafe Stain for 30 min on a shaker. The gels were destained overnight in Milli-Q water.

Protein solubility

A method from Morr et al. (1985) was modified to determine the protein solubility. Solutions of protein in regular tap water (10 mL 2% w/v) were made in triplicate. Tap water was use to mimic the conditions from the pilot-scale experiments. The proteins were dissolved for 90 min at ambient temperature using a tube rotator at 30 rpm (Rotator SB3, Stuart, United Kingdom). These solutions were then centrifuged at 4500 xg for 20 min at 4 °C and the supernatants were freeze dried. The protein contents of these, together with the protein content of the native protein isolate, were then determined in triplicate using the Dumas method. The nitrogen-to-protein conversion factors used were 5.7 for

PPI (C. Kornet et al., 2020) and 6.38 for WPI (Carunchia Whetstine et al., 2005; Elgar et al., 2020). The protein solubility index (*PSI*) was calculated using equation (7.1):

$$PSI = \frac{p_s}{p_i} \cdot 100\% \qquad\qquad (7.1)$$

in which p_s is the protein content of the supernatant and p_i the protein content of the initial sample.

The protein content (p_i) of the used WPI was higher than that of the used PPI: 87.3 ± 0.2% for WPI, versus 70.7 ± 0.2% for PPI as determined using Dumas.

Viscosity of feed solutions
The dynamic viscosity (η) of the feed solutions with different protein concentrations was analysed in triplicate at 20 °C using a rotational MCR502 rheometer (Anton Paar, Austria), equipped with a double gap measuring system (DG26.7). The shear rate was logarithmically increased from 10 to 1000 s^{-1}.

The feed solutions for the viscosity measurements were prepared by first dissolving antifoam in 1,2 propanediol in a 3:10 ratio. This was then added to hot tap water (± 55 °C) used for the feed solutions to obtain 120 ppm antifoam in the total feed. The MD and protein isolate powders were mixed and subsequently added to the water. This was stirred for at least 30 min until the powders were fully dispersed. The solutions were stored overnight in the fridge. Before the measurements, they were kept at room temperature for 5 min.

Single droplet drying
Sample preparation
Solutions with different ratios of MD38 and WPI or PPI were prepared by mixing the powder with water and stirring it overnight to obtain 20% (w/w) solutions. Dry base concentrations of PPI of 0%, 1%, 10% and 25% were used. For WPI, the same dry base concentrations were prepared, as well as an additional sample with a dry base concentration of 100% WPI.

Single droplet drying with collisions.
The single droplet drying collision platform used in this study is a sessile single droplet drying platform where fine particles can be introduced in the drying air stream to generate collisions. The droplets had an initial radius of 200 ± 15 μm, determined during free fall briefly after dispensing. To represent the fines, glass beads were used (70-110 μm, density of 3.22 kg/m³, EPCE Bouwstoffen B.V., the Netherlands). They were released at different time points to collide with partly dried droplets. For a full description of the experimental setup and the operational procedure, we refer to Eijkelboom, Rang, et al. (2024). The initial pre-heating procedure was slightly adjusted: instead of using the air stream to preheat the tunnel, the backlight of the camera was used for preheating. The light was switched off

in between experiments, and before starting an experiment it was switched on again to obtain an air temperature near the droplet and a contact surface temperature of 40 °C. At this moment, a droplet was dispensed and this triggered the drying system to supply dry air (absolute moisture content of 3.5 g/kg) of 80 °C, flowing at a rate of 10 L/min (0.4 m/s) for 30 s. The resulting temperature of the drying air near the droplet is depicted in Figure 7.1.
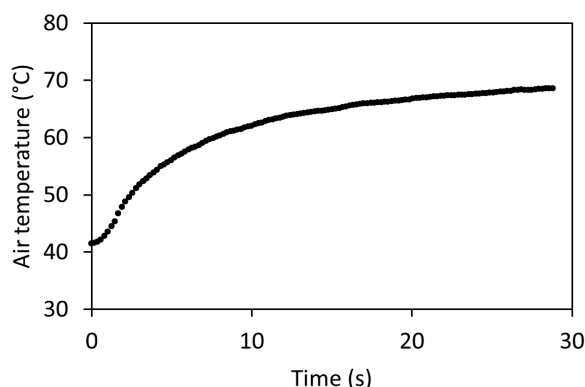
Figure 7.1. Temperature of the drying air near the droplet as applied during the drying experiments in this research.

The locking point, which is determined as the first point at which shape deviation from a sphere is visually observed (Siemons et al., 2020), as well as the collision outcomes were visually determined based on high speed camera recordings.

The total number of observed collisions is 141 for the 0% protein isolate (PI), 142 for the 1% WPI, 174 for the 10% WPI, 80 for the 25% WPI, 136 for the 100% WPI, 155 for the 1% PPI, 136 for the 10% PPI and 124 for the 25% PPI.

Data analysis for the collision outcomes
Probability plots were generated based on kernel density estimation using Python (Python Software Foundation, United States) with external libraries for data handling, statistical analysis and data visualization (Eijkelboom, Rang, et al., 2024; Hunter, 2007; McKinney, 2010; Seabold & Perktold, 2010; van Rossum & Drake, 1995; Virtanen et al., 2020).

Pilot-scale spray drying
Pilot-scale spray drying
Agglomeration trials were performed in duplicate on a DW-350 single-stage pilot-scale spray dryer (Spray Dry Works, the Netherlands). For a more detailed description of the spray dryer, we refer the reader to van Boven et al. (2023) and the set-up with extension and basket as described by van Boven et al. (2024). A SIY78/SKY16 high pressure nozzle from Spraying Systems Co. (USA) was used. The drying air had a flowrate of 585 ± 7 kg/h db

and the inlet temperature was set to 160 °C. The atomization was kept constant at a feed flow rate of 21 kg/h resulting in an outlet temperature of 83.3 ± 0.9 °C.

For the trials, MD38 feeds with 4 different levels of protein concentration (either WPI or PPI) were dried: 0%, 0.5%, 2% and 5% on dry basis. For both protein types, the trials were performed in duplicate on separate days. All feeds had a total solids (TS) content of 40%. For every trial, one batch of 50% MD38 solution was made and one batch of 38% MD38 and 2% protein was made. These were mixed together with tap water to obtain the proper ratios. The MD38 feed was made by dissolving the powder in hot tap water (± 50 °C) and stirring until the solution became transparent. The MD38-protein feeds were made by dissolving the powders in hot tap water in a double-jacketed vessel. Prior to dissolving, the powders were mixed to prevent lump formation, and antifoam was added to the water. 255 ppm antifoam (concentration in full protein feed batch) was dissolved in 1,2-propanediol in a 3.3:10 ratio before adding it to the water. After the powders were added, the solution was stirred for 30 minutes at ambient temperature, before cooling with cold tap water (± 17 °C) through the double-jacketed vessel. The protein solutions were stirred overnight under constant cooling before mixing with the MD38 feed and water to obtain the desired compositions.

During the trials, dry powder with a small particle size, referred to as "fines", was injected concentrically to the nozzle at a flowrate of 7.8 ± 0.9 kg/h using a hopper. The fines are subsequently transported to the nozzle using ambient air. For every drying condition, a sample with and without fines dosing was taken. The fines were produced separately (see *Fines production*) and do not originate from inline separation of the fine fraction from the produced powder.

Fines production
A 40% w/w MD21 feed was prepared by dissolving the MD21 in hot tap water (± 50 °C). The feed was stirred for at least one hour until the feed was transparent. A SU2A two-fluid nozzle (fluid cap 2050, air cap 70) (Spraying Systems Co., USA) was used to atomize the feed with an atomizing air pressure of 414 kPa (60 psi). The drying air inlet temperature was 160 °C and the outlet temperature was set to 100 °C, which resulted in a feed flow of 17.5 kg/h (wet basis).

To obtain the fraction with the smallest particle size, the powder was subsequently air classified using an Alpine Multi-mill system with integrated air classifier (Hosokawa Micron B.V., the Netherlands). A classifier rotor speed of 3000 rpm was used, with an inlet air flowrate of 55 m^3/h and a pressure drop over the classifier of 5.8-7.0 kPa. The fine-to-coarse ratio was 41:59 and the fine fraction had a D[4,3] of 24.5 ± 0.2 µm as determined using a Mastersizer 3000 (Malvern, U.K.).
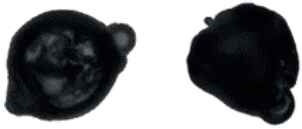
Powder morphology
Scanning Electron Microscopy (SEM) was used to visually compare powder particles. For the spray dried powders, carbon tape was used to adhere the powder to the aluminum

sample holder, after which pressurized air was used to remove any loose particles. For the dried single droplets, the tape on which the droplet was dried was put onto the carbon tape that was attached to the sample holder. The samples were sputter-coated with gold using a JEOL Smart-Coater (JEOL, Japan). Images were taken using a JCM-7000 SEM (JEOL, Japan) at an acceleration voltage of 5 kV.

Powders obtained from the pilot-scale experiments were divided into morphological classes using the Morphologi4 (Malvern, U.K.) to assess agglomeration. Per powder, 19 mm³ was dispersed onto a glass plate with a dispersion pressure of 2.5 bar. Per powder at least 38,000 particles were analyzed. Static image analysis was used to determine the descriptive shape factors. The classification used was modified from van Boven et al. (2023) (Table 7.1).

Table 7.1: Particle classes based on shape factors obtained from the Malvern Morphologi 4 software. Particles that did not belong to any of these classes were classified as 'other' (N_O) (van Boven et al., 2023). Particles with a circle-equivalent diameter ≤ 5 µm or > 100 µm were also included in the other class.

Particle class	High Sensitivity Elongation (HS) circularity		Solidity $\left(\frac{actual\ area}{convex\ hull\ area}\right)$	Example particle and corresponding CE-diameter
Primary particles (N_{pp})	≥ 0.98	< 0.1	> 0.6	47.8 µm (left) and 39.7 µm (right)
Partially coalesced particles (N_{pc})	$0.98 > \ldots \geq 0.8$	< 0.7	> 0.6	50.3 µm (left) and 82.6 µm (right)
Agglomerated particles (N_{agg})	< 0.8	< 0.7	> 0.6	82.8 µm (left) and 54.2 µm (right)

7

Results and Discussion

Protein characterisation

Protein size

The proteins in the different protein isolates can be characterized with the SDS-PAGE profiles in Figure 7.2. Under non-reducing conditions all non-covalent bonds were disrupted, while the addition of DTT in the reducing conditions also breaks down the

disulphide bonds. In both cases, there is a clear difference between WPI and PPI: WPI consists of mainly small proteins (10 and 15 kDa), together with few larger proteins. On the other hand, PPI contains many proteins of varying sizes, which is evident in bands throughout the entire lane. In both cases, the DTT breaks down some of the larger proteins, but the general pattern remains. The results are in line with earlier SDS-page results of WPI (Segat et al., 2014) and PPI (R. Kornet et al., 2021).
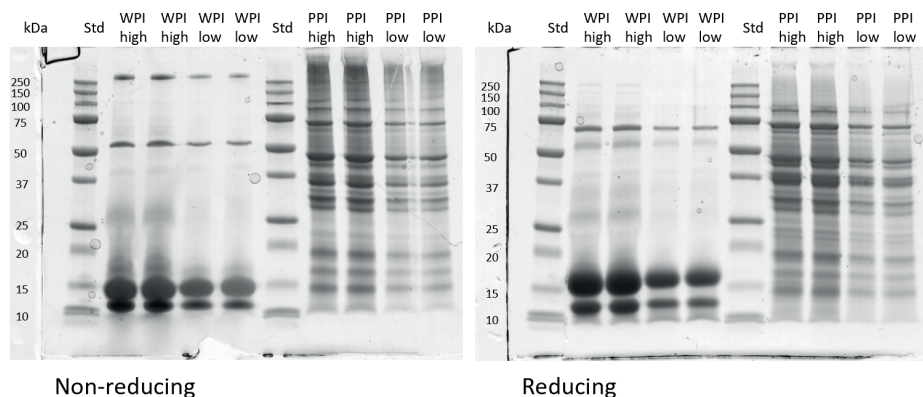
Figure 7.2. SDS-PAGE profiles of WPI and PPI under non-reducing and reducing conditions. High and low refer to the initial concentrations of the solutions (5 mg/mL and 2 mg/mL), Std means the lane is of the protein standard.

Protein solubility
The solubility of WPI was $91.5 \pm 2.3\%$, whereas that of PPI was $30.3 \pm 3.8\%$. These values are in the same order of magnitude as R. Kornet et al. (2021) found for WPI and a commercial PPI. Under non-reducing conditions, the SDS-PAGE profile of PPI sample shows some bands at 100-250 kDa, which disappear when the disulphide bonds are broken under reducing conditions (Figure 7.2). This indicates the presence of protein aggregates in the PPI, which may explain the lower solubility (R. Kornet et al., 2021).

Viscosity of feed solutions
While the feed solutions containing PPI (Figure 7.3A) behave non-Newtonian and their viscosity depends strongly on PPI content, feed solutions with WPI show little impact of the shear rate on the viscosity (Figure 7.3B). During atomization, the shear rate is higher than used in the viscosity measurements (1000 1/s) with values around 10^6 1/s reported for the atomization of emulsions with a similar nozzle (Höhne, Taboada, et al., 2024). Even though the difference in viscosity decreases upon increasing shear rate, the higher pea protein concentration still leads to higher viscosity. Generally, larger proteins or protein aggregates increase a solution's viscosity more upon increasing their concentration (Hong et al., 2017; Nicoud et al., 2015). The higher viscosity of the PPI feeds is thus due to the larger proteins present, that are shown in the SDS-PAGE analysis.
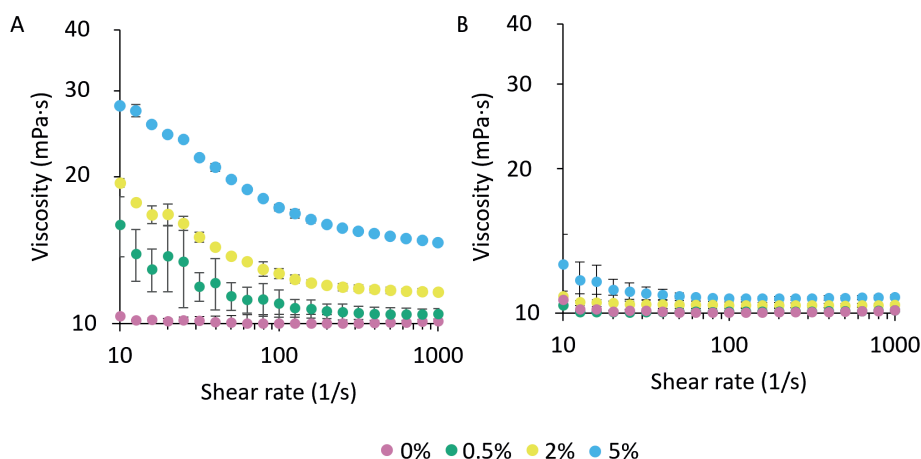
Figure 7.3. Dynamic viscosity of feed solutions with different protein concentrations. A. PPI, B. WPI. The 0% protein conditions are equal.

Single droplet drying

Locking point

During drying, droplets exhibit a point in time when their shape starts to deviate from being perfectly spherical (i.e. the locking point). This point differs for different formulations (Table 7.2). The locking point is earlier in time with an increase in protein concentration for both proteins. This is in line with previous research that showed that droplets containing solutes with a high molecular weight have an earlier locking point (Eijkelboom, Swinkels, et al., 2023; Siemons et al., 2020). Based on the molecular size differences of the protein isolates as evidenced by SDS-PAGE, it was expected that the larger PPI proteins would result in a more significant decrease of the locking point than the smaller WPI proteins. However, this is not observed. The absence of such a difference might be related to differences in accumulation of the proteins at the surface of the droplet. Dairy proteins are generally more surface active than plant proteins (Tang et al., 2023). Xu et al. (2012) found that while only working with the soluble protein fraction, the amount of protein at the surface of spray dried particles of maltodextrin/protein matrices was much lower for PPI than for WPI. As the protein needs to be present at the surface to form a skin, the lower surface protein content for PPI would lower the impact on the decrease of the locking point.

Table 7.2. Locking points (s) of drying droplets of MD38 and different dry base concentrations of protein. Note that the WPI and PPI 0% samples are the same, i.e. the sample containing only MD38.

Protein concentration (% db)	0%	1%	10%	25%	100%
WPI	6.2 ± 0.4	5.5 ± 0.3	4.5 ± 0.2	4.2 ± 0.2	2.3 ± 0.2
PPI	6.2 ± 0.4	5.5 ± 0.3	5.4 ± 0.2	4.4 ± 0.2	

Morphology

The type and concentration of protein within the drying matrix influenced the dried particle morphology (Figure 7.4). Dried particles of an MD38 solution without any protein showed a wrinkled morphology, in line with results obtained previously (Eijkelboom, Swinkels, et al., 2023; Siemons et al., 2020). As also shown by Andersson et al. (2018) and Both, Karlina, et al. (2018), the addition of WPI reduces the number of dents and wrinkles of the dried particle. Simultaneously with the decrease in the number of wrinkles, the dents become deeper. The skin becomes stiffer with an increase in protein content, making it less prone to wrinkling. As water still evaporates from the droplet, the pressure below the skin decreases, resulting in an under-pressure. The pressure gradient over the skin (between the inside of the droplet and the environment) favors deformation of the droplet (Bouman et al., 2016). Hence, as soon as a dent forms, it deepens further as a response to the evolving pressure gradient. The impact of PPI on the dried particle morphology was much smaller. For all concentrations of PPI investigated, the dried particles showed a large number of shallow wrinkles. The lower surface presence of PPI might be causing this difference: less protein at the surface results in less stiffening of the skin, which then remains more deformable (Andersson et al., 2018; Xu et al., 2012).
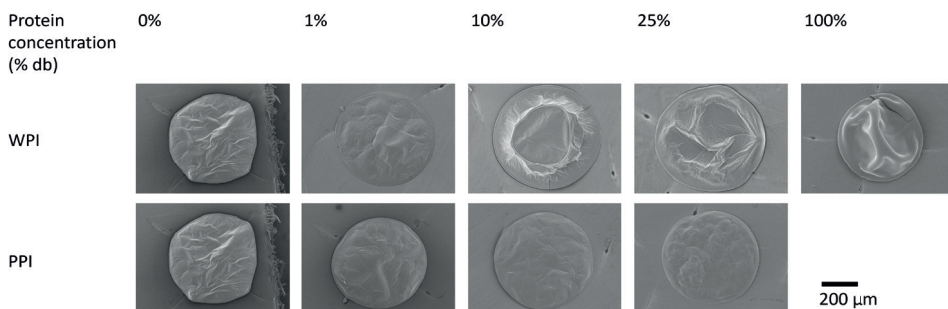
Figure 7.4. Morphology of dried single droplets of MD38 and different dry matter concentrations of protein. Note that the WPI and PPI 0% samples are the same, i.e. the sample containing only MD38.

Collisions

Depending on the drying time, either merging, sticking or bouncing can be observed during collisions between a drying droplet and glass beads (Figure 7.5). Independent of the droplet composition, there is an initial period during which all collisions result in merging, as the droplets are then still very liquid. The transition to the regime where also sticking can be observed depends on the droplet composition. The collision regimes partly overlap due to the stochastic nature of the process. Adding protein to the MD38 matrix results in an earlier onset of the sticking regime. Within a protein concentration range of 1 to 25% db, the amount of protein that was added had no impact, but the type of protein did influence the onset of the sticking regime. The sticking regime started at 6.0 s for droplets without protein, and at around 5.0 and 4.0 s for droplets consisting of maltodextrin with PPI or WPI, respectively. For the droplets with only WPI, the sticking regime started even earlier, at 3.0 s. The earlier onset of the sticking regime is in line

with the observation of earlier locking points (Eijkelboom, Rang, et al., 2024). The end of the sticking regime depended on the droplet composition as well. The addition of some (1-25 % (db)) protein to an MD38 matrix delayed the end point of the sticking regime, with a slightly later end point for PPI than for WPI containing samples. While this might not have been expected based on the later locking point, the locking point only indicates the first onset of the skin formation. It is expected that complete skin formation, with interlocking solutes at the surface, is required to end the sticking regime. By having a system consisting of multiple solutes, the transition of the skin into a locked system is expected to be more gradual than for a system containing only maltodextrin. Plasticizers reduce the intermolecular forces between polymer chains, resulting in more flexible films (Felton, 2013). Sugars are generally plasticizers for proteins, and the formation of a more flexible film on the surface may stretch the sticking regime to longer times. Droplets only containing WPI showed an earlier end point of the sticking regime. For a pure WPI system, with a sufficiently high concentration of the globular proteins in the skin of the droplet, the proteins will behave as hard spheres and will jam into a strong, semi-solid shell. This jamming of whey protein happens at a concentration of ~ 50% (w/w), whereas maltodextrin DE12, a more random-coil type molecule, remains predominantly viscous up to concentrations of ~ 70% (w/w) (Both et al., 2019). This explains the earlier locked skin formation, and thereby the end point of the sticking regime, of the pure WPI systems.

Figure 7.5. Collision outcomes over time for maltodextrin/protein systems containing different dry base concentrations of WPI or PPI. Note that the WPI and PPI 0% samples are the same, i.e. the sample containing only MD38.

While the onset and end point of the sticking regime are valid for the conditions applied in this study, it would also be valuable to know how this information can be translated to other conditions. For example, during industrial spray drying the drying air conditions and initial droplet size differ from the conditions applied at the single droplet scale. This will result in a different absolute time point of the onset of the sticking regime. To correct for this, the collision times can be normalized by using the locking point (Figure 7.6). The

locking point is co-determined by factors like drying air conditions and droplet size (Boel et al., 2020; Sadek, Schuck, et al., 2015), and is found to play an important role in collision outcomes (Eijkelboom, Rang, et al., 2024).

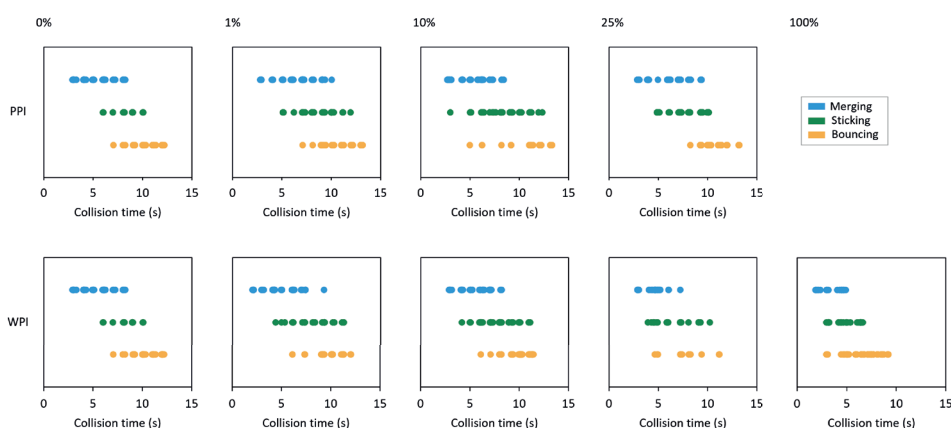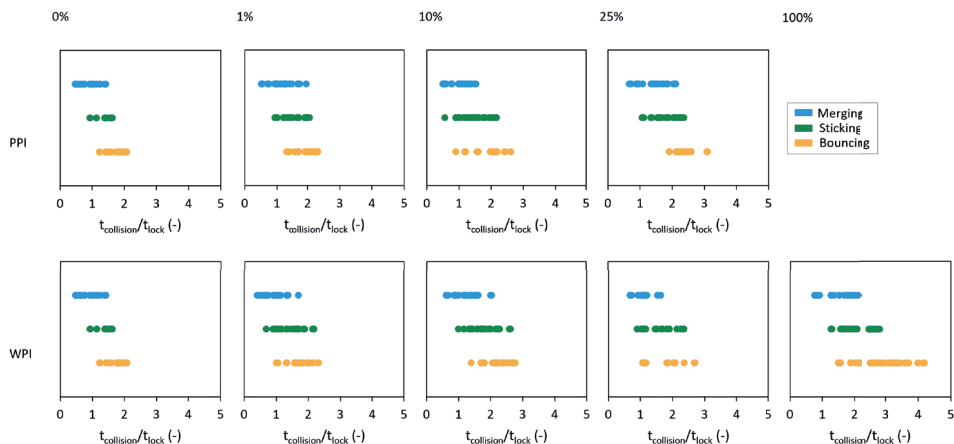

Figure 7.6. Collision outcomes over normalized collision time ($t_{collision}/t_{lock}$ (-)) for maltodextrin/ protein systems containing different dry base concentrations of WPI or PPI. Note that the WPI and PPI 0% samples are the same, i.e. the sample containing only MD38.

The normalized sticking regime depends on the composition of the drying matrix. For the MD38 droplets, the sticking regime lasted from 1.0 to 1.6 $t_{collision}/t_{lock}$. For samples with a protein concentration of 1-25% db, the normalized sticking regime also started at 1.0 $t_{collision}/t_{lock}$, but lasted till a longer normalized collision time with an increase in protein content. A droplet consisting of only WPI showed an even later offset of the normalized sticking regime, at 2.8 $t_{collision}/t_{lock}$. However, with the onset of the sticking regime for this composition being at 1.3 $t_{collision}/t_{lock}$, this was also slightly later than for the MD containing solutions. This increased duration of the normalized sticking regime for pure protein samples shows a different perspective than the observations of the sticking regime related to the real collision time. Upon protein addition, the locking point decreases. Dividing a collision time by an early locking point results in higher values, resulting in a larger sticking regime for protein-rich samples based on the normalized collision time. This normalization distorts the picture of the impact of the drying matrix on the duration of the sticking regime. Direct comparisons between different drying matrices related to the duration of the sticking regime should therefore be based on non-normalized collision times. However, normalized data can be used for the translation to different drying conditions using the same matrix. For example, if the drying conditions and corresponding locking point of the matrix dried during an industrial process are known, the sticking regime under those conditions can be determined.

As the collision outcomes are partially stochastic, it is interesting to have better insight into the probability of specific collision outcomes. Therefore, probability plots of observing different collision outcomes based on normalized collision times are shown in Figure 7.7

for the different drying matrices. Probability plots with non-normalized collision times can be found in Appendix 7.A.
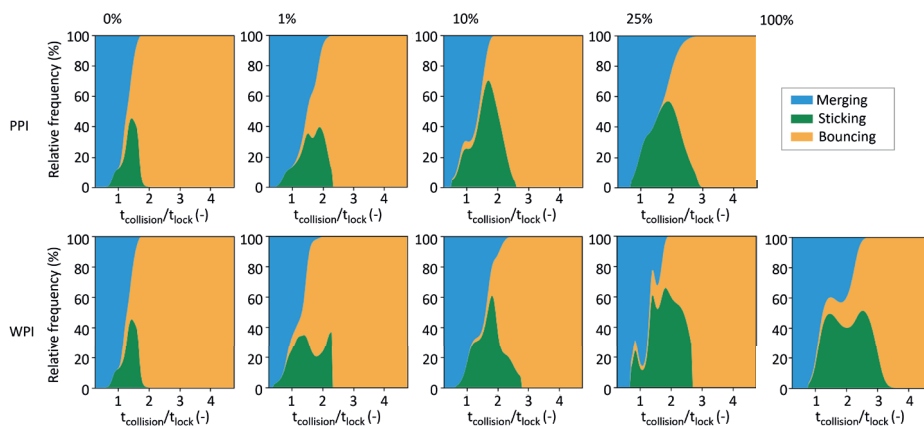
Figure 7.7. Stacked area charts for different collision outcomes for maltodextrin/protein systems containing different dry base concentrations of WPI or PPI across $t_{collision}/t_{lock}$ (-). Note that the WPI and PPI 0% samples are the same, i.e. the sample containing only MD38.

The relative frequency of sticking depends on the protein concentration. An increase in protein concentration yields an increase in the relative frequency, indicating that the chance of a collision resulting in sticking increases with increasing protein concentration. Besides influencing the skin properties (Both, Karlina, et al., 2018), the presence of proteins at the surface may further enhance sticking as proteins are known to more easily adsorb to external solid surfaces, such as that of the glass beads (Rabe et al., 2011; Zheng et al., 2019).

Pilot-scale spray drying
An adjusted sticking regime can affect both fouling and agglomeration. Therefore, pilot-scale spray drying trials were conducted to investigate the effect of protein addition on yield and agglomeration.

Yield
The absolute yield without protein or fines addition was high for all trials (89-98%, Appendix 7.B). Therefore, comparing the effect of protein addition without fines addition (Figure 7.8A) only has a limited use. To account for day-to-day variation during pilot-scale spray drying, the yield was analyzed by looking at the differences in yield compared to the condition without proteins as dried on the same day (Figure 7.8). With fines additions (Figure 7.8B), the absolute yield values for the 0% protein conditions were generally lower (83-84%, except for PPI-1 which had 98%). This is due to the dosing of the dry fines. These particles are very small and can negatively impact the yield in two ways. First, small particles have impaired flow behavior: they can remain in the cone region of the dryer or in the tubing

connecting the drying chamber to the cyclone and are thus not collected. Second, small particles are less well separated by the cyclone and may leave the system, with the drying air (Sardar et al., 2023). An improved yield can thus be caused by two reasons: 1) less powder was deposited onto the wall of the spray dryer, or 2) fines agglomerated and are therefore bigger, enabling better flow and a more efficient separation from the drying air over the cyclone.
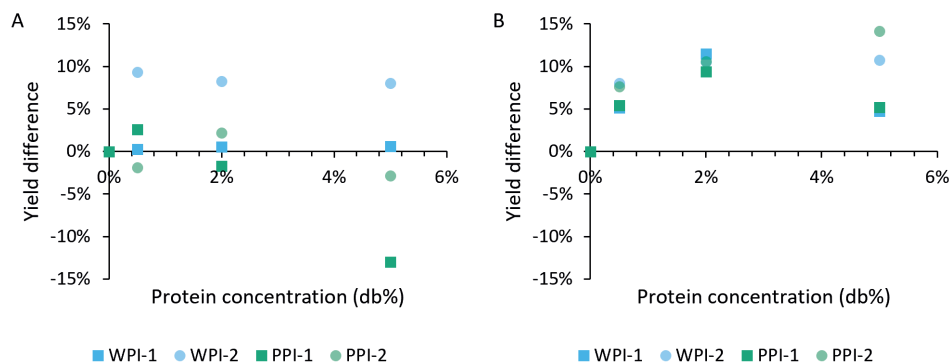
Figure 7.8. Difference in yield compared to the yield without protein addition (yield-yield(0)) for different protein conditions. A: without fines dosing, B: with fines dosing.

It is well established that adding whey protein, either as isolate or as concentrate, during spray drying of a sugar rich product can improve the yield (Bazaria & Kumar, 2016; Gong et al., 2018; Ruano Uscategui et al., 2018; Shi et al., 2013). Although our absolute yield without protein addition was too high to see large effects, we still saw this same effect during the WPI-2 trial. In our study, the concentration of the protein in the tested range did not seem to matter. This is contradictory to Mirlohi et al. (2022), who found that all proteins affect the yield in a dose-dependent manner until a saturation point is reached. Adding PPI to the feed however did not affect the yield at concentrations up to 2% db. This can be explained by the lower solubility and lower protein content of the PPI and the fact that plant-based proteins are usually less surface active (Tang et al., 2023) and thereby less efficient drying aids (Mirlohi et al., 2022). At 5% db, the PPI even negatively affected the yield. It is possible that with 5 db% pea protein the atomized droplets are bigger due to the higher viscosity. As larger droplets dry slower, at this concentration of PPI one may end up with slower drying leading to more fouling for this dryer and air flow.

During fines dosing, both proteins improved the yield (Figure 7.8B). The improved yield upon increasing protein concentration during fines addition is related to the onset of the sticking regime, as the SDD experiments showed that protein addition caused an earlier onset of the sticking regime. Fines are dosed concentrically to the nozzle, and an earlier transition to the sticking regime shifts the collision outcomes from full coalescence to sticking, resulting in larger agglomerates and thus a more efficient separation over the cyclone.

The yield is lower on the first trial compared to the second one both with and without fines dosing (PI-1 versus PI-2). This is especially visible with 5% db protein. In both cases, the PI-1 trials were performed with decreasing protein concentration, meaning that 0% protein was the final run, while the PI-2 trials were performed with ascending protein concentration (0% protein concentration as initial run). The yield improvement upon protein addition is thus larger with the reference sample as initial run. During the day fouling builds up in the dryer. After some time, wall deposits can fall off and end up in the sample, seemingly increasing the yield. When starting with the conditions that cause most fouling, this affects the yield of the later runs more. It is thus important to consider the order of experiments when planning and analyzing a trial. This is also the reason why the absolute yield for PPI-1 with fines addition exceeds 100% when proteins are present (Appendix 7.B).

Particle morphology
Similar to the particle morphology of single dried droplets, the morphology of pilot spray dried pure MD38 is wrinkled (Figure 7.9, Appendix 7.C). However, the wrinkles appear more shallow compared to those of dried single droplets, which may be due to the smaller droplet size. The droplets dried during SDD are larger than those dried during pilot-scale spray drying. The smaller surface-to-volume ratio implies longer drying times and results in later skin formation (Both, Karlina, et al., 2018). Because of the longer drying time, the components have time for redistribution through diffusion. Consequently, the surface composition of larger droplets may be different, affecting the surface rheological properties. A larger droplet size can therefore result in a different morphology (Eijkelboom, van Boven, et al., 2023). The outside of the particles obtained from SDD appears more spherical because they are dried on a flat surface and the image is a top-view only while the droplets in a spray dryer are freely moving through the drying air. From the side, the particles from SDD would not look spherical but flattened. Adding WPI during pilot-scale spray drying results in less circular particles with deeper dents that have sharp edges. This is also observed in the particles obtained from SDD and is caused by the stiffer skin resulting from the protein addition. Similar to the SDD experiments, adding PPI instead of WPI results in particles that have less wrinkles and the wrinkles are smooth instead of sharp. As previously explained, the presence of PPI protein at the surface is probably lower than for WPI protein which results in a less stiff skin.

The morphological classification (Figure 7.10) shows variance when replicated on different days, as also shown for the yield. The 0% protein conditions should be equal on WPI and PPI trial days as the feed solutions are the same, but especially in the system without fines added (Figure 7.10A) the results differ. The results are not averaged as this enables a more accurate analysis on the effect of fines addition. Without adding fines, it can be seen that increasing the protein concentration reduces the fraction of primary particles, meaning that more droplets within the atomizer cloud have agglomerated together. This matches the longer sticky regime for increasing protein concentration as shown by SDD. The samples containing PPI have a larger fraction of primary particles than the WPI
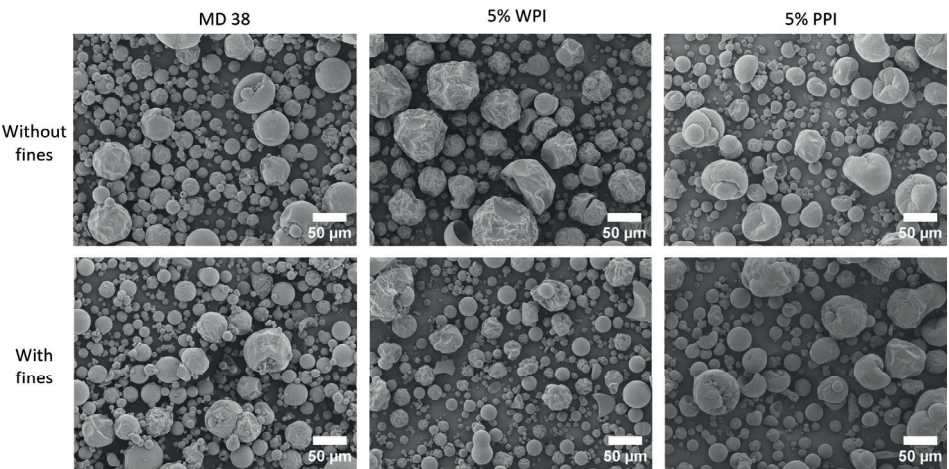
Figure 7.9. SEM images of powder obtained after pilot-scale spray drying. From left to right: no protein addition, 5% db WPI addition and 5% db PPI addition. The images in the top row are without fines dosing, the ones in the second row are with fines dosing.

Figure 7.10. Morphology classification for different levels of WPI or PPI. A: without fines dosing, B: with fines dosing. Results are presented as average of the percentages obtained from the duplicate trials.

samples, at the cost of partially coalesced particles. At the same time, the yield of the WPI samples is higher. This is in line with the earlier locking point for WPI compared to PPI observed during SDD at 10% db protein. Particles with an earlier locking point shift earlier from merging to sticking, resulting in a larger particle size. As explained before, the larger particle size contributes to a higher yield because of improved flow behavior and a more efficient separation from the drying air in the cyclone.

Upon fines addition (Figure 7.10B), the addition of protein to the feed also reduced the fraction of primary particles. More agglomeration occurred, shown by the increased fractions of partially coalesced and agglomerated particles. This agglomeration is a combination of agglomeration between droplets in the atomizer cloud and of agglomeration of droplets and dosed fines. The trend is present for both protein types, but it is more pronounced for PPI as the 0% PPI has a higher fraction of primary particles than WPI whereas this is reversed upon protein addition. Additionally, the agglomerate fraction with PPI is somewhat larger compared to the partially coalesced fraction, relative to WPI samples. This is contrary to the results without fines dosing. We hypothesize that this is due to the later end point of the sticking regime for PPI (Figure 7.5). We assume that collisions between droplets and fines occur later in the drying process than collisions between droplets within the atomizer cloud. Since PPI has a later end point of the sticking regime than WPI, collisions between droplets and fines can still result in the formation of agglomerates for droplets containing PPI, while droplets containing WPI already progressed to the bouncing regime. The fact that some samples have a larger fraction of primary particles upon fines addition is not surprising, as not all fines agglomerate within one pass (Fröhlich et al., 2023). As the used spray dryer is a single stage dryer in which fines are dosed, the obtained sample is a mixture of particles originating from the spray, unagglomerated fines and agglomerates formed by agglomeration of sprayed droplets and dry fines. This is contrary to a set-up where particles are recycled until they reach a required size.

The order of the pilot trials affected the resulting particle morphologies. With fines dosing, doing runs with an ascending protein concentration led to a larger fraction of primary particles under the same conditions, mainly at the cost of partially coalesced particles, compared to doing runs with a descending protein concentration (Appendix 7.D Figure 7.D.1). This was also seen without fines, except for the WPI 0.5% protein samples and the PPI 5% protein samples (Appendix 7.D Figure 7.D.2). As protein addition results in a longer sticking regime, starting with the highest protein concentration leads to more fouling. These wall deposits accumulate and end up in powders later during the day and thus decrease the fraction of primary particles.

Conclusion

This work aimed at developing guidelines to optimize product formulation, specifically focusing on protein addition, in order to facilitate agglomeration and reduce fouling in spray drying processes. A combined single droplet and pilot-scale spray drying research

approach was adopted. This multi-scale character enabled the identification of the mechanisms on single droplet scale and subsequent verification of their effects at pilot-scale. Binary drying droplet-particle collisions were performed to investigate the effect of protein addition on the sticking regime of drying droplets. Upon the addition of proteins, the sticking regime started earlier. Within a dry base content range of 1 to 25%, the exact protein concentration had no clear impact on the duration of the sticking regime. However, the protein concentration did influence the likelihood of a collision resulting in sticking, with an increase in the likelihood of sticking upon an increase in protein concentration.

The choice of PPI or WPI as a protein source had limited impact on the sticking outcomes, with PPI containing samples having a later end point of the sticking regime than WPI containing samples. PPI contains larger proteins than WPI, therefore PPI was expected to result in earlier, and more rigid skin formation. The lower solubility and lower surface activity of the PPI counteracted this difference.

The sticking regimes were normalized for the locking point. Since the locking point depends on factors such as droplet size, solid content and drying air temperature, this can help to link the obtained insights to agglomeration and fouling behavior during spray drying.

Pilot-scale trials were performed to investigate the effect of protein addition on fouling and agglomeration. Protein addition during trials with fines dosing increased the yield. This was caused by an earlier onset of the sticking regime, which shifted collision outcomes from full coalescence to agglomeration. This in turn led to a larger increase in particle size which enabled a higher powder recovery by a more efficient separation in the cyclone and better flow behavior. Within the tested range, up to 5% db protein, the response in yield and agglomeration was dose dependent until the protein affected the feed viscosity, resulting in different drying behavior. The morphological classification of particles confirmed that PPI addition leads to more agglomeration, due to the slightly later end point of the sticking regime for PPI than for WPI. These results highlight the importance of the time at which a collision occurs in a spray dryer.

Optimizing a spray drying process requires understanding of the interplay between formulation, drying conditions and the physical set-up of a dryer that determines when recycled fines collide with atomized droplets. The results of this study contribute to formulating guidelines to perform more controlled spray drying with protein additives. If a spray drying process shows too little agglomeration and little fouling, particles are dried too quickly. Alternatively to slower drying by adapting the temperature or air flow rate, it is also possible to use a protein inducing a longer or later sticking regime. If there is insufficient agglomeration but a lot of fouling, particles have become sticky too late and using a protein with an earlier sticking regime can improve the performance. With satisfactory agglomeration but excessive fouling, the particles remain sticky for too long. The performance can then be improved by using a protein with a shorter sticking regime.

Appendix 7.A
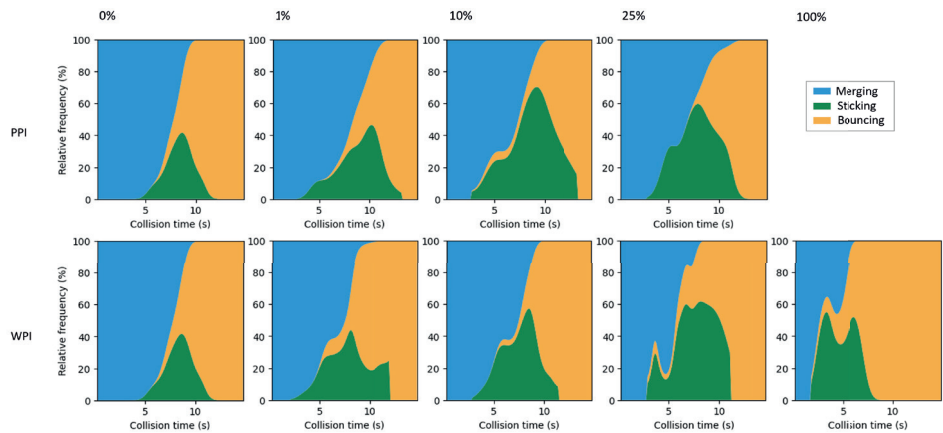
Figure 7.A.1. Stacked area charts for different collision outcomes for maltodextrin/protein systems containing different dry base concentrations of WPI or PPI. Note that the WPI and PPI 0% samples are the same, i.e. the sample containing only MD38.

Appendix 7.B

Table 7.B.1. Absolute yield values for pilot trials.

	Protein concentration (% db)	WPI-1	WPI-2	PPI-1	PPI-2
Without fines	0%	98.01%	89.25%	91.12%	94.99%
	0.50%	98.25%	98.58%	93.70%	93.13%
	2%	98.54%	97.54%	89.40%	97.17%
	5%	98.59%	97.28%	78.11%	92.12%
With fines	0%	82.78%	83.05%	97.86%	84.14%
	0.50%	87.95%	91.11%	103.30%	91.80%
	2%	94.27%	93.58%	107.24%	94.69%
	5%	87.51%	93.79%	103.03%	98.28%

Appendix 7.C

WPI PPI

No fines, 0% protein

No fines, 5% protein

With fines, 0% protein

With fines, 0.5% protein

With fines, 2% protein

With fines, 5% protein
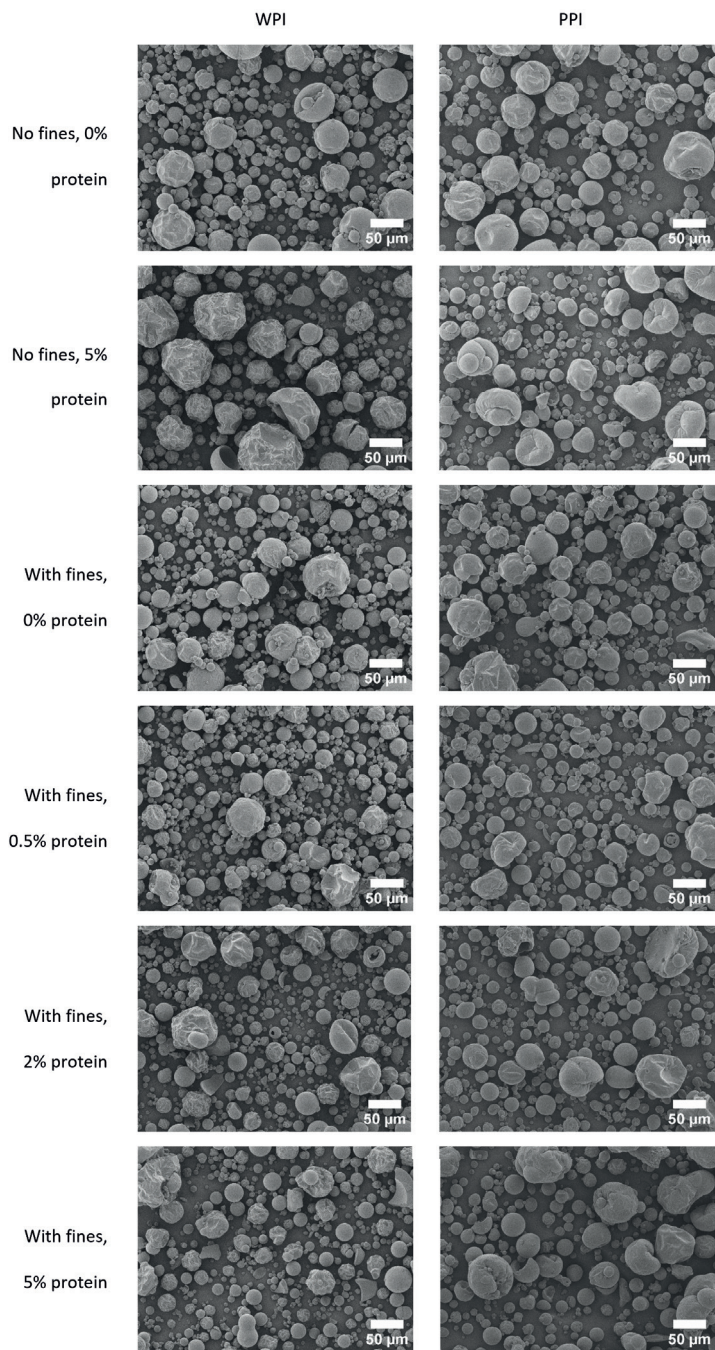
Figure 7.C.1. SEM images for powders obtained from pilot-scale spray drying.

Appendix 7.D
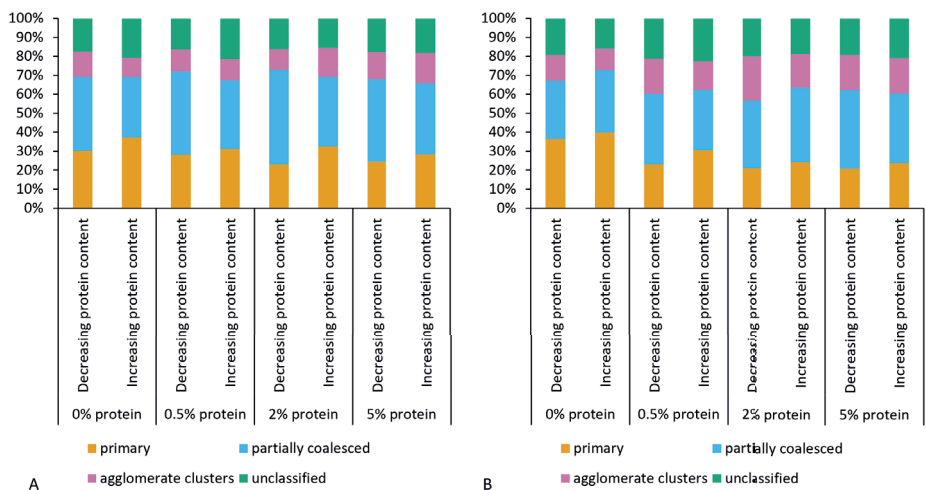
Figure 7.D.1. Effect of order of experiments on the morphological classification of powder particles <u>with fines</u> dosing. A: WPI, B: PPI.
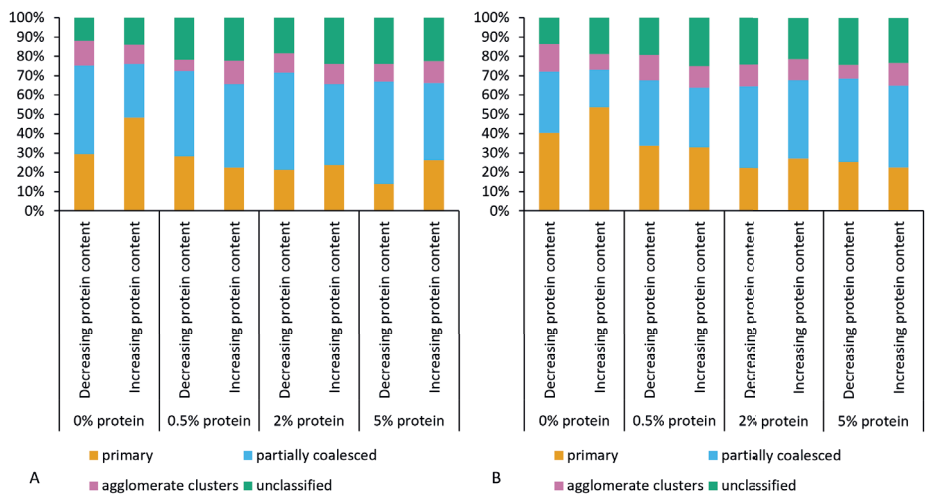
Figure 7.D.2. Effect of order of experiments on the morphological classification of powder particles <u>without fines</u> dosing. A: WPI, B: PPI.
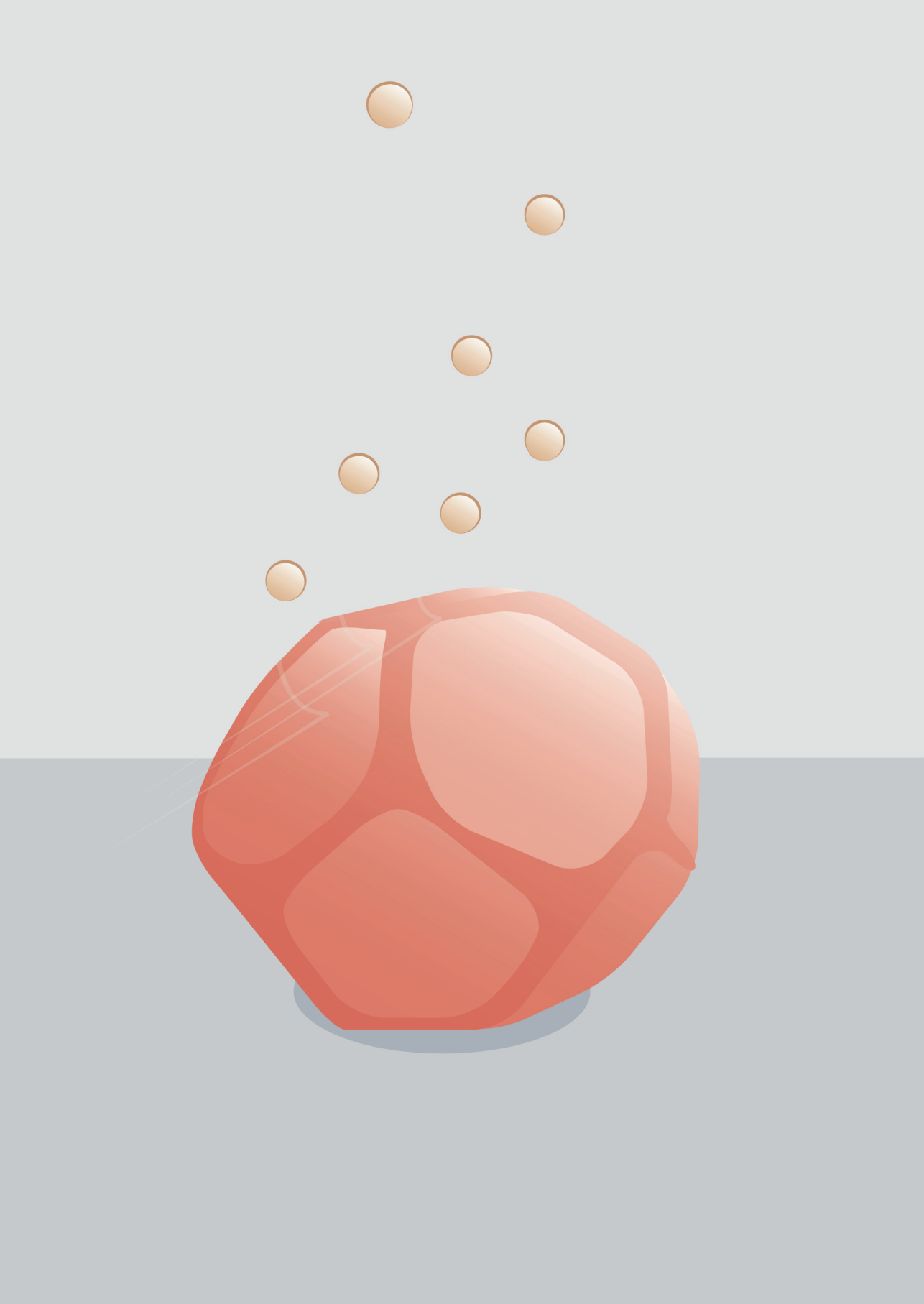
Chapter

General discussion

8

Introduction

Spray drying is widely used to convert liquid formulations into agglomerated powders. Despite its widespread use, optimal drying and agglomeration protocols in spray drying are currently still established via empirical procedures. Mechanistic understanding of droplet drying and agglomeration during spray drying can contribute to establishing better agglomeration protocols. However, the large scale and closed nature of an industrial spray dryer make it virtually impossible to obtain these insights at this scale. Single droplet drying approaches are used to assess spray drying at the scale of a single droplet, creating the opportunity to provide mechanistic insights. However, current single droplet drying systems dry droplets at a constant drying air temperature. Moreover, they cannot investigate the interactions between droplets and particles relevant for agglomeration. Improved single droplet drying approaches would therefore help to improve mechanistic understanding of the spray drying process.

The overall aim of this thesis was to characterize the physical phenomena underlying the drying and agglomeration behavior of droplets during spray drying via improved single droplet drying approaches. For this, a single droplet dryer was developed that can realistically represent changing spray drying temperature conditions. Moreover, binary collisions can be studied with the newly developed platform. This platform was then used to characterize the drying droplets, including their temperature during drying and dried surface composition, and binary collision outcomes. Numerical models were developed and employed to predict and understand drying and collision behavior.

This chapter discusses the main findings of these studies. As collision dynamics might also depend on the properties of the small particles, additional results on the impact of glass bead size on the collision outcomes will be presented. The practical implications of the work performed will be highlighted and the chapter concludes with an outlook towards the future.

Main findings and conclusions

The current status of the potential and limitations of single droplet drying to understand spray drying was discussed in **Chapter 2**. This includes the developments regarding the evolution of primary particle morphology and nozzle-zone agglomeration. A conclusion was that existing single droplet drying methods are especially suitable to characterize the particle morphology, but only extending a single droplet dryer to monitor binary collision behavior can give first insights into agglomeration behavior.

During the first steps of this research, focus was on the drying behavior of sessile single droplets. In **Chapter 3**, an existing setup that dries droplets with constant air temperatures was used. High-resolution thermography was incorporated to measure the temperature of drying droplets. Combined with visual camera observations, this showed that the droplet temperature started to increase at the visually observed locking point. Besides,

the temperature measurements worked as an indirect measurement for morphological development of the droplets; droplets that form a vacuole during drying showed a more irregular temperature increase, with a plateau of the droplet's temperature as soon as the vacuole was formed. A sessile droplet drying model was extended by incorporating conductive heat transfer to predict the drying of the droplets.

To more realistically mimic the changes in the drying environment that a droplet is subjected to in a spray dryer, a new single droplet drying platform was introduced in **Chapter 4**. The platform works with step-wise changing temperature-time trajectories, simulating the high inlet- and low outlet temperatures. The dried droplets contained β-galactosidase, of which the inactivation is used as an indicator of the thermal load applied to the dried particles. For droplets containing an initial solid content of 40% maltodextrin DE21, the initial drying air temperature (representing the inlet air of a spray dryer) hardly influenced the drying behavior and enzyme inactivation. A higher temperature at the second stage of drying (representing the outlet air of a spray dryer) did result in higher droplet temperatures and a higher thermal load, and more inactivation of the β-galactosidase. For droplets with a lower initial solute content of 20% maltodextrin DE21, different initial air temperatures did result in different drying behavior and inactivation. The coupling of a drying and an inactivation model resulted in a model that could predict the drying behavior and β-galactosidase inactivation of the droplets dried under different conditions.

While the work in the previous chapters focused on single component systems, in industrial practice multi-component systems are commonly used. Therefore, in **Chapter 5**, the drying of multicomponent, dairy-based systems was investigated. It was found that the presence of fat within a drying matrix resulted in an earlier locking point. Morphological differences were observed for droplets containing different ratios between lactose and protein, and between different types of proteins. Confocal Raman microscopy was used to qualitatively investigate the surface composition of the dried droplets. The surface of the dried dairy-based systems generally consisted of a mixture of lactose and protein, but samples with increased levels of fat or whey protein isolate showed the presence of surface fat. As the presence of fat on the surface would promote the caking of the powder, this is undesired.

Agglomeration generally improves the quality of a powder. Agglomeration can be the result of an interaction between a drying droplet and a fine particle, although such an interaction does not always result in sticking, but can also lead to merging or bouncing. In **Chapter 6** the single droplet drying platform was extended to asses binary collision outcomes between a drying droplet and glass beads. It was observed that the collision outcome depends on the collision time. The absolute time at which a transition from merging to other collision outcomes was observed depended on the DE-value of the maltodextrin present in the drying droplet. If the collision time is corrected for the locking point, the different maltodextrins exhibit similar collision outcome regimes, with the sticking regime ranging from 0.75 to 1.5 $t_{collision}/t_{lock}$. A match between the droplet

temperature increase, characteristic rheological changes and the locking point was observed when using a numerical model that combines the drying of a single droplet with the rheological properties of the matrix. The model can therefore be used to indicate the locking point, and thereby the sticking regime.

In **Chapter 7** the investigation of collision behavior was extended to multi-component systems, investigating the effect of protein addition on collision behavior. Feed solutions were used containing mixtures of maltodextrin and proteins. Both whey protein isolate and pea protein isolate were investigated as a protein source, investigating the impact of switching from dairy protein to plant protein on drying and collision behavior. Upon the addition of proteins, the sticking regime started earlier and the likelihood of a collision resulting in sticking increased. Whether pea or whey protein isolate was used as a protein source only had a limited impact on the sticking outcomes. Pilot-scale spray drying trials were performed to validate the sticking behavior by investigating agglomeration and yield upon drying of maltodextrin-protein mixtures. Protein addition during trials with fines dosing increased the fraction of agglomerated particles and improved the yield. These results highlight the importance of both the time at which a collision occurs, as well as the droplet composition, on optimizing the spray drying process.

Single droplet drying with more realistic temperature-time trajectories

As a part of this thesis, a new sessile single droplet dryer has been developed to dry droplets with a temperature-time trajectory, more realistically representing the drying conditions in a spray dryer. A reflection is given here on the usefulness of applying a temperature-time trajectory during single droplet drying.

In Chapter 4 it was demonstrated that the impact of more realistic temperature-time trajectories on the drying behavior of droplets depends on the initial solute content. Droplets containing an initial MD21 content of 40% were not influenced by a higher initial air temperature. When working with a lower initial solute content, the locking point is delayed, resulting in an increased temporal resolution. For droplets containing an initial MD21 content of 20%, an impact of the first stage air temperature was observed. Moreover, a numerical single droplet drying model was validated to predict drying behavior under different temperature-time trajectories. While models and simulations can also be used to predict the drying behavior under different temperature-time trajectories, it is important to validate such a model based on experimental results under varying conditions.

The validated numerical SDD model was also used to predict enzyme inactivation for different drying conditions. It showed that optimization procedures to maintain maximal enzyme activity differ depending on working with constant or with changing temperatures. With constant air temperatures, the SDD model predicted that minimal enzyme inactivation after drying is obtained with a low initial solute content. However, using temperature-time trajectories, a high initial solute content is predicted to be favorable

to achieve minimal enzyme inactivation. These differences illustrate the added value of including temperature-time trajectories during SDD when focusing on the inactivation of heat-sensitive compounds.

More realistic temperature-time trajectories were also applied upon the drying of dairy systems, as described in Chapter 5. Here it was observed that the surface composition of a small droplet (400 μm) dried with a more realistic temperature-time trajectory differed from that of previous research by Both, Nuzzo, et al. (2018). For example, drying of fat-free samples with a temperature-time trajectory showed evidence of stratification of small components on the surface of the dried droplet. In contrast, for larger droplets (800-1200 μm) dried at a constant temperature (70-90 °C) Both, Nuzzo, et al. (2018) observed a very thin layer of protein at the surface. This difference in surface composition is probably caused by differences in the drying rate. Stratification of small components at the surface may only occur when the solvent evaporation rate is sufficiently high. As the temperature-time trajectories applied in our work are more in line with realistic spray drying conditions, it is expected that these give a better indication of the surface composition achieved in industrial spray dried powders.

While Chapters 4 and 5 show the added value of single droplet drying with more realistic temperature-time trajectories, one has to be critical about the trajectories applied. While they do represent the changing air conditions within a spray dryer more realistically than using a constant air temperature, they are still not a perfect representation of the drying conditions within an industrial spray dryer. The conditions of the air surrounding the droplet cannot change rapidly enough to fully recreate the fast changeover that is present within a spray dryer.

Another difference between the drying environment in a spray dryer and in the single droplet dryer that is still present, is the relative humidity of the air. During single droplet drying, dry air is used. In a spray dryer, the air that enters the dryer is dry, but due to moisture evaporation from the feed the relative humidity of the air increases towards the outlet of the dryer. While the initial drying of a droplet is limited by the external rate of mass and heat transfer, internal diffusive mass transfer becomes limiting after the locking point. It is, therefore, expected that the drying behavior will only be influenced if the relative humidity vastly increases before the locking point. The high inlet air temperatures used in the spray drying industry result in very early locking points, therefore, the overall impact of a relative humidity profile on the drying behavior of a single droplet is expected to be limited.

A downside of applying more realistic temperature-time trajectories becomes visible upon the investigation of collisions. For the investigation of collisions where a drying droplet is involved, very fast initial drying is undesired. In the case of fast initial drying it will not take long until all collisions result in bouncing. Therefore, to properly investigate the change in collision outcomes over time, working at more moderate drying conditions is desired.

Influence of the fines particle size on collision outcomes

Next to the properties of the drying droplets, the properties of the dry fines are expected to have an influence on the collision outcomes. Chapters 5 and 6 investigated the collision between drying droplets (initial diameter of 400 μm) and glass beads of a fixed size (70-110 μm). In a spray dryer, the size (ratio) of interacting particles varies much more, and this will impact the collision behavior. To investigate this, experiments were performed on the collisions between drying maltodextrin DE38 droplets and glass beads of different sizes. The drying procedures were kept identical to those applied in Chapter 6. The locking point was visually observed to be 6.5 ± 0.2 s. Glass beads with different size distributions were obtained from EPCE Bouwstoffen B.V. (the Netherlands) (Figure 8.1). The total number of observed collisions is 117 for the glass beads of 0-50 μm, 128 for the glass beads of 70-110 μm, 116 for the glass beads of 90-150 μm and 109 for the glass beads of 150-250 μm.
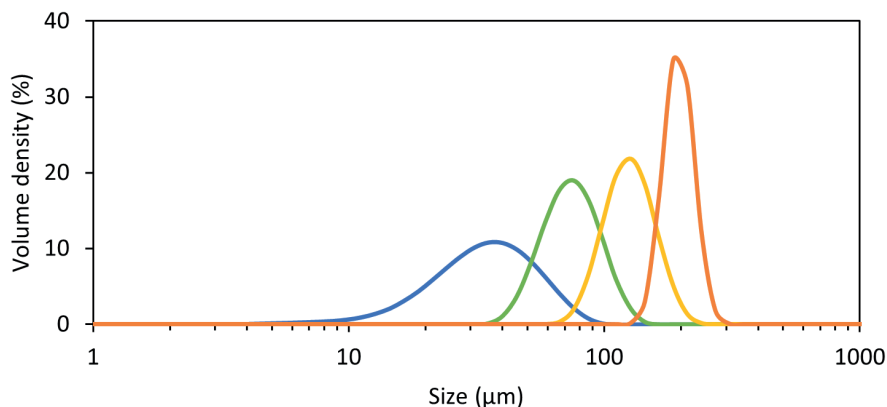
Figure 8.1. Measured size distribution of the different glass beads that are by the supplier indicated as 0-50 μm (blue), 70-110 μm (green), 90-150 μm (yellow) and 150-250 μm (orange).

During collisions between drying MD38 droplets and glass beads of different sizes, an impact of the glass bead size on the sticking regime was observed (Figure 8.2). For the three largest size ranges of glass beads (70-110, 90-150 and 150-250 μm), the sticking regime lasts longer with an increasing bead size. Moreover, the chance of observing sticking as the collision outcome increases, especially at the expense of having fewer bouncing collisions. It is expected that this shift from bouncing to sticking is related to the increase in inertial forces, making it easier for the large droplets to indent and penetrate the surface and stick (Gao et al., 2017). Besides, the increase in the contact area between droplet and bead upon increasing glass bead sizes might promote sticking. However, these observations do not hold for the glass pearls of the smallest size range investigated (0-50 μm). The different observations for the smaller beads might have to do with the increasing relative strength of adhesive forces upon decreasing particle sizes. It is known that micron-sized

particles tend to form agglomerates upon collision due to inter-particle attractive forces being relatively much higher than the gravitational or inertial forces involved (Li et al., 2011). This increase in inter-particle attractive forces might help to keep the glass beads adhered to the surface of the drying droplet, also resulting in sticking.
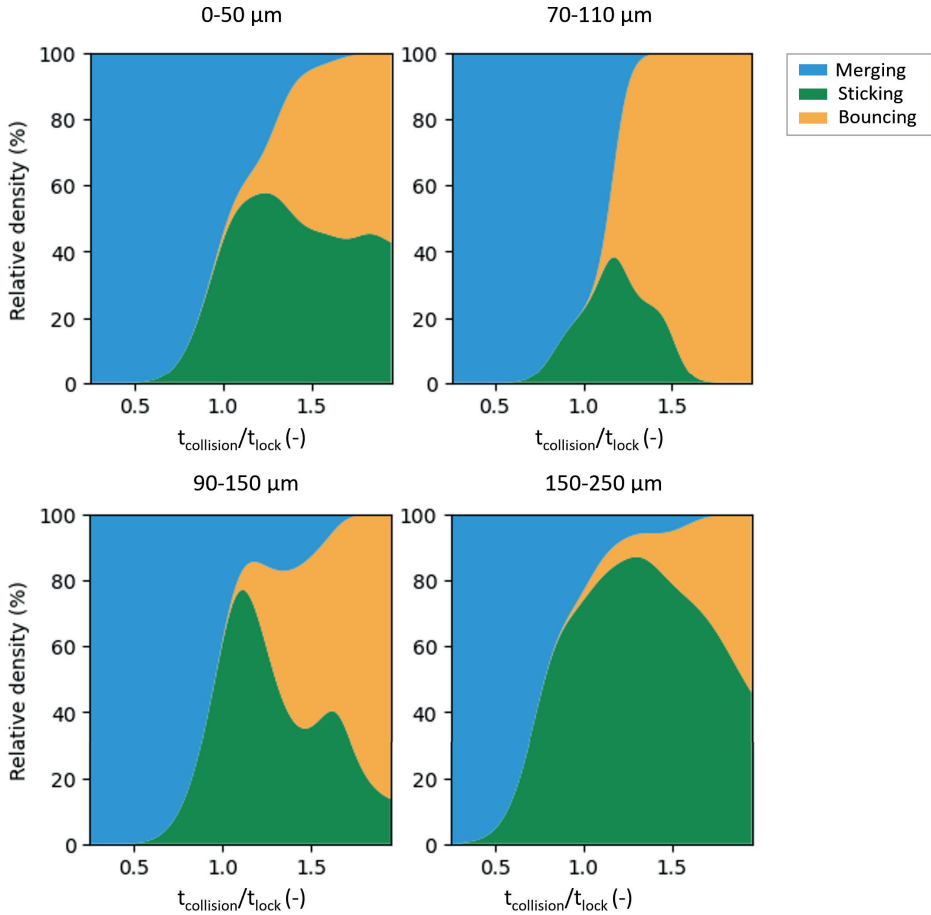
Figure 8.2. Stacked area charts for the collisions between drying MD38 droplets and glass beads of different sizes based on kernel density estimation values relative for each collision outcome across $t_{collision}/t_{lock}$ (-).

Differences in the stickiness range for glass beads of different sizes might also have to do with differences in collision speeds. Upon decreasing the glass bead sizes, the average collision speed increased (Figure 8.3). This might be caused by larger kinetic energy losses upon interactions with the wall of the powder tube for the larger beads. Moreover, a larger spread in collision speeds was observed for the smaller glass beads. The air flow within the drying tunnel is not completely laminar, and smaller particles are more susceptible for changing directions caused by turbulence eddies (Vames & Hanratty, 2004).
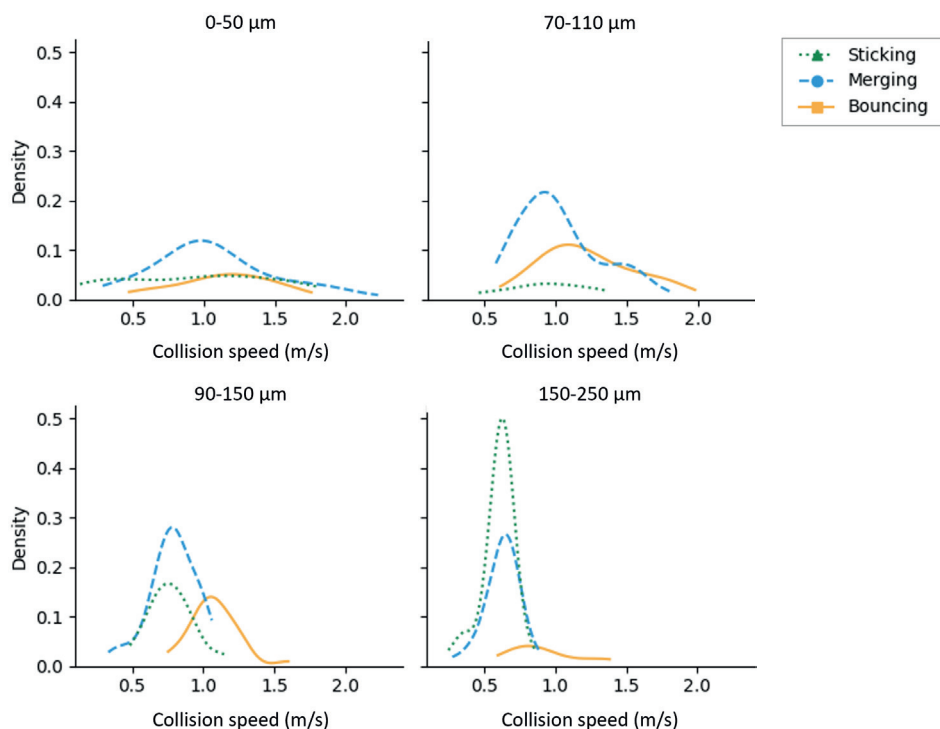
Figure 8.3. Density plots for collision speed, comparing glass bead sizes and collision outcomes.

The distribution of the collision speeds for the different collision outcomes reveals that higher velocities result more often in bouncing (Figure 8.3). For micron sized particles, it is known that the collision speed needs to be above a certain critical velocity to overcome adhesive forces and to result in bouncing (Chen, Li, & Yang, 2015; Konstandopoulos, 2006). Although the dominance of adhesion forces related to sticking behavior is not expected for our larger glass beads, it does seem like there is a critical velocity that is required for the bead to bounce off the droplet. As also observed by Chen et al. (2015) and Konstandopoulos (2006), this critical velocity depends on the particle size. The critical velocity for agglomeration is known to also depend on the particle density. As it increases with a decreasing density, it will create a wider window in which the relative velocity is below the critical velocity and in which agglomeration can occur (Hussain et al., 2022). The density of fines within a spray dryer is generally lower than that of the glass beads used in our research (3220 kg/m³). It is therefore expected that this lower density of real fines will result in more sticking. It will be worthwhile to investigate the relation between particle density and collision outcomes in more detail.

While the research presented within this thesis focused on the collision dynamics between a drying droplet and a dry particle, within a spray dryer collisions can also occur between two drying droplets. As these types of collisions can also result in agglomeration, it would

be of interest to investigate them as well. Replacing the dry glass bead for a drying droplet influences the stickiness properties of the colliding object. It is expected that the chance of the collision resulting in agglomeration will increase if the colliding object itself is also sticky. As an intermediate step collisions with dry particles having different surface properties, such as hydrophilicity, might also be of interest. Hydrophilic particles are attracted to water, and are therefore expected to have a later onset of the sticking and bouncing regime than hydrophobic particles.

Practical implications

Screening of complex systems
One of the initial ideas behind the development of single droplet drying systems, was to use it as a screening tool for complex systems to be spray dried. A rapid, small-scale investigation on the suitability of a material to be spray-dried is deemed very valuable for the drying industry. As shown throughout this thesis, it can, for example, be used to understand the drying kinetics of systems, to investigate the morphology and surface composition of the dried particles, or to investigate the inactivation of heat-sensitive compounds within the specific matrix. Optimization procedures, based on drying conditions or matrix formulations, can also benefit from initial screening at the single droplet level. Being able to reduce the number of large-scale trials would reduce the amount of energy and raw materials needed as well as the time required for the screening procedures.

Steering of agglomeration
Based on the work presented in this thesis, several lessons have been learned that can have direct implications to optimize industrial spray drying processes. First of all, when it comes to the drying conditions applied, the drying air temperature impacts drying behavior. A higher inlet air temperature will result in an earlier locking point. As the locking point influences the sticking behavior, the inlet air temperature can be changed to adjust the sticking regime for optimal agglomeration.

Both the timing of the collision as well as the (surface) composition of the drying droplets play an important role in agglomeration. The positioning of the fines return in the spray dryer is an important factor in the timing of the collisions. Fines colliding with the droplets while they are in their sticking regime will give agglomeration that results in loose grape structures. The formation of onion-like agglomerates indicates that the collisions occur too early. Adapting the position of the fines return to delay the collision time between droplets and fines will enhance the formation of grape-like agglomerates. A low observed level of agglomeration, and a high remaining level of fines indicate that the collisions occur too late. Relocating the fines return to a position higher up in the dryer to induce earlier collisions between the droplets and fines will enhance the desired agglomeration.

The composition of the drying droplets influences the locking point and hence the sticking regime. When working with maltodextrin-containing matrices, the DE value of

the maltodextrin present can be changed. In Chapter 6 it was shown that a lower DE value can be used to create an earlier onset of the sticking regime, while a high DE value maltodextrin can be used to make the sticking regime last longer. As described in Chapter 7, the addition of small amounts of proteins can be beneficial to enhance agglomeration in sugar rich products, when too little agglomeration is observed. The addition of proteins results in both an earlier onset and a later ending of the sticking regime, as well as an increased probability of a collision resulting in sticking.

Future outlook

The experimental platform that was developed in the context of this thesis, allowed in-line monitoring of the temperature and volume of drying droplets. The composition of the surface of dried particles could only be investigated off-line. For more complex matrices, the development of the surface properties of a drying droplet is expected to be important in collision dynamics, and thus would be valuable to measure in-line as well. However, this is challenging for a process that is as fast as drying droplets. Confocal Raman measurements, as applied in Chapter 5, require long measurement times compared to the drying time of our small droplets. Also for other techniques, like X-ray photoelectron spectroscopy or energy dispersive X-ray analysis, the temporal resolution is not sufficient to track the surface composition of our small, rapidly drying droplets over time. It might be possible to artificially stop the drying process at a specified time point, but this will introduce new artifacts. In this PhD project, some initial attempts were made to flash-freeze the droplet with liquid nitrogen, but direct application of liquid nitrogen onto the drying droplet was not feasible due to its rapid evaporation once in contact with applicational devices such as pipettes. The use of a cryogenic sprayer was investigated, but the ejection force of the nitrogen was too large to keep the small drying droplets in place. As an alternative to experimentally obtaining inline information about the changing surface composition, numerical models can provide additional information. Within this thesis, single droplet drying models were already used to accurately predict several characteristics of rapidly drying, small droplets. Extending the model to include predictions on the surface composition can give insights that could otherwise not be obtained at the short timescale relevant for the droplet drying process.

The work presented in the thesis included some first steps to link the single droplet drying observations to pilot scale spray drying. For the spray drying industry, the impact of non-soluble solids on the drying behavior would be an interesting topic for further research. In Chapter 7, the presence of non-soluble solids in the pea protein isolate seemed to influence agglomeration and yield. Besides, it would be relevant to extend this work to investigate the mechanistic insights behind processes such as crystallization, emulsion stability, or volatile retention during drying. Single droplet drying models might also be extended further to predict these processes without the need for extremely complex experimental designs. Moreover, creating experimentally validated drying models that use the input of single droplet drying research to predict drying and collision behavior at the large scale

would be another great step forward to support knowledge-based decision making in the spray drying industry. If this work would also be confirmed at the pilot-scale, it will be even more effective to create the opportunity to optimally steer the agglomeration in spray dryers.

Conclusion

This thesis aimed to characterize the physical phenomena underlying the drying and agglomeration behavior of droplets during spray drying via improved single droplet drying approaches. High-resolution thermography helped to obtain relevant information throughout the drying process. A new single droplet drying platform was developed that more realistically represents spray drying conditions by allowing temperature-time trajectories. These changing temperature conditions were found to influence the drying behavior of a droplet. This impacted, for example, the inactivation of β-galactosidase and the surface composition of dried dairy-based droplets. The new single droplet drying platform was extended to study binary collisions between drying droplets and glass beads. These studies showed the influence of the droplet composition on the sticking regime. The single droplet drying studies were extended with pilot-scale trials in which both agglomeration and yield were investigated. This showed that the learnings obtained at the single droplet scale provided useful insights for the optimization of spray drying processes.

8
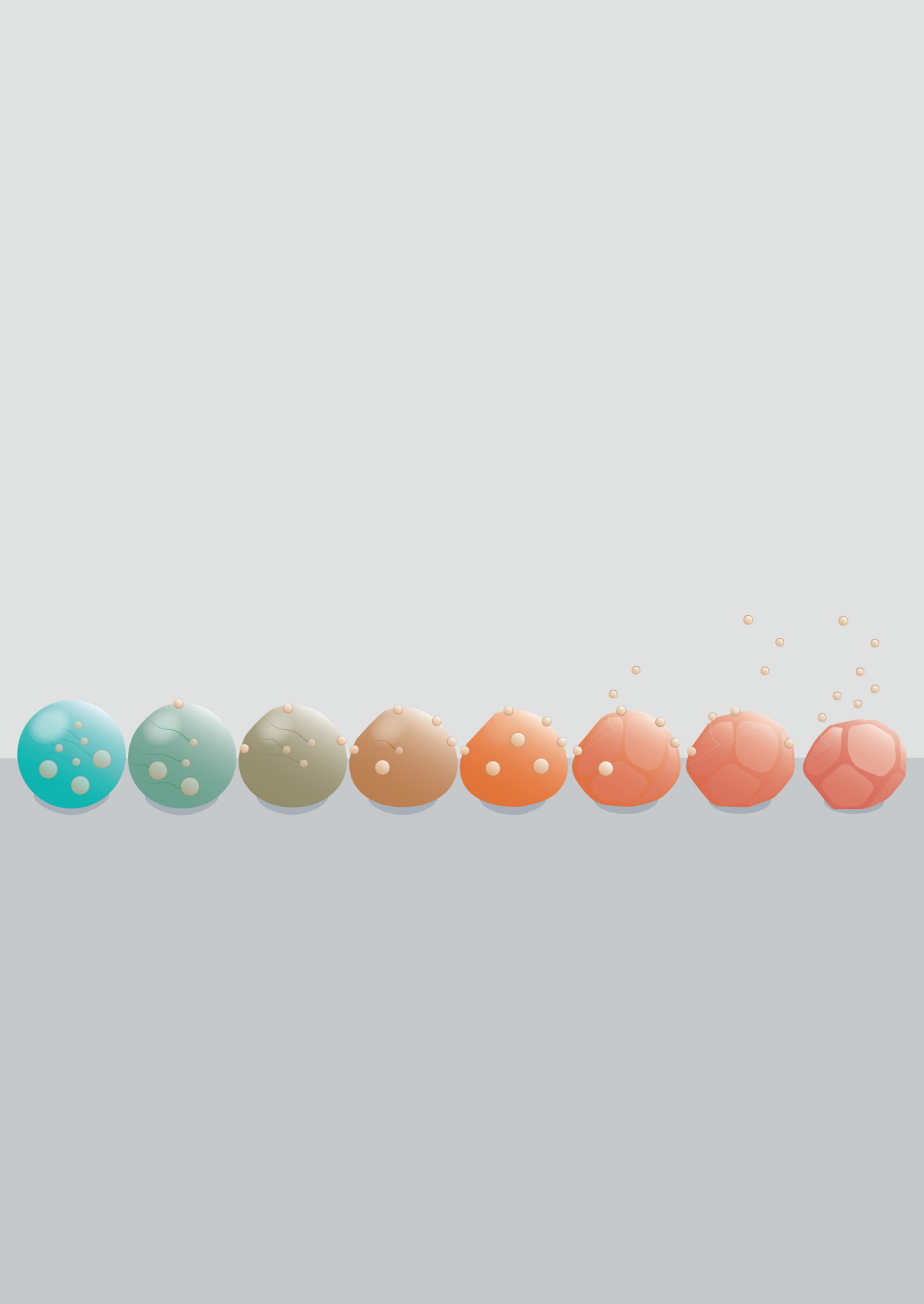
References

Adhikari, B., Howes, T., Bhandari, B. R., & Troung, V. (2004). Effect of addition of maltodextrin on drying kinetics and stickiness of sugar and acid-rich foods during convective drying: experiments and modelling. Journal of Food Engineering, 62, 53–68. https://doi.org/10.1016/S0260-8774(03)00171-7

Adhikari, B., Howes, T., Bhandari, B. R., & Truong, V. (2000). Experimental studies and kinetics of single drop drying and their relevance in drying of sugar-rich foods: A review. International Journal of Food Properties, 3(3), 323–351. https://doi.org/10.1080/10942910009524639

Adhikari, B., Howes, T., Bhandari, B. R., Yamamoto, S., & Truong, V. (2002). Application of a simplified method based on regular regime approach to determine the effective moisture diffusivity of mixture of low molecular weight sugars and maltodextrin during desorption. Journal of Food Engineering, 54, 157–165. https://doi.org/https://doi.org/10.1016/S0260-8774(01)00203-5

Alamilla-Beltrán, L., Chanona-Pérez, J. J., Jiménez-Aparicio, A. R., & Gutiérrez-Lopez, G. F. (2005). Description of morphological changes of particles along spray drying. Journal of Food Engineering, 67(1–2), 179–184. https://doi.org/10.1016/j.jfoodeng.2004.05.063

Anandharamakrishnan, P. C., & Ishwarya, S. (2015). Spray Drying Techniques for Food Ingredient Encapsulation (First edition). https://doi.org/10.1002/9781118863985

Andersson, I. M., Glantz, M., Alexander, M., Millqvist-Fureby, A., Paulsson, M., & Bergenståhl, B. (2018). Impact of surface properties on morphology of spray-dried milk serum protein/lactose systems. International Dairy Journal, 85, 86–95. https://doi.org/10.1016/j.idairyj.2018.04.011

Archer, J., Walker, J. S., Gregson, F. K. A., Hardy, D. A., & Reid, J. P. (2020). Drying Kinetics and Particle Formation from Dilute Colloidal Suspensions in Aerosol Droplets. Langmuir, 36, 12481–12493. https://doi.org/10.1021/acs.langmuir.0c01830

Bazaria, B., & Kumar, P. (2016). Effect of whey protein concentrate as drying aid and drying parameters on physicochemical and functional properties of spray dried beetroot juice concentrate. Food Bioscience, 14, 21–27. https://doi.org/10.1016/j.fbio.2015.11.002

Boel, E., Koekoekx, R., Dedroog, S., Babkin, I., Vetrano, M. R., Clasen, C., & Van den Mooter, G. (2020). Unraveling particle formation: From single droplet drying to spray drying and electrospraying. Pharmaceutics, 12(7), 1–58. https://doi.org/10.3390/pharmaceutics12070625

Both, E. M., Boom, R. M., & Schutyser, M. A. I. (2020). Particle morphology and powder properties during spray drying of maltodextrin and whey protein mixtures. Powder Technology, 363, 519–524. https://doi.org/10.1016/j.powtec.2020.01.001

Both, E. M., Karlina, A. M., Boom, R. M., & Schutyser, M. A. I. (2018). Morphology development during sessile single droplet drying of mixed maltodextrin and whey protein solutions. Food Hydrocolloids, 75, 202–210. https://doi.org/10.1016/j.foodhyd.2017.08.022

Both, E. M., Nuzzo, M., Millqvist-Fureby, A., Boom, R. M., & Schutyser, M. A. I. (2018). Morphology development during single droplet drying of mixed component formulations and milk. Food Research International, 109, 448–454. https://doi.org/10.1016/j.foodres.2018.04.043

Both, E. M., Siemons, I., Boom, R. M., & Schutyser, M. A. I. (2019). The role of viscosity in morphology development during single droplet drying. Food Hydrocolloids, 94, 510–518. https://doi.org/10.1016/j.foodhyd.2019.03.023

Both, E. M., Tersteeg, S. M. B., Boom, R. M., & Schutyser, M. A. I. (2020). Drying kinetics and viscoelastic properties of concentrated thin films as a model system for spray drying. Colloids and Surfaces A: Physicochemical and Engineering Aspects, 585, 124075. https://doi.org/10.1016/j.colsurfa.2019.124075

Bouman, J., Venema, P., de Vries, R. J., van der Linden, E., & Schutyser, M. A. I. (2016). Hole and vacuole formation during drying of sessile whey protein droplets. Food Research International, 84, 128–135. https://doi.org/10.1016/j.foodres.2016.03.027

Buchholz, M., Haus, J., Pietsch-braune, S., Kleine, F., & Heinrich, S. (2022). CFD-aided population balance modeling of a spray drying process. Advanced Powder Technology, 33(7), 103636. https://doi.org/10.1016/j.apt.2022.103636

Buck, B., Lunewski, J., Tang, Y., Deen, N. G., Kuipers, J. A. M., & Heinrich S. (2018). Numerical Investigation of Collision Dynamics of Wet Particles via Force Balance. Chemical Engineering Research and Design, 132, 1143–59. doi:10.1016/j.cherd.2018.02.026

Capece, M., Ho, R., Strong, J., & Gao, P. (2015). Prediction of powder flow performance using a multi-component granular Bond number. Powder Technology, 286, 561–571. https://doi.org/10.1016/j.powtec.2015.08.031

Carunchia Whetstine, M. E., Croissant, A. E., & Drake, M. A. (2005). Characterization of dried whey protein concentrate and isolate flavor. Journal of Dairy Science, 88(11), 3826–3839. https://doi.org/10.3168/jds.S0022-0302(05)73068-X

Charalampous, G., & Hardalupas, Y. (2017). Collisions of droplets on spherical particles. Physics of Fluids, 29(10). doi:10.1063/1.5005124

Charlesworth, D. H., & Marshall, W. R. (1960). Evaporation from drops containing dissolved solids. AIChE Journal, 6(1), 9–23. https://doi.org/10.1002/aic.690060104

Chen, P., Toubal, M., Carlier, J., Harmand, S., Nongaillard, B., & Bigerelle, M. (2016). Evaporation of Binary Sessile Drops: Infrared and Acoustic Methods To Track Alcohol Concentration at the Interface and on the Surface. Langmuir, 32, 9836–9845. https://doi.org/10.1021/acs.langmuir.6b02564

Chen, S., Li, S., & Yang, M. (2015). Sticking/rebound criterion for collisions of small adhesive particles: Effects of impact parameter and particle size. Powder Technology, 274, 431–440. https://doi.org/10.1016/j.powtec.2015.01.051

References

Chen, Y., Dai, J., Zhou, X., Liu, Y., Zhang, W., & Peng, G. (2014). Raman spectroscopy analysis of the biochemical characteristics of molecules associated with the malignant transformation of gastric mucosa. PLoS ONE, 9(4). https://doi.org/10.1371/journal.pone.0093906

Cheuyglintase, K. (2009). Spray drying of fruit juice with vegetable fibre as a carrier. [Doctoral thesis, University of Canterburry]. http://dx.doi.org/10.26021/2181

CNIEL. (2016). The World Dairy Situation 2016. Bulletin of the International Dairy Federation 485. www.fil-idf.org.

Colberg, C. A., Krieger, U. K., & Peter, T. (2004). Morphological Investigations of Single Levitated H2SO 4/NH3/H2O Aerosol Particles during Deliquescence/Efflorescence Experiments. Journal of Physical Chemistry A, 108(14), 2700–2709. https://doi.org/10.1021/jp037628r

Coulter, S. T. (1956). Dry Milk Manufacture. Journal of Dairy Science, 39(6), 843–46. https://doi.org/10.3168/jds.S0022-0302(56)91211-5

Dahl, J. F., Gregersen, S. B., Andersen, U., & Corredig, M. (2023). Confocal Raman microscopy to evaluate anisotropic structures and hydration development. Methodological considerations. Soft Matter, 19, 4208–4222. https://doi.org/10.1039/d3sm00170a

Dairy Industries International. (2018). Germany's Dairy Market Report. https://www.dairyindustries.com/news/30833/germanys-dairy-market-report/

De Souza Lima, R., Ré, M.-I., & Arlabosse, P. (2020). Drying droplet as a template for solid formation: A review. Powder Technology, 359, 161–171. https://doi.org/10.1016/j.powtec.2019.09.052

Du, J., Strenzke, G., Bück, A., & Tsotsas, E. (2022). Monte Carlo modeling of spray agglomeration in a cylindrical fluidized bed: From batch-wise to continuous processes. Powder Technology, 396, 113–126. https://doi.org/10.1016/j.powtec.2021.10.051

Duranty, E. R., Mccardle, H., Reichert, W. M., & Davis, J. H. (2020). Acoustic levitation and infrared thermography: a sound approach to studying droplet evaporation †. This Journal Is Cite This: Chem. Commun, 56, 4224. https://doi.org/10.1039/c9cc09856a

Eagle, J. (2016). GEA Installs 'second of Its Kind' World's Largest Spray Dryer at Fonterra Milk Powder Plant. Dairy Reporter. https://www.dairyreporter.com/Article/2016/11/04/GEA-installs-second-world-s-largest-spray-dryer-at-Fonterra

Eijkelboom, N. M., van Boven, A. P., Siemons, I., Wilms, P. F. C., Boom, R. M., Kohlus, R., & Schutyser, M. A. I. (2023). Particle structure development during spray drying from a single droplet to pilot-scale perspective. Journal of Food Engineering, 337. https://doi.org/10.1016/j.jfoodeng.2022.111222

Eijkelboom, N. M., Gawronska, K., Vollenbroek, J. M., Kraaijveld, G. J. C., Boom, R. M., Wilms, P. F. C., & Schutyser, M. A. I. (2024). Single droplet drying with stepwise changing temperature-time trajectories: Influence on heat sensitive constituents. Food Research International, 182. https://doi.org/10.1016/j.foodres.2024.114194

Eijkelboom, N. M., Rang, V. J., Breevaart, S., Boom, R. M., Wilms, P. F. C., & Schutyser, M. A. I. (2024). Binary collisions of drying maltodextrin droplets and glass beads. Journal of Food Engineering, 112110. https://doi.org/10.1016/j.jfoodeng.2024.112110

Eijkelboom, N. M., Swinkels, A. C. M., de Ruiter, J., Boom, R. M., Wilms, P. F. C., & Schutyser, M. A. I. (2023). High-resolution thermography and modelling allows for improved characterization of drying sessile single droplets. Journal of Food Engineering, 341. https://doi.org/10.1016/j.jfoodeng.2022.111340

Elgar, D. F., Hill, J. P., Holroyd, S. E., & Peddie, G. S. (2020). Comparison of analytical methods for measuring protein content of whey protein products and investigation of influences on nitrogen conversion factors. International Journal of Dairy Technology, 73(4), 790–794. https://doi.org/10.1111/1471-0307.12709

El-Sayed, T. M., Wallack, D. A., & King, C. J. (1990). Changes in particle morphology during drying of drops of carbohydrate solutions and food liquids. 1. Effect of composition and drying conditions. Industrial & Engineering Chemistry Research, 29(12), 2346–2354. https://doi.org/10.1021/ie00108a007

Euston, S. R., & Hirst, R. L. (2000). The Emulsifying Properties of Commercial Milk Protein Products in Simple Oil-in-Water Emulsions and in a Model Food System. Journal of Food Science, 65(6). https://doi.org/10.1111/j.1365-2621.2000.tb09396.x

Everall, N. J. (2010). Confocal Raman microscopy: Common errors and artefacts. In Analyst (Vol. 135, Issue 10, pp. 2512–2522). Royal Society of Chemistry. https://doi.org/10.1039/c0an00371a

Fang, Y., Rogers, S., Selomulya, C., & Dong, X. (2012). Functionality of milk protein concentrate : Effect of spray drying temperature. Biochemical Engineering Journal, 62, 101–105. https://doi.org/10.1016/j.bej.2011.05.007

FAO. (2011). "Energy-Smart" Food for People and Climate. https://www.fao.org/4/i2454e/i2454e00.pdf

Felton, L. A. (2013). Mechanisms of polymeric film formation. International journal of pharmaceutics, 457(2), 423-427. https://doi.org/10.1016/j.ijpharm.2012.12.027

Filková, I., Xin Huang, L., & Mujumdar, A. S. (2006). Industrial Spray Drying Systems. In Handbook of Industrial Drying, Third Edition (pp. 191–226). https://doi.org/10.1201/9781420017618.ch10

R

References

Finotello, G., De, S., Vrouwenvelder, J. C. R., Padding, J. T., Buist, K. A., Jongsma, A., Innings, F., & Kuipers, J. A. M. (2018). Experimental investigation of non-Newtonian droplet collisions: the role of extensional viscosity. Experiments in Fluids, 59(7), 113. https://doi.org/10.1007/s00348-018-2568-2

Finotello, G., Kooiman, R. F., Padding, J. T., Buist, K. A., Jongsma, A., Innings, F., & Kuipers, J. A. M. (2018). The dynamics of milk droplet–droplet collisions. Experiments in Fluids, 59(1), 17. https://doi.org/10.1007/s00348-017-2471-2

Focke, C., Kuschel, M., Sommerfeld, M., & Bothe, D. (2013). Collision between high and low viscosity droplets: Direct Numerical Simulations and experiments. International Journal of Multiphase Flow, 56, 81–92. https://doi.org/10.1016/j.ijmultiphaseflow.2013.05.008

Foerster, M., Gengenbach, T., Woo, W., & Selomulya, C. (2016). The impact of atomization on the surface composition of spray-dried milk droplets. Colloids and Surfaces B: Biointerfaces, 140, 460–471. https://doi.org/10.1016/j.colsurfb.2016.01.012

Fortini, A., & Sear, R. P. (2017). Stratification and Size Segregation of Ternary and Polydisperse Colloidal Suspensions during Drying. Langmuir, 33(19), 4796–4805. https://doi.org/10.1021/acs.langmuir.7b00946

Fortini, A., Martín-Fabiani, I., De La Haye, J. L., Dugas, P. Y., Lansalot, M., D'Agosto, F., Bourgeat-Lami, E., Keddie, J. L., & Sear, R. P. (2016). Dynamic Stratification in Drying Films of Colloidal Mixtures. Physical Review Letters, 116(11). https://doi.org/10.1103/PhysRevLett.116.118301

Foster, K. D., Bronlund, J. E., & Paterson, A. H. J. (2005). The contribution of milk fat towards the caking of dairy powders. International Dairy Journal, 15(1), 85–91. https://doi.org/10.1016/j.idairyj.2004.05.005

Fox, B., Bellini, G., & Pellegrini, L. (2014). Drying. In Fermentation and Biochemical Engineering Handbook (pp. 283-305). William Andrew Publishing. https://doi.org/10.1016/B978-1-4557-2553-3.00014-3

Fröhlich, J. A., Raiber, T. V., Hinrichs, J., & Kohlus, R. (2021). Nozzle zone agglomeration in spray dryers: Influence of total solid content on agglomerate properties. Powder Technology, 390, 292–302. https://doi.org/10.1016/j.powtec.2021.05.094

Fröhlich, J. A., Ruprecht, N. A., & Kohlus, R. (2023). Nozzle zone agglomeration in spray dryers: Determination of the agglomeration efficiency in the fines return by means of agglomerate properties and residence time distribution. Drying Technology. https://doi.org/10.1080/07373937.2023.2203224

Fröhlich, J. A., Ruprecht, N. A., Hinrichs, J., & Kohlus, R. (2020). Nozzle zone agglomeration in spray dryers: Effect of powder addition on particle coalescence. Powder Technology, 374, 223–232. https://doi.org/10.1016/j.powtec.2020.07.009

Fu, N., Woo, M. W., & Chen, X. D. (2012). Single Droplet Drying Technique to Study Drying Kinetics Measurement and Particle Functionality: A Review. Drying Technology, 30(15), 1771–1785. https://doi.org/10.1080/07373937.2012.708002

Fu, N., Woo, M. W., Selomulya, C., & Chen, X. D. (2013). Shrinkage behaviour of skim milk droplets during air drying. Journal of Food Engineering, 116(1), 37–44. https://doi.org/10.1016/j.jfoodeng.2012.11.005

Fu, N., Xiao, J., Woo, M., & Chen, X. D. (2020). Frontiers in Spray Drying. CRC Press. https://doi.org/10.1201/9780429429859

Fu, Nan, Wai Woo, M., Lin, S. X. Q., Zhou, Z., & Dong Chen, X. (2011). Reaction Engineering Approach (REA) to model the drying kinetics of droplets with different initial sizes-experiments and analyses. Chemical Engineering Science, 66(8), 1738–1747. https://doi.org/10.1016/j.ces.2011.01.009

Gallier, S., Vocking, K., Post, J. A., Van De Heijning, B., Acton, D., Van Der Beek, E. M., & Van Baalen, T. (2015). A novel infant milk formula concept: Mimicking the human milk fat globule structure. Colloids and Surfaces B: Biointerfaces, 136, 329–339. https://doi.org/10.1016/j.colsurfb.2015.09.024

Gao, Y., Mitra, S., Wanless, E. J., Moreno-Atanasio, R., & Evans, G. M. (2017). Interaction of a spherical particle with a neutrally buoyant immiscible droplet in salt solution. Chemical Engineering Science, 172, 182-198. https://doi.org/10.1016/j.ces.2017.06.018

García Llamas, C., Swami, V. V., Timmermans, B. A. G., Buist, K. A., Kuipers, J. A. M., & Baltussen, M. W. (2024). Numerical simulation of binary droplet collisions using a front tracking interface technique. Chemical Engineering Science, 284, 119510. https://doi.org/10.1016/j.ces.2023.119510

Ge, Y. (2005). 3D Numerical study on droplet-solid collisions in the Leidenfrost regime. The Ohio State University.

Gianfrancesco, A., Turchiuli, C., & Dumoulin, E. (2008). Powder agglomeration during the spray-drying process: Measurements of air properties. Dairy Science and Technology, 88(1), 53–64. https://doi.org/10.1051/dst:2007008

Gianfrancesco, A., Turchiuli, C., Dumoulin, E., & Palzer, S. (2009). Prediction of powder stickiness along spray drying process in relation to agglomeration. Particulate Science and Technology, 27(5), 415–427. https://doi.org/10.1080/02726350903129987

Gianfrancesco, A., Turchiuli, C., Flick, D., & Dumoulin, E. (2010). CFD Modeling and Simulation of Maltodextrin Solutions Spray Drying to Control Stickiness. Food and Bioprocess Technology, 3(6), 946–955. https://doi.org/10.1007/s11947-010-0352-2

Gong, Z., Yu, M., Wang, W., & Shi, X. (2018). Functionality of spray-dried strawberry powder: Effects of whey protein isolate and maltodextrin. International Journal of Food Properties, 21(1), 2229–2238. https://doi.org/10.1080/10942912.2018.1506477

R

Gouaou, I., Shamaei, S., Koutchoukali, M. S., Bouhelassa, M., Tsotsas, E., & Kharaghani, A. (2019). Impact of operating conditions on a single droplet and spray drying of hydroxypropylated pea starch: Process performance and final powder properties. Asia-Pacific Journal of Chemical Engineering, 14(1), e2268. https://doi.org/10.1002/apj.2268

Granelli, K., Fäldt, P., Appelqvist, L. Å., & Bergenståhl, B. (1996). Influence of surface structure on cholesterol oxidation in model food powders. Journal of the Science of Food and Agriculture, 71(1), 75–82. https://doi.org/10.1002/(SICI)1097-0010(199605)71:1<75::AID-JSFA551>3.0.CO;2-J

Gregson, F. K. A., Robinson, J. F., Miles, R. E. H., Royall, C. P., & Reid, J. P. (2019). Drying Kinetics of Salt Solution Droplets: Water Evaporation Rates and Crystallization. The Journal of Physical Chemistry, 123, 266–276. https://doi.org/10.1021/acs.jpcb.8b09584

Griesing, M., Grosshans, H., Hellwig, T., Sedelmayer, R., Gopireddy, S. R., Pauer, W., Gutheil, E., & Moritz, H. U. (2016). Influence of Air Humidity on the Particle Formation of Single Mannitol-Water Droplets during Drying. Chemie-Ingenieur-Technik, 88(7), 929–936. https://doi.org/10.1002/cite.201500087

Groenewold, C., Möser, C., Groenewold, H., & Tsotsas, E. (2002). Determination of single-particle drying kinetics in an acoustic levitator. Chemical Engineering Journal, 86(1–2), 217–222. https://doi.org/10.1016/S1385-8947(01)00292-3

Grosshans, H., Griesing, M., Mönckedieck, M., Hellwig, T., Walther, B., Gopireddy, S. R., Sedelmayer, R., Pauer, W., Moritz, H. U., Urbanetz, N. A., & Gutheil, E. (2016). Numerical and experimental study of the drying of bi-component droplets under various drying conditions. International Journal of Heat and Mass Transfer, 96, 97–109. https://doi.org/10.1016/j.ijheatmasstransfer.2015.12.062

Han, K., Song, G., Ma, X., & Yang, B. (2016). An experimental and theoretical study of the effect of suspended thermocouple on the single droplet evaporation. Applied Thermal Engineering, 10, 568–575. https://doi.org/10.1016/j.applthermaleng.2015.12.022

Hardy, D. A., Archer, J., Lemaitre, P., Vehring, R., Reid, J. P., & Walker, J. S. (2021). High time resolution measurements of droplet evaporation kinetics and particle crystallisation. Physical Chemistry Chemical Physics, 23(34), 18568–18579. https://doi.org/10.1039/d1cp02840e

Harvie, D. J.E., T. A.G. Langrish, and D. F. Fletcher. 2002. "A Computational Fluid Dynamics Study of a Tall-Form Spray Dryer." Food and Bioproducts Processing: Transactions of the Institution of of Chemical Engineers, Part C 80(3): 163–75. doi:10.1205/096030802760309188.

Heitor, M. V, & Moreira, A. L. N. (1993). Thermocouples and sample probes for combustion studies. Progress in Energy and Combustion Science, 19, 259–278. https://doi.org/https://doi.org/10.1016/0360-1285(93)90017-9

Höhne, S., & Gaukel, V. (2024). Impact of the drying rate on product properties of spray dried emulsions to enable a targeted product design. Drying Technology. https://doi.org/10.1080/07373937.2024.2306525

Höhne, S., Taboada, M. L., Schröder, J., Gomez, C., Karbstein, H. P., & Gaukel, V. (2024). Influence of Nozzle Geometry and Scale-Up on Oil Droplet Breakup in the Atomization Step during Spray Drying of Emulsions. Fluids, 9(3). https://doi.org/10.3390/fluids9030070

Hong, T., Iwashita, K., & Shiraki, K. (2017). Viscosity Control of Protein Solution by Small Solutes: A Review. Current Protein & Peptide Science, 19(8), 746–758. https://doi.org/10.2174/1389203719666171213114919

Hooiveld, E., Dols, M., van der Gucht, J., Sprakel, J., & van der Kooij, H. M. (2023). Quantitative imaging methods for heterogeneous multi-component films. Soft Matter, 19. https://doi.org/10.1039/d3sm01212c

Huang, S., Vignolles, M. L., Chen, X. D., Le Loir, Y., Jan, G., Schuck, P., & Jeantet, R. (2017). Spray drying of probiotics and other food-grade bacteria: A review. Trends in Food Science and Technology, 63, 1–17. https://doi.org/10.1016/j.tifs.2017.02.007

Huelsmann, R., Esper, G. J., & Kohlus, R. (2020). Using an acoustic levitator to investigate the drying kinetics and solids forming process of individual droplets during spray drying. Progress in Agricultural Engineering Sciences, 16(1), 41–49. https://doi.org/10.1556/446.2020.00011

Hülsmann, R., Mast, M., Schnorr, C., Esper, G. J., & Kohlus, R. (2022). Implementation of an acoustic levitator experimental setup for the investigation into drying kinetics of single droplets. Drying Technology, 40(7), 1436-1450. doi:10.1080/07373937.2021.1872609

Hunter, J. D. (2007). Matplotlib: A 2D Graphics Environment. Computing in Science & Engineering, 9(3), 90–95. https://doi.org/10.1109/MCSE.2007.55

Hussain, F., Jaskulski, M., Piatkowski, M., & Tsotsas, E. (2022). CFD simulation of agglomeration and coalescence in spray dryer. Chemical Engineering Science, 247. https://doi.org/10.1016/j.ces.2021.117064

Janocha, M., & Tsotsas, E. (2022). Coating layer formation from deposited droplets: A comparison of nanofluid, microfluid and solution. Powder Technology, 399. https://doi.org/10.1016/j.powtec.2022.117202

Khan, H. M. H., McCarthy, U., Esmonde-White, K., Casey, I., & O'Shea, N. (2023). Potential of Raman spectroscopy for in-line measurement of raw milk composition. Food Control, 152. https://doi.org/10.1016/j.foodcont.2023.109862

Kim, S. S., & Bhowmik, S. R. (1990). Survival of Lactic Acid Bacteria during Spray Drying of Plain Yogurt. Journal of Food Science, 55(4), 1008–1010. https://doi.org/10.1111/j.1365-2621.1990.tb01585.x

R

Kluyver, T., Ragan-Kelley, B., Pérez, F., Granger, B., Bussonnier, M., Frederic, J., Kelley, K., Hamrick, J., Grout, J., Corlay, S., Ivanov, P., Avila, D., Abdalla, S., & Willing, C. (2016). Jupyter Notebooks—a publishing format for reproducible computational workflows. Positioning and Power in Academic Publishing: Players, Agents and Agendas - Proceedings of the 20th International Conference on Electronic Publishing, ELPUB 2016, 87–90. https://doi.org/10.3233/978-1-61499-649-1-87

Konstandopoulos, A. G. (2006). Particle sticking/rebound criteria at oblique impact. Journal of Aerosol Science, 37(3), 292–305. https://doi.org/10.1016/j.jaerosci.2005.05.019

Kornet, C., Venema, P., Nijsse, J., van der Linden, E., van der Goot, A. J., & Meinders, M. (2020). Yellow pea aqueous fractionation increases the specific volume fraction and viscosity of its dispersions. Food Hydrocolloids, 99. https://doi.org/10.1016/j.foodhyd.2019.105332

Kornet, R., Shek, C., Venema, P., Jan van der Goot, A., Meinders, M., & van der Linden, E. (2021). Substitution of whey protein by pea protein is facilitated by specific fractionation routes. Food Hydrocolloids, 117. https://doi.org/10.1016/j.foodhyd.2021.106691

Langevin, D. (2020). Emulsions, Microemulsions and foams. Springer Nature. https://doi.org/https://doi.org/10.1007/978-3-030-55681-5

Leniger, H. A., & Beverloo, W. A. (1975). Food process engineering. D. Reidel Publishing Company.

Li, H., Kuschel, M., & Sommerfeld, M. (2016). Experimental investigation and modeling of coalescence and agglomeration for spray drying of solutions. In Process-Spray: Functional Particles Produced in Spray Processes (pp. 205–233). Springer International Publishing. https://doi.org/10.1007/978-3-319-32370-1_6

Li, S., Marshall, J. S., Liu, G., & Yao, Q. (2011). Adhesive particulate flow: The discrete-element method and its application in energy and environmental engineering. Progress in Energy and Combustion Science, 37(6), 633–668. https://doi.org/10.1016/j.pecs.2011.02.001

Lin, S. X. Q., & Chen, X. D. (2002). Improving the glass-filament method for accurate measurement of drying kinetics of liquid droplets. Chemical Engineering Research and Design, 80(4), 400–409. https://doi.org/10.1205/026387602317446443

Linke, A., Weiss, J., & Kohlus, R. (2020). Factors determining the surface oil concentration of encapsulated lipid particles: impact of the emulsion oil droplet size. European Food Research and Technology, 246(10), 1933–1943. https://doi.org/10.1007/s00217-020-03545-5

Littringer, E. M., Paus, R., Mescher, A., Schroettner, H., Walzel, P., & Urbanetz, N. A. (2013). The morphology of spray dried mannitol particles-The vital importance of droplet size. Powder Technology, 239, 162–174. https://doi.org/10.1016/j.powtec.2013.01.065

Macdonald, A. M., & Vaughan, A. S. (2007). Numerical simulations of confocal Raman spectroscopic depth profiles of materials: A photon scattering approach. Journal of Raman Spectroscopy, 38(5), 584–592. https://doi.org/10.1002/jrs.1706

Mallamace, F., Corsaro, C., Mallamace, D., Baglioni, P., Stanley, H. E., & Chen, S. H. (2011). A possible role of water in the protein folding process. Journal of Physical Chemistry B, 115(48), 14280–14294. https://doi.org/10.1021/jp205285t

McColl, I. H., Blanch, E. W., Gill, A. C., Rhie, A. G. O., Ritchie, M. A., Hecht, L., Nielsen, K., & Barron, L. D. (2003). A new perspective on β-sheet structures using vibrational raman optical activity: From poly(L-lysine) to the prion protein. Journal of the American Chemical Society, 125(33), 10019–10026. https://doi.org/10.1021/ja021464v

McKinney, W. (2010). Data structures for statistical computing in python. Proceedings of the 9th Python in Science Conference.

Mezhericher, M., Levy, A., & Borde, I. (2015). Multi-Scale Multiphase Modeling of Transport Phenomena in Spray-Drying Processes. Drying Technology, 33(1), 2–23. https://doi.org/10.1080/07373937.2014.941110

Michalski, M. C., Briard, V., Michel, F., Tasson, F., & Poulain, P. (2005). Size distribution of fat globules in human colostrum, breast milk, and infant formula. Journal of Dairy Science, 88(6), 1927–1940. https://doi.org/10.3168/jds.S0022-0302(05)72868-X

Mirlohi, M., Manickavasagan, A., & Ali, A. (2022). The effect of protein drying aids on the quantity and quality of spray dried sugar-rich powders: a systematic review. Drying Technology, 40(6), 1068–1082. https://doi.org/10.1080/07373937.2020.1856131

Mitra, S., Doroodchi, E., Pareek, V., Joshi, J. B., & Evans, G. M. (2014). Collision behaviour of a smaller particle into a larger stationary droplet. Advanced Powder Technology, 26, 280–295. https://doi.org/10.1016/j.apt.2014.10.008

Mondragón, R., Juliá, J. E., Hernández, L., & Jarque, J. C. (2013). Influence of Particle Size on the Drying Kinetics of Single Droplets Containing Mixtures of Nanoparticles and Microparticles: Modeling and Pilot-Scale Validation. Drying Technology, 31(7), 759–768. https://doi.org/10.1080/07373937.2012.757233

Morr, C. V., German, B., Kinsella, J. E., Regenstein, J. M., Buren, J. P. V., Kilara, A., Lewis, B. A., & Mangino, M. E. (1985). A Collaborative Study to Develop a Standardized Food Protein Solubility Procedure. Journal of Food Science, 50(6), 1715–1718. https://doi.org/10.1111/j.1365-2621.1985.tb10572.x

Mulet-Cabero, A. I., Mackie, A. R., Wilde, P. J., Fenelon, M. A., & Brodkorb, A. (2019). Structural mechanism and kinetics of in vitro gastric digestion are affected by process-induced changes in bovine milk. Food Hydrocolloids, 86, 172–183. https://doi.org/10.1016/j.foodhyd.2018.03.035

R

Nhumaio, G. C. S., Watkins, A. P., & John Yule, A. (2004). Experiments and CFD Predictions of Two Overlapping Water Sprays Issued from Air-Assist Atomizers. 19th Annual Meeting of the Institute for Liquid Atomization and Spray Systems (Europe).

Nhumaio, G. C. S., Watkins, A. P., Yule, A. J., & Verdurmen, R. E. M. (2005). CFD Predictions of Three Overlapping Sprays Discharged in Hot Turbulent Flows. Proc. 20th Annual Conference of ILASS-Europe.

Nicoud, L., Lattuada, M., Yates, A., & Morbidelli, M. (2015). Impact of aggregate formation on the viscosity of protein solutions. Soft Matter, 11(27), 5513–5522. https://doi.org/10.1039/c5sm00513b

Nuzzo, M., Millqvist-Fureby, A., Sloth, J., & Bergenstahl, B. (2015). Surface Composition and Morphology of Particles Dried Individually and by Spray Drying. Drying Technology, 33, 757–767. https://doi.org/10.1080/07373937.2014.990566

Nuzzo, M., Sloth Overgaard, J., Bergenståhl, B., & Millqvist-Fureby, A. (2017). The morphology and internal composition of dried particles from whole milk—From single droplet to full scale drying. Food Structure, 13, 35–44. https://doi.org/10.1016/j.foostr.2017.02.001

Nuzzo, M., Sloth, J., Brandner, B., Bergenstahl, B., & Millqvist-Fureby, A. (2015). Confocal Raman microscopy for mapping phase segregation in individually dried particles composed of lactose and macromolecules. Colloids and Surfaces A: Physicochemical and Engineering Aspects, 481, 229–236. https://doi.org/10.1016/j.colsurfa.2015.04.044

Ozmen, L., & Langrish, T. A. G. (2003). An experimental investigation of the wall deposition of milk powder in a pilot-scale spray dryer. Drying Technology, 21(7), 1253–1272. https://doi.org/10.1081/DRT-120023179

Palzer, S. (2005). The effect of glass transition on the desired and undesired agglomeration of amorphous food powders. Chemical Engineering Science, 60(14), 3959–3968. https://doi.org/10.1016/j.ces.2005.02.015

Paramita, V., Iida, K., Yoshii, H., & Furuta, T. (2010). Effect of additives on the morphology of spray dried powder. Drying Technology, 28(3), 323–329. https://doi.org/10.1080/07373931003627098323

Patel, K. C., & Chen, X. D. (2008). Surface-center temperature differences within milk droplets during convective drying and drying-based Biot number analysis. AIChE Journal, 54(12), 3273–3290. https://doi.org/10.1002/aic.11608

Pawar, S. K., Henrikson, F., Finotello, G., Padding, J. T., Deen, N. G., Jongsma, A., Innings, F., & Kuipers, J. A. M. H. (2016). An experimental study of droplet-particle collisions. Powder Technology, 300, 157-163. https://doi.org/10.1016/j.powtec.2016.06.005

Pax, A. P., & Sheehan, J. J. (2020). Novel application of confocal Raman microscopy to determine the microstructure of fermented dairy products including the spatial distribution of proteins, lipids and carbohydrates. Biomedical Spectroscopy and Imaging, 9(1–2), 33–45. https://doi.org/10.3233/bsi-200201

Pearce, D. L. (2007). A Novel Way to Measure the Concentration of a Spray in a Spray Dryer. Drying Technology, 24(6), 777–781. https://doi.org/10.1080/03602550600685366

Peighambardoust, S. H., Golshan Tafti, A., & Hesari, J. (2011). Application of spray drying for preservation of lactic acid starter cultures: A review. Trends in Food Science and Technology, 22(5), 215–224. https://doi.org/10.1016/j.tifs.2011.01.009

Percy, S. R. (1872). Improvement in drying and concentrating liquid substances by atomization (Patent No. 125,406).

Perdana, J., Fox, M. B., Schutyser, M. A. I., & Boom, R. M. (2013). Mimicking Spray Drying by Drying of Single Droplets Deposited on a Flat Surface. Food and Bioprocess Technology, 6(4), 964–977. https://doi.org/10.1007/s11947-011-0767-4

Perusko, M., Ghnimi, S., Simovic, A., Stevanovic, N., Radomirovic, M., Gharsallaoui, A., Smiljanic, K., Van Haute, S., Stanic-Vucinic, D., & Cirkovic Velickovic, T. (2021). Maillard reaction products formation and antioxidative power of spray dried camel milk powders increases with the inlet temperature of drying. Lwt, 143, 111091. https://doi.org/10.1016/j.lwt.2021.111091

Petersen, T. (2015). Model of Stickiness in Spray Drying. [Doctoral thesis, Technical University of Denmark]. https://findit.dtu.dk/en/catalog/57f3d20b15252c3a0f00000c

Písecký, J. (2012). Handbook of milk powder manufacture. GEA Process Engineering A/S.

Poozesh, S., & Bilgili, E. (2019). Scale-up of pharmaceutical spray drying using scale-up rules: A review. International Journal of Pharmaceutics, 562, 271–292. https://doi.org/10.1016/j.ijpharm.2019.03.047

Porowska, A., Dosta, M., Fries, L., Gianfrancesco, A., Heinrich, S., & Palzer, S. (2016). Predicting the surface composition of a spray-dried particle by modelling component reorganization in a drying droplet. Chemical Engineering Research and Design, 110, 131–140. https://doi.org/10.1016/j.cherd.2016.03.007

Qian, J., & Law, C. K. (1997). Regimes of coalescence and separation in droplet collision. Journal of Fluid Mechanics, 331, 59–80. https://doi.org/10.1017/S0022112096003722

Rabe, C., Malet, J., & Feuillebois, F. (2010). Experimental investigation of water droplet binary collisions and description of outcomes with a symmetric Weber number. Phys. Fluids, 22. https://doi.org/10.1063/1.3392768

Rabe, M., Verdes, D., & Seeger, S. (2011). Understanding protein adsorption phenomena at solid surfaces. In Advances in Colloid and Interface Science (Vol. 162, Issues 1–2, pp. 87–106). Elsevier B.V. https://doi.org/10.1016/j.cis.2010.12.007

R

Räderer, M., Besson, A., & Sommer, K. (2002). A thin film dryer approach for the determination of water diffusion coefficients in viscous products. In Chemical Engineering Journal (Vol. 86).

Ramírez, C. A., Patel M., & Blok K. (2006). From Fluid Milk to Milk Powder: Energy Use and Energy Efficiency in the European Dairy Industry. Energy, 31(12), 1984–2004. doi:10.1016/j.energy.2005.10.014

Rogers, S., Duo, W., Lin, S. X. Q., & Dong, X. (2012). Particle shrinkage and morphology of milk powder made with a monodisperse. Biochemical Engineering Journal, 62, 92–100. https://doi.org/10.1016/j.bej.2011.11.002

Ruano Uscategui, D. C., Ciro Velásquez, H. J., & Sepúlveda Valencia, J. U. (2018). Concentrates of sugarcane juice and whey protein: Study of a new powder product obtained by spray drying of their combinations. Powder Technology, 333, 429–438. https://doi.org/10.1016/j.powtec.2018.04.025

Ruprecht, N. A., Bürger, J. V., & Kohlus, R. (2023). Using phycocyanin as a marker to investigate drying history and structure formation in spray drying. Drying Technology, 1–14. https://doi.org/10.1080/07373937.2023.2193977

Sadek, C., Hervétabuteau, H., Schuck, P., Fallourd, Y., Pradeau, N., Cécile, C., Floch-Fouéré, L., Fouéré, F., & Jeantet, R. (2013). Shape, Shell, and Vacuole Formation during the Drying of a Single Concentrated Whey Protein Droplet. Langmuir, 29(50), 15606–15613. https://doi.org/10.1021/la404108v

Sadek, C., Li, H., Schuck, P., Fallourd, Y., Pradeau, N., Le Floch-Fouéré, C., & Jeantet, R. (2014). Protein kind driven particle morphology and resulting dairy powder properties. 19th International Drying Symposium (IDS 2014).

Sadek, C., Pauchard, L., Schuck, P., Fallourd, Y., Pradeau, N., Le Floch-Fouéré, C., & Jeantet, R. (2015). Mechanical properties of milk protein skin layers after drying: Understanding the mechanisms of particle formation from whey protein isolate and native phosphocaseinate. Food Hydrocolloids, 48, 8–16. https://doi.org/10.1016/j.foodhyd.2015.01.014

Sadek, C., Schuck, P., Fallourd, Y., Pradeau, N., Jeantet, R., & Le Floch-Fouéré, C. (2016). Buckling and collapse during drying of a single aqueous dispersion of casein micelle droplet. Food Hydrocolloids, 52, 161–166. https://doi.org/10.1016/j.foodhyd.2015.06.016

Sadek, C., Schuck, P., Fallourd, Y., Pradeau, N., Le Floch-Fouéré, C., & Jeantet, R. (2015). Drying of a single droplet to investigate process–structure–function relationships: a review. Dairy Science & Technology, 95(6), 771–794. https://doi.org/10.1007/s13594-014-0186-1

Samborska, K., Guiavarc'h, Y., Van Loey, A., & Hendrickx, M. (2005). The influence of moisture content on the thermostability of Aspergillus oryzae α-amylase. Enzyme and Microbial Technology, 37(2), 167–174. https://doi.org/10.1016/j.enzmictec.2004.06.017

Samborska, K., Sarabandi, K., Tonon, R., Topuz, A., Eroğlu, E., Kaymak-Ertekin, F., Malekjani, N., & Jafari, S. M. (2023). Recent progress in the stickiness reduction of sugar-rich foods during spray drying. Drying Technology, 1–20. https://doi.org/10.1080/07373937.2023.2229916

Santos, D., Maurício, A. C., Sencadas, V., Santos, J. D., Fernandes, M. H., & Gomes, P. S. (2018). Spray drying: an overview. In Biomaterials - Physics and Chemistry (pp. 9–35). IntechOpen.

Santos, J., Trujillo-Cayado, L. A., Carrillo, F., López-Castejón, M. L., & Alfaro-Rodríguez, M. C. (2022). Relation between Droplet Size Distributions and Physical Stability for Zein Microfluidized Emulsions. Polymers, 14(11). https://doi.org/10.3390/polym14112195

Sardar, R., Oh, J., Kim, M., Lee, J. E., Kim, S., & Kim, K. C. (2023). The effect of inlet velocity, gas temperature and particle size on the performance of double cyclone separator. Chemical Engineering and Processing - Process Intensification, 191. https://doi.org/10.1016/j.cep.2023.109469

Schaefer, J., & Lee, G. (2015). Arrhenius activation energy of damage to catalase during spray-drying. International Journal of Pharmaceutics, 489(1–2), 124–130. https://doi.org/10.1016/j.ijpharm.2015.04.078

Schiffter, H., & Lee, G. (2007). Single-Droplet Evaporation Kinetics and Particle Formation in an Acoustic Levitator. Part 1 : Evaporation of Water Microdroplets Assessed using Boundary-Layer and Acoustic Levitation Theories. Journal of Pharmaceutical Sciences, 96(9), 2274–2283. https://doi.org/10.1002/jps.20860

Schulz, M., & Keddie, J. L. (2018). A critical and quantitative review of the stratification of particles during the drying of colloidal films. Soft Matter, 14(30), 6181–6197. https://doi.org/10.1039/c8sm01025k

Schutyser, M. A. I., Both, E. M., Siemons, I., Vaessen, E. M. J., & Zhang, L. (2019). Gaining insight on spray drying behavior of foods via single droplet drying analyses. Drying Technology, 37(5). https://doi.org/10.1080/07373937.2018.1482908

Schutyser, M. A. I., Perdana, J., & Boom, R. M. (2012). Single droplet drying for optimal spray drying of enzymes and probiotics. Trends in Food Science and Technology, 27(2), 73–82. https://doi.org/10.1016/j.tifs.2012.05.006

Schwartzbach, C., & Masters, K. (2001). Performance of spray dryer with integrated filter and fluid bed. Drying Technology, 19(8), 1909–1923. https://doi.org/10.1081/DRT-100107279

Seabold, S., & Perktold, J. (2010). Statsmodels: Econometric and statistical modeling with python. Proceedings of the 9th Python in Science Conference.

R

Segat, A., Misra, N. N., Fabbro, A., Buchini, F., Lippe, G., Cullen, P. J., & Innocente, N. (2014). Effects of ozone processing on chemical, structural and functional properties of whey protein isolate. Food Research International, 66, 365–372. https://doi.org/10.1016/j.foodres.2014.10.002

Selvamuthukumaran, M., Tranchant, C., & Shi, J. (2020). Spraying Drying Concept, Application and Its Recent Advances in Food Processing. In M. Selvamuthukumaran (Ed.), Handbook on Spray Drying Application for Food Industries (pp. 1–30). Taylor and Francis Group.

Sewalt, E.J.G. (2024). Predicting collision outcomes of partially-dried droplets in spray drying. [Doctoral thesis, Delft University of Technology]. https://doi.org/10.4233/uuid:8204cf4d-a5fd-4e20-956c-37aba9bf3dd7

Sewalt, E. J. G., Zhang, F., Steijn, V. van, Ommen, J. R. van, & Meesters, G. M. H. (2020). Static and Dynamic Stickiness Tests to Measure Particle Stickiness. KONA Powder and Particle Journal, 38(0), 26–41. https://doi.org/10.14356/KONA.2021017

Shamaei, S., Kharaghani, A., Seiiedlou, S. S., Aghbashlo, M., Sondej, F., & Tsotsas, E. (2016). Drying behavior and locking point of single droplets containing functional oil. Advanced Powder Technology, 27(4), 1750–1760. https://doi.org/10.1016/j.apt.2016.06.006

Shamaei, S., Seiiedlou, S. S., Aghbashlo, M., & Valizadeh, H. (2017). Mathematical modeling of drying behavior of single emulsion droplets containing functional oil. Food and Bioproducts Processing, 101, 100–109. https://doi.org/10.1016/j.fbp.2016.10.012

Shi, Q., Fang, Z., & Bhandari, B. (2013). Effect of Addition of Whey Protein Isolate on Spray-Drying Behavior of Honey with Maltodextrin as a Carrier Material. Drying Technology, 31(13–14), 1681–1692. https://doi.org/10.1080/07373937.2013.783593

Siccama, J. W., Pegiou, E., Eijkelboom, N. M., Zhang, L., Mumm, R., Hall, R. D., & Schutyser, M. A. (2021). The effect of partial replacement of maltodextrin with vegetable fibres in spray-dried white asparagus powder on its physical and aroma properties. Food Chemistry, 356, 129567. doi:10.1016/j.foodchem.2021.129567

Siemons, I., Politiek, R. G. A., Boom, R. M., van der Sman, R. G. M., & Schutyser, M. A. I. (2020). Dextrose equivalence of maltodextrins determines particle morphology development during single sessile droplet drying. Food Research International, 131. https://doi.org/10.1016/j.foodres.2020.108988

Siemons, I., Vaessen, E. M. J., Oosterbaan Van Peski, S. E., Boom, R. M., & Schutyser, M. A. I. (2021). Protective effect of carrier matrices on survival of Lactobacillus plantarum WCFS1 during single droplet drying explained by particle morphology development. Journal of Food Engineering, 292. https://doi.org/10.1016/j.jfoodeng.2020.110263

Siemons, I., Veser, J., Boom, R. M., Schutyser, M. A. I., & van der Sman, R. G. M. (2022). Rheological behaviour of concentrated maltodextrins describes skin formation and morphology development during droplet drying. Food Hydrocolloids, 126, 107442. https://doi.org/10.1016/j.foodhyd.2021.107442

Siguemoto, E., Atmani, L., Mestres, C., & Meot, J. M. (2023). Modelling cowpea beans α-galactosidase inactivation dependence on temperature and moisture content. LWT, 190. https://doi.org/10.1016/j.lwt.2023.115571

Sugiyama, Y., Larsen, R. J., Kim, J.-W., & Weitz, D. A. (2006). Buckling and Crumpling of Drying Droplets of Colloid–Polymer Suspensions. Langmuir, 22(14), 6024–6030. https://doi.org/10.1021/LA053419H

Tabatabaei, M., Ebrahimi, B., Rajaei, A., Movahednejad, M. H., Rastegari, H., Taghavi, E., Aghbashlo, M., Gupta, V. K., & Lam, S. S. (2022). Producing submicron chitosan-stabilized oil Pickering emulsion powder by an electrostatic collector-equipped spray dryer. Carbohydrate Polymers, 294. https://doi.org/10.1016/j.carbpol.2022.119791

Taboada, M. L., Schäfer, A. C., Karbstein, H. P., & Gaukel, V. (2021). Oil droplet breakup during pressure swirl atomization of food emulsions: Influence of atomization pressure and initial oil droplet size. Journal of Food Process Engineering, 44(1). https://doi.org/10.1111/jfpe.13598

Takeiti, C. Y., Kieckbusch, T. G., & Collares-Queiroz, F. P. (2008). Morphological and physicochemical characterization of commercial maltodextrins with different degrees of dextrose-equivalent. International Journal of Food Properties, 13(2), 411–425. https://doi.org/10.1080/10942910802181024

Tang, Q., Roos, Y. H., & Miao, S. (2023). Plant Protein versus Dairy Proteins: A pH-Dependency Investigation on Their Structure and Functional Properties. Foods, 12(2). https://doi.org/10.3390/foods12020368

Terrazas-Velarde Korina, K., Peglow, M., & Tsotsas, E. (2011). Kinetics of fluidized bed spray agglomeration for compact and porous particles. Chemical Engineering Science, 66(9), 1866–1878. https://doi.org/10.1016/j.ces.2011.01.037

Tran, T. T. H., Avila-Acevedo, J. G., & Tsotsas, E. (2016). Enhanced methods for experimental investigation of single droplet drying kinetics and application to lactose/water. Drying Technology, 34(10), 1185–1195. https://doi.org/10.1080/07373937.2015.1100202

Tran, T. T. H., Jaskulski, M., & Tsotsas, E. (2017). Reduction of a model for single droplet drying and application to CFD of skim milk spray drying. Drying Technology, 35(13), 1571–1583. https://doi.org/10.1080/07373937.2016.1263204

Turchiuli, C., Gianfrancesco, A., Palzer, S., & Dumoulin, E. (2011). Evolution of particle properties during spray drying in relation with stickiness and agglomeration control. Powder Technology, 208(2), 433–440. https://doi.org/10.1016/j.powtec.2010.08.040

R

Ullum, T., Sloth, J., Brask, A., & Wahlberg, M. (2010). Predicting spray dryer deposits by CFD and an empirical drying model. Drying Technology, 28(5), 723–729. https://doi.org/10.1080/07373931003799319

Vames, J. S., & Hanratty, T. J. (2004). Turbulent dispersion of droplets for air flow in a pipe. Experiments in Fluids, 6(2), 94–104. https://doi.org/10.1007/BF00196459

van Boven, A. P., Calderon Novoa, S. M., Kohlus, R., & Schutyser, M. A. I. (2023). Investigation on nozzle zone agglomeration during spray drying using response surface methodology. Powder Technology, 429, 118910. https://doi.org/10.1016/j.powtec.2023.118910

van Boven, A. P., Dubbelboer, A., Janssen, T. J. A., Schröder, J., Sewalt, J. J. W., Kohlus, R., & Schutyser, M. A. I. (2024). Investigating the impact of air distribution on spray dryer operability using CFD simulations and pilot-scale experiments. Powder Technology, 440, 119779. https://doi.org/10.1016/j.powtec.2024.119779

van der Hoeven, M. (2008). Particle-droplet collisions in spray drying. [Doctoral thesis, The University of Queensland]. https://doi.org/10.14264/178950

van Rossum, G., & Drake, F. L. (1995). Python Tutorial. Centrum Voor Wiskunde En Informatica Amsterdam, 620.

Vehring, R., Foss, W. R., & Lechuga-Ballesteros, D. (2007). Particle formation in spray drying. Journal of Aerosol Science, 38, 728–746. https://doi.org/10.1016/j.jaerosci.2007.04.005

Verdurmen, R. E. M., Van Houwelingen, G., Gunsing, M., Verschueren, M., & Straatsma, J. (2006). Agglomeration in spray drying installations (the EDECAD project): Stickiness measurements and simulation results. Drying Technology, 24(6), 721–726. https://doi.org/10.1080/07373930600684973

Virtanen, P., Gommers, R., Oliphant, T. E., Haberland, M., Reddy, T., Cournapeau, D., Burovski, E., Peterson, P., Weckesser, W., Bright, J., van der Walt, S. J., Brett, M., Wilson, J., Millman, K. J., Mayorov, N., Nelson, A. R. J., Jones, E., Kern, R., Larson, E., … Vázquez-Baeza, Y. (2020). SciPy 1.0: fundamental algorithms for scientific computing in Python. Nature Methods, 17(3), 261–272. https://doi.org/10.1038/s41592-019-0686-2

Walton, D. E. (2000). The morphology of spray-dried particles a qualitative view. Drying Technology, 18(9), 1943–1986. https://doi.org/https://doi.org/10.1080/07373930008917822

Wegener, M., Paul, N., & Kraume, M. (2014). Fluid dynamics and mass transfer at single droplets in liquid/liquid systems. International Journal of Heat and Mass Transfer, 71, 475–495. https://doi.org/10.1016/J.IJHEATMASSTRANSFER.2013.12.024

Williams, A. M., Jones, J. R., Paterson, A. H. J., & Pearce, D. L. (2009). Effect of fines on agglomeration in spray dryers: An experimental study. International Journal of Food Engineering, 5(2). https://doi.org/10.2202/1556-3758.1635

Winborne, D. A., Nordine, P. C., Rosner, D. E., & Marley, N. F. (1976). Aerodynamic Levitation Technique for Containerless High Temperature Studies on Liquid and Solid Samples. Metallurgical Transactions B, 7B, 711. https://doi.org/10.1007/BF02698607

Woo, M. W., Daud, W. R. W., Mujumdar, A. S., Talib, M. Z. M., Hua, W. Z., & Tasirin, S. M. (2008). Comparative study of droplet drying models for CFD modelling. Chemical Engineering Research and Design, 86(9), 1038–1048. https://doi.org/10.1016/j.cherd.2008.04.003

Xu, Y. Y., Howes, T., Adhikari, B., & Bhandari, B. (2012). Investigation of Relationship between Surface Tension of Feed Solution Containing Various Proteins and Surface Composition and Morphology of Powder Particles. Drying Technology, 30(14), 1548–1562. https://doi.org/10.1080/07373937.2012.696571

Yamamoto, S., & Sano, Y. (1992). Drying of enzymes: enzyme retention during drying of a single droplet. Chemical Engineering Science, 47(1), 177–183. https://doi.org/https://doi.org/10.1016/0009-2509(92)80211-T

Yang, K., Hong, F., & Cheng, P. (2014). A fully coupled numerical simulation of sessile droplet evaporation using Arbitrary Lagrangian-Eulerian formulation. International Journal of Heat and Mass Transfer, 70, 409–420. https://doi.org/10.1016/j.ijheatmasstransfer.2013.11.017

Yu, M., Le Floch-Fouéré, C., Pauchard, L., Boissel, F., Fu, N., Chen, X. D., Saint-Jalmes, A., Jeantet, R., & Lanotte, L. (2021). Skin layer stratification in drying droplets of dairy colloids. Colloids and Surfaces A: Physicochemical and Engineering Aspects, 620. https://doi.org/10.1016/j.colsurfa.2021.126560

Zbicinski, I., Ciesielski, K., & Ge, B. (2022). Mechanism of Particle Agglomeration for Single and Multi-Nozzle Atomization in Spray Drying: A Review. Processes, 10(727). https://doi.org/https://doi.org/10.3390/pr10040727

Zhang, L., Chen, X. D., Boom, R. M., & Schutyser, M. A. I. (2017). Thermal inactivation kinetics of β-galactosidase during bread baking. Food Chemistry, 225, 107–113. https://doi.org/10.1016/j.foodchem.2017.01.010

Zhang, X., Zhou, Q., Huang, Y., Li, Z., & Zhang, Z. (2011). Contrastive analysis of the Raman spectra of polychlorinated benzene: Hexachlorobenzene and benzene. Sensors, 11(12), 11510–11515. https://doi.org/10.3390/s111211510

Zheng, K., Kapp, M., & Boccaccini, A. R. (2019). Protein interactions with bioactive glass surfaces: A review. In Applied Materials Today (Vol. 15, pp. 350–371). Elsevier Ltd. https://doi.org/10.1016/j.apmt.2019.02.003

Zheng, Z., & Huang, Y. (2017). Investigation on the interaction among multi-sprays generated from pressure-swirl atomizers. Atomization and Sprays, 27(6), 477–491. https://doi.org/10.1615/AtomizSpr.2017018229

R
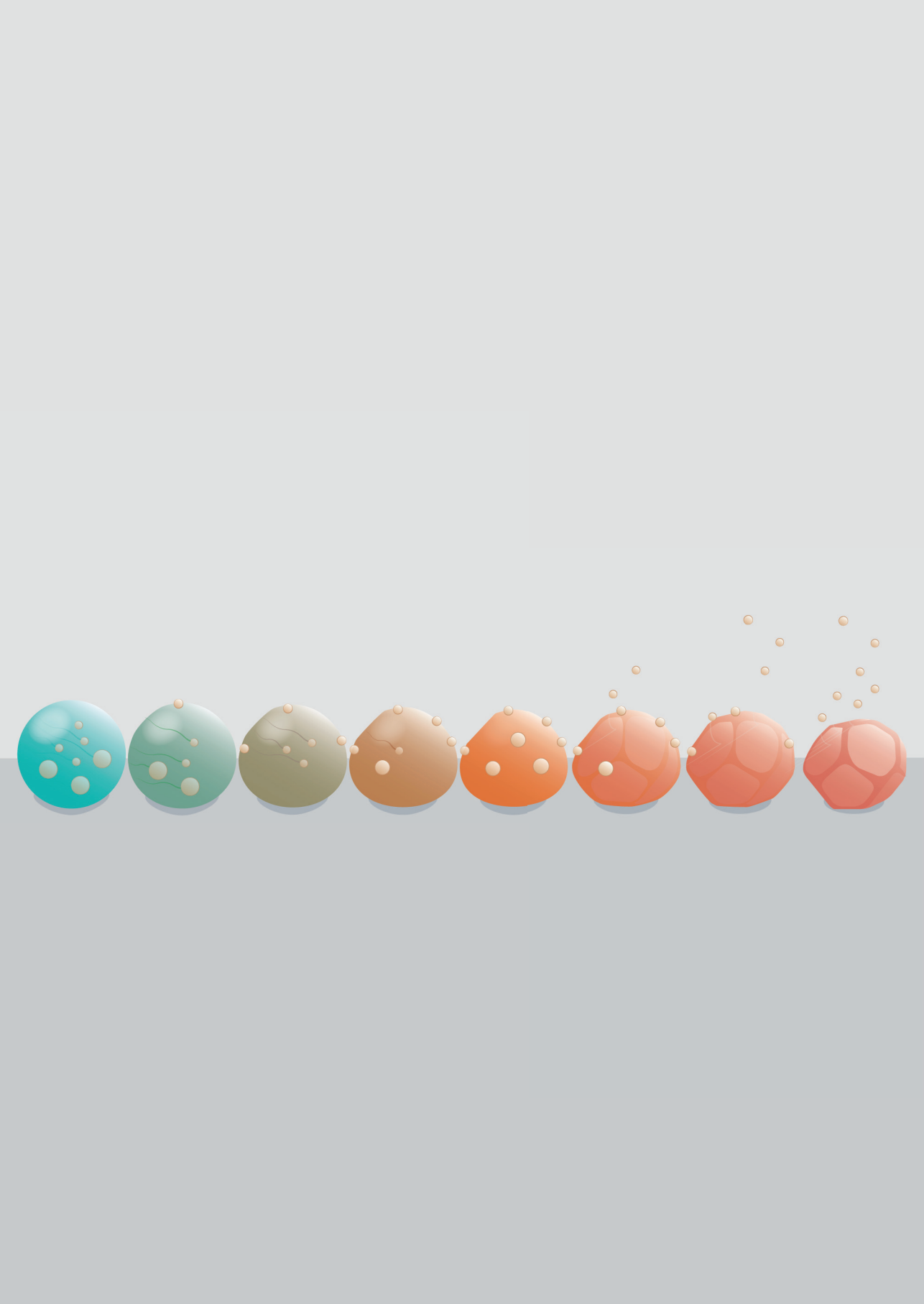
Summary

English summary

Nederlandse samenvatting

S

English summary

Large scale food processes allow mass-production of well-preservable food materials, such as powders produced by spray drying. However, the food industry is consuming a lot of energy, and drying is one of its most energy consuming processes. During spray drying, countless very small droplets are contacted with hot air to dry. The droplets interact, resulting in coalescence, agglomeration or bouncing. Agglomeration is an important factor for steering towards high product quality. It generally improves the flowability and reconstitution behavior of a powder. An insufficient level of agglomeration can lead to off-spec product formation, dust formation and fouling. This all leads to an unnecessary increase in the energy consumption of the powder production chain. Despite its widespread use, optimal drying and agglomeration protocols in spray drying are still established via empirical procedures. Mechanistic understanding of droplet drying and agglomeration during spray drying can contribute to more optimal agglomeration protocols for spray drying. Therefore, the overall aim of this thesis was to characterize the physical phenomena underlying the drying and agglomeration behavior of droplets during spray drying via advanced single droplet drying experimentation.

Single droplet drying approaches have been employed to study the development of the primary particle morphology and drying kinetics of droplets under well-defined conditions. These studies shed light on the underlying drying mechanisms, but have less often been related to realistic drying conditions and agglomeration behavior. **Chapter 2** reviews the potential and the limitations of single droplet drying approaches to unravel the evolution of primary particle morphology and nozzle-zone agglomeration phenomena during spray drying. It discusses the different single droplet drying methods that currently exist and the analyses that have been performed on drying droplets. This showed that current SDD methods are intrinsically not suitable to characterize nozzle zone agglomeration, but that they may be complemented with binary collision studies of droplets and/or particles. Further understanding of nozzle-zone agglomeration requires the use of pilot-scale spray dryer set-ups that allow for controlled agglomeration. Ultimately, advanced CFD modelling approaches could prove useful to fully integrate the insights gained at the SDD and pilot-scale. However, fully resolved CFD based models have to cover multiple scales of space and time and thus are computationally very intensive. Insights generated by SDD experiments can help us to develop coarse-grained or lumped models that are more computationally realistic and may be directly used to find generic guidelines for industrial application.

While visual camera observations have been used to gain insights into the drying kinetics of drying sessile single droplets until the locking point, they failed until now to obtain relevant information further in the drying process. To understand the drying behavior of a droplet during spray drying, in **Chapter 3** high-resolution thermography was used to obtain more relevant information during the entire drying process. This study found that the drying kinetics during the constant rate period depend on the drying air temperature, but not on the composition of the droplet. The duration of the constant rate period

was found to be matrix-specific and related to the morphological locking point of the droplet. At the locking point, the temperature of the droplet no longer stayed at the wet-bulb temperature but started to increase. The time-temperature results obtained by high-resolution thermography were found to serve as an indirect measure for morphological development of the droplet. Droplets that form a vacuole during drying show a more irregular temperature increase, with a plateau of the droplet's temperature when the vacuole is formed. In this chapter, the drying behavior of the droplets was shown to be predicted with a single droplet drying model.

While existing single droplet drying platforms employed an airstream of a constant temperature to dry droplets, within a spray dryer the temperature around the droplet decreases considerably over time. **Chapter 4** therefore focuses on the development of a new sessile single droplet drying system that can simulate the changing conditions in a spray dryer. This new setup was used to dry droplets of solutions containing β-galactosidase and maltodextrin with different temperature-time trajectories. The inactivation of the enzyme was used as an indicator for the thermal load on the droplet. The locking point was found to be an important parameter for enzyme inactivation; the air temperature before this point did not influence the enzyme inactivation much, but a high air temperature after the locking point resulted in significant inactivation. The drying behavior and β-galactosidase inactivation was correctly predicted using a numerical single droplet drying model. This model was also used to estimate parameters that cannot be measured experimentally.

In industrial spray drying, typically multicomponent feed solutions are used. This adds another level of complexity. The composition of such a feed system may influence the locking point and morphology development of the obtained powder particles. Moreover, an inhomogeneous component distribution could develop during drying, influencing the final powder quality and product performance. In **Chapter 5** drying droplets of multicomponent dairy-based systems were studied at simulated temperature-time trajectories. This included the influence of varying composition, drying conditions and emulsion droplet size on the drying behavior, morphological development and surface composition. The presence of fat within the drying matrix reduced the moisture diffusivity, thereby resulting in an earlier locking point. The ratios between lactose and protein, and between different types of protein, influenced the morphology of the dried particle. Systems high in lactose formed smoother particles, while high protein contents resulted in hollow particles. A high casein content resulted in wrinkling, while a high whey protein content resulted in smooth particles with a vacuole. Confocal Raman microscopy revealed that the initial fat, lactose and protein content influences the dry surface composition. Surface fat was detected for the matrix high in fat and for the matrix high in whey protein isolate.

A next step to deepen the insight in spray drying is to include collision dynamics at the single droplet scale. Therefore, **Chapter 6** reports on extending the single droplet drying platform to perform binary collisions. Drying droplets of maltodextrins with different dextrose equivalents were subjected to collisions with glass beads at different time points

S

in the drying process. A shift in the collision outcome was observed during drying. A transition from merging as the sole collision outcome to a regime in which also sticking and bouncing were observed was linked to the locking point of the drying droplet. The sticking regime was only observed for a short period during the drying process, ranging from 0.75 to 1.5 times the locking point. For all investigated systems, the observed collision outcome over time was stochastic, with a higher maximum probability of sticking for the viscous skin forming maltodextrin DE38. A numerical single droplet drying model predicted the locking point of a drying maltodextrin droplet, which was then linked to the observed sticking regime.

In **Chapter 7** collision studies have been extended to investigate the impact of protein addition on the agglomeration behavior. The addition of protein prolongs the sticking regime, and enhances the chance of a collision resulting in sticking. Moreover, pilot scale spray drying experiments have been performed to confirm the observed sticking behavior. This showed that the altered sticking regime upon addition of protein increased both the agglomeration and the overall yield. Industrially, these results can be used to steer product formulations to obtain optimal agglomeration and yield.

Finally, in **Chapter 8**, a discussion on the overall results obtained in this thesis is provided. In addition, some work related to the impact of the particle size of the fines on binary collisions is presented, in which glass beads were used to represent fine particles. With an increase in glass bead size, the end of the sticking regime was prolonged and the probability of a collision resulting in sticking increased. Further, the practical implications obtained from the work performed are discussed, and some guidelines are proposed.

This thesis demonstrates that improved single droplet drying approaches can be used to characterize the physical phenomena underlying the drying and agglomeration behavior of droplets during spray drying. The learnings obtained at the single droplet scale provided important new insights that can be used to steer particle agglomeration during spray drying processes.

Nederlandse samenvatting

Grootschalige processen in de voedingsindustrie maken de massaproductie van houdbare voedingsmiddelen mogelijk. Een voorbeeld is de productie van poeders door middel van sproeidrogen. De voedingsindustrie verbruikt echter veel energie, waarbij drogen een van de grootste energiegebruikers is. In een sproeidroger worden talloze zeer kleine druppeltjes gedroogd met warme lucht. Tijdens dit droogproces botsen de druppels, wat kan leiden tot het coalesceren, aan elkaar plakken zonder volledig coalesceren, of botsen van de individuele druppels. Het aan elkaar blijven plakken wordt ook wel agglomeratie genoemd. Agglomeratie is een belangrijke factor voor de kwaliteit van het uiteindelijke poeder, en zorgt over het algemeen voor een verbeterd poederstromingsgedrag en oplosbaarheid van poeder. Een incorrecte mate van agglomeratie kan ervoor zorgen dat poeder niet aan de gestelde kwaliteitseisen voldoet of dat het zich ophoopt in de sproeidroger. Omdat dit poeder niet goed genoeg is om te verkopen, zal het worden afgekeurd en moet er meer poeder gemaakt worden. Dit zorgt voor een onnodige toename van afval en energieverbruik in de poederproductieketen. Ondanks het grootschalige gebruik van sproeidrogers wordt de optimalisatie van droog- en agglomeratieprotocollen nog steeds gedaan op basis van praktische ervaring. Mechanistisch begrip van het drogen en het aan elkaar blijven plakken van druppels tijdens sproeidrogen kan bijdragen aan het opstellen van betere protocollen voor procesoptimalisatie. Dit proefschrift is daarom gericht op het karakteriseren van de fysische verschijnselen die ten grondslag liggen aan het droog- en agglomeratiegedrag van druppels tijdens sproeidrogen door gebruik te maken van geavanceerde experimentele techieken voor het drogen van individuele druppels.

Eerder onderzoek richtte zich op het drogen van individuele druppels om de morfologie en de droogkinetiek van druppels onder gecontroleerde omstandigheden te bestuderen. Deze studies geven inzicht in de onderliggende droogmechanismes, maar konden niet worden uitgevoerd onder industriële droogcondities en konden niet worden gebruikt voor het bestuderen van agglomeratie. **Hoofdstuk 2** geeft een overzicht van de mogelijkheden en beperkingen van het volgen van het drogen van individuele druppels om morfologische ontwikkeling en agglomeratie gedurende het sproeidrogen beter te begrijpen. Verschillende methoden om individuele druppels te drogen worden besproken inclusief de analyses die gedaan kunnen worden. De huidige methodes om druppels te drogen zijn niet geschikt om agglomeratie te karakteriseren, maar kunnen wel aangevuld worden om botsingen tussen twee druppels en/of deeltjes te bestuderen. Uiteindelijk kunnen de resultaten worden opgenomen in numerieke modellen om de inzichten die zijn opgedaan tijdens het experimentele onderzoek op individuele druppel en pilot-schaal volledig te integreren. Dergelijke modellen vergen echter erg veel rekentijd, omdat ze meerdere tijd- en lengteschalen moeten overbruggen. De experimentele waarnemingen kunnen daarom ook gebruikt worden om deze modellen te versimpelen, waardoor ze sneller resultaten kunnen geven, en daarom gemakkelijker gebruikt kunnen worden voor het opstellen van aanbevelingen voor toepassing op industriële schaal.

Visuele waarnemingen via cameraopnamen kunnen goed worden gebruikt om te kijken naar de ontwikkeling van de morfologie van een druppel tijdens het drogen. Daarnaast worden deze camerabeelden gebruikt om inzicht te krijgen in de droogkinetiek van druppels tot het moment waarop er een vaste schil wordt gevormd aan de buitenkant van de druppel (het 'locking point'). Na het locking point kan het volume van de druppel aan de hand van deze camerabeelden echter niet meer goed worden bepaald, waardoor geen betrouwbare informatie over de droogkinetiek na het locking point kan worden verkregen. Om inzicht te krijgen in de droogkinetiek gedurende het gehele droogproces, wordt in **Hoofdstuk 3** het droogproces van een druppel met behulp van een hoge-resolutie infraroodcamera bestudeerd. Dit liet zien dat de droogkinetiek gedurende de periode waarin de droogsnelheid constant is afhankelijk is van de temperatuur van de lucht waarmee gedroogd wordt. De duur van deze periode waarin de droogsnelheid constant is bleek afhankelijk te zijn van de samenstelling van de druppel en was gelinkt aan het locking point. Rond het locking point bleef de temperatuur van de druppel niet langer op de natteboltemperatuur, maar begon deze te stijgen. De tijd-temperatuurresultaten verkregen met de hoge-resolutie infraroodcamera kunnen dienen als een indirecte maat voor de morfologische ontwikkeling van de druppel. Druppels die een vacuole vormen tijdens het drogen vertoonden een meer onregelmatige temperatuurstijging, met een afvlakking van de temperatuurstijging wanneer de vacuole werd gevormd. Dit hoofdstuk liet ook zien dat het drooggedrag van individuele druppels inderdaad met een druppeldroogmodel voorspeld kan worden.

Terwijl bestaande opstellingen voor het drogen van individuele druppels gebruik maken van een luchtstroom van constante temperatuur, koelt de lucht rond een druppel in een sproeidroger in de loop van de tijd snel af. **Hoofdstuk 4** richt zich daarom op de ontwikkeling van een nieuwe druppeldroger die de veranderende omstandigheden van de luchttemperatuur in een sproeidroger beter kan simuleren. Deze nieuwe opstelling werd daarna gebruikt om druppels van oplossingen met het enzym β-galactosidase en maltodextrine te drogen onder verschillende temperatuur-tijd trajecten. De inactivering van het enzym werd gebruikt als indicator voor de thermische belasting van de druppel. Het locking point bleek een belangrijke parameter te zijn voor de inactivering van het enzym; voor dit punt had de luchttemperatuur weinig invloed op de inactivering van het enzym, maar na dit punt leidde een hoge luchttemperatuur tot significante inactivering. Het drooggedrag en de inactivering van β-galactosidase in een maltodextrine-matrix werd succesvol voorspeld met behulp van een numeriek droogmodel. Daarnaast werd het model gebruikt om parameters te schatten die experimenteel niet gemeten konden worden.

Tijdens industrieel sproeidrogen wordt over het algemeen een oplossing gedroogd die uit meerdere componenten bestaat. De samenstelling van zo'n systeem kan het locking point en de morfologieontwikkeling van de poederdeeltjes beïnvloeden. Bovendien kan er tijdens het drogen een inhomogene verdeling van de componenten ontstaan, wat de uiteindelijke poederkwaliteit beïnvloedt. In **Hoofdstuk 5** is daarom gekeken naar het drogen van op zuivel gebaseerde druppels die meerdere componenten bevatten. Hierbij is gekeken naar de invloed van de samenstelling, de grootte van de oliedruppels in de emulsie,

S

en de droogcondities op het drooggedrag en de morfologische ontwikkeling, inclusief de oppervlaktesamenstelling. De aanwezigheid van vet in de droogmatrix vertraagde de diffusie van water, wat resulteerde in een eerder locking point. De verhoudingen tussen lactose en eiwit, en tussen verschillende soorten eiwit, beïnvloedde de morfologie van het gedroogde deeltje. Systemen met een hoog lactosegehalte resulteerden in poederdeeltjes met een gladder oppervlak, terwijl hoge eiwitgehaltes resulteerden in holle deeltjes. Een hoog gehalte aan caseïne resulteerde in gerimpelde deeltjes, terwijl een hoog gehalte aan wei-eiwit resulteerde in gladde deeltjes met een vacuole. Confocale Raman microscopie liet zien dat de initiële vet-, lactose- en eiwitgehalten de oppervlaktesamenstelling van de gedroogde druppels beïnvloedden. Oppervlaktevet werd gedetecteerd voor de druppels met een hoog gehalte aan vet of wei-eiwit.

Om verder inzicht te verkrijgen in de processen in een sproeidroger, is een volgende stap het meenemen van druppelinteracties. Daarom is in **Hoofdstuk 6** het druppeldroog-platform uitgebreid om botsingen tussen een drogende druppel en een droog deeltje te kunnen bestuderen. Drogende maltodextrinedruppels werden op verschillende tijdstippen in het droogproces onderworpen aan botsingen met glasparels, gebruikt als model voor droge deeltjes. Tijdens het drogen werd een verandering in het botsingsresultaat waargenomen. Een overgang van samensmelten als enige botsingsresultaat naar een regime waarbij ook plakken en afketsen werden waargenomen, kon worden gerelateerd aan het locking point van de druppel. Het regime waar plakken werd waargenomen duurde van 0.75 tot 1.5 maal het locking point. Voor alle onderzochte systemen bleek het botsingsresultaat als functie van de droogtijd stochastisch te zijn. Een hogere maximale kans op plakken werd waargenomen in systemen waarvan de droge laag die zich aan de buitenkant van de druppel vormt overwegend viskeus is dan wanneer zich een overwegend elastische laag vormt. Een numeriek droogmodel voor een individuele druppel was gebruikt om het locking point van een drogende maltodextrinedruppel te voorspellen, dat vervolgens werd gekoppeld aan het regime waarin plakken plaatsvindt.

In **Hoofdstuk 7** zijn de botsingsstudies uitgebreid om de invloed van het toevoegen van eiwitten op het plakken te bestuderen. Dit verlengde het regime waar plakken werd waargenomen, en verhoogde de kans dat een botsing in plakken resulteerde. Om deze waarneming te bevestigen, zijn experimenten met een sproeidroger op pilot-schaal uitgevoerd. Dit liet zien dat het gewijzigde regime waarbinnen plakken werd waargenomen zowel de agglomeratie, maar ook de algehele opbrengst van het proces verbeterde. In de industrie kunnen deze resultaten worden gebruikt om productformulaties aan te passen om agglomeratie en opbrengst te optimaliseren.

Tot slot geeft **Hoofdstuk 8** een discussie over de gezamenlijke resultaten van dit proefschrift. Dit is aangevuld met extra metingen naar de invloed van de grootte van glasparels, als modelsysteem voor kleine droge deeltjes, op botsingen. Een toename in de grootte van glasparels leidde tot een later eind van het regime waar plakken werd waargenomen, en de kans dat een botsing in plakken resulteerde nam toe. Het hoofdstuk eindigt met het delen van een aantal praktische implicaties van het uitgevoerde onderzoek.

Dit proefschrift toont aan dat het drogen van individuele druppels gebruikt kan worden voor het karakteriseren van de fysische verschijnselen die ten grondslag liggen aan het droog- en agglomeratiegedrag van druppels tijdens sproeidrogen. De kennis die werd verkregen op de schaal van een individuele druppel levert belangrijk inzicht op die het beter sturen van deeltjesagglomeratie tijdens sproeidroogprocessen mogelijk maakt.

S

Appendices

A
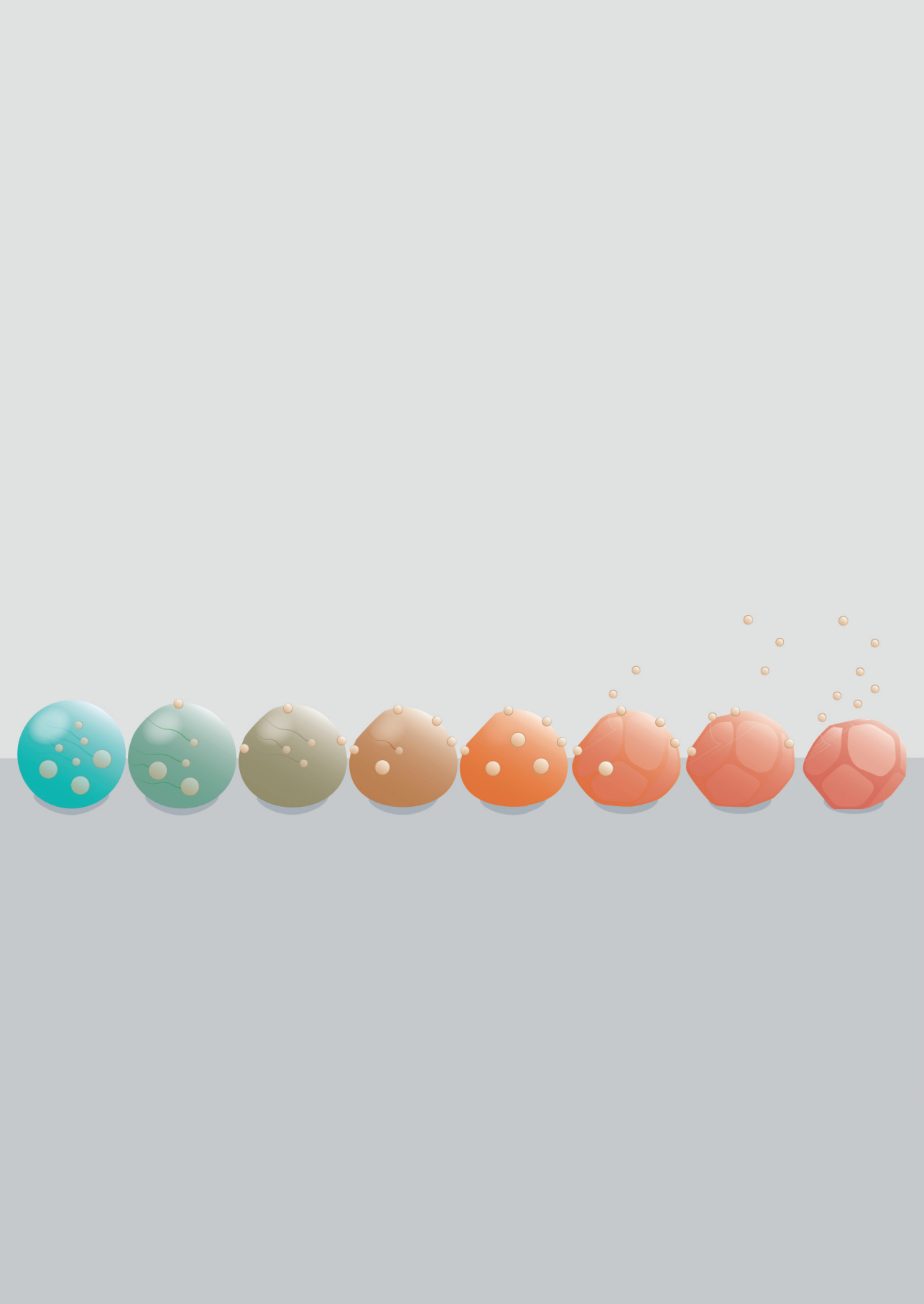
Acknowledgements - Dankwoord

Over the past four years of working on my thesis, I have had the pleasure of being surrounded by many supportive, talented and kind people. Each of them contributed to this thesis in their own way, and I would like to express my sincere gratitude to all of them.

I would like to thank my promotors and co-promotors. *Maarten*, jij hebt mij gedurende mijn gehele promotietraject bijgestaan met jouw oneindige kennis op het gebied van drogen. De inspirerende discussies en constructieve feedback hebben geholpen om mijn onderzoek naar een hoger niveau te tillen. *Jolet*, gedurende het eerste jaar van mijn project ben jij als co-promotor betrokken geweest. Jouw enthousiasme, interesse, behulpzaamheid en ontelbare hoeveelheid nieuwe ideeën hebben enorm bijgedragen aan het opstarten van mijn onderzoek, dankjewel. *Patrick*, wat ben ik blij dat jij na een jaar mijn promotieteam kwam versterken. Jij maakte je het onderwerp snel eigen, stelde scherpe vragen, en hielp mij daarmee om ook zelf kritisch te blijven. Bedankt voor het enthousiasme en de positiviteit waarmee jij iedere meeting in ging, dit werkte voor mij erg motiverend. *Remko*, ook jou mocht ik na mijn eerste jaar aan mijn promotieteam toevoegen. Jouw gedrevenheid en scherpe blik leidde altijd weer tot nieuwe inzichten.

I would also like to acknowledge the support of the partners from the StAggloP project. The industrial project partners; *Guido, Jasper, Jewe, Joost, Joris, Koen and Marc,* thank you for all your valuable contributions. I really appreciated the inspiring meetings, the visits to your companies, and all the insights into the world of industrial spray drying that you shared. *Anne en Annemijn*, bedankt voor de coördinatie vanuit ISPT. *Anneloes*, het was erg fijn om jou als project maatje te hebben. Bedankt voor de gezelligheid tijdens de gezamenlijke meetings, bedrijfsbezoeken en congressen, en voor de goede inhoudelijke discussies welke tot twee mooie gezamenlijke papers hebben geleid. I am happy that the research on single droplet drying continues within the Dragons Egg project. *Suzan*, ik heb met veel plezier vanaf de zijlijn meegekeken hoe jij dit onderzoek vol enthousiasme oppakt. Ik ben benieuwd naar jouw resultaten.

I have had the pleasure of supervising several bachelor and master students during their research projects. *Anne, Lisanne, Sabine, Klaudia, Johannes, Vincent, Koen and Kiki,* thank you for all your contributions to the single droplet drying research.

Voor de analyse van meer complexe experimentele data heb ik het geluk gehad om fijne samenwerkingen aan te kunnen gaan. *Ellard*, toen ik je vroeg om even op het lab te helpen met de confocal Raman microscoop bood jij al snel aan om ook mee te kijken met de verdere analyse van de data. Bedankt voor de waardevolle samenwerking die hier uit voortvloeide. *Sander*, bedankt voor je hulp met de data analyse van de botsingsstudies. Om hiervoor met iemand samen te kunnen werken die niet alleen heel kundig is op het gebied van data analyse, maar ook veel kennis heeft op het gebied van levensmiddelentechnologie was erg prettig.

Mijn onderzoek zou nooit vorm hebben gekregen zonder de hulp van de Technical Development Studio, in het bijzonder van *Hans, Hans en Jeroen.* Gedurende de afgelopen

vier jaar hebben jullie continu meegewerkt aan het vormgeven en verbeteren van de nieuwe single droplet dryer. Bedankt voor de vriendelijkheid en de can-do mentaliteit gedurende de talloze keren dat ik bij jullie aanklopte om iets te laten aanpassen of repareren.

Within the lab, I could always count on the great team of FPE technicians; *Jarno, Jos, Kasia, Lyneth, Martin, Maurice and Wouter.* Your dedication keeps the labs running smoothly, and your expertise and assistance with all the equipment has been very valuable. Martin, ook bedankt voor je hulp met de financiële zaken. Op administratief en organisatorisch gebied kon ik altijd rekenen op de hulp van het FPE secretariaat; *Ilona, Marjan, Esther, Evelyn en Ilone*, dank jullie wel.

To all the amazing colleagues at FPE, thank you for contributing to a great working environment. From big events like PhD trips to daily activities like the lunch breaks, it was all so much more fun because of you. You are with too many to name you all individually, but I hope you all feel appreciated. Special thanks to *Sicong* and *Joanne* for showing me how great FPE is during my BSc and MSc thesis. *Isabel*, dank je wel voor de introductie in de wereld van de drogende druppels. *Julia*, I have really enjoyed our modelling meetings. Your enthusiasm for modelling is inspiring, thank you for sharing all your tips and tricks, for thinking along, and for the fun talks about work and non-work related things. My office mates; *Nienke, Yizhou, Nattawan, Asif and Jolien*, thank you for all the great conversations and laughs we shared. The 2022 Christmas dinner committee; *Iris, Kieke, Lyneth, Maurice, Ting and Wouter*, the 2023 Chinese New Year Hotpot committee; *Luc, Miek, Solange, Yafei, and Yifeng*, and the 2024 FPE PhD study trip committee; *Aadi, Aryo, Koen, Lyneth, Maurice, Melanie and Ting*, thank you for all the good times organizing these events together.

Mijn lieve *vrienden en familie*, bedankt voor al jullie support en voor de momenten van ontspanning. *Opa*, bedankt voor al je interesse in mijn werk, en voor hoe trots jij altijd bent op wat ik doe. *Papa en mama*, bedankt voor jullie onvoorwaardelijke steun en vertrouwen. Bij jullie kan ik altijd terecht, of het nou is om met mij mee te denken, om even te relativeren en tot rust te komen, of gewoon voor de gezelligheid. *Arjen*, bedankt voor de prachtige voorkant en opmaak van mijn thesis. *Anouk*, vroeger liep ik vaak achter jou aan en wilde ik doen wat jij ook deed. Zo was het ook een beetje toen jij het er over had een PhD te willen doen, dit zette mij aan het denken of dit ook iets voor mij zou zijn. Bedankt daarvoor, want ik zou het zo weer over doen.

A

About the author

Nienke Maria Eijkelboom was born on March 9th, 1998 in Best, the Netherlands. She attended 'RSG Pantarijn' in Wageningen, where she obtained her high school diploma in 2015.

In the same year, Nienke started the bachelor Food Technology at the Wageningen University. Her BSc included a four-months exchange program at the University of Sydney, Australia in 2017. For her BSc thesis, Nienke worked on *"Screening methodology development and identification of potential materials used for 3D food printing"* at the department of Food Process Engineering. She finished her BSc cum laude in 2018. Nienke continued with the master Food Technology in Wageningen. In 2019, she came back to the department of Food Process Engineering to work on her MSc thesis entitled *"Influence of carrier formulations on physical properties and aroma profile of spray-dried asparagus powders"*. After completing her thesis, Nienke performed an internship at the Research & Development department of Sanorice Holding B.V., working on the development of a new product.

After obtaining her MSc degree in 2020, Nienke started as a PhD candidate in the department of Food Process Engineering at Wageningen University. She worked on the characterization of the physical phenomena underlying the drying and agglomeration behavior of droplets during spray drying via single droplet drying experimentation. The results of her PhD project are presented in this thesis.

A

Publications

This thesis

Eijkelboom, N. M.[1], van Boven, A. P.[1], Siemons, I., Wilms, P. F. C., Boom, R. M., Kohlus, R., & Schutyser, M. A. I. (2023). Particle structure development during spray drying from a single droplet to pilot-scale perspective. *Journal of Food Engineering*, *337*. https://doi.org/10.1016/j.jfoodeng.2022.111222

Eijkelboom, N. M., Swinkels, A. C. M., de Ruiter, J., Boom, R. M., Wilms, P. F. C., & Schutyser, M. A. I. (2023). High-resolution thermography and modelling allows for improved characterization of drying sessile single droplets. *Journal of Food Engineering*, *341*. https://doi.org/10.1016/j.jfoodeng.2022.111340

Eijkelboom, N. M., Gawronska, K., Vollenbroek, J. M., Kraaijveld, G. J. C., Boom, R. M., Wilms, P. F. C., & Schutyser, M. A. I. (2024). Single droplet drying with stepwise changing temperature-time trajectories: Influence on heat sensitive constituents. *Food Research International, 182*. https://doi.org/10.1016/j.foodres.2024.114194

Eijkelboom, N. M., Rang, V. J., Breevaart, S., Boom, R. M., Wilms, P. F. C., & Schutyser, M. A. I. (2024). Binary collisions of drying maltodextrin droplets and glass beads. *Journal of Food Engineering, 378*. https://doi.org/10.1016/j.jfoodeng.2024.112110

Eijkelboom, N. M., Hooiveld, E., Kingma, J., Boom, R. M., Wilms, P. F. C., & Schutyser, M. A. I. (2024). Single droplet drying of dairy-based systems at spray drying like temperature-time trajectories. *International journal of Dairy Technology, 77*. http://doi.org/10.1111/1471-0307.13106

van Boven, A. P.[1], **Eijkelboom, N. M.**[1], Fentsahm, K.J., Gruson, M.J., Boom, R. M., Wilms, P. F. C., Kohlus, R., & Schutyser, M. A. I. A multiscale investigation on protein addition toward steering agglomeration and yield in spray drying. *Submitted for publication.*

Other publications

Siccama, J. W.[1], Pegiou, E.[1], **Eijkelboom, N. M.**, Zhang, L., Mumm, R., Hall, R. D., & Schutyser, M. A. I. (2021). The effect of partial replacement of maltodextrin with vegetable fibres in spray-dried white asparagus powder on its physical and aroma properties. *Food Chemistry*, *356*. https://doi.org/10.1016/j.foodchem.2021.129567

[1] Shared first authorship: these authors contributed equally.

A

Overview of completed training activities

Discipline specific activities

Conferences

NWGD Symposium (Online)	2020
International Conference on Droplets (Online)	2021
NWGD Symposium (Online)	2021
International Drying Symposium (Worcester, the United States of America)[o]	2022
NWGD Symposium (Wageningen, the Netherlands)[p]	2022
European Drying Conference (Lodz, Poland)[o]	2023
NWGD Symposium (Wageningen, the Netherlands)[p,o]	2023
EFFoST International Conference (Valencia, Spain)[p]	2023
NWGD Symposium (Wageningen, the Netherlands)[p,o]	2024

Courses

Drying – Fundamentals and Applications (Online)	2021
Rheology: the do's and don'ts (Wageningen, the Netherlands)	2021
European School on Rheology (Leuven, Belgium)	2022

General courses

VLAG PhD week (Diessen, the Netherlands)	2021
Presenting with impact (Online)	2021
Posters and pitching (Online)	2021
PhD Carousel (Online)	2021
Supervising BSc & MSc thesis students (Wageningen, the Netherlands)	2021
Effective behaviour in your professional surroundings (Wageningen, the Netherlands)	2021
Scientific writing (Wageningen, the Netherlands)	2021
Introduction to R (Wageningen, the Netherlands)	2022

Other activities

Preparation of the research proposal	2020
FPE weekly group meetings	2020-2024
VLAG PhD Council	2021-2023
PhD study tour to Singapore[p,o]	2022
PhD study tour to England[p,o]	2024
Organizing PhD study tour to England	2024

[p] poster presentation

[o] oral presentation

A